Interrogating mitochondrial dysfunction in facial appearance and ageing

Roisin B. Stout, BSc. (Hons), MRes.

Thesis submitted for the degree of Doctor of Philosophy

Newcastle University
Faculty of Medical Sciences
Translational and Clinical Research

March 2022

Abstract

Mitochondrial dysfunction is found in ageing tissues and has been specifically implicated in the progression of extrinsic ageing in skin through a cycle of oxidative stress and dysfunction. Primary mitochondrial disease (PMD) is caused by genetic abnormalities that effect mitochondrial oxidative phosphorylation and patients may present prematurely with age-related disorders such as dementia, sensorineural hearing loss, and muscle weakness. This thesis aims to explore the link between chronic and extrinsic ageing, and mitochondrial dysfunction using primary mitochondrial disease as a model.

HDFn cells are commonly cultured in high glucose media supplemented with 10% FBS, which ensures continuous growth. However, the level of glucose is not physiologically relevant. Cells in this media; a glucose free media to induce mitochondrial energy production; and a 2% FBS supplementation to reduce cell growth, were stressed with solar light to determine the effect of dose and culture condition on response to solar light irradiation. High glucose DMEM supplemented with 10% FBS had reduced mtDNA repair in response to solar stress and increase mitochondrial ROS, therefore this culture condition could artificially increase the damage response. Chronic repeated doses of solar light, as opposed to single acute doses, had an accumulative increase of mtDNA damage and resulted in reduced oxidative damage post solar stress, thereby having a protective effect against subsequent doses. After solar stress, fibroblasts reduced the majority of mtDNA damage between 8 and 24 hours, and mtDNA network returns to control levels within 8 hours. Overall, culture conditions affect mitochondrial damage response from solar stress and highly proliferative cells grown in high glucose media may not reflect a physiological environment. Low glucose media provides a physiologically relevant alternative to high glucose media, and further investigation into appropriate addition of growth serum would be beneficial to optimise solar stress studies. This study also optimised the appropriate times to study mtDNA damage and mitochondrial network response to solar light damage in dermal fibroblasts cells.

Premature facial ageing and clinical facial features were assessed in PMD patients by systematic review of case reports and cohort studies; a pilot study was conducted in adult PMD patients to assess facial ageing using human evaluators and a convolution neural network.

Results from the systematic review found ocular manifestations of mitochondrial disease include ptosis (eyelid drooping) and ophthalmoplegia (restricted eye movement) that are predominately found in patients with mtDNA deletions in the mitochondrial genome, and highest in patients with single large-scale deletions. However, the overall facial appearance in

patients is underreported and under-investigated. Ptosis in patients may be linked to increased perceived age, though patients on average had reduced levels of sun damage in the form of UV spots. This patient study found there could be a confounding effect between skin appearance and overall facial structure when assessing perceived age between the PMD patient cohort and controls. Notably, no previous literature existed on premature ageing in PMD. Ptosis could be a substantial contributor to overall perceived age and future expansion of the study would benefit from interrogating a larger cohort of patients harbouring large-scale single and multiple mtDNA deletions.

Declaration

This thesis is submitted for the degree of Doctor of Philosophy. The research for this submission was performed in the Department of Dermatological Sciences, Translational and Clinical Research, Newcastle University, United Kingdom from September 2017 to March 2022, under the academic supervision of Professor Mark A. Birch-Machin, Professor Gráinne Gorman and Dr Renae Stefanetti. All work is original unless acknowledged via reference. None of the material has been submitted previously for a degree or any other qualification at this university or any other institution.

Acknowledgements

First and foremost, I am grateful to the NIHR for not only funding my project and giving me this opportunity, but also for their ongoing encouragement during studentship, the pre-COVID breakfasts, training workshops, and their unfailing support during such uncertain times. Without the NIHR this thesis wouldn't be here, so thank you to everybody at the BRC Newcastle for making this happen.

To my academic supervisor, Prof Mark Birch-Machin, thank you for providing me with an environment in which I could grow my own ideas and pursue areas of research that have been integral to my growth as a researcher. I would like to thank my secondary supervisors Prof Gráinne Gorman and Dr Renae Stefanetti of the Mitochondrial Research Group for facilitating the patient study, and for their support and guidance throughout.

The staff and facilities of Newcastle University have been enormously helpful to my work in this project. I would like to give a special thanks to Dr Glyn Nelson and Dr David Bulmer for answering my many questions on microscopy and image analysis, and to Ms Carly Knill for teaching me the ropes in flow. I am incredibly grateful to Dr Kim Pearce for her knowledge of statistics, and for translating it so effectively. Also, to Dr Alastair Blain for his analysis of the systemic review data.

To the MBM group past and present who have provided support, training, in depth scientific discussion, encouragement, commiserations, general conversation, and plenty food; I thank Dr Amy Bowman, Dr Eyman Rashdan, Dr Matt Jackson, Dr Becky Hanna, and the future Drs Ms Catherine Bonn, Ms Gewei Zhu, Ms Lizzie Ruddy, Mr Wil Reynolds and Ms Jess Moore. And thanks to the rest of the dermatology department for the same reasons, I couldn't have asked for a better group to work with. I would like to give a special thanks to Ms Lizzie Ruddy for her collaboration during the skin swab optimisation, and to Mr Wil Reynolds for reading this thesis and providing invaluable feedback.

Thank you to my friends and family for their ongoing support throughout my PhD. I especially want to thank Ross Galloway for listening to endless talk about mitochondria, and for being endlessly positive.

Table of Contents

Table of Figures

Table of Tables

Abbreviations

ADP	Adenosine diphosphate
AF	Auto fluorescence
ATP	Adenosine triphosphate
ATP6, ATP8	Adenosine triphosphate synthase subunits
BSA	Bovine serum albumin
CCCP	carbonyl cyanide m-chlorophenylhydrazone
CNN	Convolution neural network
CO2	Carbon dioxide
COX1 to 3	Cytochrome oxidase subunits
CPEO	Chronic progressive external ophthalmoplegia
Ct	Cycle threshold
DAPI	4′,6-diamidino-2-phenylindole
DCF-DA	2',7'-dichlorodihydrofluorescein diacetate
D-loop	Dissociation loop region
DMEM	Dulbecco's Modified Eagles Medium
DMSO	Dimethyl sulfoxide
DNA	Deoxyribonucleic acid
EDTA	Ethylenediaminetetraacetic acid
ETC	Electron transfer chain
FADH2	Flavin adenine dinucleotide
FBS	Foetal bovine serum
FCCP	Carbonyl cyanide-p-trifluoromethoxyphenylhydrazone
FSC-a	Forward scatter area
FSC-h	Forward scatter height
GFP	Green fluorescent protein
GIT	gastrointestinal tract
GLUT1 and GLUT4	Glucose transporters 1 and 4
H2O2	Hydrogen peroxide
HDFn	Neonatal human dermal fibroblasts
HEt	Hydroethidine
HGPS	Hutchinson-Gilford progeria syndrome
HMW	High molecular weight
H-strand	Heavy strand
LHON	Leber's hereditary optic neuropathy
LMW	Low molecular weight
L-strand	Light strand
MD	Mitochondrial disease
MED	Minimum erythemal dose
MELAS	Mitochondrial encephalopathy, lactic acidosis and stroke- like episodes
MERRF	myoclonic epilepsy with ragged red fibres
MFI	Mean fluorescent index
MIDD	Mitochondrial inherited diabetes mellitus and deafness
mRNA	Messenger ribonucleic acid
mROS	Mitochondrial reactive oxygen species
mtDNA	Mitochondrial deoxyribonucleic acid

MMP	Matrix metalloproteinase
MTS	3-(4,5-dimethylthiazol-2-yl)-5-(3-carboxymethoxyphenyl)-2-(4-sulfophenyl)-2H-tetrazolium, inner salt
NADH	Nicotinamide adenine dinucleotide (reduced)
NADH2	Nicotinamide adenine dinucleotide
NCR	Non-coding region
ND1 to 6	Nicotinamide adenine dinucleotide dehydrogenase subunits
nDNA	Nuclear deoxyribonucleic acid
NFM	Non-fat milk
NO	Nitric oxide
ONOO	Peroxynitrite
OXPHOS	Oxidative phosphorylation
P/S	Penicillin Streptomycin
P53	Tumour protein p53
p53R2	p53-inducible ribonucleic acid subunit
PBS	Phosphate buffered saline
PI	Propidium iodide
PMA	Phorbol myristate acetate
PMD	Primary mitochondrial disease
POLG	Polymerase gamma
qPCR	Quantitative polymerase chain reaction
RFP	Red fluorescent protein
ROS	Reactive oxygen species
ROX	Carboxyrhodamine
RRAD	Ras Related Glycolysis Inhibitor and Calcium Channel Regulator
rRNA	Ribosomal ribonucleic acid
RRM2B	Ribonucleotide reductase M2B
SANDO	Sensory ataxia neuropathy, dysarthria and ophthalmoparesis
SED	Standard erythemal dose
SLE	stroke-like episodes
SMD	Secondary mitochondrial disease
SOD	Superoxide dismutase
TAE	Tris acetate EDTA
TBE	Tris borate EDTA
TBS	Tris buffered saline
TBS-T	Tris buffered saline with tween 20
TCA	Tricarboxylic acid
TE	Trypsin-ethylenediaminetetra-acetic acid
TFAM	Mitochondrial transcription factor A
TIGAR	TP53 Induced Glycolysis Regulatory Phosphatase
TMRE	Tetramethylrhodamine, Ethyl Ester, Perchlorate
tRNA	Transfer ribonucleic acid
UVR	Ultraviolet radiation
UVA	Ultraviolet A
UVB	Ultraviolet B
γH2AX	Gamma H2A histone family member X

Chapter 1. General Introduction

1.1 Skin structure and function

The skin is the largest organ of the body and provides a barrier to water and the external environment; it protects against ultraviolet radiation (UVR), pathogens, and injury from both mechanical and chemical stressors. The main structure can be broadly divided into three main layers: the epidermis, the dermis, and the hypodermis. The outer epidermal layer is further sectioned by five distinct stratum layers, the dermis has two undefined layers and contains other skin appendages such as blood vessels and hair follicles, and the hypodermis is the deepest layer which consists mostly of adipose tissue.

Skin properties vary depending on sex, body region, age, ethnic origin, among other disease and lifestyle factors. Factors affecting skin differences in sex is predominantly affected by sex steroids altering both epidermal and dermal thickness and immune function (Dao and Kazin, 2007). There are vast anatomical regional variations in the epidermal thickness (Sandby-Moller et al., 2003). Within the face area alone there are differences in total skin thickness including dermis to epidermis ratio (Chopra et al., 2015); vascular patterns, and sebaceous- and sweat gland population (Moretti et al., 1959). Anatomic skin region can see changes in roughness, hydration and trans-epidermal water loss, sebum secretion, elasticity, and pH (Dąbrowska et al., 2018). Certain lifestyle factors can promote skin ageing and ageing itself has a negative impact on many of these skin changes; this is reviewed later.

1.1.1 Epidermis

The epidermis' five layers begin from keratinocyte production and follow a path of keratinisation to produce an outer layer of skin with protective corneocytes and a high lipid content as a water barrier.

Epidermal keratinocyte production begins at the **stratum basale** of the epidermis; a single layer of cuboidal keratinocytes and active stem cells, melanin producing melanocytes, and Merkel receptor cells are attached to the basement layer separating the epidermis from the dermis (Kolarsick et al., 2011).

The **stratum spinosum** constitutes of around 5-10 layers of cells and continues from the stratum basale. The shape and composition of these cells transforms as they mature and progress from the lower to upper layers of the spinosum. Keratinocytes start accumulating lamellar bodies and keratin fibres which cause the cells to appear flatter. This layer also hosts

interspersed Langerhans cells which function to engulf bacteria, debris and other dysfunctional cells (Yousef et al., 2019).

The outer cells continue through to the **stratum granulosum**, a 3-5 cell thick layer where the keratinocytes no longer divide, and continue keratin and lamellar body production. Keratohyalin granules are formed to promote cell dehydration and death mainly by the release of filaggrin to form keratin aggregates, and the degradation of nuclear material and cellular organelles follows (Eckhart et al., 2013). Lipids and peptides are released from lamellar bodies which provide both a water barrier and antimicrobial enzymatic defence (Feingold, 2012).

The **stratum corneum** is the outermost layer of skin where cells have fully undergone terminal differentiation into corneocytes. Cells are dense with keratin aggregates and a lipid surround, that inevitably undergoes shedding (desquamation) (Marks, 2004). In healthy skin, this layer can be up to 30 corneocytes thick and provides effective protection against trans-epidermal water loss, pathogen invasion, and extrinsic stressors (Yousef et al., 2019).

Between the stratum corneum and stratum granulosum, the **stratum lucidum** is found in thicker regions of skin- in the palms and soles. It provides an extra water barrier for areas which are more prone to damage and contains the keratohyalin transformation product and keratin precursor, eleiden (Yousef et al., 2019).

1.1.2 Dermis

The dermis is a fibrous supportive layer of connective tissue, situated between the epidermis and the hypodermis. Collagen and elastic tissue provide a supportive network for the upper epidermal layer, dermal fibroblasts, immune and stem cells, and adipocytes. The papillary dermis lies beneath the basement layer of the epidermis. It is packed with capillary loops and fibroblasts, with a loose connective tissue structure, and hosts mast cells and macrophage immune cells. In comparison, the majority of the dermis comprises of the underlying dense reticular dermis with collagen and elastic fibres, sweat glands, pilar erector muscles, hair follicles, and blood vessels. Sensory and nerve receptors are present throughout the dermis.

The main function of fibroblasts in the dermis is to produce collagen and elastin for connective tissue. However, there is heterogeneity of fibroblasts in the dermis and diversity is apparent between anatomical regions, dermal layers, developmental stages, and even between cells. As previously reviewed by *Driskell and Watt* (2015); dermal fibroblast lineages arise from different origins depending on anatomical site, and further differentiation to papillary or reticular dermis alters gene expression which increases fibroblast heterogeneity.

The indistinct border between reticular and papillary dermis is lined with the superficial subpapillary vascular plexus, which supplies the papillary dermis and capillary loops in the dermal papillae. The deep dermal vascular plexus lies below the reticular dermis above the hypodermis.

1.1.3 Melanocytes and melanin production

Melanin molecules are capable of absorbing light, which can protect skin from harmful UVR, and provide thermoregulatory properties (D'Mello et al., 2016). Importantly, melanin significantly reduces the level of UVR that reaches the dermal fibroblasts, but not the basal layer of the epidermis (Miyamura et al., 2007). Melanocytes account for around 1% of epidermal cells and transfer melanosome organoids into surrounding epidermal keratinocytes to synthesise and store melanin (Seiberg, 2001); the process of melanin production has been extensively reviewed and is further discussed later (D'Mello et al., 2016).

Skin colour is predominantly determined by melanin pigment and haemoglobin in the skin (Stamatas et al., 2004); there are two types of melanin which produce either a brown or black pigment (eumelanin) or a reddish pigment (pheomelanin). The ratio of pheomelanin to eumelanin is related to skin type; production of each increases in response to UVR, but only the degree of eumelanin production correlates with the appearance of skin tanning (Thody et al., 1991). Melanin production in response to UVA light is immediate and temporary, and proposed to be directly activated by reactive oxygen species (ROS) production (Miyamura et al., 2007). Conversely, UVB causes a postponed induction of melanin, through tyrosinase activation, and can persist in the form of hyper-pigmented spots after chronic exposure (Awad et al., 2021, Rok et al., 2021).

1.2 **Mitochondria**

1.2.1 Structure

Mitochondria are cellular organelles located in the cytoplasm and are primarily responsible for the majority of cellular energy supply, they also have essential roles in cell signalling and macromolecule synthesis. The dual membrane structure comprises of an outer membrane, intermembrane space, and an inner membrane with infolding creating cristae to increase surface area.

The mitochondrion works with the cellular machinery in endosymbiosis. The main theory for eukaryotes' ability to establish complex form begins with the phagocytosis of the prokaryotic

mitochondria, thus offering the energetic advantage to both parties and the driving force for the development of the large nuclear genome and greater cellular size of eukaryotes. This theory is well reviewed by Lane and Martin (2010), providing evidence for mitochondria's pivotal role in the evolution of multicellular organisms. The alternative theory poses mitochondria was engulfed by an anaerobic eukaryote and worked to detoxify ROS. This theory is problematic as mitochondria are major ROS producers and could have added to the issue, however proposed prokaryotes similar to mitochondria do not have an ATP translocator so it is likely mitochondria served an initial purpose prior to energy production (reviewed by Kurland and Andersson (2000)).

1.2.2 Function

1.2.2.1 Oxidative phosphorylation

Energy is produced through respiratory complexes spanning the inner membrane during the oxidative phosphorylation process; Figure 1-1 shows the electron transport chain respiratory complexes I-IV and ATP synthase (complex V) in the inner membrane.

Oxidisation of NADH at complex I (NADH- ubiquinone oxidoreductase) or flavin adenine dinucleotide ($FADH_2$) at complex II (succinate-CoQ reductase) is catalysed by the reduction of coenzyme Q (Q in Figure 1-1) (Alcázar-Fabra et al., 2016); NADH and $FADH_2$ are generated in the tricarboxylic acid (TCA) cycle and during β-oxidation. Hydrogen ions (protons) from each reaction are transported to the intermembrane space of the cristae through complexes I and III, this is powered by the transfer of the electrons from complex I and II to complex III by the lipid electron carrier coenzyme Q. Electron donation at complex II by $FADH_2$ results in fewer transferred protons as it essentially bypasses complex I (Ehinger et al., 2016), though four times greater NADH is produced in the TCA cycle.

Complex III (coenzyme Q: cytochrome c – oxidoreductase) transfers electrons to cytochrome c, taking up protons from the matrix and pumping extra protons from the reaction into the intermembrane space. Electron transfer continues via cytochrome c to complex IV (cytochrome c oxidase), where they are used to produce water molecules along with matrix hydrogen ions and O_2; more protons are transferred to the inter membrane space during this process.

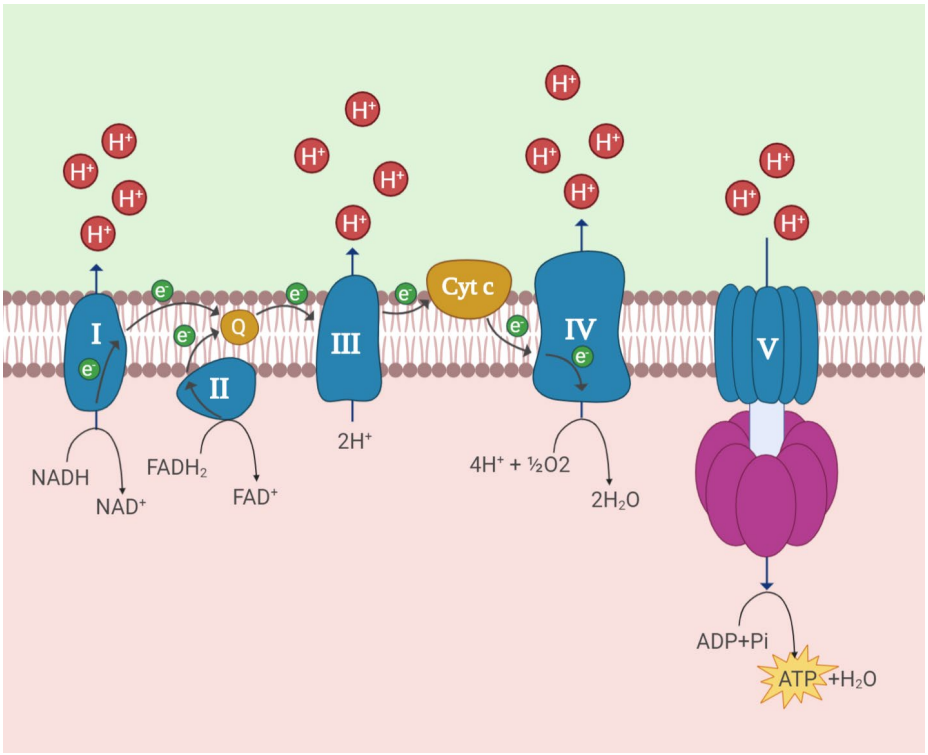

Figure 1-1 Oxidative phosphorylation process in the mitochodnrial inner membrane.
Green area represents mitochodnrial matrix and pink area represents the innermembrane space. Blue figures represent the mitochondrial complexes of OXPHOS I-V. Created in Biorender.com

A positive proton concentration gradient and electrical potential is created in the intermembrane space which drives a proton motive force to the matrix. When coupled with complex V (ATP synthase), this supplies the energy required to phosphorylate adenosine diphosphate (ADP) into adenosine triphosphate (ATP) energy (ATP synthase reviewed by Jonckheere et al. (2012)). The proton gradient can be disrupted by regulated or unregulated uncoupling of complex V, or through cation influx into the mitochondrial matrix. This mechanism is further discussed by Berry et al. (2018), which details involvement in thermogenesis in brown adipose tissue, and in unfolded protein degradation and stress response mediated by the generation of ROS.

1.2.2.2 ROS production

ROS are defined as any oxygen containing molecule with the capacity to initiate some form of reaction. They are essential cell signalling molecules in response to stress, such as; T-cell proliferation, differentiation and activation (reviewed by Yarosz and Chang (2018)); migratory precision of neutrophils (Wang et al., 2016b); hypoxia regulation (reviewed by Movafagh et al. (2015)); and wound healing (reviewed by Dunnill et al. (2017)). H_2O_2 released by immune

cells can directly modify pathogen signalling and reduce virulence as a defence mechanism (Alvarez et al., 2016). ROS reacts both reversibly and irreversibly with lipids, proteins and nucleic acid in a signalling capacity, and the resulting conformational changes can alter membrane permeability (Wang et al., 2016c), modify transcription factors (Klotz et al., 2015), enzyme activity status and mRNA stability (mitochondrial redox signalling review by Schulz et al. (2014)). Mild increases in ROS can have a cytoprotective response, but these modifications can become detrimental when ROS production and antioxidants become imbalanced (the concept of mitochondrial hormesis is explored in this review by Ristow and Zarse (2010)). Both chronic and acute stress can induce ROS generation; the main detrimental effects of ROS are by products of lipid peroxidation, protein oxidation and damage to nucleic acid.

ROS are produced by both damage and inflammation, and are produced through normal physiological processes. This can make precise measurements difficult to attribute to specific experimental conditions and inhibition impossible without affecting a large proportion of cellular mechanisms. An update in this field by the European Consortium in Science and Technology highlights the problems with using the blanket term 'ROS' to describe many interacting species (Egea et al., 2017). As the field has now progressed its understanding of ROS species, it is clear that location and quantity are both interplaying factors in the downstream consequences. Secondary sources of ROS are signalled through primary ROS in a 'cascade of ROS amplification'; mitochondrial ROS formation is a prime example of this.

Mitochondria are well-documented producers of ROS, due to their oxygen and electron rich environments. Mitochondrial ROS (mROS) production is predominantly in the form of superoxide ($O_2^{\bullet-}$) as a direct result of single electron leak in the ETC and reduction of O_2. This will mainly undergo rapid dismutation to hydrogen peroxide (H_2O_2) by superoxide dismutases (SODs: SOD1 specific to cytoplasm and SOD2 specific to mitochondria); electron leak in pairs contributes to hydrogen peroxide formation. Superoxide can also react with nitric oxide (NO) to form the oxidant peroxynitrite ($ONOO^-$). Hydrogen peroxide is considered a non- radical ROS as it relatively stable with no unpaired electrons, and it requires further oxidation to become reactive. It can either be dissociated into H_2O and O_2 by catalase, or form hydroxyl radicals in the presence of iron (II) or copper (I) salts via the Fenton reaction (the chemical formations of these molecules are reviewed in further detail by Halliwell and Gutteridge (1984)). Singlet oxygen ($^1O_2$) is formed in the mitochondria by lipid peroxidation, and in turn can directly oxidise lipids. The interaction of mitochondrial membrane lipid cardiolipin and

cytochrome c in the ETC has been demonstrated to release $^{1}O_2$ *ex vivo* (Miyamoto et al., 2012), and is proposed as a key pathway in mitochondrial induction of apoptosis.

1.2.2.3 Stress response and cell death

Apoptosis is a highly conserved process of cell death, whereby cells undergo self-destruction in response to extrinsic and intrinsic triggers. The mitochondrial pathway of apoptosis is activated in high stress conditions, including mitochondrial DNA (mtDNA) damage and growth factor deprivation, whereby the mitochondrial membrane transition pore in the inner mitochondrial membrane opens, changing the membrane from highly impermeable to a permeable state. The resulting osmotic disturbance in the mitochondrial matrix and an increase in permeability of the outer mitochondrial membrane cause the release of apoptosis signalling proteins including cytochrome *c* and apoptosis inducing factor (reviewed by Redza-Dutordoir and Averill-Bates (2016)). While low dose ROS activates cell repair and survival pathways, high ROS can activate cell death in the form of apoptosis and necroptosis. Activation and stabilisation of tumour suppressor p53 by low-level ROS can trigger cell survival by inducing cell cycle arrest, promoting DNA repair, and inducing cell senescence. In normal conditions, p53 promotes mitochondrial energy production by supressing the glycolysis pathway through suppression of GLUT1 and GLUT4 glucose transporters, inhibiting glucose-6-dehydrogenase activity, and activating RRAD and TIGAR inhibitors of glycolysis (reviewed by Gnanapradeepan et al. (2018)). In high stress conditions, p53 regulates the transcription of pro- and anti-apoptotic proteins that translocate to the mitochondria to directly interact with apoptotic proteins, and therefore promoting mitochondrial induced apoptosis (Redza-Dutordoir and Averill-Bates, 2016).

1.2.3 Mitochondrial genome

1.2.3.1 Structure

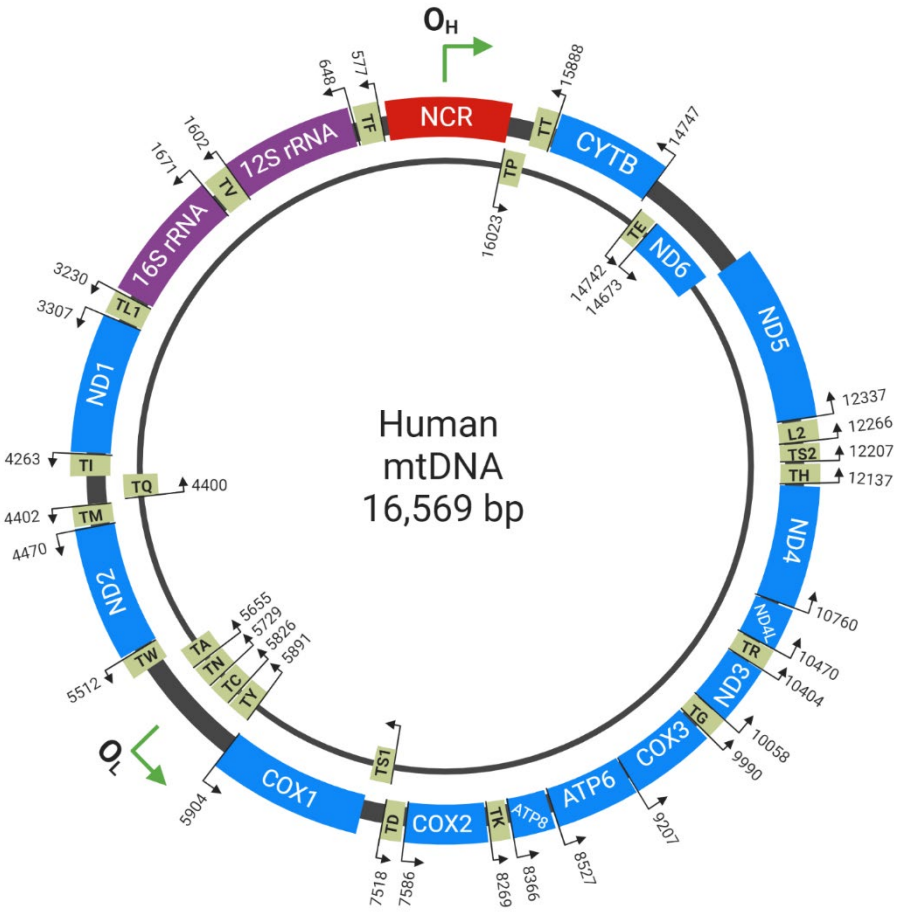

Figure 1-2. Human mtDNA showing the 2 mitoribosomes (purple), 13 polypeptides (blue) and 22 tRNA genes (beige) with corresponding transcription start regions. Heavy strand origin of replication = O_H; Light strand origin of replication= O_L; and Non-coding region= NCR. Created in Biorender.com.

Multiple copies of mtDNA reside in the mitochondrial matrix, independent of nuclear DNA (nDNA). Depicted in Figure 1-2, the double stranded mitochondrial genome is 16,569 bp in size, with a heavy and a light strand, which host 37 genes in total: 2 ribosomal RNAs (rRNA), 22 transfer RNAs (tRNA) and 13 polypeptides. The polypeptides are all components of the OXPHOS machinery: cytochrome b (CYTB), NADH dehydrogenase subunits (ND1, ND2, ND3, ND4, ND4L, ND5 and ND6), cytochrome oxidase subunits (COX1, COX2 and COX3), and ATP synthase subunits (ATP6 and ATP8) are encoded in mtDNA (Figure 1-2). The rRNAs are 2 sub-units (12S and 16S) of the mitoribosomes responsible for mitochondrial protein

translation, and the 22 tRNAs code all 20 amino acids with two for leucine (UUR and CUN) and two for serine (UCN and AGY).

Unlike nDNA, mtDNA is not packaged in protective histones and is located in close proximity to high levels of ROS from the ETC, which is widely believed to increase susceptibility to mutations (Rong et al., 2021). Even though the mutation rate in mtDNA is higher than nDNA (Allio et al., 2017), mtDNA is not completely unprotected. Copies are distributed throughout the mitochondria in nucleoid structures, with an average estimation of anything between 2.4 and 7.8 copies per nucleoid (reviewed by Bogenhagen (2012)). mtDNA is compacted by binding to mitochondrial transcription factor A (TFAM) at specific sites, which in turn shortens the DNA and condenses it into a dense globular state to aid the binding of multiple DNA genomes (Brett et al., 2007). Consequently, defects in TFAM result in catastrophic mtDNA depletion and reduction of nucleoids (Stiles et al., 2016). Localisation and segregation of mtDNA is an important factor the expansion of mtDNA variants.

mtDNA polymorphisms in human populations are found throughout the world, and populations which share similar mtDNA sequences are defined as 'haplogroups'. Some haplotypes have been suggested to have evolved as biological adaptation with functional consequences, including; non-shivering thermogenesis response in cold climates (Nishimura et al., 2017), and maximal oxygen uptake (Martínez-Redondo et al., 2010). Subsequent phenotypical manifestations of variants in the mitochondrial genome can be associated with particular haplotypes (reviewed by Chinnery and Gomez-Duran (2018)), creating further complexity in the study of mitochondrial dysfunction.

Mitochondrial function relies on the interaction with the nuclear genome; there are around 1300 nuclear gene products imported into the mitochondria. The respiratory chain requires around 70 nuclear encoded proteins and only the rRNA sub-units of the mitoribosomes are derived from mtDNA, the other polypeptides are translated by cytoplasmic ribosomes and transferred into the mitochondria for assembly (Bogenhagen et al., 2018).

mtDNA heteroplasmy arises when one or more variant/s of the mitochondrial genome is present due to inheritance, somatic variants, and/or incorrect replication/repair resulting in errors or deletions. Variants can be benign or dysfunctional, and there is a threshold effect whereby the ratio of dysfunctional to functional mtDNA can determine whether the disease phenotype becomes apparent. mtDNA heteroplasmy shows tissue variation, and it is theorised that cells with a high turnover rate are less likely to accumulate dysfunctional genotypes; this is apparent in blood in which heteroplasmy of dysfunctional variants declines with age (Grady

et al., 2018). Interestingly, after sequencing 12 tissues from 152 healthy individuals, Li et al. (2015) found a positive selection for specific variants in liver; it was suggested that this reduction in mitochondrial metabolism may be beneficial to the liver by reducing by-product, though the functional significance of the variant is unknown. The has been found in a further independent study with the same position specific variant (nucleotide position 72) was found in the liver, though higher levels of overall heteroplasmy were found in the skeletal muscle (Naue et al., 2015). These studies demonstrate tissue specification of heteroplasmy that occur in high levels in the liver, kidney, and skeletal muscle; lower levels of heteroplasmy are found in other tissues. However, this mechanism is not well understood, and could arise from positive/negative selection of variants on a tissue/cell specific basis with age or from clonal expansion during tissue differentiation. Regardless of mechanism, tissue specificity of heteroplasmy is a further complexity to consider with mitochondrial studies and is of importance during this thesis (particularly in chapter 5) when assessing the effect of genetic mitochondrial disease in facial appearance and skin ageing.

1.2.3.2 Repair mechanisms

mtDNA was once widely believed to have very limited repair mechanisms, and damaged mitochondrial was thought to only undergo degradation by mitophagy alone. Though the understanding of mtDNA repair has progressed, it is still less understood than nuclear repair. Repair mechanisms in mitochondria has been the subject of several recent reviews (Fontana and Gahlon, 2020, Zinovkina, 2018, Rong et al., 2021). Base excision repair is considered the main repair mechanism and involves the removal of non-bulky DNA lesions, including; AP sites (missing purine/pyrimidine base), de-animation (hydrolysis of cytosine to uracil), oxidised bases, and alkylated bases; followed by cleavage of the site, and patching (Krokan and Bjørås, 2013). Single strand break repair is considered part of the base excision repair pathway (Meagher and Lightowlers, 2014). Repair of double strand breaks occurs through accurate re-joining of breaks during the late S to G_2 phase of replication, using the homologous strand as a template for repair (Vítor et al., 2020). Proteins involved in homologous repair translocate to the mitochondria upon induction of double strand breaks and various tissues are shown to have such repair mechanism/s (Dahal et al., 2018). In contrast, non-homologous end joining is an error prone ligation of the broken ends which occurs throughout the cells cycle but predominantly during G_1 phase (Vítor et al., 2020). Microhomology mediate end joining, a subset of non-homologous end joining, is active in mitochondria and proposed to mediate

end joining at other points in the cells cycle (Tadi et al., 2016). This method uses 'microhomologous sequences' within the DNA, usually short repeating sequences, to align the broken ends (McVey and Lee, 2008). mtDNA deletions are proposed to be a consequence of this repair mechanism, and deletions in the mtDNA are often flanked by short repeating sequences (Bua et al., 2006).

1.2.4 Mitochondrial role in skin

Skin cells have a reduced energy requirement compared to other tissues, but mitochondria still maintain functional roles in the skin besides energy production, including stratum corneum development, melanin production, microbial defence, and hypoxic response. In response to staphylococcus infection; glycolysis and ATP production have been found to rapidly increase (Wickersham et al., 2017), and mitochondrial ROS signalling is activated through electron transport of complex I which induces hypoxia-inducible factor 1-alpha (HIF1α) activation and promotes immune cell recruitment (McGettrick and O'Neill, 2020, Hamanaka and Chandel, 2009). Mitochondrial role in epidermal differentiation is further discussed in section 5.5.1, and melanin production in 1.3.3.

1.3 **Skin ageing**

1.3.1 Intrinsic

Cutaneous (intrinsic) skin ageing is a combination of the inevitable loss of type I and III procollagen, reduced collagen density (Varani et al., 2006), connective tissue alterations, and an increase in collagen degrading matrix metalloproteases with increasing age (Varani et al., 2000); this leads to the development of fine lines. Age dependant changes to the cornification envelope in the stratum corneum resulting in barrier dysfunction and xerosis (Rogers et al., 1996, Rinnerthaler et al., 2013). Fine lines, breakdown of the skin structure, reddening due to increased visible vasculature and a reduction of elasticity are the main clinical features of intrinsic ageing; extrinsic ageing produces much deeper wrinkles, dryer skin, spider veins and uneven pigmentation (Naidoo and Birch-Machin, 2017).

1.3.2 Extrinsic

Sun damage is a well-known cause of skin cancer and ageing, and photoageing is the process of chronic sun exposure leading to extrinsic skin ageing.

The most striking representative images of the effects of sun damage on skin ageing come from an image of a 69 year old truck driver first published by Gordon and Brieva (2012). After years of unilateral sun exposure on the left side of his face, subsequently has deep wrinkles and solar elastosis to that side but only fine lines on the other (Gordon and Brieva, 2012). Solar light is composed of ultraviolet radiation (UVR) (10–380nm), visible light (380–780nm) and infrared radiation (above 780nm). UVR is the most notorious for causing skin damage, so protection against both UVA (315-400nm) and UVB (280-315 nm) is found in most sunscreens. UVB radiation was once believed to be the only contributor to photoageing due to higher energy levels than UVA, but it is now proven that UVA is also a key inducer of DNA damage, though each affects skin through different pathways. UVA makes up the majority of solar UVR but only affects DNA indirectly through ROS production and oxidative stress, whereas UVB radiation represents a smaller portion but causes direct DNA damage (Rünger et al., 1995). Penetration of light into the skin increases with wavelength, and thicker stratum corneum results in reduced light penetration (Finlayson et al., 2021). Other factors involved in light penetration include ethnicity, site of skin, and hydration (Sklar et al., 2012). Melanin absorption of UVR is protective against damage (Swalwell et al., 2012), and higher melanin has an inverse correlation with total DNA photoproducts in humans (Wenczl et al., 1998, Tadokoro et al., 2003). mtDNA damage is repeatedly seen in higher levels in photo-exposed skin, leading to an accumulation of cellular damage and reduced mitochondrial activity (Birket and Birch-Machin, 2007, Bowman and Birch-Machin, 2016, Krishnan et al., 2004, Berneburg et al., 1997).

Collagen reduction, mtDNA damage and increased ROS production are all key features of photoageing, although mechanisms are not yet fully characterised. Inflammation induces the breakdown of matrix proteins to help the recruitment and migration of immune cells, therefore chronic inflammation can result in the detrimental breakdown of tissues (Manicone and McGuire, 2008). Inflammation due to UVA and UVB exposure has been shown to induce the enzymatic activity of matrix metalloproteinases (MMPs) in the dermis and epidermis, respectively, through ROS signalling and the activation of transcription factor AP-1 and NFκB (Vicentini et al., 2011, Kang et al., 2003, Tewari et al., 2014, Chiang et al., 2012). AP-1 production reduces synthesis of procollagen type I and III, thereby disrupting the formation of new collagen and concurrently degrading it (Fisher et al., 2000). This is supported by the presence of ultrastructural changes and degradation of collagen fibre bundles from the dermis in photo-exposed areas of human skin and UVR irradiated mouse models (Edwards et al., 2001). Therefore, sun exposure is directly linked to the active breakdown of collagen and the

reduction of collagen synthesis through ROS signalling, leading to the formation of deep wrinkles and extrinsic skin ageing.

Pollution can induce extrinsic ageing in addition to UVR. With climate change a major danger to human health, research into the effects of air pollution has received growing attention. Outdoor pollutants predominantly originate from vehicle emissions, combustion of fossil fuels and industrial processes. Small particulate matter (PM2.5) and ozone has been shown to increase DNA and protein damage through ROS and oxidative stress in vitro and in mouse models (Piao et al., 2018, Valacchi et al., 2002), and have a positive association with skin ageing through pigmentation spots and skin wrinkling (Ding et al., 2017, Vierkötter et al., 2010). Furthermore, particulate matter increases DNA double strand breaks and MMP production in a dose dependant manner (Reynolds et al., 2020).

Lentigines are hyperpigmented lesions in the skin resulting from excess melanocytes that often become more abundant during ageing. Solar lentigines are associated with the level of sun exposure of the skin (Bastiaens et al., 2004), and are the product of excess melanin production. Traffic-associated particles and soot have also been associated with the formation of these pigment spots on the forehead and cheeks (Vierkötter et al., 2010, Hüls et al., 2016), suggesting a common mechanism between UVR and pollution stressors. It has been suggested that this could in part be due to the age-dependent decline of mitochondrial complex II: succinate dehydrogenase (Chang, 2016). Complex II is entirely transcribed by nuclear DNA and has been shown to have an age dependant decrease in activity in senescent cells in comparison to complex I and IV, predominantly in the epidermis (Bowman and Birch-Machin, 2016). Inducing hyperpigmentation in melanoma cells results in an increase of complex II activity, but not complex I or III, and an initial increase in superoxide ROS formation (Boulton and Birch-Machin, 2015). Additionally, complex II activity reduces co-enzyme Q_{10} which provides antioxidant properties, and reduced complex II activity is linked to increased ROS production (Wojtovich et al., 2013). Therefore, lentigine formation has been proposed as a protective mechanism against the increase in ROS production from senescent skin cells, due to a decline in complex II function.

Melatonin is a hormone predominantly produced in the brain to regulate sleep, and its metabolism relies heavily on mitochondria and ROS signalling (Slominski et al., 2017). It exhibits antioxidant effects and can inhibit melanogenesis in animal models at high concentrations, which can help modulate coat colour (Slominski and Pruski, 1993). Studies observing changes in human skin pigmentation with intake of oral melatonin found no effects

over a 30-day period in patients with hyperpigmentation of varying causes (Nordlund and Lerner, 1977), melanoma patients or a control group (McElhinney et al., 1994). However, melatonin and its metabolites have been detected in human skin in vivo, and all were found to inhibit melanocyte proliferation and tyrosinase activity in vitro (Kim et al., 2015). All the above suggests that mitochondrial function is a modulator of skin pigmentation, and dysfunction could interfere with melanin production both directly and indirectly through excessive ROS signalling and melatonin production.

1.3.3 Pigmentation

Melanin pigment is formed in response to oxidation reactions in melanocytes. Pheomelanin is the yellow-red pigment associated with red hair and freckles and eumelanin which is more prevalent in dark haired individuals, the ratio of these is regulated by the melanocortin 1 receptor (MC1R) gene which has been previously reviewed (Denat et al., 2014). Pheomelanin has been shown to have higher pro-oxidant effects on cells as it sequesters cysteine and glutathione antioxidant during synthesis, and loss-of-function in MC1R results in an inability to produce eumelanin in response to α-melanocyte-stimulating-hormone (α-MSH), the process of which produces some antioxidant properties (Song et al., 2009b). In terms of skin ageing, loss of MC1R function has been linked to increased perceived age by an average of two years and heterozygous variants with only a reduced MC1R function was associated with an increased perceived age of one year on average (Liu et al., 2016). In humans, a six-fold increase in photoageing was observed in those with homozygous loss of MC1R gene variants compared to wild type (Elfakir et al., 2010). It was suggested that this could be due to either the oxidative effects of pheomelanin production or changes to fibroblast function in the absence of MC1R activity (Liu et al., 2016). In relation to mitochondrial function, melanocytes pre-treated with α-MSH have been shown to have a protective effect on mtDNA copy number in response to UVB light. This could infer that stimulation of eumelanin rather than pheomelanin could have photo-protective properties; however, no quantification of pheomelanin/eumelanin was performed (Böhm and Hill, 2016). Links between mitochondrial function, mtDNA and pheomelanin/eumelanin ratio have not yet been formally researched, which could provide an insight into the mechanisms involved in skin ageing though oxidative stress.

In addition to the pro-oxidative effects of pheomelanin synthesis, the process of photo-degradation of melanin is also a pro-oxidant process as it results in singlet oxygen production (Żądło et al., 2020), and UVA irradiation of pheomelanin exhibited conformational changes in

catalase antioxidant which was attenuated with a singlet oxygen quencher (Maresca et al., 2006). This suggests that photo-degradation of melanin could also be an important inducer of the oxidative stress and mtDNA damage exhibited in photo-exposed skin.

Uneven pigmentation is one of the hallmarks of skin ageing. Mitochondria have even been associated with the biosynthesis of melanin in melanocytes, required to create pigmentation in response to UVR. Prohibitin proteins found localised in the inner mitochondrial membrane were found to bind directly to melanogenin, a synthetic pigmentation promotor. Prohibitin silencing directly interferes with melanogenin activity and is thought to be involved in the regulation of the rate limiting melanin enzyme tyrosinase (Snyder et al., 2005). In addition to this, mitochondria in melanocytes have been shown to interact with melanosomes, suggesting a functional role in melanosome biogenesis and therefore melanin production (Daniele et al., 2014).

Portions of this on skin ageing section have been previously published (Stout and Birch-Machin, 2019).

1.4 Oxidative stress, ageing healthspan and lifespan

The free radical theory of ageing hypothesises that oxidative stress is a leading cause of both intrinsic and extrinsic skin ageing (Harman, 1956). The mitochondrial theory of ageing proposes damage to the mitochondria from endogenous and exogenous stressors causes damage to mtDNA. This accumulates over time, causing OXPHOS dysfunction, increased ROS production and more mtDNA damage in a cycle of stress and oxidative damage (Kowald, 2001, Ziada et al., 2020). Mitochondrial decline has been documented in skin ageing and exacerbated by exogenous stress, this could be a result of the central role mitochondria plays in ROS production (Sreedhar et al., 2020). How the free radical and mitochondrial theory of ageing expands to overall ageing health and lifespan is still lacking conclusive evidence (Sanz and Stefanatos, 2008, Sanz et al., 2006). The theory is difficult to prove in humans due to the length of lifespan, cell culture experiments are prone to confounding factors, and models in animals and organisms with shorter lifespans do not replicate the metabolism of humans (Gruber et al., 2008). However, there is some good evidence for the free radical theory in ageing health, if not ageing lifespan.

Caenorhabditis elegans (C. elegans) nematodes provide a good basic model to study ROS and lifespan factors due to their fully mapped genome, availability of mutant variants and short lifespan (~20-80 days). Schaar et al. (2015) provide evidence for the differential effects of

cytoplasmic and mitochondrial ROS on the lifespan of *clk-1* mutated *C. elegans*; the *clk-1* mutation results in an increase in ROS production due to altered synthesis in coenzyme Q and reduced ETC function. *Clk-1* variants have increased basal antioxidant gene transcription compared to wild-type and show increased lifespan after chronic exposure to 4mM paraquat-induced oxidative stress when compared to wild-type. Combined *clk-1* mutation and mutations of superoxide dismutases of the cytoplasm (*sod-1* or *sod-5*) or mitochondria (*sod-2* or *sod-3*) can achieve increased superoxide in specific cellular compartments. Increased mitochondrial superoxide (*clk-1/sod-2* mut) significantly increased lifespan, a result which was also seen in two separate *sod-2* single mutant variants (gk257 and ok1030) (Van Raamsdonk and Hekimi, 2009); whereas increased cytoplasmic superoxide (*clk-1/sod-1* and *clk-1/sod-5* mut) significantly decreased lifespan which was not seen in *sod-1* and *sod-5* single mutant variants (Van Raamsdonk and Hekimi, 2009). This research demonstrated the opposing effects of mitochondrial and cytoplasmic superoxide, but was unable to quantify initial ROS differences in each compartment. Compared to wild-type, *clk-1* variants have greater basal *sod-1* transcription than *sod-2*, and isolated mitochondria from *clk-1* variants had no change in mitochondrial superoxide but a significant increase in overall ROS (Yang and Hekimi, 2010). This could be evidence of high cytoplasmic stress or could be indicative of the difficulties in mROS measurements, as superoxide can be readily dismutated to H_2O_2 and transported to the cytoplasm (Bienert and Chaumont, 2014). Nematode models have been integral in exploring the involvement of ROS production in overall health and lifespan, and this study is a prime example of the difference ROS species and location can make in a particular model. It also highlights the difficulty in determining relative ROS levels and the balance at which ROS is beneficial, making the true impact of ROS on lifespan and health difficult to extrapolate.

Mice studies provide a more complex model than nematodes for investigating lifespan in response to oxidative stress, however mice have a relatively short life of 12-18 months (in comparison to humans) and can be maintained in controlled conditions making them a suitable model for lifespan studies. Oxidative damage to nDNA and mtDNA has been found to accumulate in different tissues with increasing age in mice. This may not be due to a reduced ability to repair oxidative DNA damage as it has been shown that DNA damage is removed in mice in response to radiation (Hamilton Michelle et al., 2001). However, the older mice were still more susceptible to damage from acute radiation than younger mice. $SOD1^{-/-}$ (cytoplasmic) null mice can be used to model increased cytoplasmic superoxide, as with *C. elegans* models. These variants have been found to have a decrease in lifespan that can be recovered with dietary

restriction (Zhang et al., 2017), an established method of oxidative damage reduction (Walsh et al., 2014). Further studies with $SOD1^{-/-}$ mice have found premature aging phenotypes, including hearing loss, macular degeneration, cataracts, thinning skin and bone fragility (Hamilton et al., 2012, Keithley et al., 2005, Muller et al., 2006). Taken together, this suggests that mice with increased cytoplasmic stress age prematurely and subsequently have a reduced lifespan. SOD2 (mitochondrial) homozygous knockout is embryonically lethal in mice, and heterozygous SOD2 knockdown mice exhibit premature mitochondrial decline and apoptosis (Kokoszka Jason et al., 2001, Liang and Patel, 2004). Overexpression of SOD2 was found to have no effect on lifespan, however it resulted in lower oxidative damage (protein carbonyls) with no age dependent increase in lipid peroxidation in the muscle (Jang et al., 2009). Finally, lifespan was increased by 4.5 months in male and female mice by increased mitochondrial catalase activity (Schriner Samuel et al., 2005). This contrasted with a non-significant increase in lifespan when the catalase was increased in the nucleus, and a 3.5 month when in peroxisomes. Taken together, loss of mitochondrial superoxide is more detrimental than cytoplasmic in mice. However, it is the expression of catalase in the mitochondria that is linked to lifespan, suggesting the reduction of mitochondrial superoxide is not enough to improve lifespan, and the removal of H_2O_2 could be key in reducing oxidative stress induced cellular decline. However, overexpression of antioxidants have mixed effects, and lifespan is not always affected (Pérez et al., 2009). The differing results could be due to mice species, location of antioxidant or due to maximal age of mice without an exogenous stressor. Evidence for the effect of oxidative stress on lifespan and healthspan in mice is prevalent, and these studies propose a critical role of oxidative stress in ageing.

While increase in antioxidant levels have limited effect on lifespan, reduction of antioxidants and therefore increased oxidative stress is linked to ageing phenotypes. Other ageing mice models include the POLG mutator mice, which induces mitochondrial deletions and dysfunction, and causes increased oxidative damage to skeletal muscle (Kolesar et al., 2014). Using dietary restriction as a model for reduced oxidative stress, Forni et al. (2017) found increased mitochondrial function in the dermis of POLG mutator mice, in addition to fur remodelling. In terms of skin ageing, this suggests a rejuvenation of the skin by preventing skin thinning and hair loss indicative of chronological ageing.

There is some contention in the field surrounding the impact of mitochondrial ROS on ageing, health, and lifespan. ROS can be beneficial or detrimental to lifespan depending on model organism, but also within model species. The main issues surrounding ROS in research is the

dual purpose and effect of crucial signalling and reactivity. The dynamic nature of ROS and their sources makes it difficult to balance pro- and anti-oxidative effects in experimental models. The key question here is: how much ROS is too much? A question which cannot be generalised to the whole body, as it plays cell, tissue, and organ dependant roles.

1.5 Primary mitochondrial disease

1.5.1 Background

Mitochondrial diseases are complex disorders due to pathogenic variants of either mtDNA or nDNA, with a minimum prevalence of 1 in 4,300 (Gorman et al., 2015). In primary mitochondrial disease these variants are germline, and directly affect either mtDNA or nDNA genes encoding ETC proteins or tRNAs, or interfere with OXPHOS function through the formation of mtDNA deletions. Multiple mtDNA deletions arise from defects in nuclear encoded genes of mitochondrial maintenance, and the precise mechanism of formation is dependent on the affected gene.(Niyazov et al., 2016). *POLG* and *Twink* are specifically involved in mtDNA replication, *POLG* encodes the catalytic subunit of polymerase γ (defects in *POLG2* accessory subunit can also induce mtDNA deletions) and *Twink* encodes the mtDNA helicase. Dysfunction in either of these genes leads to incorrect replication and therefore deletions and/or depletion of mtDNA (Rahman and Copeland, 2019). Other genes involved in dysfunctional mtDNA maintenance include those which affect dNTP metabolism, such as: *RRM2B, TYMP, SLC25A4, DGUOK* (Rahman and Copeland, 2019). Defects in such genes can decrease the nucleotide pool during mtDNA replication and repair. Additionally, genes involved in mitochondrial dynamics can induce the formation of mtDNA deletions. For example, *OPA1* is involved in mitochondrial fusion, though also plays a role in TFAM binding and mtDNA transcription, leading to mtDNA deletions or depletion when dysfunctional (Yang et al., 2020). While multiple deletions are from nuclear origin, single large-scale deletions can vary in size from 1.3-10kb (Rocha et al., 2018), and those involved in PMD are typically thought to occur through a replication error during embryogenesis (Jeppesen et al., 2020). Pathogenesis of large-scale deletions occurs through the loss of genes in the mtDNA due to the deletion.

Secondary mitochondrial dysfunction (SMD) can indirectly disrupt mitochondrial bioenergetics through germline variants in non-OXPHOS genes, or as a result of mtDNA damage due to ageing or mitotoxic drugs (Anna and Adam, 2013). Although the onset of PMD

can occur at any age, paediatric cases tend to be more severe with greater consequences as growth and development can be disrupted (Cao et al., 2018).

PMDs can be inherited maternally, through mtDNA, or Mendelian, in nDNA; variants can also be sporadic. Despite the genetic inheritance, diagnosis of PMD is complex. Families with nuclear encoded defects can be easier to identify as it can be traced through multiple generations. However, recessive defects can remain undetected for generations and certain dominant defects can have a subtle onset. The inheritance and distribution of mtDNA variants is further complicated by the level of mtDNA heteroplasmy from parent to offspring, which can vary greatly. This can be explained by a 'bottleneck effect' during pre-natal oogenesis, believed to exist to specify the selection of mitochondria passed on to the next generation, although the precise mechanisms have not yet been identified (Marlow, 2017). This has been debated, and although it is generally considered a bottleneck occurs, there is more evidence that it affects post- natal maturation as opposed to primary oocyte formation (Cao et al., 2009). Regardless, it is agreed that mtDNA undergo segregation and subsequent clonal expansion which results in varied mutational load in offspring. Low levels of heteroplasmy in the oocyte during conception could result in low heteroplasmy at birth in a mother with high heteroplasmy and prominent symptoms, or vice versa. After birth, it is hypothesised that mature oocytes experience random genetic drift and are susceptible to increased mutational load over time. For example, the common 4977 bp deletion in mtDNA has an age-dependant increase in mutational load in parallel with decreasing mtDNA copy number (Chan et al., 2005, Keefe et al., 1995, Zabihi Diba et al., 2016, Zheng et al., 2012), further influencing the transmission of mtDNA and making it difficult to construct models to investigate this phenomenon.

Disease severity does not always reflect the scale of DNA damage, and symptoms can be vague or present as other multi-factorial diseases, often impeding recognition of mitochondrial dysfunction as the source. For example, Leber's hereditary optic neuropathy (LHON), commonly caused by mtDNA pathogenic variants at nucleotide positions 3460, 1178 or 14484 affecting NADH dehydrogenase sub-units, most often results in painless bilateral vision loss (Meyerson et al., 2015). In contrast, a point variant at nucleotide position 3243 is known to exhibit phenotypic heterogeneity including Mitochondrial Encephalopathy, Lactic Acidosis and Stroke- like episodes (MELAS), and Maternally Inherited Diabetes mellitus and Deafness (MIDD) (Naing et al., 2014, Zhang et al., 2015). These are both very different syndromes resulting from the same variant, which also brings into question whether there are nuclear modifiers contributing the phenotypes (Pickett et al., 2018).

Typically, 60-80% heterogeneity of mtDNA variants is considered the threshold in which tissues can harbour variants before resulting in disease phenotype, this can vary between tissues, individuals and variant (Craven et al., 2017). This is not always the case, as there can often be no relationship between mutation load and phenotype, and asymptomatic members of MD patients can have higher heteroplasmy (Wong, 2007).

1.5.2 PMD links to skin and ageing

Only one study so far has attempted to assess premature ageing skin in PMD. Quantification of skin thickness, collagen synthesis and re-epithelialisation rate were assessed in 28 patients harbouring the mt.3243A>G pathogenic variant, with no significant findings compared to controls (Karvonen et al., 1999). However, in this study there were no details of age matched controls nor were subjects controlled for age in the comparison. Vitiligo was observed in three of the unrelated patients (11%), as opposed to a population prevalence of <2% (Zhang et al., 2016). While this is a crude estimation of vitiligo in patients with this variant, it could suggest defective melanin production in these patients, which as a by-product would increase their susceptibility to UVR damage. Retinal pigment epithelial cells derived from induced pluripotent stem cell clones of dermal fibroblasts with m.3243A>G variant, have ultrastructural changes to both the mitochondria and melanosomes in cells with 50-70% heteroplasmy (Chichagova et al., 2017). This is an interesting observation, and while this could affect the pigment within these cells, there is little information on how this could link back to the skin.

Hutchinson-Gilford progeria syndrome (HGPS) is a rare premature ageing disorder, caused by a sporadic mutation in the LMNA gene which results in expression of the mutated form of lamin A, progerin, causing altered nuclear membrane (Gonzalo et al., 2017). HGPS patient fibroblasts demonstrate severe mitochondrial dysfunction (Rivera-Torres et al., 2013), and treatment with methylene blue recovers nuclear instability associated with HGPS (Xiong et al., 2016). Methylene blue is an electron donor and acceptor in mitochondria OXPHOS which both stimulates respiration and provides antioxidant properties. This research suggests that mitochondrial dysfunction has a key role in the premature skin ageing phenotype associated with this disease.

Several PMDs do have symptoms analogous to premature ageing, particularly with the early onset of Alzheimer's disease (Hutchin et al., 1997), parkinsonism (Siciliano et al., 2001), muscle weakness, vision loss (Schrier and Falk, 2011) and deafness (Kokotas et al., 2007).

A recent comprehensive review of skin and variants affecting mtDNA found some key variants associated with premature ageing (Hussain et al. (2021). Though the variants in the review are not specific to mitochondria and also affect nuclear DNA, they result in mitochondrial dysfunction. Specifically, dysfunction to the RecQ DNA helicases causes altered DNA repair and an increased in DNA defects. Rothmund-Thomas syndrome (RECQL4 loss of function) causes hypo- and hyper-pigmentation, atrophy, and cell senescence in the skin, coupled with random mtDNA variants in the D-loop and inactivated SOD2. Patients with Werners syndrome, caused by defects in the WRN RecQ helicase, exhibit premature skin wrinkling, hair loss and hair greying, in addition to other ageing syndromes. Hussain et al. (2021) noted that WRN is not found in the mitochondria, however can be associated with the outer membrane and is linked with an increase in mitochondrial ROS. Finally, Cockayne syndrome group B protein translocates to the mitochondria under oxidative stress, and is involved in mitochondrial base excision repair. Dysfunction in Cockayne syndrome leads to a range of dermatological aberrations including photosensitivity and pigmentation. No studies have specifically characterised premature ageing or susceptibility to UVR damage in PMD patients, which could help further understand how mitochondrial dysfunction is involved in the ageing and photoageing process.

Chapter 2. Materials and Methods

2.1 Cell culture

2.1.1 Neonatal human dermal fibroblast (HDFn) cell line

Cells were cultured in high glucose Dulbecco's Modified Eagles Medium (DMEM) (Gibco, UK) supplemented with 10% foetal bovine serum (FBS) (Invitrogen, UK) and 100 $U.ml^{-1}$ Penicillin and 100 $mg.ml^{-1}$ streptomycin (P/S) (Invitrogen, UK) (complete DMEM). Cells were maintained in a humidified incubator containing 5% (v/v) CO_2 at 37˚C. Cells were passaged 2 times per week by washing once in phosphate buffered saline solution (PBS) (Lonza, UK), and dissociated with 2ml of trypsin-ethylenediaminetetra-acetic acid (TE) (Lonza, UK) for 5 mins at 37˚C. TE was neutralised by adding 8ml of complete media and split into a new T175 flask (Sarstedt, Germany).

2.1.2 Immortalised primary cell culture

Immortalised primary dermal fibroblasts were provided as a kind gift from the Mitochondrial Research group at Newcastle University. Two patient cell lines (M1096 and M1582) and two control cell lines (M1171 and M0528) from arm biopsies were cultured in high glucose DMEM supplemented with 10% FBS, 1% non-essential amino acids and P/S, and stored and passaged as per the HDFn cell line.

2.1.3 Storage

Cells were transferred to -80˚C for short term, or to liquid nitrogen for long term storage. Cells were washed once with PBS before disassociation with TE and incubated at 37 ˚C for 5 mins. TE was neutralised with complete DMEM and pelleted by centrifugation at 12000rpm for 5mins before resuspension in 1ml per half T175 flask of complete DMEM with 10% dimethyl sulfoxide (DMSO) (Fisher Scientific, UK), and transferred to a 1.6 ml cryotube vial (Sarstedt, Germany) for immediate freezing using a CoolCell (Corning, USA) at -80 ˚C. After 24 hours, vials could be transferred to liquid nitrogen for long term storage. Cells were thawed rapidly and immediately transferred to 20ml of complete DMEM and incubated at 37 ˚C at 5% (v/v) CO_2 for 24 hours before replacing the media.

2.1.4 Cell seeding

Cells were washed once in PBS and dissociated with TE and incubated at 37˚C for 5-10 mins to single cell suspension. They were counted using a haemocytometer (Gallenkamp, UK) and diluted to concentration using appropriate media, before seeding into 6-well plates with a total of 2ml media per well and incubated at 37˚C at 5% (v/v) CO_2 overnight before treatment.

2.1.5 Cell harvesting for DNA extraction

Cells were washed once in PBS and dissociated with TE and incubated at 37˚C for 5 mins. Cells were collected in 1 ml of media and centrifuged at 8000 rpm for 3 mins, washed with PBS and re-centrifuged. PBS was removed and dry pellets were stored at -20 ˚C prior to DNA extraction.

2.1.6 Cell dosing with solar simulator

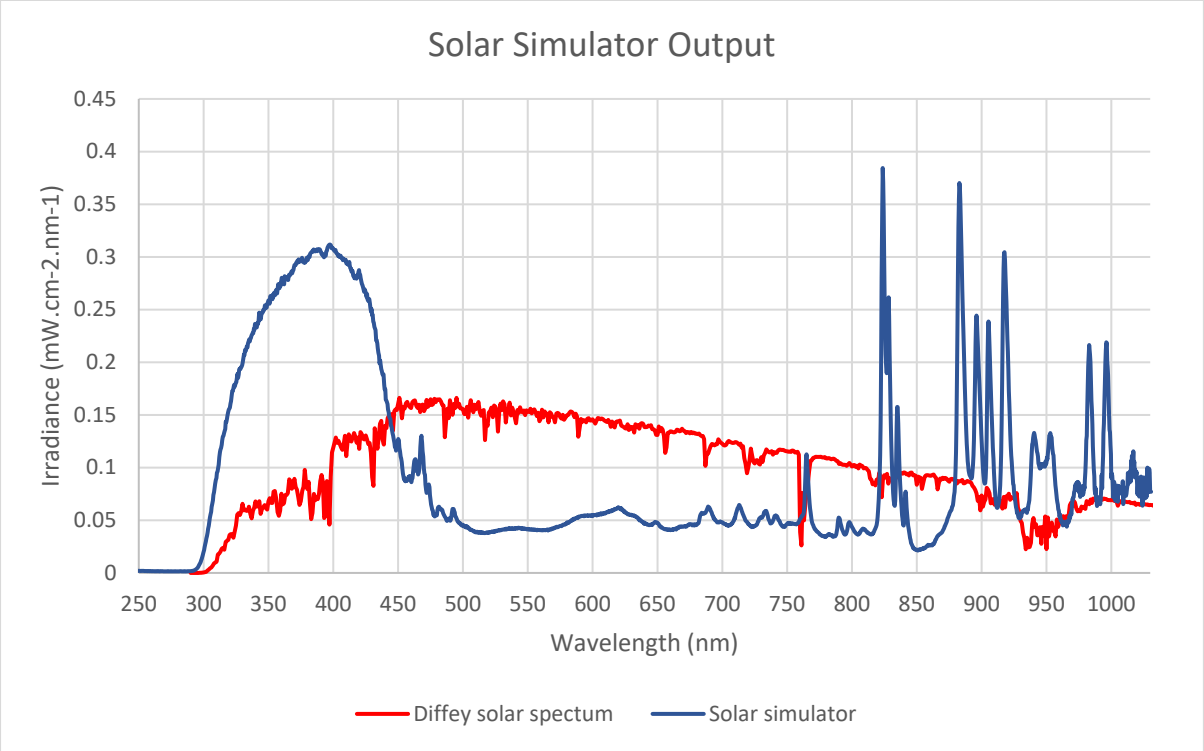

Figure 2-1. Solar spectrum from solar simulator and Diffey solar spectrum.
Diffey spectrum as calculated for 45° latitude at 12 noon in midsummer. Image made by Dr Catherine Bonn.

Total solar light was simulated using a solar simulator (Newport), which was retrofitted with an infrared heat filter by the Medical Physics department in Newcastle University making it broadly consistent with the sol-UV6 model. Spectrum of the solar simulator was measured by

Dr Catherine Bonn with the FLAME spectroradiometer (Blue line in Figure 2-1). Prior to each irradiation event, total solar light was measured using a radiometer (International Light Technologies). The meter readings in mW/cm^2 were converted into standard erythemal dose (SED) which was developed as a weighted erythemal measure of exposure equivalent to 100 $J.m^{-2}$ (Lucas et al., 2006). Equivalent SED dose was calculated using Diffey solar spectrum for equivalent time in solar sun at 45° latitude at 12 noon in midsummer (red line in Figure 2-1) (Diffey, 2015). The Diffey solar spectrum is a calculated spectrum for specific latitudes/times/dates; while this specification used to calculate equivalent time to SED is not available as a measured output, Figure 2-2 shows the solar output of the ASTM reference spectrum at 48° latitude for comparison. Media was replaced with PBS, irradiating in phenol red and FBS free media has previously been found to increase production of H_2O_2 in the media so was not used during irradiation (Yoshimoto et al., 2018).

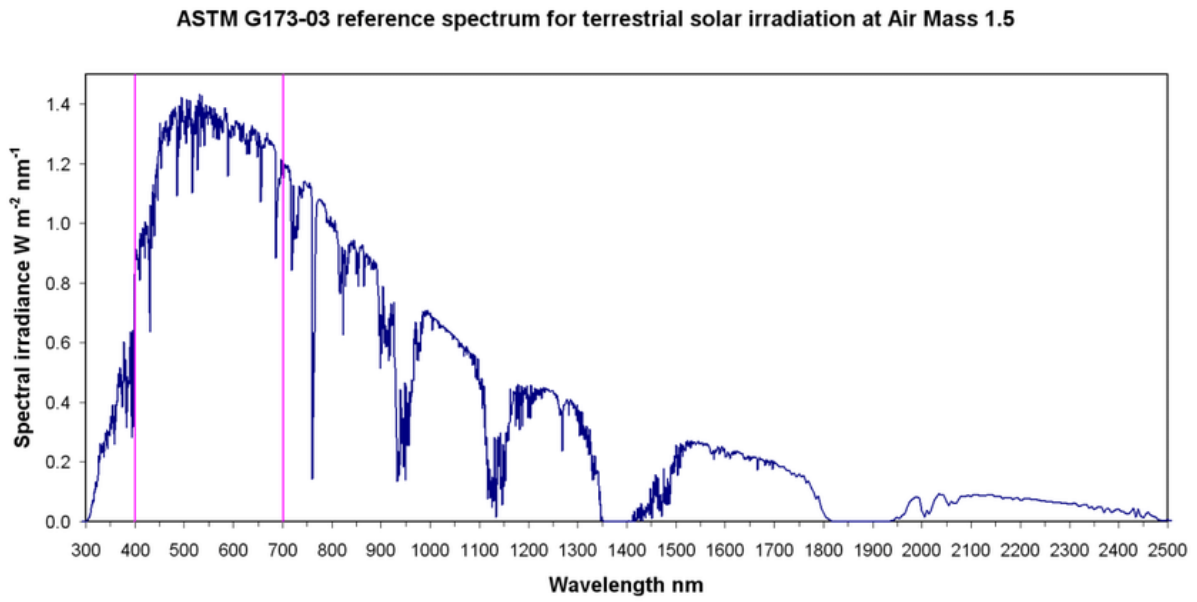

Figure 2-2. ASTM G173-03 reference spectrum for solar irradiance at sea level at 48° latitude (Pockett, 2010)

2.2 Quantitative PCR

2.2.1 MtDNA damage markers: qPCR theory

The 1 kb and 11 kb qPCR assays both work by the same principle. Each is run after the short 83 bp housekeeping amplicon and amplifies a selected region in the mitochondrial genome. Correctly amplified products have no damage to the genome that would disrupt the polymerase;

this would include double-stranded and some single-stranded breaks, and certain oxidative damage.

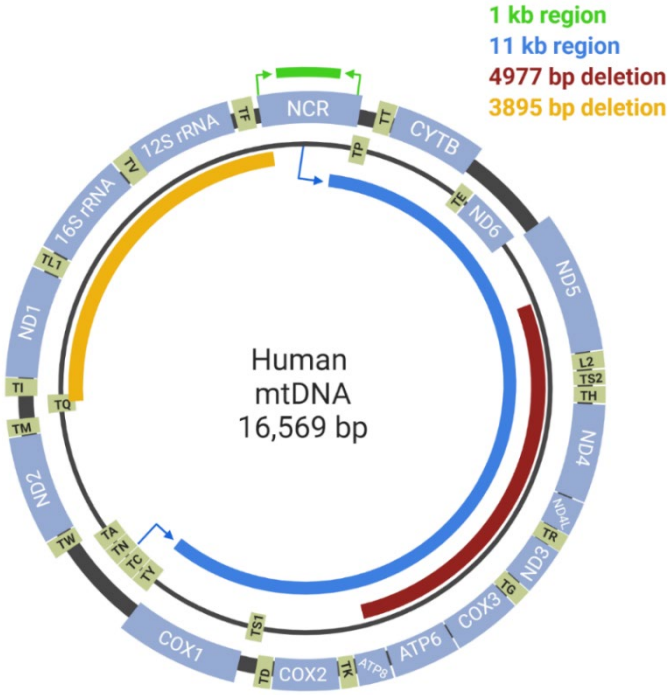

Figure 2-3. mtDNA denoting long range PCR primer regions (1 kb in green and 11 kb in blue) and 4977 bp (red) and 3895 bp (orange) deletions. Created with BioRender.com

The housekeeping amplicon is small enough to amplify the region on most of the mtDNA present in the sample and quantifies the mtDNA; DNA quantification of mtDNA by Nanodrop is imprecise as there is a much larger quantity of nDNA, though the Nanodrop is used to dilute the sample to within the linear range. The 83 bp amplifies a region in the D-loop of the non-coding region (NCR) (16,062 bp to 16,102 bp). Figure 2-3 shows the 1 kb region (green) encompasses most of the NCR from 16,040 bp to 404 bp (Full size of NCR= 16,024 to 576 bp). Both primer sets attach to the H (heavy) strand. The 11 kb region (blue) amplifies a large portion of the coding region on the L (light) strand (5781 bp to 256 bp); this incorporates 14/22 tRNAs, and 11/13 proteins (Figure 2-3). The dynamic linear range of the 11 kb PCR was previously determined as 10-50 ng of DNA (Hanna et al., 2019), 40 ng was used as it was close to the peak concentration but high enough to ensure mtDNA in the treatment groups would still be in the linear range.

The fold change was calculated by the 'Pfaffl method' using individual efficiencies of each reaction (Pfaffl, 2001). These can be calculated using a standard curve by including a serial dilution on each plate:

$$Fold\ change = \frac{E_{target}^{(sample-control)}}{E_{housekeeping}^{(sample-control)}}$$ *Equation 1. Pfaffl method*

The deletion assays use a method in which amplification will only occur if the deletion is present. When the breakpoint occurs, the ends at either side of the deletion ligate together. The primers bind to either side of this and amplify the region over the breakpoint, the TaqMan probe then binds over the breakpoint. Using a short elongation time during the qPCR cycle, the short region over the breakpoint would only amplify if the deletion is present, and the probe will only fluoresce if it attaches the new breakpoint sequence. Figure 2-3 shows the 4977bp 'common deletion' region in red and the 3895 bp 'UVR specific deletion' region in orange.

2.2.2 DNA extraction and quantification from cell pellet

DNA was extracted from whole cells using commercially available QiaAMP mini kit (Qiagen). Cell pellets were re-suspended in 200 µl PBS, 20 µl proteinase K was added and then 200 µl Buffer AL (lysis buffer) was added. Solutions were pulse vortexed for 15s, incubated for 10 mins at 56˚C on a heat block, pulse spun to remove condensation in the lid, and 200 µl of ethanol (100%) was added before pulse vortexing for 15s and a final pulse spin. The full volume was transferred to a spin column and centrifuged at 6000xg for 1 min. The collection tube was replaced, ensuring the outside of the spin column was dry to avoid contamination each time. 500 µl AW1 buffer was added to the spin column, centrifuged for 1 min at 6000xg and the collection tube was replaced. 500 µl of AW2 was then added and the column was spun at maximum speed (16,000xg) for 3 mins. Finally, the spin column was placed in a clean and sterile 1.5 ml microfuge tube and 60 µl Buffer AE was added to the column, incubated at room temperature for 5 mins and centrifuged at 6000xg for 1 min. DNA was quantified using NanoDrop 2000 (Thermo Scientific). Absorbance ratios were taken to assess DNA purification quality, and A260/280 and A260/230 ratios were considered pure at ~1.8-2 and over 2, respectively.

All subsequent quantitative polymerase chain reaction (qPCR) assays were performed using either StepOnePlus Real-Time PCR System (Applied Biosciences, UK) using StepOne Software v2.3 (Applied Biosciences, UK) to view results; or QuantStudio 3 (QS3) Real-Time PCR system (Applied Biosciences, UK) using Design and Analysis app (ThermoFisher, UK). Each master mix was assembled on ice, and reactions were performed in a MicroAmp Fast Optical 96-well reaction plate (Applied Biosciences, UK).

2.2.3 Amplification of 83 bp and 93 bp region to normalise mtDNA copy number

A small, 83 bp region of mtDNA was amplified to normalise mtDNA copy number. A 93 bp region in the B2M gene on chromosome 15 was amplified to determine nDNA copy number. PCR was performed in 20 µl reaction containing: 2 µl of each DNA sample, 400 µM of each primer, 1x SYBR® Green JumpStart™ *Taq* ReadyMix™ and 1x ROX passive reference dye (Sigma) and made up to the correct volume using UVR sterile, high grade PCR water. Primer sequences are in Table 2-1. Cycling condition were as follows: 2 min initial denaturation stage at 94°C followed by 35 cycles of 15s denaturation at 94°C, 45s annealing at 60°C and 45s extension at 72°C, and a 2 min final extension at 72°C. Melt curves were performed at the end of each reaction to assess the PCR product.

Primer	Region	Sequence
Forward IS1	mtDNA D-Loop	5'- GATTTGGGTACCACCCAAGTATTG -3'
Reverse IS2		5'- AATATTCATGGTGGCTGGCAGTA -3'
Forward B2M F2	nDNA B2M (15q)	5'- GCTGGGTAGCTCTAAACAATGTATTCA -3'
Reverse B2M R2	gene	5'- CCATGTACTAACAAATGTCTAAAATGGT -3'

Table 2-1: 83 bp mtDNA primer sequence (Koch et al., 2001) and 93 bp nDNA primer sequence (Matsuzaki et al., 2015)

2.2.4 Amplification of 1 kb region to assess mtDNA damage

A 1 kb pair region across the mtDNA D-Loop was amplified to quantify double strand breaks over the D-loop origin of heavy strand replication. The assay was optimised for the StepOnePlus and QS3 using the same run cycles, but a lower level of ROX in the master mix for the QS3 due to its higher ROX sensitivity. PCR was performed in a 20 µl reaction containing: 1x SensiFAST^{TM}SYBR kit (Bioline) Hi-ROX for StepOnePlus and Lo-ROX for QS3, 250 µM of each primer and made up to the correct volume using high grade PCR water. Primer sequences are in Table 2-2. Cycling conditions were as follows: 10 min initial denaturation stage at 95°C followed by 40 cycles of 15s denaturation at 95°C, 15s annealing at 60°C and 55s extension at 72°C, and a 7 min final extension at 72°C. Melt curves were performed at the end of each reaction to assess the PCR product.

Primer	Sequence
Forward AL4F	5'- CTGTTCTTTCATGGGGAAGC -3'
Reverse AS1R	5'- AAAGTGCATACCGCCAAAAG -3'

Table 2-2: 1kb primer sequence (Rothfuss et al., 2009).

2.2.5 Amplification of 11 kb region of mtDNA to assess mtDNA damage

A large 11 kb region of mtDNA was amplified to quantify mtDNA double stranded breaks. The whole region of DNA amplifies as a single product with a melt temperature of 84 in the absence of damage to the region, therefore the Ct value correlates with the level of mtDNA breaks which can quantify the damage occurring in mtDNA under different conditions. PCR was performed in 20 µl reaction containing: 500 µM PCR nucleotide mix (Sigma), 300 µM each primer, 0.1x SYBR® Green I nucleic acid stain from a 5x working solution (Lonza) and 1x ROX passive reference dye (Life Technologies), and made up to the correct volume using high grade PCR water. Primer sequences are in Table 2-3. Cycling conditions were as follows: 2 min initial denaturation stage at 94°C followed by 10 cycles of 15s denaturation at 94°C, 30s annealing at 60°C and 9 min extension at 72°C; then 25 cycles of 15s denaturation at 94°C, 30s annealing at 60°C and 8 min 50 sec (+10s per cycle) extension at 72°C. Melt curves were performed at the end of each reaction to assess the PCR product. The 11 kb strand break assay was previously optimised for the StepOnePlus by Rebecca Hanna (Hanna et al., 2019).

Primer	Sequence
Forward D1B	5'- ATGATGTCTGTGTGGAAAGTGGCTGTGC -3'
Reverse OLA	5'- GGGAGAAGCCCCGGCAGGTTTGAAGC -3'

Table 2-3: 11kb primer sequences (Hanna et al., 2019).

2.3 Gel electrophoresis

Gel electrophoresis was performed to confirm PCR products.

Low molecular weight products below 1000 nucleotides were ran on a 3-4% (w/v) agarose gel in 1x Tris Borate EDTA (TBE) buffer (0.1 M Tris base; 0.1 M boric acid; 2 mM EDTA). For high molecular weight products of up to 15,000 nucleotides, a gel of 0.5-0.8% (w/v) agarose in 1x Tris Acetate EDTA (TAE) buffer (40 mM Tris base; 20 mM acetic acid; 1 mM EDTA) was cast. Agarose and buffer were microwaved at full power to dissolve the agarose, and 1x GelRed nucleic acid stain (Biotium) was added before pouring. Samples were run with either a low (LMW DNA ladder, New England Biolabs) or high (GelPilot High Range ladder, Qiagen) molecular weight ladder, and samples were diluted with each ladder's corresponding dye at 1:6 dilution (LMW) or 1:5 (HMW). Electrophoresis was performed at 70 V initially while the samples migrated out the well and 100 V thereafter until the dye front had migrate far enough down the gel.

Samples were visualised using LICOR Odyssey Fc imaging system for 2 mins at 600 nm.

2.4 Cloning of positive control plasmid for skin swab qPCR analysis

Skin swab qPCR analysis (chapter 5) was carried out on multiple plates, and it was necessary to have a reliable positive control between batches. Previous methods of skin swab analysis used a ratio method of the target Ct value divided by the housekeeping Ct value, but this method produces different results depending on the starting concentration on mtDNA. For example, assuming 100% efficiency, if the target Ct is 15 and the housekeeping Ct is 17, this results in a ratio of 0.882. If the DNA is 32x more dilute, which would result in 5 Ct higher result for both the target and housekeeping, the target would now be 20 and the housekeeping 22, giving a ratio of 0.909. Interpolation from a standard curve to produce a percentage of DNA amplified was determined to be the most appropriate method of standardisation. Cell DNA of a known concentration can be subject to degradation from storage, even at -20˚C, and would be subject to natural variation between samples. Inserting a positive control region into a plasmid would provide a standard control to ensure accurate interpretation of qPCR results between batches, and plasmid DNA is stable when stored at -20˚C for over 3 years (Nguyen et al., 2018). The region of amplification for 83 bp housekeeping assay is located within the region of the 1 kb probing region on the mtDNA (Figure 2-4), therefore primers were designed to insert this PCR amplicon into a vector backbone.

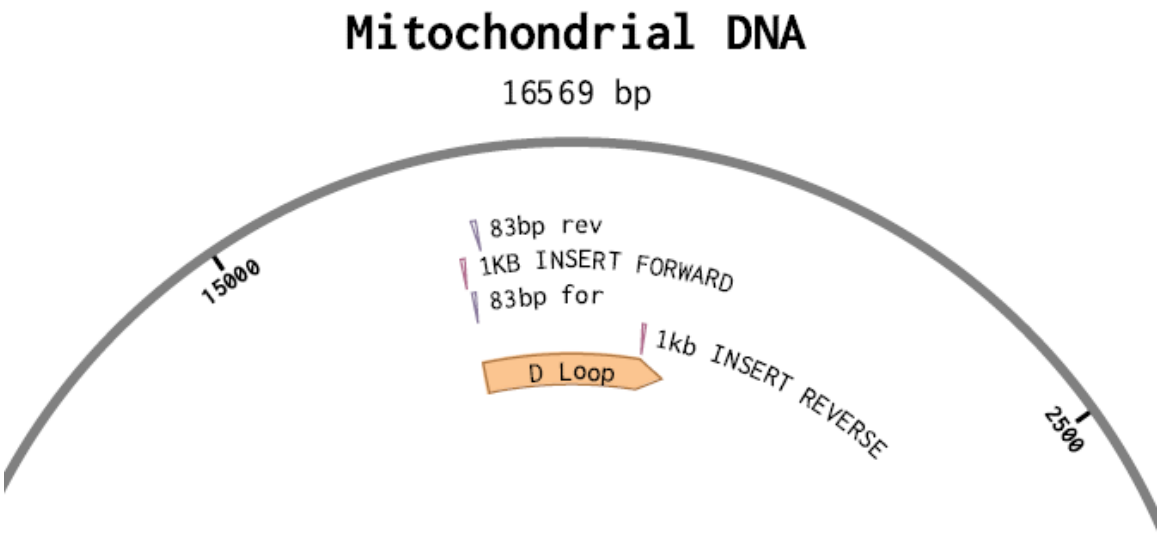

Figure 2-4. 1 kb insert and 83 bp housekeeping gene amplification region with D-loop annotated. Image taken from Benchling.com.

Primer and experimental protocol design by Roisin Stout, procedure carried out by Dr Lizzie Ruddy and Dr Gewei Zhu. The type of cloning vector did not impact the final product as it was not necessary for gene expression, a pCMV backbone (a kind gift from Magomet Aushav used in chapter 6) with ampicillin resistance was used for selection (see method 6.3.2.1 for full transformation and purification method). The 1 kb insert product was amplified using DNA obtained from HDFn cells.

Primer	Sequence
Vector Reverse	5' GCTTCCCCATGAAAGAACAGGGAGCCACCCTTCGAGTGG 3'
Vector Forward	5' CTTTTGGCGGTATGCACTTTGGGACTCCAGCCAAAGGCAG 3'
Insert Forward	5' CCACTCGAAGGGTGGCTCCCTGTTCTTTCATGGGGAAGC 3'
Insert Reverse	5' CTGCCTTTGGCTGGAGTCCCAAAGTGCATACCGCCAAAAG 3'

Table 2-4. Primer sequences for PCR amplification of cloning components.
Sequence in red corresponds with the annealing region and black region is overhang region.

Cohesion end cloning procedure was used to assemble the final product, primers were designed with overhang sequences corresponding to the complement region (Table 2-4). Prior to amplification, the primers were checked using the NEBuilder online assembly tool (nebuilder.neb.com) to confirm the final assemble product was correct. PCR was performed using a Q5 High Fidelity 2x Master Mix (New England BioLabs, USA) as per manufacturer's instructions with the final concentrations: 1x Q5 reaction buffer, 200 µM PCR nucleotide mix

(Sigma), 0.5 µM of each primer, 0.02 U/µl Q5 polymerase, and 1x GC enhancer. DNA Engine Peltier Thermal Cycler (PTC-200) using the cycle conditions in (Table 2-5).

	Insert		Vector	
	Temp (˚C)	Time	Temp (˚C)	Time
Initial Denaturation	95	03:00	98	00:30
Denaturation	98	00:10	98	00:10
Annealing	72	00:15	72	00:30
Extension	72	00:55	72	04:37
Final extension	72	02:00	72	02:00
Hold	/		4	

Table 2-5. Cycle conditions for amplification of insert and vector region.

PCR products were confirmed by gel electrophoresis with 0.8% agarose in TAE buffer. The size difference between the vector plasmid and PCR product was relatively similar and difficult to confirm by gel electrophoresis, therefore a diagnostic restriction digest was performed on the vector product using PvuI enzyme (reaction mixture (New England Biolabs): 10 µl PCR product, 1x NEB buffer, 20 units PvuI) for 1 hour at 37˚C and inhibited at 80˚C for 20 mins. Expected digestion products were determined using Benchling online research tool (benchling.com) to run the digestion simulation (Figure 2-5A). Pvu1 has 2 cut sites on the vector plasmid, creating 3 products in the linear PCR product, and only 2 products on the circular plasmid.

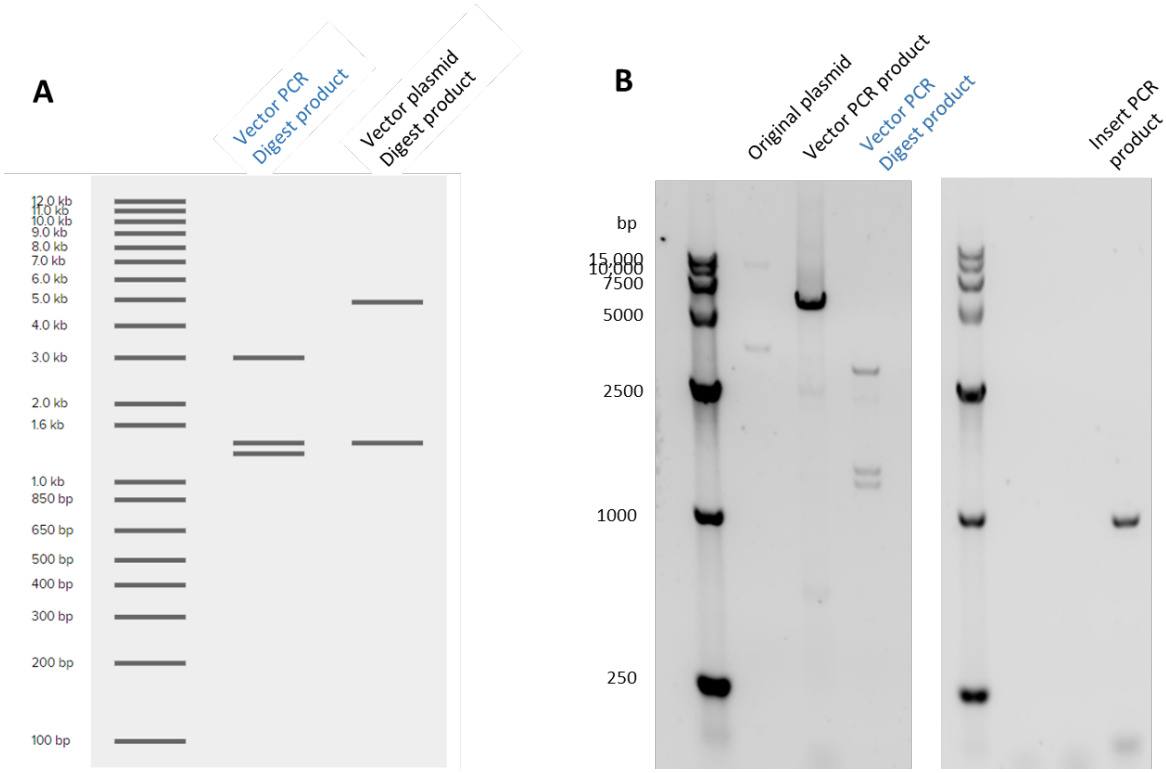

Figure 2-5. Confirmation of PCR products using gel electrophoresis
A. Simulation using Benchling online tool; lane 1 shows the expected PVUI digestion products from the 1 kb PCR product and lane 2 shows PVUI digestion on the initial vector. B. Gel electrophoresis of vector 1 kb PCR product digestion shows the PCR successfully created the required vector product and the PCR product from the insert was correct at 1 kb.

Dpn1 digestion was performed on the vector to remove any of the original plasmid DNA; Dpn1 cleaves at *E.coli* Dam methylase-methylated sites of plasmid DNA so does not cleave PCR product; this stops the original plasmid from being transformed into the competent cells. Reaction components for Dpn1 digestion (ThermoFisher) (10 µl of vector PCR product, 1x Buffer Tango, 20 units of Dpn1 in nuclease free water) were incubated for 1 hour at 37 ˚C and heat inactivated at 80 ˚C for 20 mins. PCR products were cleaned using QIAquick PCR purification kit (Qiagen, UK) spin column to remove impurities as per manufacturers' instructions. The final product concentrations were calculated using NanoDrop 3000 (ThermoFisher, UK).

Assembly of vector and 1 kb insert was carried out using NEBuilder Hifi DNA assembly cloning kit (New England BioLabs) as per manufacturer's reaction protocol. After the PCR cleanup, the final concentrations of insert and vector were 9 ng/µl and 16.2 ng/µl, respectively. The assembly reaction required 2:1 ratio of insert:vector, the total amount of fragments in picomoles was calculated by: pmols = (weight in ng)*1000/(base pairs*650 daltons). The

reaction mixture (0.06 pmols of insert; 0.03 pmols of vector; 10 µl Master Mix) was incubated at 50˚C for 15 mins and stored at -20˚C until transformation.

Post transformation and plasmid purification, the qPCR to amplify the 83 bp housekeeping and 1 kb region were performed on plasmid DNA and compared to amplification from HDFn cell DNA of concentrations 110 ng to 0.011 ng in 1:10 serial dilutions (Figure 2-6). The 83 bp assay has a similar reaction efficiency in both the plasmid (E=1.99; R^2=0.99) and cell DNA (E=1.99; R^2=0.99). The 1 kb assay had a different efficiency of 1.91 for cell DNA and 1.84 for plasmid (R^2=0.99 for both). The difference in efficiencies was minor, and using the plasmid as a control for comparison between runs was considered a more consistent method than using cell DNA as there could be batch inconsistencies in cell DNA. Efficiencies of qPCR analysis of skin swab DNA was found to be comparable to that of the plasmid at E= 1.96 for the 83 bp reaction (R^2=0.99) and E=1.93 for the 1 kb (R^2=0.99).

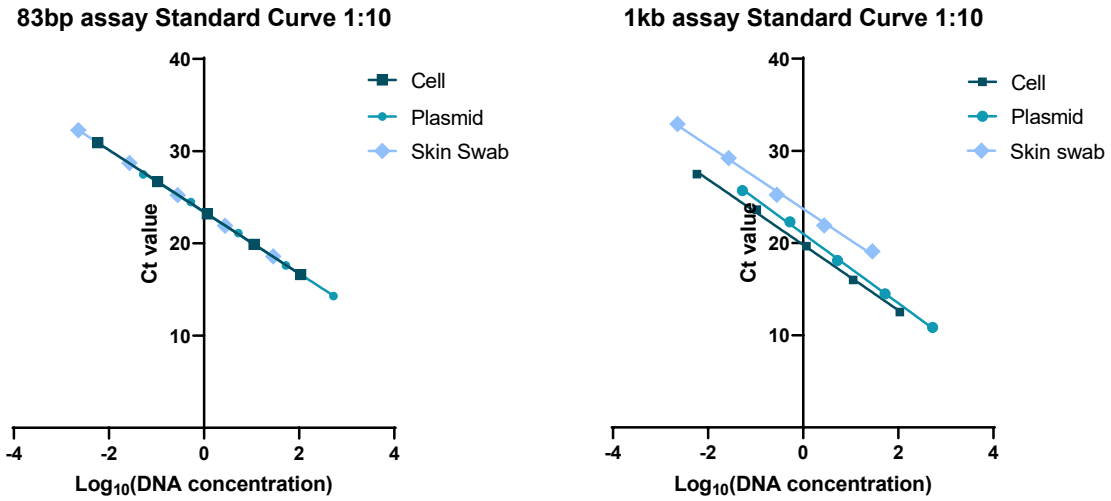

Figure 2-6. qPCR standard curve the 1 kb assay positive control plasmid.
83 bp and 1 kb amplification of plasmid dilutions compared to HDFn cell DNA of known quantity and skin swab DNA; 1:10 dilution. Linear regression used to determine primer efficiencies; n=1.

Chapter 3. Systematic Review of Facial Appearance in Primary Mitochondrial Disease

3.1 Chapter Overview

Facial appearance undergoes morphological changes with age and certain characteristics, such as fat redistribution and loss of muscle tone, develop over time and contribute to the perceived age of an individual. The methods in Chapter 5 use perceived age in combination with skin markers to determine the effect of mitochondrial dysfunction on ageing in patients with primary mitochondrial disease (PMD). This systematic review of the literature was undertaken to investigate specific facial features/characteristics reported in patients with PMD, supported by other systemic clinical features, which are characteristic of ageing. This chapter also explores the diagnostic potential of facial appearances as a non-invasive screening method for PMD.

Presenting features concerning the visual appearance of the eye area are reported in different forms of PMD. Ophthalmoplegia is characterised by the progressive paralysis of the extraocular muscle, resulting in the restriction of gaze which can occur uni- or bi-laterally and have varying directional severity. Ptosis (dropping eyelids) may present synonymously or independent of ophthalmoplegia. Ophthalmoplegia has been found to correspond with extraocular muscle atrophy irrespective of the form of PMD (Pitceathly et al., 2016), and gives rise to the nomenclature of MDs such as chronic progressive ophthalmoplegia (CPEO) and sensory ataxia neuropathy, dysarthria and ophthalmoparesis (SANDO). Compensatory adjustments to ptosis/ophthalmoplegia can present with elevation of frontalis (forehead) muscles or head tilting, which can cause it to go unnoticed by the patient for longer (Fraser et al., 2010). Extraocular symptoms have been found in a variety of mitochondrial point variants, single large-scale deletions as well as nDNA defects with multiple mtDNA deletions, and it has been reported that single large-scale mtDNA deletions resulted in the greatest severity (Yu-Wai-Man et al., 2014).

Subcutaneous fat redistribution, in combination with a loss of skin elasticity and muscle weakness, leads to ‘sagging’ characteristic of facial ageing (Coleman and Grover, 2006). Twenty eight morphological changes through various ages were described in healthy individuals by Kaur et al. (2015). Of these age-related morphological changes, three are associated with PMD; ptosis, upper eyelid muscle reduction, and transverse forehead lines, of which all increased in severity with age. However, facial muscle weakness with PMD can reduce the ability to move the muscles required for transverse forehead wrinkles. Ptosis was

either absent or minimal in all subjects aged 30-40 years, 74% had marked ptosis at 40-50 years, and prominent ptosis was found in 74% of patients aged 50-60 years which increased to 96% at 60+ years. A similar pattern, whereby severity increased with age, was evident in the presentation of eyelid muscle reduction. Transverse forehead lines are not explicitly a feature in PMD in isolation, however, their presence can indicate an over-activity of the frontalis muscle to compensate for ptosis (Ezure and Amano, 2010). Ptosis and reduced eyelid muscle function can restrict a patient's ability to see as the eyelid can cover the pupil so can be clinically significant. However, the other 25 morphological ageing features as described by Kaur et al. (2015) are superficial without any clinical implications for a patient, and therefore are unlikely to be reported in the context of PMD. Ophthalmoplegia has not been associated with ageing without co-morbidities; progressive symptoms are a hallmark of mitochondrial disease, usually preceded by ptosis.

Features involving facial muscles are less commonly described in PMD cases. Case reports note severe cases with visual facial weakness and electromyography (EMG) testing sometimes includes facial muscles, but there is no specific research into this feature. Weakness of the facial muscles is often in concordance with ptosis and ophthalmoplegia, but not always (McFarland et al., 2004, Tulinius et al., 2005), and not linked to any specific DNA alterations. EMG studies have shown elderly require a higher percentage of maximal jaw muscle (masseter) and temporal muscle activity for mastication compared to young subjects, suggesting a reduced muscle function with age (Galo et al., 2007); although other factors, such as tooth loss and swallowing difficulties may also interfere with eating in elderly. Less than 25% of orofacial muscle (i.e., the tongue and muscles responsible for movement of the mouth and lips) function is required for speech (Solomon et al., 2017), thus a significant loss of function would be required to affect articulation (dysphagia) and only a 40% reduction in bite force was found when comparing participants aged 23-30 years to those aged 60-75 years. Nevertheless, dysphasia can be indicators of facial muscle weakness (Ekberg et al., 2002). While ageing can result in muscle weakness, subsequent loss of tissue and skin thinning in the face during ageing results in greater muscle pull, which can cause increased facial expression (Swift et al., 2021). Premature facial muscle weakness as a result of PMD could cause reduced facial movement, and as a result, reduce wrinkle formation with age.

It is evident that while PMD has some overlapping facial characteristics, symptom presentation is disease specific. Therefore, a combination of these symptoms could be a valuable non-invasive diagnostic tool if fully characterised.

3.2 Chapter aims

To explore the current literature for information on facial appearance and ageing in mitochondrial dysfunction.

- Investigate the link between specific mitochondrial variants and facial appearance, perceived age, and skin ageing
- Determine any prospective diagnostic capabilities of facial appearance in primary mitochondrial disease.

3.3 Chapter specific methods

3.3.1 Literature search strategy

Search criteria was developed and peer reviewed with an experienced librarian prior to execution. Three databases were searched (MedLine, Embase and Scopus) from inception until 16 April 2019 with no restrictions imposed. The search strategy used across databases were translated as closely as possible; a variety of keyword and subject heading terms were included depending upon the thesaurus terms available in each database. See 1.3.2 for search terms used. Backward citation searching was performed; bibliographies of included articles were hand searched for additional articles. Meeting abstracts and non-English articles were not included. Articles were imported using EndNote for de-duplicating and screening. Duplicates of included articles were excluded, multiple articles containing the same patients were assessed and any additional data that met the eligibility criteria was collated. Full details of the process are described in the PRISMA diagram (Figure 3-1).

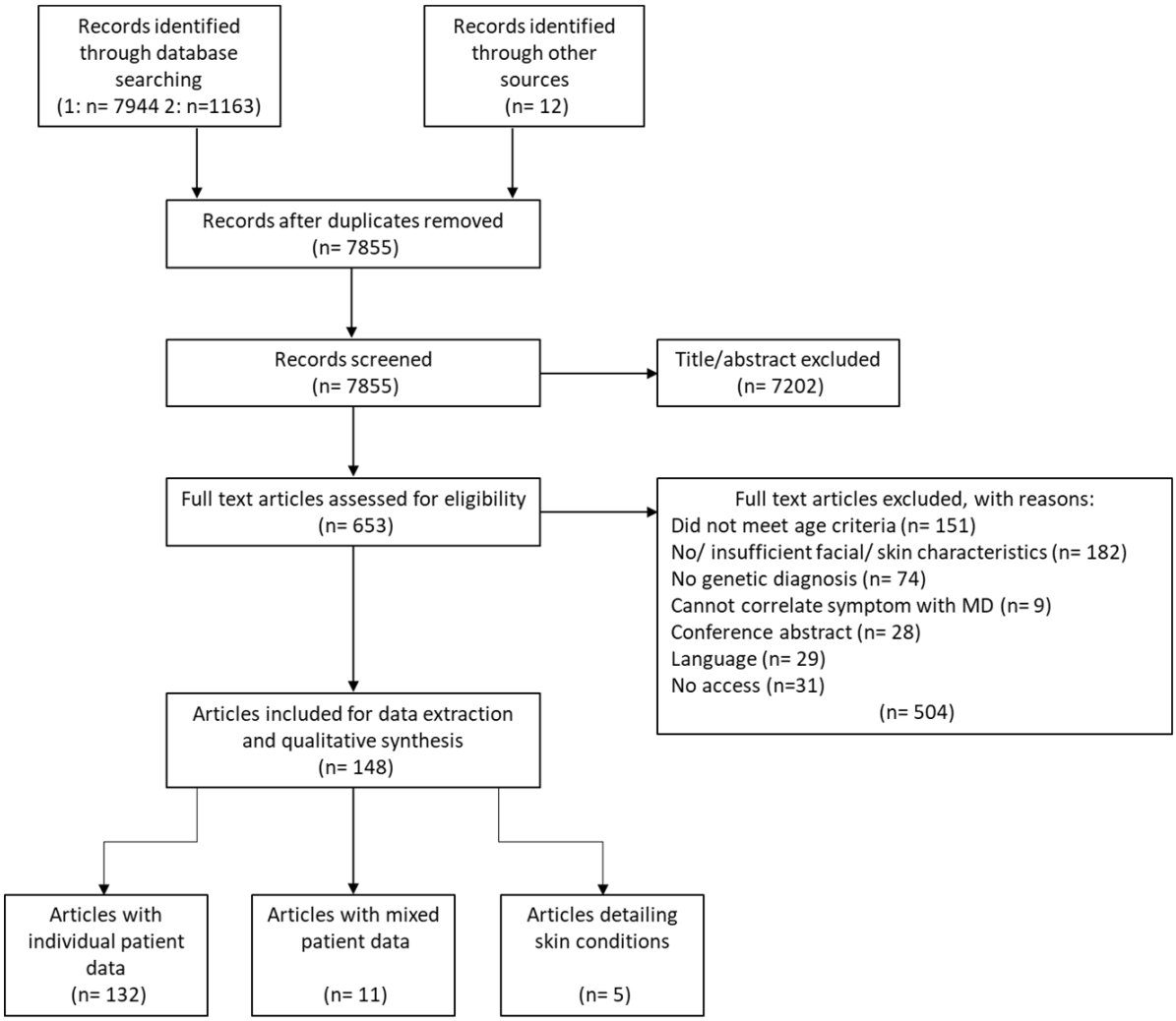

Figure 3-1. PRISMA diagram of searched articles.
Abbreviations: MD, mitochondrial disease

3.3.2 Search terms

3.3.2.1 MedLine

[DNA, Mitochondrial/ AND exp Mitochondrial diseases/ AND (Face/ OR exp Skin/ OR exp Capillaries/ OR infrared rays/ OR sunlight/ OR ultraviolet rays/ OR exp Aging/ OR Physical Appearance, Body/) NOT exp Neoplasms/] limit to humans

3.3.2.2 Embase

[mitochondrial DNA/ AND "disorders of mitochondrial functions"/ AND (exp face/ OR face malformation/ OR exp skin/ OR exp capillary/ OR exp ultraviolet radiation/ OR exp aging/ OR exp clinical feature/ OR physical appearance/) NOT exp malignant neoplasm/] limit to humans

3.3.2.3 Scopus

TITLE-ABS-KEY (("mitochondrial disease*" AND "mitochondrial dysfunction") AND mtDNA AND (face* OR facial OR uv OR ultraviolet OR sun OR capillar* OR ageing OR aging OR age OR appearance* OR morphology OR characteristic* OR skin*) AND NOT (neoplasm OR cancer OR carcinoma OR mice OR mouse OR zebrafish OR pig eon OR animals))

3.3.3 Eligibility criteria

3.3.3.1 Inclusion

Original articles which detailed the presence or absence of any reported facial characteristic in adults with a genetically diagnosed primary mitochondrial disease were eligible for inclusion. Articles were eligible where patients presented with symptoms at ≥ 16 years old. Articles were considered for inclusion if the patient had a history of vague symptoms, such as exercise intolerance and muscle weakness before aged 16 years, provided that the patient had a genetically confirmed diagnosis. Studies which detailed skin conditions, premature ageing or altered fat distribution were also included, provided they could be attributed to the PMD.

3.3.3.2 Exclusion

Articles were excluded if patients had secondary mitochondrial disease triggered by drug therapy or another condition, or had mitochondrial dysfunction as a natural by-product of

ageing. Case reports in which the symptoms could not be correlated to disease, or where there was insufficient data to distinguish individual features of patients were not included. Papers were excluded whereby a clear phenotype could not be attributed to the genotype. Conference abstracts, unpublished reports and abstracts where the full paper was unavailable were also excluded, however every effort to gain access was first attempted

Studies involving large cohorts were assessed independently from case reports. Studies were permitted which did not distinguish between highly frequent clinical features of mitochondrial disease- ptosis and ophthalmoplegia. Cases were critically appraised using the Joanna Briggs critical appraisal tools checklists.

3.3.4 Statistical analysis

There was limited data for statistical tests from this review, data was assessed by Dr Alasdair Blain using the Kruskal-Wallis test to determine differences between the variant groups.

3.4 **Results**

3.4.1 Cohort studies

Seven retrospective cohort studies met the eligibility criteria. Of these, four were carried out in an Italian population either through the 'nation-wide Italian collaborative network of mitochondrial disease' by Mancuso et al.(Mancuso et al., 2014, Mancuso et al., 2015, Mancuso et al., 2013) or University of Milan by Sciacco et al. (Sciacco et al., 2001); six of these were carried out in Europe (Dvorakova et al., 2016, De Laat et al., 2012, Garone et al., 2011), with only one study on single largescale deletions in centres in Japan (Yamashita et al., 2008). Results were collated into mtDNA point variants or deletions, and then further categorised into m.3243A>G, m.8344A>G, single large-scale deletion, and multiple deletions/ nuclear defects. Full list of studies and clinical symptoms is detailed in Table 3-1.

mtDNA point variants had the lowest prevalence of ophthalmoplegia and/or ptosis, with 35.2% of 264 cases with m.3243A>G and 29.4% of 34 cases with m.8344A>G presenting. Multiple deletions/ nuclear defects had a greater prevalence at 72.5% of 51 cases, and single large-scale deletions had the highest prevalence with 96.8% of 412 total cases. The m.3243A>G cases were a combination of 5 individual studies between which there was little variation in prevalence of between 20.0% and 45.1%; the study with the lowest number of cases had only 15 patients and three of the studies had cases between with a prevalence of between 44.1% and 45.1%. The three studies that detailed single large-scale deletions had only 7% variation in

reported prevalence, between 93 and 100%. Age was reported differently in each cohort, the m.3243A>G studies reported the highest maximum ages (77 and 78 years old), though more were reported as a range with no median to gauge the spread, nor was the age of onset reported. Sex was unreported in 5/10 studies, though more female patients were included in those reported.

Group	mtDNA point variants							Multiple deletions/ nuclear defects	Single large-scale deletion			
	(m.3243 A>G)						(m.8344 A>G)					
Author (year)	**De Laat et al. (2012)**	**Mancuso et al. (2014)**	**(Dvorakova et al., 2016)**	**Sciacco et al. (2001)**	**Sciacco et al. (2001)**	**Total**	**(Mancuso et al., 2013)**	**Sciacco et al. (2001)**	**Sciacco et al. (2001)**	**(Mancuso et al., 2015)**	**(Yamashita et al., 2008)**	**Total**
Demogr	**Netherlands**	**Italy**	**Czech Republic**	**Italy**	**Italy**		**Italy**	**Italy**	**Italy**	**Italy**	**Japan**	
Patients (n)	71	126	34	18	15	264	34	51	57	228	127	412
Sex (M/F)	25/ 46	65/ 61	7/26				22/ 20			90/ 144		
Age range (years)	34-55 (IQR)	1-77	17-78	10-59	11-55		45.6 average	12-65	1-52	41.3 average	0-65	
Ptosis/ Ophth	32 (45.1%)	35 (27.8%)	15 (44.1%)	8 (44.4%)	3 (20.0%)	93 (35.2%)	10 (29.4%)	37 (72.5%)	53 (93.0%)	219 (96.1%)	127 (100%)	399 (96.8%)

Table 3-1. Cohort patient features and demographics.
Percent of total shown in brackets. Demogr= demographic, ophth= ophthalmoplegia

3.4.2 Case reports

Data from 132 case reports (n= 397 patients) was extracted. Presence or absence of at least one facial feature was reported in each case report, including; ophthalmoplegia (total n=316, 79.6%), ptosis (n=295, 74.3%), facial weakness (n=93, 23.4%), nystagmus (n=17, 4.3%), muscles tremors or spasms (n=10, 2.5%), muscle tightness (n=2, 0.5%), palsy (n=2, 0.5%) and frontalis muscle over-activity (n=1, 0.3%) (Table 3-2). During data extraction, 182 studies had no/insufficient detail of facial features, therefore only 42% of reports had sufficient facial features for inclusion.

Features were assessed in 3 groups: mtDNA point variants (patient n=91), multiple mtDNA deletions/ nuclear defects (n=235), and single large-scale deletions (n=71). Each group had a similar split of males to females and a slight difference between the mean age of each group. Single large-scale deletions had 29 male patients compared to 41 females, with the lowest average age of onset (23.6 years old); point variants was split 43 males to 45 females with an average age of onset of 30.2 years; and multiple deletions/nuclear defects was exactly 50:50 and had an average age of onset of 35.6 years.

Ptosis, ophthalmoplegia and facial weakness all had significant differences between the three variant groups ($p<0.001$), and each group had a similar prevalence to that found in the cohort study analysis. Ptosis was present in 95.6% of single large-scale deletions, 81.3% of multiple mtDNA deletions/ nuclear defects, and 39.6% of mtDNA point variants. Each group had a higher percentage of cases with ophthalmoplegia, which was present in in 98.6% of single large-scale deletions, 87.7% of multiple mtDNA deletions/ nuclear defects, and 44.0% of mtDNA point variants. There was a significant correlation between the presence of ptosis and ophthalmoplegia ($R=0.61$, $p<0.001$) Of these case reports, point variants had the highest number that did not report either ptosis or ophthalmoplegia (ptosis n=17 and ophthalmoplegia n=1, 18.7% of total cases), followed by multiple mtDNA deletions/ nuclear defects (ptosis=11 and ophthalmoplegia=4, 6.4% of total cases) and single large-scale deletions only had one case that did not mention presence or absence of ptosis (1.4% of total cases).

Further details of any other feature related to the face was sparse. Tremors or spasms in the facial muscles and lipomatosis was predominantly found in point variants (8.8% of total cases for each), and nystagmus as a sign of epilepsy was similarly found in cases of multiple deletions/nuclear defects (4.7%) and point variants (6.6%). Skin features and premature ageing were only mentioned in 4 cases, skin discolouration and premature ageing were reported in

individual cases of single large-scale deletions, and two cases with point variants reported premature ageing.

	Multiple deletions/ nuclear defects	mtDNA point variants	Single large-scale mtDNA deletions	Total
Patients (n)	235	91	71	397
Age of onset (years)	35.6(±14.3)	30.2(±12.3)	23.6 (±14.7)	33.7±14.23
Sex (%)				
Male	44.7	47.2	40.8	44.2
Female	44.7	49.5	57.8	50.7
Frequency of clinical features (n) **Eyes**				
Ptosis	191 (81.3)	36 (39.6)	68 (95.8)	295 (74.3)
Ophthalmoplegia	206 (87.7)	40 (44.0)	70 (98.6)	316 (79.6)
Nystagmus	11 (4.7)	6 (6.6)	0	17 (4.3)
Facial appearance				
Tremor/spasm	2 (0.9)	8 (8.8)	0	10 (2.5)
Muscle tightness	0	2 (2.2)	0	2 (0.5)
Frontalis over-action	1 (0.4)	0	0	1 (0.3)
Muscle weakness	54 (23.0)	17 (18.7)	22 (31.0)	93 (23.4)
Palsy	0	2 (2.2)	0	2 (0.5)
Other appearance				
Premature ageing	1 (0.4)	2 (2.2)	0	3 (0.8)
Skin discolouration	0	0	1 (1.4)	1 (0.3)
Lipomatosis	0	8 (8.8)	0	8 (2.0)

Table 3-2**.** Case reports symptoms and demographics.
Frequency of symptoms in whole numbers with percent of total in brackets, age of onset mean±SD.

The heterogeneity of mtDNA variants was too large to group patients further categories for statistical analysis, however they have been further categorised in Table 3-3 (multiple mtDNA deletions/nuclear defects), Table 3-4 (mtDNA point variants) and Table 3-5 (single large-scale deletions).

Defects in genes of mtDNA replication, *POLG* and *Twink*, accounted for almost half of the nuclear defect reports (48.5% of total cases). Of the cases which reported facial features, ptosis, ophthalmoplegia and facial weakness were reported as present more frequently in *POLG* compared to *Twink* by ~10% (POLG mutations resulted in a prevalence of 92.8% ptosis; 95.5% ophthalmoplegia; 74.3% facial weakness). However, in total, facial weakness was unreported in 57.9% of POLG cases. Defects in genes affecting dNTP metabolism accounted for 24% of total nuclear defect cases, with the most reported being *RRM2B* (11.1%), followed by *TYMP* (9.8%). Defects in *RRM2B* gene reported a much higher frequency of ophthalmoplegia

compared to *TYMP* (100% compared to 43.5%), and 10% more cases presenting with ptosis (88.0 to 78.3%). Facial weakness had a similar frequency in both groups (23.1% *RRM2B* and 26.1% *TYMP*), though again this was unreported in 51.1% of cases. Other genes of mitochondrial maintenance included *OPA1* (10.2%)*, SP7* (5.5%) and *MTFMTI* (0.4%), which accounted for 16.1% of total cases. Facial weakness was not reported in any cases of *SP7* defects and was unreported in 62.5% of *OPA1* cases. *OPA1* defects reported only 50.0% of the cases were present with ophthalmoplegia, compared to 75.0% of cases which presented with ptosis. Conversely, *SP7* defects reported a higher number of cases with ophthalmoplegia compared to ptosis (84.6% to 61.5%). Multiple deletions with no genetic diagnosis accounted for 11.5% of cases and had the highest frequency of reported facial weakness at 81.8%, however it was unreported in more than half of cases (59.3%).

mtDNA point variants occurred predominantly in tRNA genes (n=69, 75.8% of total cases) compared to OXPHOS protein genes (n= 22, 24.2%). Of the cases from tRNA genes, m.3243A>G variant accounted for 25.3% of total cases (n=23), m.8344A>G variant for 14.3% (n=13), and other variants involving other tRNA genes for the remaining 36.6% (n=33). Cases with the m.3243A>G had the highest prevalence of ptosis and ophthalmoplegia (58.8% and 69.6%, respectively), but the lowest reported cases of facial weakness of 40.0% and 56.5% of cases with unreported facial weakness. Other tRNA genes had the second highest prevalence of ptosis and ophthalmoplegia (44.8% and 30.3%, respectively), but lower prevalence of facial weakness at 54.5% compared to m.8344A>G variant with 75.0%. However, facial weakness was reported in only 4 cases of m.8344A>G variant; this group had the highest percentage of unreported facial weakness cases (69.2%) and only 23.1% of cases reported either ptosis or ophthalmoplegia. Variants in genes encoding OXPHOS proteins included *ATP6, ND1-6* and *COX3*, however the individual cases for each gene were too low to comment on in detail. Of the 22 cases reported with defect in OXPHOS proteins, 55.6% reported presence of ptosis and 52.4% ophthalmoplegia. Facial weakness was only reported in 45.5% of cases and was reported as present in 60.0% percent of cases.

Single large-scale deletions had the highest reporting of facial weakness, which was reported in 72.2% of all cases (n=71), only 1 case of each ptosis and ophthalmoplegia was unreported in those which mentioned a facial feature.

Compared to the cohort studies, single large-scale deletions had a similar prevalence of ptosis/ophthalmoplegia, with cohort studies reporting presence in 96.8% of cases and case reports 95.8% for ptosis and 98.6% for ophthalmoplegia. M.3243A>G variant group had higher

presence of ptosis and ophthalmoplegia in case reports (58.8% and 69.6%) compared to cohort studies with only 35.2%. Conversely, the m.8344A>G variant group had a higher prevalence in the cohort studies (29.4%) compared to the case reports (21.3%). Finally, nuclear defects/multiple mtDNA deletions had 8.8% higher prevalence of ptosis and 15.2% higher ophthalmoplegia compared to cohort studies (72.5% cases of ptosis/ophthalmoplegia).

Multiple deletions/nuclear defects (n=235)	**Ptosis**	**Ophthalmoplegia**	**Facial Weakness**
POLG	n= 78/84;	n= 86/90	n= 29/39;
(n=90; 38.3%)	NR (n=6)	NR (n=0)	NR (n=51)
RRM2B	n= 22/25;	n= 26/26	n= 3/13;
(n=26; 11.1%)	NR (n=1)	NR (n=0)	NR (n=13)
Twink	n= 19/23;	n= 20/23;	n= 5/8;
(n =24; 10.2%)	NR (n=1)	NR (n=1)	NR (n=15)
OPA1	n= 18/24;	n= 14/24	n= 1/1;
(n=24; 10.2%)	NR (n=1)	NR (n=0)	NR (n=23)
TYMP	n= 18/23;	n= 10/23	n= 6/11;
(n=23; 9.8%)	NR (n=10)	NR (n=0)	NR (n=23)
SPG7	n= 8/13	n= 11/13	ND
(n=13; 5.5%)	NR (n=0)	NR (n=0)	NR (n=13)
Multiple deletions	n= 25/27	n= 24/27	n= 9/11
(n=27; 11.5%)	NR (n=0)	NR (n=0)	NR (n=16)
DGUOK	n= 3/3	n= 3/3	n= 2;
(n=3; 1.4%)	NR (n=0)	NR (n=0)	N/R (n=1)
TK2	n= 0/1;	n= 1/1;	n= 1/1;
(n=2; 0.9%)	NR (n=1)	NR (n=1)	NR (n=1)
MTFMT	NR (n=1)	n= 1/1	n= 1/1
(n=1; 0.4%)	NR (n=0)	NR (n=0)	NR (n=0)
SLC25A4	n= 1/1	n= 0/1	NR (n=1)
(n=1; 0.4%)	NR (n=0)	NR (n=0)	NR (n=0)
EGCF1	n= 1/1	n= 1/1	ND
(n=1; 0.4%)	NR (n=0)	NR (n=0)	N/R (n=1)

Table 3-3. Ptosis, ophthalmoplegia and facial weakness data, variant types and affected genes of multiple deletion/ nuclear defects involved in case report data.

mtDNA point variants (n=91)	Ptosis	Ophthalmoplegia	Facial Weakness
m.3243A>G (*MT-TL1*)	n= 10/17	n= 16/23	n= 4/10;
(n=23; 25.3%)	NR (n=6)	NR (n=0)	NR (n=13)
m.8344A>G (*MT-TK*)	n= 3/13	n= 3/13	n= 3/4
(n=13; 14.3%)	NR (n=0)	NR (n=0)	NR (n=9)
m.9176T>C (*MT-ATP6*)	n= 1/1	n= 1/1	ND
(n=1; 1.1%)	NR (n=0)	NR (n=0)	NR (n=1)
MT-ND5	n= 4/6	n= 3/6	n= 1/1
(n=6; 6.6%) [m.13094T>C (n=4); m.13565C>A (n=1); m.13805C>G (n=1)]	NR (n=0)	NR (n=0)	N/R (n=4)
(*MT-ND4*)	n= 2/5	n= 2/5	n= 2/4
(n=5; 5.5%) [m.11778G>A (n=4); m.11232T>C (n=1)]	NR (n=0)	NR (n=0)	NR (n=1)
(*MT-ND1*)	n= 1/2	n= 1/3	n= 1/1
(n=3; 3.3%) [m.3365T>C (n=1); m.4175G>A (n=1); m.3460G>A (n=1)]	NR (n=1)	NR (n=0)	NR (n=2)
m.9478T>C (m.*COX3*)	n= 0/2	n= 1/2	n= 1/2
(n=2; 2.2%)	NR (n=0)	NR (n=0)	NR (n=0)
m.4810G>A *(MT-ND2)*	n= 1/1	n= 1/2	n= 0/1
(n=2; 2.2%)	NR (n=1)	NR (n=0)	NR (n=1)
(MT-ND6)	n= 1/1; NR (n=1)	n= 2/2	ND
(n=2; 2.2%) [m.14459G>A (n=1); m.14484T>C (n=1)]	NR (n=1)	NR (n=0)	NR (n=2)
Other mt tRNA	n= 13/28	n= 10	n= 6/11
(n=33; 36.3%)	NR (n=5)	NR (n=0)	NR (n=22)
m.10197G>A *(MT-ND3)*	ND	ND	n=1/1
(n=1; 1.1%)	NR (n=1)	NR (n=1)	NR (n=0)

Table 3-4. Ptosis, ophthalmoplegia and facial weakness data mtDNA point variant types and affected genes involved in case report data.

	Ptosis	Ophthalmoplegia	Facial Weakness
Single large-scale mtDNA deletions (n=71 patients)	68/70	68/70	22/52
	NR (n=1)	NR (n=1)	NR (n=19)

Table 3-5. Ptosis, ophthalmoplegia and facial weakness data for single large-scale deletions in case report data.

Asymmetry could be inferred from the description of ptosis or facial weakness in some patient case reports. This was often through the description of the clinical assessment of ptosis severity (mild, moderate, or severe) on one side compared to the other, or facial feature presentation on one or both sides. Asymmetrical facial weakness or paresis was reported in a total four case reports [point variant m.8344A>G (n = 2) and in the ND3 gene region (n = 1), and a single 3.5 kb deletion (n = 1)]. 118 out of 397 cases (29.7%) specified the presence or absence of ptosis in each eye (single large-scale deletion n = 11; nuclear defects/ multiple deletions n = 78; single point variants n = 31). A total of 59 mentioned the severity in each eye, of which ptosis had asymmetrical severity in 20 cases [single large-scale deletions (n = 3/7; 42.9%); point variants (n = 9 out of 15; 60.0%); nuclear DNA defects/ multiple mtDNA deletions (n = 7/37; 18.9%)]. Of the 39 cases with symmetrical ptosis; 30 had nuclear defects/multiple mtDNA deletions, 4 had point variants, and 3 had single large-scale deletions.

In summary, patients with single large-scale mtDNA deletions most frequently had either ptosis or ophthalmoplegia. More cases with nuclear defects/multiple mtDNA deletions were included in this analysis than point variants or single large-scale deletions, though in total less than half of the total reports from the initial search reported any facial symptoms at all. A higher percentage of patients with point variants had ptosis without ophthalmoplegia, but the opposite was true for nuclear defects and single large-scale deletions. In all groups, most cases had both symptoms concurrently and ptosis significantly correlated with ophthalmoplegia. Facial weakness was reported most in single large-scale deletions, followed by nuclear defects/multiple mtDNA deletions, and then point variants. Analysis of symmetry was inconclusive as the number of cases specifying severity of each eye was too low.

3.5 **Discussion**

This is the first review of full facial appearance in mitochondrial disease, to date. The case report and case studies were categorised into variant type to assess the full extent of facial characteristics reported in the literature, as well as other symptoms which may have an impact on the overall patient phenotype.

The most reported and characterised facial features were ptosis and ophthalmoplegia, other features reported that appeared on the face included nystagmus; facial muscle weakness, tightness, spasms, tremors; facial palsy; and frontalis muscle over-action. Generalised premature ageing without further details, skin discolouration and lipomas were also reported. Case reports of patients with nuclear defects/ multiple mtDNA deletions reported a greater number of patients with at least one facial characteristic, compared to mtDNA point variants or single large-scale deletions, with most cases displaying either ptosis or ophthalmoplegia. However, of those cases single large-scale deletions reported the highest prevalence of ptosis/ ophthalmoplegia. This is in keeping with the current literature, whereby patients harbouring single large-scale deletions are shown to have the highest prevalence of ocular manifestations and nuclear defects/multiple mtDNA deletions, (Orsucci et al., 2017). Prevalence of facial weakness was similar in all groups; this did not seem to reflect the incidences of patients with either ptosis or ophthalmoplegia.

In comparison to case report data, cohort studies had a similar number of reported patients with ophthalmoplegia/ptosis in cases with single large-scale deletions and the m.8344A>G variant. Cases with the nuclear defects/ multiple mtDNA deletions and the m.3243A>G variant had lower prevalence. Disparities between data sets could either reflect selection bias or and the fact that the majority of the case study data was from the Italian Network database. Case reports which did not report ptosis or ophthalmoplegia were excluded rather than assumed as negative, which could affect the frequency of negative cases if reports do not mention an absent feature. Likewise, case reports frequently report uncommon symptoms which can skew the data from the average population, though have also provided a broader range of point variants than the cohort study data. Furthermore, surgical correction of ptosis could further complicate the reporting if absent post-surgery. Overall, the disparities between the two groups highlight a necessity for standardised reporting of features in patients, and also the deficit in data on facial appearance.

The main connection between PMD facial appearance and ageing lies in ptosis, as no other specific age-related features are reported in detail. Somatic deletions in mtDNA are

accumulated with age in both muscle and skin, and the increase in ptosis seen in ageing links with the high prevalence of ptosis in PMD patients. This could suggest an accelerated facial ageing phenotype, though there were no reports of any facial/ skin ageing in any patients. Researching facial ageing and specific mitochondrial dysfunction could provide a valuable insight into mitochondrial specific roles in ageing by assessing genotype/ phenotype correlations.

From this review, limited information is evident about facial appearance in PMD beyond ptosis and ophthalmoplegia, with little standardisation on the specific detail involved in reporting of these features within case reports. Importantly, there is some evidence of homogeneity of facial symptoms within variant groups, which could provide both diagnostic value and insight into mitochondria's role in ageing with further characterisation.

3.6 **Summary of main findings**

- Reporting of facial features in patients with PMD is inconsistent and there is a lack of specific detail
- Details of facial and skin ageing in PMD patients is not present in the literature
- There is some heterogeneity in the presence of ptosis and/or ophthalmoplegia within variant groups, but this would need further research to fully characterise.

Chapter 4. Mitochondrial Stress and Damage with Intermittent Solar Light Dosing

4.1 Chapter Overview

This chapter investigates the effect of chronic low doses and acute high doses of solar light on mtDNA damage and repair, using physiologically relevant doses to assess cumulative effects of sun exposure on mtDNA. Three media conditions were used to reflect normal growth media, induced mitochondrial OXPHOS, and reduced cell growth.

Unprotected exposure to UVB is the most effective method of producing endogenous Vitamin D, the length of exposure is dependent on skin type and area of exposed skin, with more melanin in the skin requiring greater sun exposure (Webb et al., 2018a). Standard erythemal dose (SED) is a skin type independent, weighted measurement of sun exposure equivalent to 100 Jm^{-2}, as opposed to minimal erythemal dose (MED) which is the lowest dose required to produce erythema in an individual. It is recommended that outdoor workers receive no more than 1-1.3 SED of acute exposure per day, and anything over 2 SED would be expected to cause sunburn in melano-compromised skin (ICNIRP, 2007). A regime of 1 SED per day at noon from March to September would be required to produce enough vitamin D for the entire year (Webb et al., 2018b). The daily doses used in this study are 1.08 SED, both in line with the maximum recommended daily dose of sun for melanocyte deficient skin and the amount required for adequate vitamin D production; the acute dose would be expected to cause sunburn.

Catalase is an enzyme integral in the conversion of H_2O_2 into water and oxygen, but it can be inactivated by UVR exposure (Zigman et al., 1996). A relatively small study by Rhie et al. (2001), found catalase activity from donors dropped by 50% in skin which had received 2x the MED of UVR on skin from the buttocks and had not returned to original levels by 72h. In older donors, catalase activity was increased in the epidermis and decreased in the dermis compared to young donors, and the ratio of activity in sun exposed (forearm) to non-exposed (upper inner arm) was higher in the old compared to the young skin, which suggests that catalase activity increases over time in response to chronic sun exposure and the resulting increase in ROS. Total skin mRNA expression of catalase was unchanged between the two age groups, which further indicates that this change in activity is not a result of levels of catalase. This same effect has been repeated in chronic and acute doses, and the reduced catalase activity has also been found to correlate with increased H_2O_2 (Reviewed by Afaq and Mukhtar (2001)). This data

suggests high doses of UVR could potentially produce greater amounts of ROS damage by reducing antioxidant activity, while chronic low exposure and ageing could provide a protective mechanism.

Obtaining physiologically relevant data in cell culture is challenging. Fibroblast cell culture conditions generally use a high glucose medium supplemented with 10% FBS as standard, this concentration of 25mM is much greater than what would be considered a high blood glucose level (5.5mM), and this would not substantially decrease over time as the media is generally changed regularly (McKay et al., 1983, Mitra et al., 2018). High glucose levels in blood have previously been correlated with a higher perceived age, which in terms of skin ageing is theorised to be through the induction of advanced glycation end-products leading to collagen cross-linkage or replicative senescence (Noordam et al., 2013). Cells cultured in galactose media without glucose undergo galactolysis, which has no net ATP output and forces the cells to use mitochondrial OXPHOS as an energy source, whereas cells cultured in high glucose can facilitate glycolysis as an energy source, bypassing mitochondrial machinery. Oxidative stress has been found to increase in cells cultured in galactose medium due to the increased stress on mitochondrial OXPHOS, but autophagy is also seen to increase in galactose treated cells compared to glucose as well as a reduction in lipid peroxidation, which could suggest a better cellular quality control system activated during galactose treatment (González-Casacuberta et al., 2019). In theory, high glucose cells would be expected to produce less ROS and have less initial mitochondrial damage in response to stress, but galactose medium would be expected to restore mitochondrial health to ensure OXPHOS efficiency.

The addition of 10% FBS ensures continuous replication, but in reality, a large population of fibroblasts in the skin are in a quiescent state whereby they remain in the G_0 phase of the cell cycle with the ability to enter G_1 upon stimulation (Rognoni et al., 2018). Neonatal cells are proliferative by nature, but post-natal cells switch to an extra-cellular matrix remodelling role with higher metabolic activity and reduced proliferation. Neonatal dermal fibroblasts are commonly used in research as they are easy to obtain and isolate, however reducing cell growth may provide a more suitable model, and this chapter aims to determine whether reducing cell growth impacts mitochondrial damage after exposure to the sun. However, quiescence can have differing ‘depths’ and monolayer culture conditions are unable to fully replicate the complexity of this state as cells are all exposed to the same culture conditions (reviewed by Fujimaki et al. (2019)).

4.2 Chapter aims

- To investigate the effects of chronic and acute solar irradiation stress on dermal fibroblasts by:
    - Quantifying the mitochondrial production of mROS (superoxide) and whole cell ROS (hydrogen peroxide).
    - Quantifying mtDNA damage in each condition.
- Probe different regions of mitochondrial genome to determine mtDNA damage and repair under each condition 24 hours post irradiation.
- Explore the effects of stress under different metabolic and growth conditions using induced mitochondrial metabolism and serum deprivation.

4.3 Chapter specific methods

4.3.1 Cell culture conditions

Galactose conditions were obtained by converting to DMEM without glucose media (Gibco, UK) supplemented with 5mM galactose (Sigma, UK), 1mM sodium pyruvate (ThermoFisher, UK), 10% FBS and P/S after 1 passage. Cells were dissociated as before, and the appropriate dilution transferred into galactose DMEM and spun down to a pellet to remove any excess glucose containing media. Cells were re-suspended in galactose media and transferred to a new flask where they were grown for experiments.

Cells were cultured in high glucose DMEM supplemented with 2% FBS by gradually reducing the concentration of FBS on each passage from 10% to 7% then finally 4% FBS, where cells were cultured in flasks for subsequent experiments. After dissociation with TE, 4% FBS medium was added to the flasks to collect the cells and then used for seeding, and serum concentration was reduced to 2% after attachment.

4.3.2 Solar light dosing

HDFn cells were seeded for each experiment in a 6-well plate; one full plate was seeded per condition, with an extra plate for control stains. The 10% FBS in glucose and galactose media conditions were seeded at 70,000 cells per well for the 4x 1.08 SED dose condition and 40,000 cells for well for the control, 1x 1.08 SED and 1x 4.32 SED conditions. The 2% FBS in glucose media condition cells were seeded at 100,000 cells per well.

Prior to dosing with solar light, media was replaced with 2 ml PBS for each condition. Cells for the intermittent dosing condition were irradiated with complete solar light at 1.08 SED every 24 ± 3 hours for 4 days, as per methods chapter, and all conditions were returned to media within 20 mins. On day 4, the 1x 1.08 SED and 1x 4.32 SED condition were irradiated along with the 4x1.08 SED.

Immediately after the final dose, flow cytometry was performed on cells from two wells, and a further two wells were harvested for DNA extraction at 0 hours (details in methods chapter). The last two wells were placed in media and incubated at 37˚C at 5% CO_2 for 24 ± 3 hours before harvesting for 24 hour sample DNA extraction.

4.3.3 Crystal violet measurement of cell density

Cells were seeded at 6000 cells per well in a 96 well plate. For each dose, all wells were replaced with 200 µl PBS and irradiated. After the final dose, the PBS was removed, and the

plate was tapped gently on blue roll to remove excess fluid. 50 µl of crystal violet stain (0.5% (w/v) crystal violet powder in 20% methanol solution) was added to each well and incubated at room temperature for 20 mins on a shaking rocker at 20 opm. Each well was washed 6 times with water, then the water was removed, and plates were left to dry overnight. Crystal violet stain was dissociated in 200 µl of 1% SDS solution on a shaking rocker at 20 opm before reading at 570nm.

4.3.4 Flow cytometry analysis of ROS

Flow cytometry of live cells was used to assess ROS using MitoSOX™ Red Mitochondrial Superoxide stain (ThermoFisher Scientific, UK) and 2',7'-dichlorodihydrofluorescein diacetate (DCF-DA) (Thermo Fisher Scientific, UK). Tetramethylrhodamine, Ethyl Ester, Perchlorate (TMRE) (ThermoFisher Scientific, UK) was used in combination with MitoSOX to assess mitochondrial membrane permeability and propidium iodide (PI) (Abcam, UK) was used with DCF-DA to assess cell viability. Following treatment, cells were dissociated using 200 µl TE for 5-10 mins at 37°C into single cell suspension. TE was neutralised in 1ml of appropriate media with FBS and cells were collected in 5ml round bottom polystyrene tubes (Falcon, UK) and spun to a pellet at 12000 rpm for 5 mins. Cells were washed once in PBS to remove phenol red.

MitoSOX and TMRE were diluted in appropriate media (galactose or glucose DMEM) depending on experimental condition. Cells were stained with 480 µl of 5 µM MitoSOX for 20mins before adding 20 µl of 1 µM TMRE (40 nM final concentration) for a further 10 mins for combined staining, and single stains of each were performed for compensation using the same concentrations for 30 mins or 10 mins, respectively. DCF-DA was diluted in PBS to a 1.5 µM working stock, and incubated for 30mins, before 0.5 µl of 50 µg/ µl PI stain was added immediately before flow analysis for a final concentration of 13 µM. Cells were all incubated at 37°C at 5% (v/v) CO_2. After staining, cells were spun down at 12000 rpm for 5 mins, washed twice with PBS and re-suspended in 500 µl chilled PBS, put immediately on ice and analysed within 1 hour.

Stain	Laser	Bandpass Filter
MitoSOX	488 nm	610/20
TMRE	561 nm	586/15
DCF-DA	488 nm	530/30
PI	561 nm	610/20

Table 4-1. Laser and bandpass filter for each stain

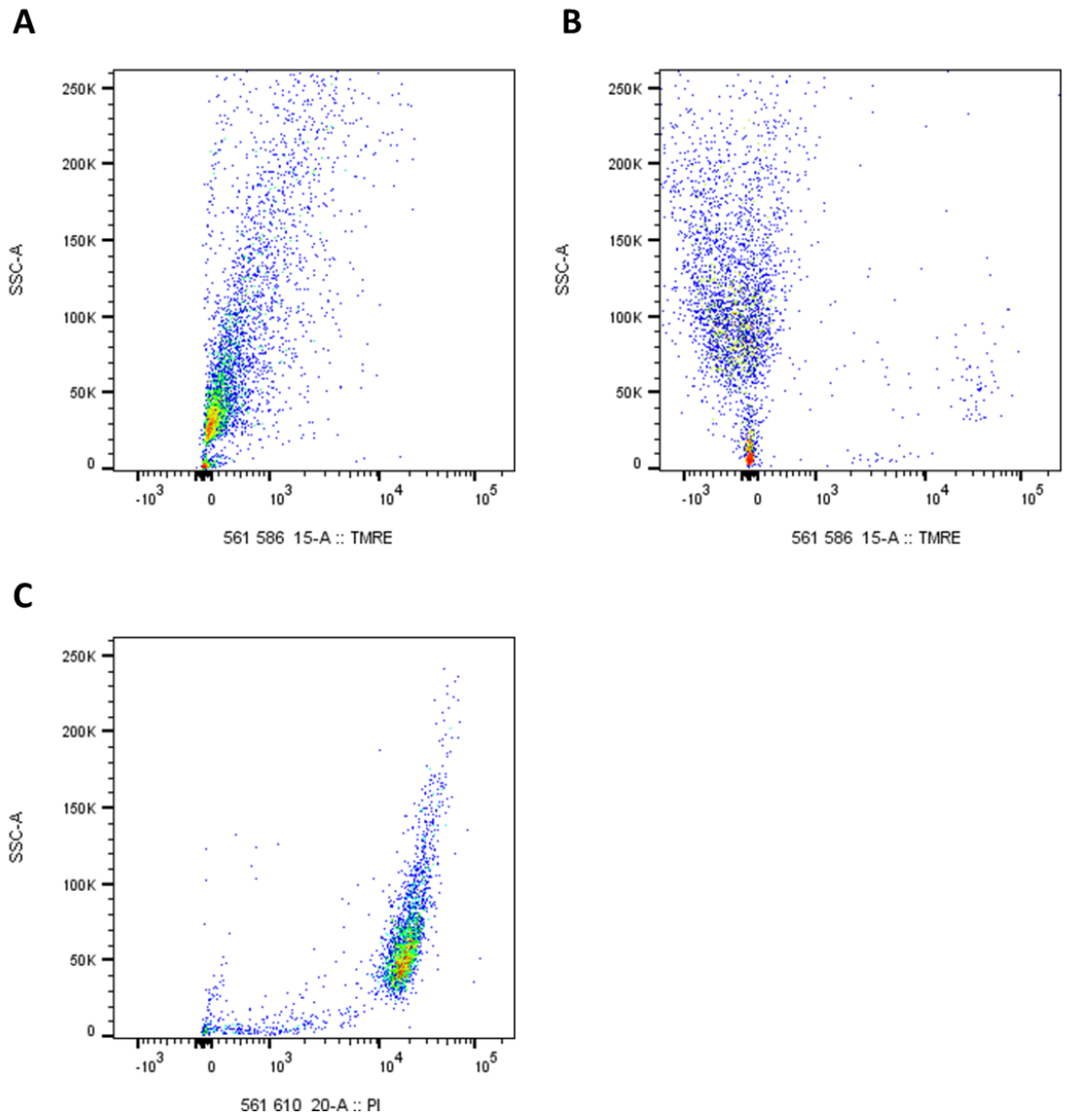

Figure 4-1. FlowJo analysis of TMRE stain and PI stain for mitochondrial membrane potential and cell death.
A) Cells were treated with FCCP for 1 hour prior to TMRE staining to deplete mitochondrial membrane potential. B and C) Cells were incubated at 56˚C for 45 mins prior to TMRE staining (B) and PI staining (C) to induce cell death.

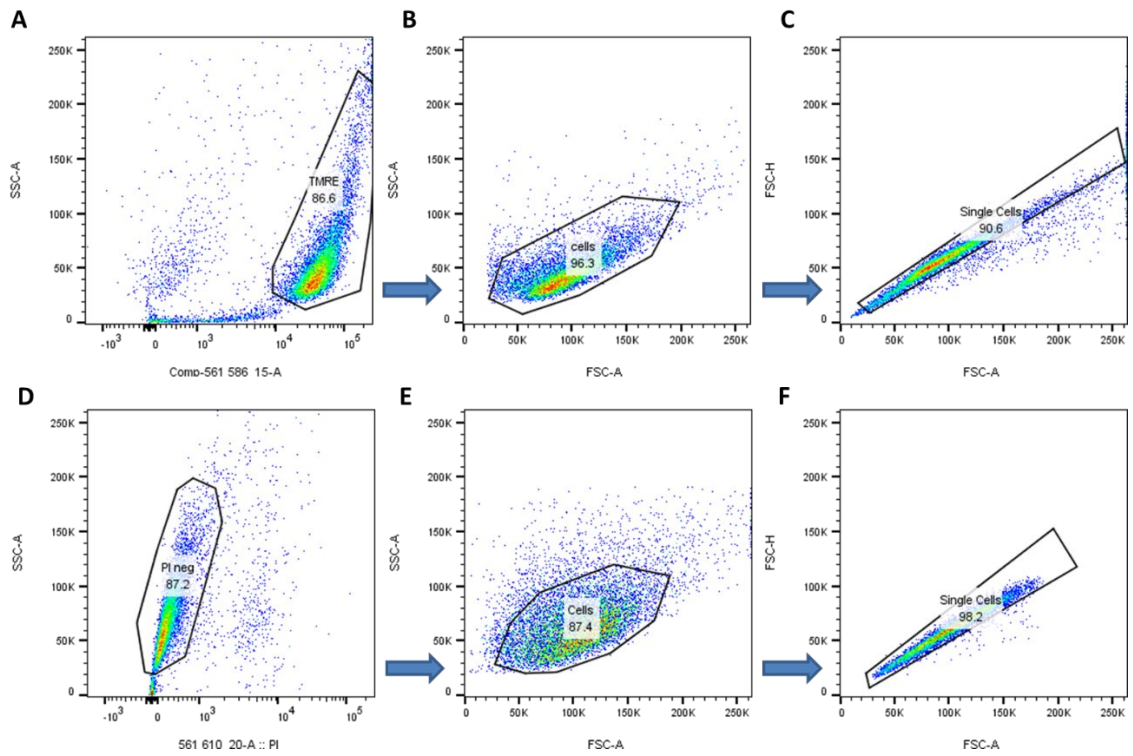

Figure 4-2. Example gating in FlowJo for MitoSOX and DCF-DA analysis of cellular ROS.
A) MitoSOX assay was gated on TMRE positive to include those with intact membrane potential. D) DCF-DA assay was first gated on PI negative cells so only live cells were included. B and E) Both were gated around the densest area of cells using FCS-a v SSC-a view to capture the average population. C and F) FSC-a v FSC-h view to exclude doublet cells.

MitoSOX experiments were compensated using a single stain of each MitoSOX and TMRE and an unstained sample using FACSDiva™ Software (BD Biosciences). Experiments were re-compensated when media or treatments conditions were changed. Each experiment was run with a non- viable control of cells heated to 56°C for 45 mins prior to staining (Figure 4-1) and an unstained sample to assess baseline auto-fluorescence with a minimum of 10000 total events collected for each experiment. Gating was carried out on FlowJo v.10 as shown in Figure 4-2, using the flow channels shown in Table 4-1.

Once cells were gated, median size adjusted mean fluorescence index (MFI) was calculated to control for the impact on cell size on total fluorescence:

$$\frac{Median\ MFI\ stain - Median\ MFI\ unstained}{Median\ FSC\ A}$$

Equation 2. Size adjustement

The size adjusted MFI of each condition was normalised to the control sample to obtain a percentage of the control fluorescence:

$$\frac{Median\ MFI\ condition}{Median\ MFI\ control} \times 100$$

Equation 3. Relative to control

4.3.5 MTS assay

MTS (3-(4,5-dimethylthiazol-2-yl)-5-(3-carboxymethoxyphenyl)-2-(4-sulfophenyl)-2H-tetrazolium), is a measure of metabolic activity based on the activity of NAD(P)H dehydrogenase enzymes. Cells were seeded into a flat bottom 96-well plate at the previously described densities. Media was removed, washed with PBS, and replaced with phenol red free media, with the appropriate concentration of FBS for either 24 hours of 48 hours prior to MTS treatment. Phenol red free media is used during incubation to limit the interference imparted from phenol red. 20% (v/v) of MTS reagent (Promega, UK) was added to the media as per the protocol and incubated in the dark at 37°C with 5% CO_2 for 1 hour prior to reading at 495 nm. Each condition with cells was compared to a negative control containing media with the respective FBS concentration and no cells. Results were plotted as the mean of the group as a percentage of the control group (10% FBS condition).

4.3.6 mtDNA damage quantification

Details of the 83 bp housekeeping, 1 kb and 11 kb amplicon qPCR assays can be found in the chapter 2.

4.3.7 Amplification of 4977 bp and 3895 bp deletion regions

Two common mitochondrial deletions of sizes 4977 bp and 3895 bp were quantified using TaqMan™ fast advanced master mix (ThermoFisher) and custom primers and probe mix (ThermoFisher), as per the manufacturer guidelines. Primer sequences are stated in Table 4-2. Cycle conditions were as follows: 10 min denaturation at 95 °C, followed by 40 cycles of 15s annealing at 95 °C and 1 min extension at 60 °C for both reactions. This produced a short 108 bp product if the 4977 bp deletion is present and a 131 bp product for the presence of the 3895 bp deletion. The TaqMan probe for each binds on both sides of the break point therefore can only attach if the deletion is present and the ends have re-joined in the mtDNA.

Primer	**Sequence**
Forward 4977	5’- ACCCCCATACTCCTTACACTATTCC -3’
Reverse 4977	5’- AAGGTATTCCTGCTAATGCTAGGCT -3’
4977 probe	5’- ACACAAACTACCACCTACCTCCCTCACCA -3’FAM
Forward 3895	5’- CAACCCTCGCCCATCCTA -3’
Reverse 3895	5’- CCTGCAAAGATGGTAGAGTAGATGAC -3’
3895 probe	5’- TGCTAACCCCATACCCCGAAAATGTTGG -3’FAM

Table 4-2. 4977 bp (Koch et al., 2001) and 3895 bp (Harbottle and Birch-Machin, 2006) deletion primer and probe sequences

4.3.8 Statistical analysis

Analysis of fractional and fold change data was first log2 transformed prior to statistical analysis. As per the law of logarithms, the geometric means were assessed and the null hypothesis assumes ratio of these is 1, therefore a significant result is considered when the confidence intervals do not contain 1. Statistical differences were determined using GraphPad Prism 8 or SPSS (IBM) software, where appropriate.

4.4 Results

4.4.1 Preliminary results and optimisation

4.4.1.1 Optimisation of ROS assessment technique

Cellular ROS measurement was initially determined using DCF-DA in a plate-based assay, however cells appeared to be removed during the wash steps between dosing. A crystal violet assay was performed to determine change in cell density during the protocol. The chronic dose condition was found to decrease the cell density on average by 40%, whereas only 12% reduction in cell density was seen for low dose and acute dose when dosing with the final chronic dose. When the low and acute doses were performed with the initial dose, there was a 44% decrease in cell density for acute and 22% for low dose. This demonstrated that both dose and media changes affected the number of cells in the well, and therefore a cell number independent method of staining was required to assess ROS. Flow cytometry is independent of cell number as cell fluorescence is measured on an individual cell basis, and therefore selected as the most appropriate method for ROS analysis.

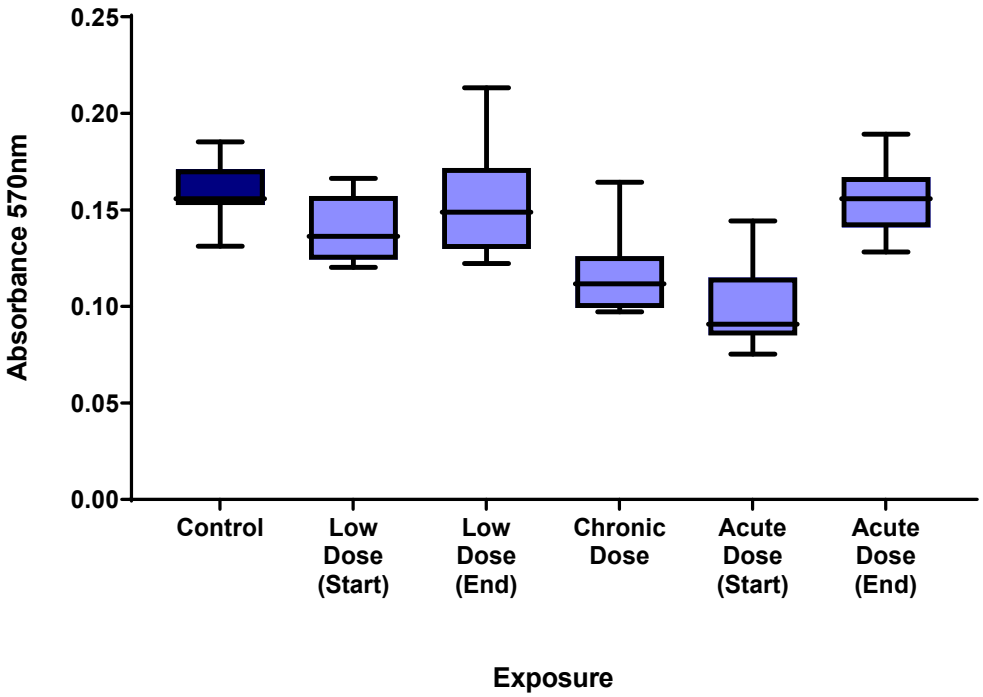

Figure 4-3. Crystal violet measurement of cell density post solar irradiation exposure.
The high and low dose were administered with either the first chronic dose (start) or last chronic dose (end). Control= no iradiation, low dose= 1x 1.08 SED, chonic dose= 4x 1.08 SED (1x every 2 hours), acute dose= 1x 4.32 SED; All conditions were washed with PBS prior to the chronic dose for consistency; N=8, n=1.

4.4.1.2 Reduced FBS concentration reduces cell growth and maintains metabolism

Research on the effects of reducing FBS concentration suggest a gradual decrease can limit cell growth but not metabolic activity (Mignon et al., 2017), but there was no detailed protocol available. Cell number was counted daily to assess proliferation and an MTS viability assay was performed to determine an appropriate protocol of reducing FBS concentration in HDFn cells.

Cell proliferation was measured by overnight seeding of cells from a flask cultured at 4% FBS concentration before changing the media to growth conditions. Cells were counted with a haemocytometer and the number of cells per well was calculated based on the volume of media they were in.

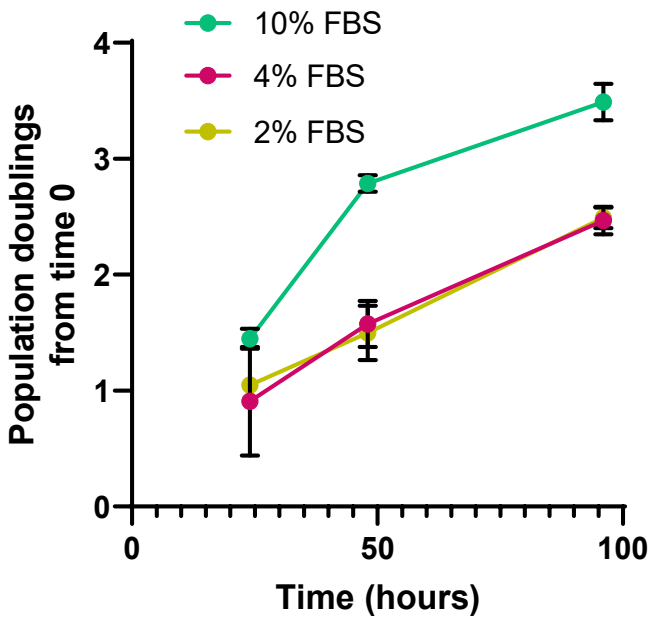

Figure 4-4. Population doublings from time 0 following 24h, 48h and 96h growth at each FBS concentration growth condition.
Cells were cultured initially in 4% FBS and seeded at 40,000 cells per well in respective FBS concentrations; 0 hour count is 24 hours after seeding (n=2). Data represents mean±SD.

Figure 4-4 shows cell growth for the 10% FBS concentration was greater than the growth of cells in 4% and 2% FBS. Cells seeded in 2% FBS had a lower initial count (25,700 cells per well) than cells seeded at 4% (35,500 cells) and 10% FBS (37,700 cells) conditions. From these results, it was determined that seeding cells in 2% FBS had some impact on the cells ability to adhere and therefore seeding at 4% FBS would be used for future experiments. There was no significant difference in population doubling between 4% and 2% FBS growth conditions at any time point. Though not significantly different at 24 hours, cells grown at 10% FBS doubled

in population 1.2 times more than the 2% and 4% conditions (p=0.004 and p=0.006, respectively) after 48 hours. At 96h their growth rate had slowed down, likely due to their confluency, and had a doubling of 1 times more than the 2 and 4% conditions (p=0.002 and p=0.019, respectively).

MTS assay assessed cell metabolism at each FBS concentration. Cells were cultured at either 10% or 4% FBS concentration, before changing to experimental FBS concentration for 48 hours. Initial MTS experiments were incubated a maximum of 4 hours as per manufacturer's recommendation of between 1 and 4 hours. However, microscopic examination found cells in higher FBS concentrations died but the cells at lower FBS concentrations remained adhered at 4 hours (n=2, no image data). The subsequent experiments were read after 1 hour incubation which did not cause any cell death.

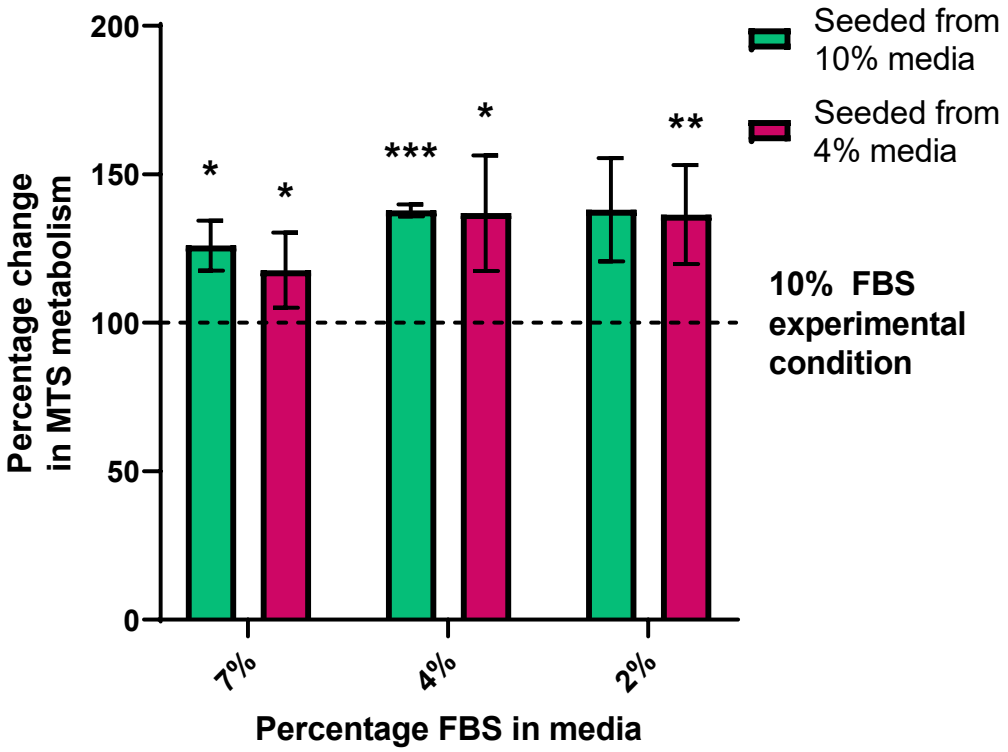

Figure 4-5. MTS metabolism at differing FBS concentrations, as a percentage change from 10% FBS conditions.

Effect of FBS concentration on MTS metabolism at 48 hours post media change, cells were incubated for 48h in respective FBS concentration media with high glucose DMEM; statistical differences from the 10% FBS experimental media condition was determined one sample t-test with hypothetical mean set as 100; ***p<0.001, **p<0.01, *p<0.05 N=8, n=5 (4%) and n=3 (10%); Data represents mean±SD.

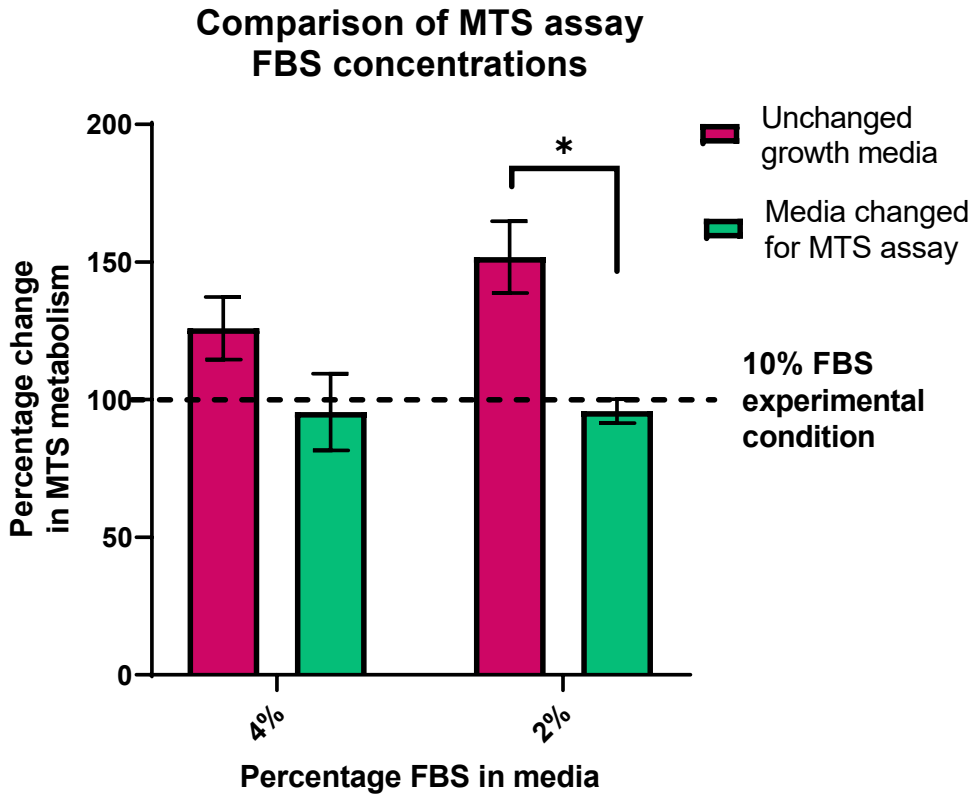

Figure 4-6. Comparison of FBS concentration during MTS assay.
Unchanged growth media MTS assay was carried out in respective FBS concentrations and media changed condition MTS assay was carried out in 2% FBS; statistical differences determined by t-test between the corresponding FBS concentrations and one sample t-test from the 10% FBS condition with hypothetical mean set to 100; *$p<0.05$; N=6, n=2; data represents mean±SD.

With decreasing FBS concentration, there was an increasing trend in MTS metabolism both for cells starting at 10% and 4% FBS as shown in Figure 4-5. When cells were seeded from a culture of 10% FBS growth condition, there was a 38% increase in MTS metabolism when cells were then cultured in 4% FBS ($p=0.001$) and 26% increase in 7% FBS ($p=0.033$). When cells were seeded from a 4% FBS concentration, the 4% and 2% FBS experimental conditions had a 37% increase in MTS metabolism compared to the 10% FBS experimental condition ($p=0.013$ and p-=0.008, respectively), and a 18% increase in 7% FBS ($p=0.035$). There was no significant difference in each growth condition between the 10% FBS and 4% FBS starting concentrations.

These results were the inverse of those expected from the data in Figure 4-4, and further research found that FBS can inhibit the MTS assay which is not mentioned in the manufacturer's protocol. The assay was repeated to test this, by culturing cells in their respective FBS concentrations and then changing the media to 2% FBS for the MTS assay for

1 hour. When the MTS assay was carried out in the same FBS concentration, there was no difference between the MTS metabolism. Though not significant likely due to the small sample size, there is an increasing trend again for reduced FBS concentrations, the 4% FBS condition increased on average by 26% (p=0.117) from the 10% FBS condition, and 2% FBS by 52% (p=0.093) (Figure 4-5). There was a significant change from 10% FBS condition between the changed and unchanged media of the 2% FBS condition, the unchanged media had 56% greater metabolism than the changed media (p=0.022). This result taken with the results of cell number from Figure 4-4 imply that the cells grown in 2% could have a higher metabolism still, as at 48h post media change, cells grown in 10% FBS had undergone 2.73 population doubling compared to cells in 2% FBS which had only undergone 1.66. Theoretically, this would expect at least 2 times more cells in the 10% FBS media condition and therefore the equal MTS assay results are indicative of a greater MTS metabolism per cell of those culture in 2% FBS.

4.4.1.3 Flow cytometry auto fluorescence and dosing condition

Cell auto-fluorescence (AF) can interfere with flow cytometry results; therefore, each experiment should be run alongside appropriate unstained controls to account for this, particularly as lipofuscin accumulation in senescent cells has a wide range emission and excitation, which covers the range of MitoSOX stain and DCF-DA. MitoSOX stain had a high background AF and had a much weaker fluorescence than DCF-DA so was more likely to be impacted by AF. Each experiment was carried out with an unstained control from the control condition population, it was later found this would not account for auto-fluorescence in the dosed conditions. Lipofuscin auto-fluorescence is correlated with cell size (Jackson, 2018), and cell size was already taken into account during the flow cytometry analysis. It was necessary to retrospectively assess the difference between AF and size correction to confirm the validity of the results.

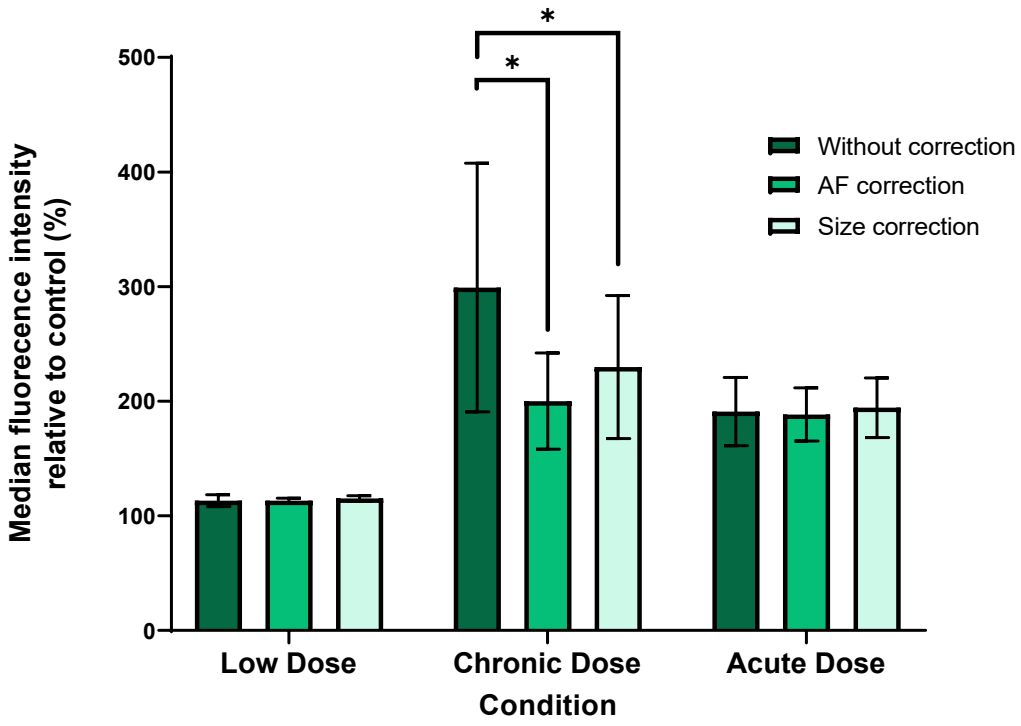

Figure 4-7. Comparison between results of size v AF correction of MitoSOX data.
Chronic solar dose equivelant to 1.08 SED of solar simulated light each day for 4 days, low dose equivalent to a single 1.08 SED dose on the final day, acute dose equivalent to 4.32 SED solar simulated light on final day. *p<0.05; Statistical differences were between analysis conditions were determined by paired t-test; n=3; data represents mean±SD.

This experiment was carried out as detailed in the methods, but with an unstained control for each condition. Uncorrected MitoSOX fluorescence following chronic dose was 100% higher than AF correction (p=0.045) and 70% higher than size correction (p=0.039), there was no significant difference between AF and size correction (p=0.129). No differences were found between the corrections for the low dose (p=0.373) and the acute dose (p=0.205).

4.4.1.4 Cell harvest technique for mtDNA qPCR analysis

Initially, the full experimental procedure was implemented for high glucose and galactose condition before extending to include the low serum condition. Results from this showed a decrease in mtDNA damage 24 hours post irradiation compared to the 0 hour cells. The initial cell harvesting procedure first washed the cells with PBS and then added trypsin, where both the media and PBS were discarded. The high glucose media experimental condition was repeated, and both media and PBS from the wash step were collected with the cells. This technique would include any detached cells from the supernatant in the qPCR analysis to exclude loss of damaged cells as a cause for the reduction in mtDNA damage.

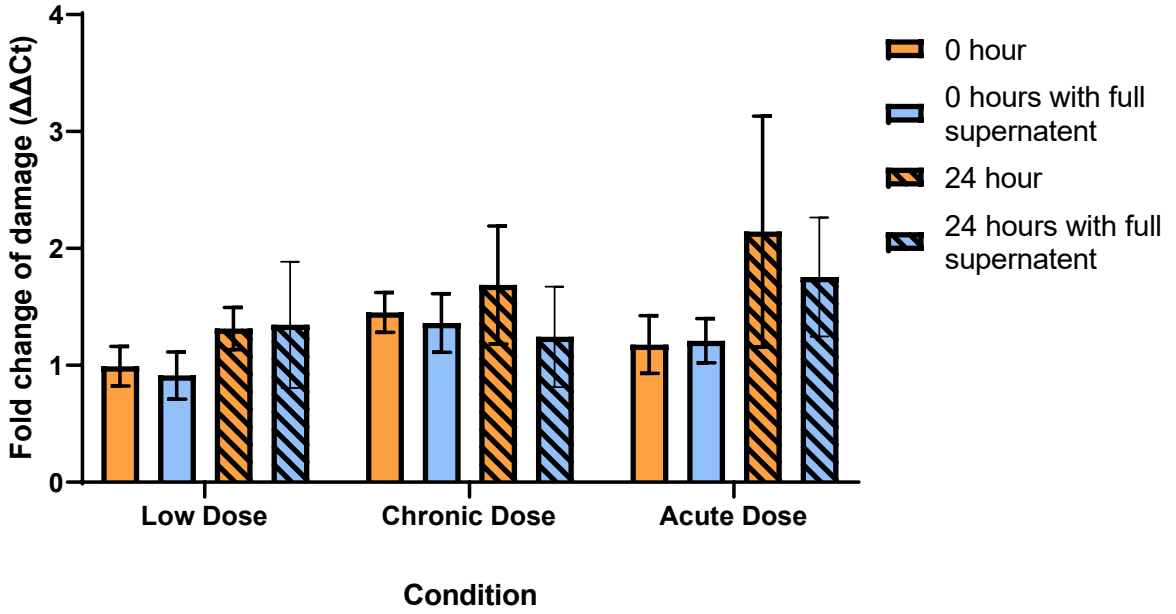

Figure 4-8. mtDNA damage using qPCR to amplify 1 kb of non-coding region.
Chronic solar dose equivelant to 1.08 SED of solar simulated light each day for 4 days, low dose equivalent to a single 1.08 SED dose on the final day, acute dose equivalent to 4.32 SED solar simulated light on final day. Statistical differences between 0h and 24h for each collection method determined using one-way ANOVA on Log2 transformed data; n=3; data represents mean±SD.

Microscopic examination of the cells at 24 hours post irradiation found no apparent cell detachment in the media. No significant differences were found between the no supernatant and full supernatant conditions (1x1.08 SED p=0.245; 4x1.08 SED p=0.549; 1x 4.32 SED p=0.179) (Figure 4-8). While the loss of cells did not have a significant effect on the mtDNA damage produced, there was an overall decreasing trend in mtDNA damage when the supernatant was collected compared to no supernatant collection. Theoretically, the collection of supernatant would include damaged cells and an increase in mtDNA damage would be expected. It was therefore determined that any difference between the two harvesting methods was purely biological variation and not related to detached cells in the media.

4.4.2 Glucose and serum concentrations affect fibroblasts ROS production in response to solar stress

The flow cytometry data in this experiment aimed to answer whether chronic or acute stress produced more ROS production in cells; how glucose and FBS concentration impacted ROS production; and whether these factors contributed to mitochondrial superoxide production and whole cell hydrogen peroxide.

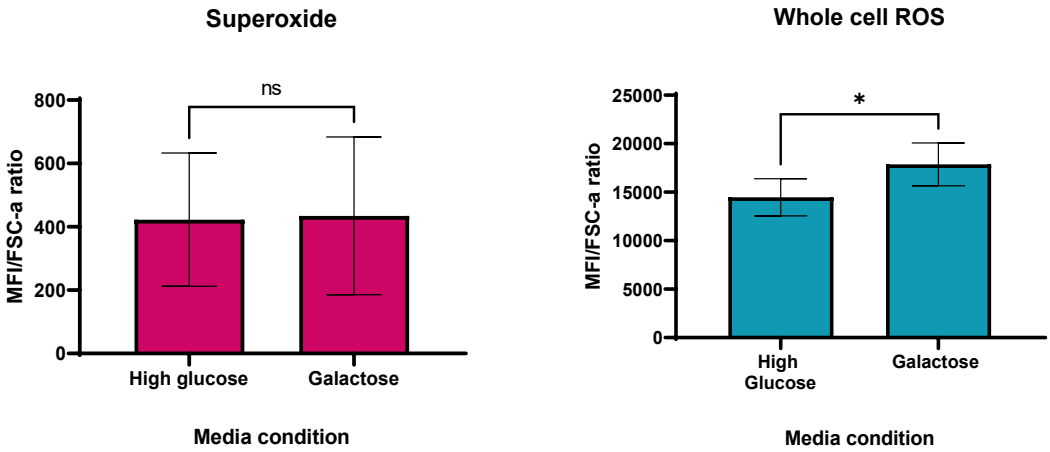

Figure 4-9. Comparison of control cell ROS production.
Mitochondrial (MitoSOX) and whole cell (DCF-DA) ROS production in cells from both media conditions (high glucose= 25mM glucose DMEM and galactose= 25mM galactose in no glucose DMEM) were measured on the same day and were analysed using identical gating procedures after flow cytometry; statistical analysis performed using unpaired two-tailed t-test (Welch's test); *$p<0.05$); MFI/FSC-a ratio = mean fluorescence index/ forward scatter measurement of fluorescence controlled to cell size; n=6; data represents mean±SD.

Normal growth of HDFn cells in high glucose DMEM supplemented with 10% FBS growth serum was compared to galactose medium with 10% FBS, and high glucose supplemented with 2% FBS for low serum condition. Four daily doses of 1.08 SED solar light irradiation were used to model chronic low level stress, and the large 4.32 SED dose was equivalent to the total of the daily doses in one acute dose. The single 1.08 SED dose was performed to compare both conditions with a single low dose. Basal ROS level comparisons showed cells cultured in galactose medium had no change in basal superoxide ($p=0.43$) and 23% increased production of basal whole cell oxidative stress ($p=0.018$) compared to cells cultured in high glucose medium condition (Figure 4-9).

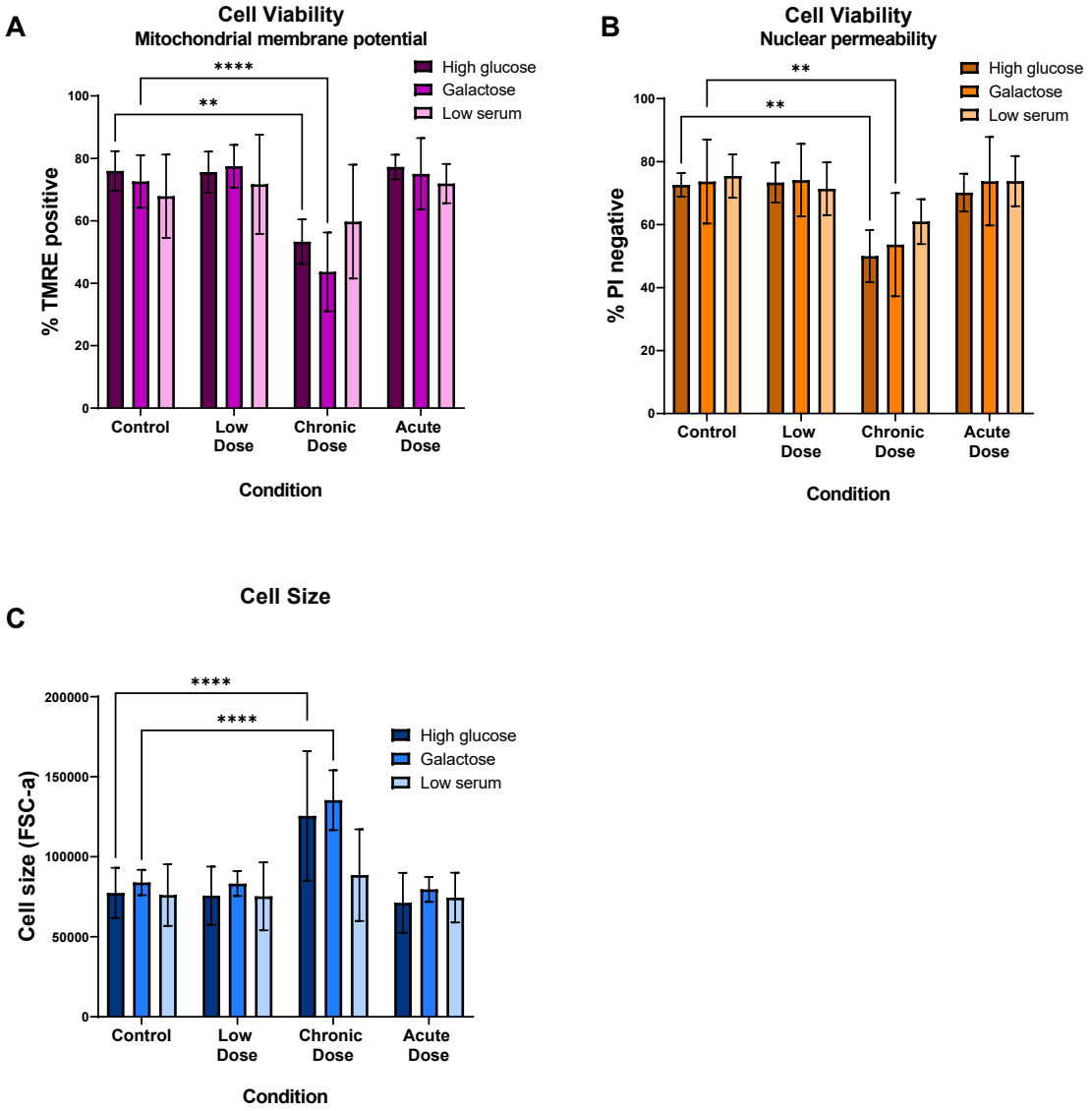

Figure 4-10. Cell viability and size as determined by flow cytometry in each dosing condition. Chronic solar dose equivelant to 1.08 SED of solar simulated light each day for 4 days, low dose equivalent to a single 1.08 SED dose on the final day, acute dose equivalent to 4.32 SED solar simulated light on final day. High glucose media condtion equals 25mM glucose DMEM with 10% FBS, glactose equals 25mM galactose in glucose free DMEM with 10% FBS and low serum equals 25mM glucose DMEM with 2% FBS. A) Mitochondrial membrane potential was determined by the percentage of TMRE positive cells after gating. B) Nuclear permeability was determined by the percentage of propidium iodide positive cells. C) Cell size was determined by forward scatter area. Statistical differences between control and each dose was determined using two-way ANOVA with Bonforonni's correction; **p<0.01, ****p<0.0001; n≥4; data represents mean±SD.

Cell viability was determined to be significantly lower following chronic dosing when cells were cultured in high glucose and galactose medium, as measured by negative mitochondrial membrane potential and positive nuclear permeability (Figure 4-10). In high glucose medium, cells were 23% less viable by both measurements after chronic dosing (TMRE p=0.004; PI p=0.001); in galactose medium, cells were 29% less viable as measure by TMRE staining

(p<0.0001) and 20% less viable via PI (p=0.008). Cell size was significantly larger than control after chronic dosing in both high glucose and galactose media (p<0.0001), but there was no significant change in size in the low serum medium.

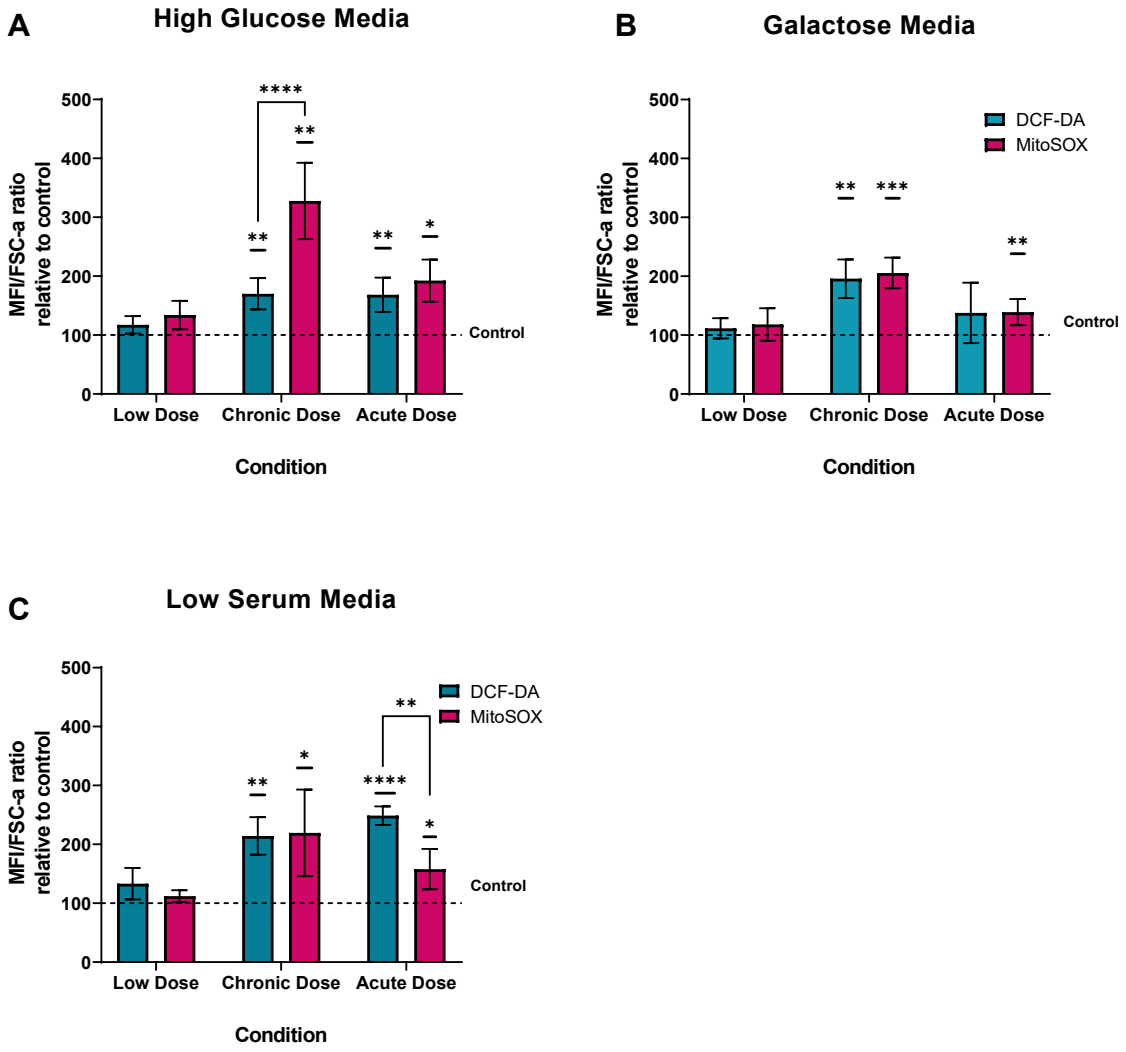

Figure 4-11. Whole cell ROS (DCF-DA) and superoxide (MitoSOX) production per media condition after chronic and acute solar irradiation.
Chronic solar dose equivelant to 1.08 SED of solar simulated light each day for 4 days, low dose equivalent to a single 1.08 SED dose on the final day, acute dose equivalent to 4.32 SED solar simulated light on final day. High glucose media condtion equals 25mM glucose DMEM with 10% FBS, glactose equals 25mM galactose in glucose free DMEM with 10% FBS and low serum equals 25mM glucose DMEM with 2% FBS. A) High glucose medium; DCF-DA n=5, MitoSOX n=4. B) Galactose medium; DCF-DA n=>4, MitoSOX n=>5. C) Low serum medium; DCF-DA n=4, MitoSOX n=5; ***p<0.001,**p<0.01, *p<0.05; Statistical difference determined of log2 transformed data, between ROS species and dose was determined from factorial measures ANOVA and change from control

determined by one sample t-test from theoretical mean; data represents mean±SD.

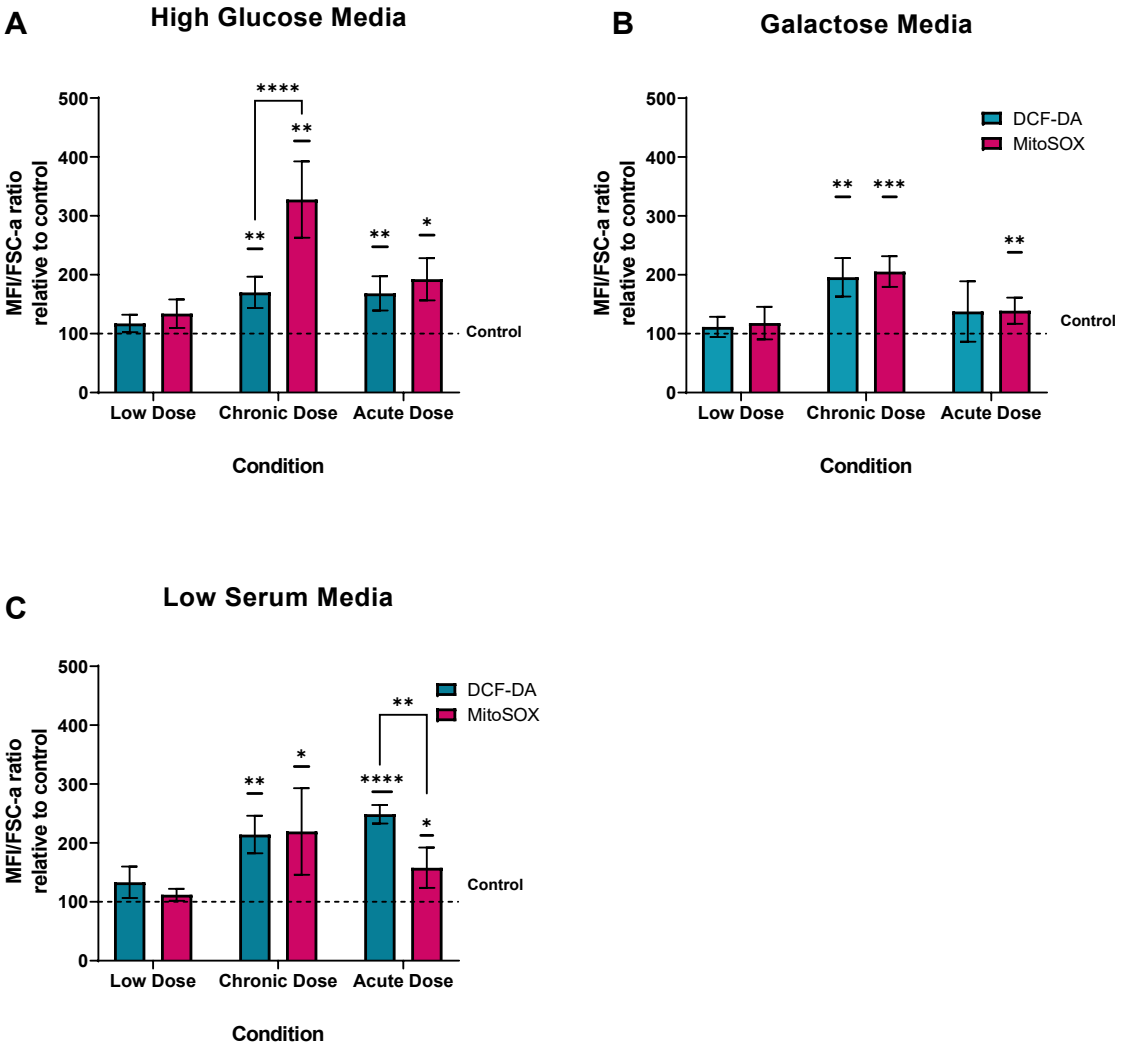

Figure 4-11 compares the whole cell ROS and superoxide formation with each media condition. When the cells were cultured in high glucose media, the chronic and acute doses resulted in the same increase in whole cell ROS production, with a 70% ($p=0.002$) and 68% ($p=0.0024$) increase from control, respectively. Superoxide production was increased by 237% ($p=0.001$) after chronic dosing, which was significantly greater than the 70% increase in whole cell ROS observed at this dose ($p<0.0001$). Superoxide production following the acute dose in high glucose had a 105% increase from control ($p=0.006$), significantly less than that produced after chronic dosing ($p=0.039$). Chronic dose resulted in a greater production of mitochondrial superoxide compared to the low and acute dose ($P<0.0001$), but whole cell ROS was not different between the dosing conditions.

Cells cultured in galactose medium had similar superoxide production and whole cell ROS production with both chronic and acute dosing. Chronic dosing similarly raised the production

of both superoxide and whole cell ROS to 105% (p=0.0002) and 95% (p=0.005) above control levels, respectively. The acute dose induced a 39% increase in mitochondrial superoxide (p=0.005), but no significant increase in whole cell ROS. There were no significant differences between each ROS species within each dosing condition. Chronic dose resulted in increased whole cell ROS compared to the low (P=0.0007) and acute (p=0.03) dose, and increased mitochondrial superoxide from low (p=0.0002) and acute (p=0.004) dose.

Reducing the growth serum resulted in a similar increase in ROS production after chronic dosing, whereby superoxide increased by 119% (p=0.009) and whole cell ROS by 114% (p=0.002). The acute dose induced significantly less superoxide than whole cell ROS (p=0.008), superoxide increased by 58% (p=0.01) but whole cell ROS had a 149% increase (p<0.0001). Chronic dose increased mitochondrial ROS (p=0.0009) and whole cell ROS (p=0.03) compared to the low dose, but the acute dose only elevated whole cell dose compared to low dose (p=0.0014).

Overall, high glucose media caused an imbalance in ROS production between mitochondrial superoxide and whole cell ROS. In high serum media, superoxide formation is greater than whole cell ROS after chronic doses; in low serum media, whole cell ROS is produced more than superoxide. Cells cultured in galactose media produced more ROS overall in response to the chronic dosing condition than the low or acute dose, whereas in high glucose media (high serum) only mitochondrial superoxide had a dose dependant change. Dose had a different effect on both ROS species when cultured in low serum media.

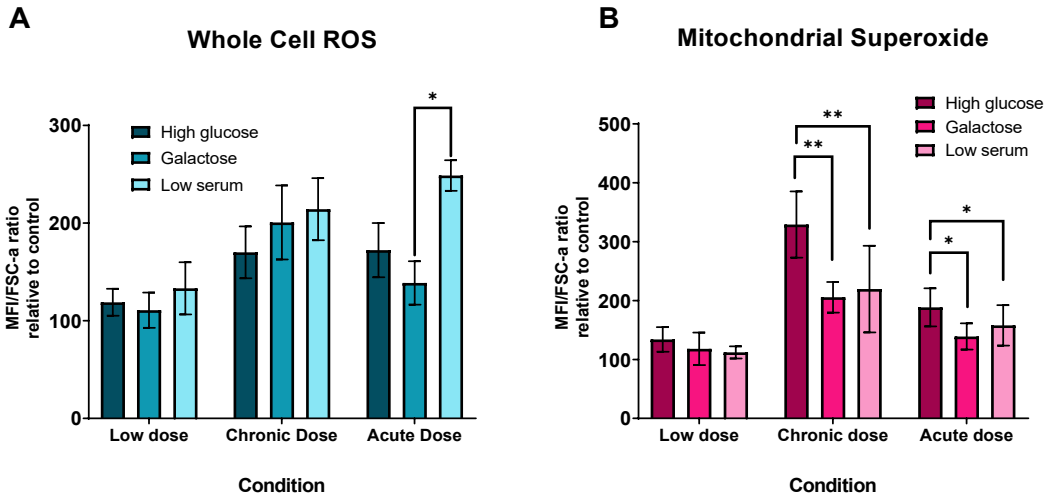

Figure 4-12. Effect of media condition on whole cell ROS and superoxide production after low, chronic and acute solar irradiation.
Chronic solar dose equivelant to 1.08 SED of solar simulated light each day for 4 days, low dose equivalent to a single 1.08 SED dose on the final day, acute dose equivalent to 4.32 SED solar simulated light on final day. High glucose media condtion equals 25mM glucose DMEM with 10% FBS, glactose equals 25mM galactose in glucose free DMEM with 10% FBS and low serum equals 25mM glucose DMEM with 2% FBS. Data from Figure 4-11 was re-plotted to compare media conditions. A) Hydrogen peroxide production measured in median fluorescent intensity of DCF-DA (n=4-6). B) Superoxide production measured in median fluorescent intensity of MitoSOX (n>=4-6). **p<0.01, *p<0.05; Statistical difference determined from one-way ANOVA with Welch's correction of log2 transformed data; data represents mean±SD.

When the media conditions are compared as in Figure 4-12, there is a distinct effect on ROS production following chronic and acute dosing. Whole cell ROS formation had the greatest difference between media conditions following the acute dose; cells in low serum medium produced 110% greater ROS than cells cultured in galactose media (p=0.033). There was also a borderline significant increase of 76% from cells in high glucose medium (p=0.052). Following chronic dosing, only a borderline non-significant difference of whole cell ROS was seen between the media conditions (p=0.057). Superoxide formation in cells after chronic dosing spiked in high glucose media with a 109% greater production compared to cells in galactose media (p=0.007), and 123% compared to cells in low serum media (p=0.004). The acute dose caused a smaller superoxide spike in high glucose medium, this increase was 49% greater than in galactose medium, and 30.5% greater than in low serum media (p=0.011 and p=0.047, respectively). Under all conditions, there was only ever a minor, non-significant increase in each ROS after a single 1.08 SED dose (superoxide p=0.181, whole cell p=0.526).

4.4.3 Chronic dosing has a protective effect on mtDNA

mtDNA damage was assessed through qPCR to determine damage in the non-coding region (1 kb assay) and coding regions of mtDNA (11 kb assay), and whether the amount of damage changed within a 24 hour period. The 11 kb assay and the 1 kb assay were performed on cells harvested immediately after solar irradiation and 24±3 hours after. The 11 kb region encompasses a large proportion of the L-strand coding region of the mitochondrial genome, whereas the 1 kb region is specifically in the non-coding region (NCR).

Figure 4-13 shows that mtDNA damage can decrease in the coding region within 24 hours of solar irradiation, but either stays consistent or increases in the NCR. Results of the 11 kb amplification assay were plotted as raw Ct value, where all conditions were assayed on the same plate after dilution to control for mtDNA content after an 83 bp housekeeping assay. The 1 kb assay was plotted as fold change using individual efficiencies of each reaction by using a standard curve on each plate.

Results from the 11 kb assay showed cells cultured in high glucose medium had time independent differences between treatments (Figure 4-13A). There was a mean increase in damage following each dosing condition compared to control; low dose resulted in a 0.97 Ct increase in damage ($p=0.004$), chronic dosing increased damage by 3.2 Ct ($p=0.0009$), and the acute dose resulted in the greatest level of damage with 5.03 Ct difference from the control ($p<0.0001$). Cells cultured in galactose medium had a significant reduction in damage 24 hours following each dosing condition. Damage following repeated doses had the greatest reduction in damage of 1.82 Ct ($p=<0.0001$), followed by the acute dosing condition (1.15 Ct; $p=0.0001$) and the low dose had the smallest reduction (0.6 Ct; $p=0.016$). The low dose had the smallest initial increase in damage of 1.45 Ct difference from control ($p=0.0024$), this reduced back to control levels over 24h as the difference was non-significant ($p=0.078$). Each dosing condition was significantly greater than the control at 0h, and the chronic and acute doses remained significantly greater than control after 24h. The chronic dose reduced from a 3.9 Ct increase ($p=0.0004$) to 2.3 Ct increase ($p=0.021$), and the acute dose had the greatest level of damage starting at 5.6 Ct difference at 0h ($p=0.0008$) and reducing to 4.6 Ct increase over 24h ($p=0.0029$). No significance was found between the high glucose and galactose media conditions when the damage after each treatment and time point was compared.

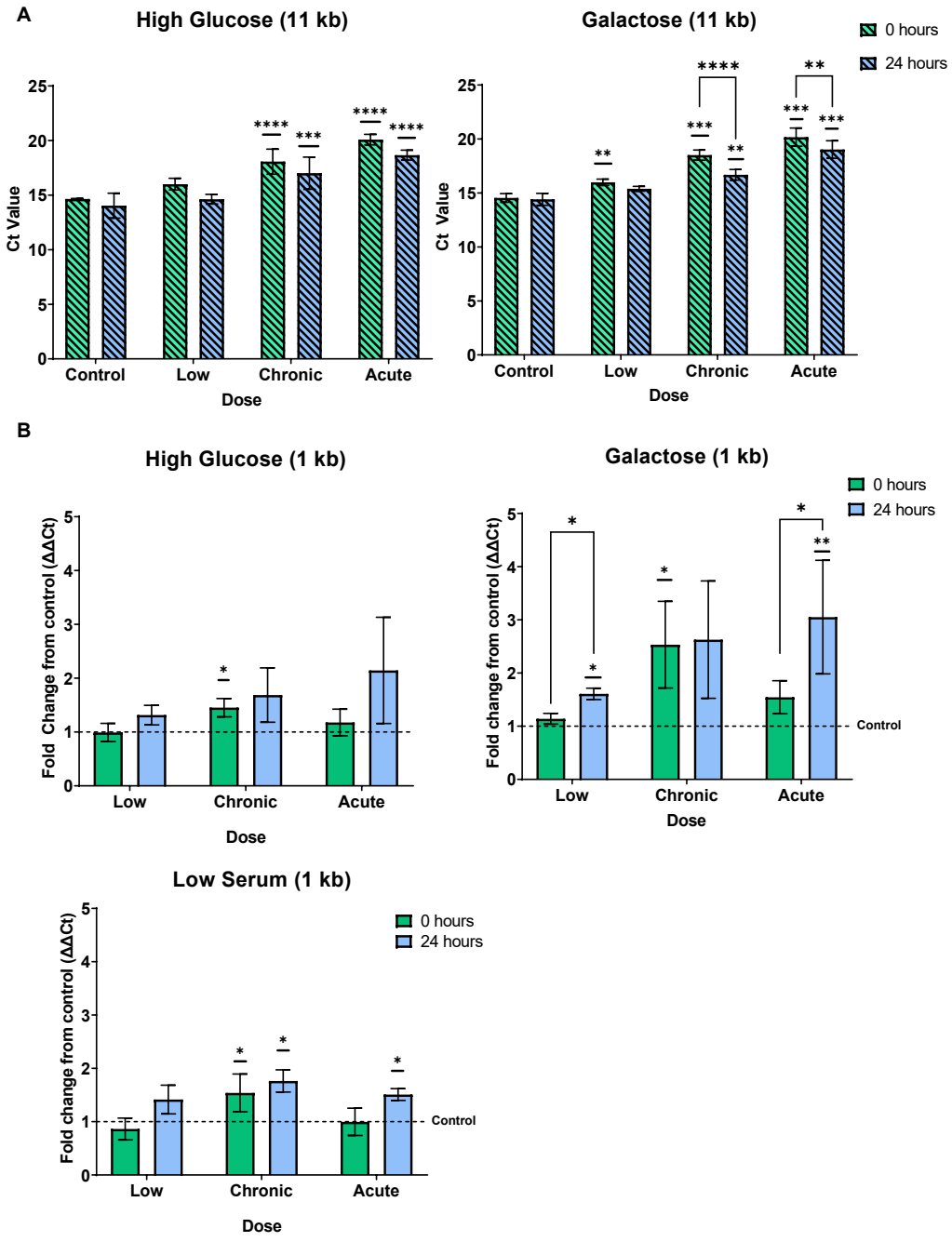

Figure 4-13. Immediate and delayed mtDNA damage in coding region and non-coding region under chronic and acute stress.

Chronic solar dose equivelant to 1.08 SED of solar simulated light each day for 4 days, low dose equivalent to a single 1.08 SED dose on the final day, acute dose equivalent to 4.32 SED solar simulated light on final day. High glucose media condtion equals 25mM glucose DMEM with 10% FBS, glactose equals 25mM galactose in glucose free DMEM with 10% FBS and low serum equals 25mM glucose DMEM with 2% FBS. A) Coding region of cells in high glucose media, n=4-6; and galactose media, n=4-6. B) Non-coding region of cells in high glucose media, n=3; galactose media; n=3; and low serum media, n=3. ****p<0.0001, ***p<0.001, **p<0.01, *p<0.05; statistical difference between treatments within each media condition was determined from factorial measures ANOVA, and differences between media conditions with one-way ANOVA with Welch's correction, of log2 transformed data, differences from control was determined by one sample t-test from theoretical mean of 1; significance above bars denotes change from control, brackets between time points; data represents mean±SD.

The 1 kb assay was performed with a standard curve, so the interpolation of fold change was performed based on the efficiencies of each PCR run. Only the cells cultured in the galactose medium condition showed any significant interactions between dose and time (Figure 4-13B); over 24 hours, the low dose resulted in a 0.47 fold increase in damage, and damage following the acute dose increased by 1.51 fold ($p=0.044$ and $p=0.02$, respectively) which was significantly different from the control at 0 hours ($p=0.035$). There was no change in damage after chronic dose over 24 hours, however at 0 hours there was 1.53 times more damage than the control ($p=0.047$), and the damage was still borderline significant from the control at 24 hours ($p=0.058$). Cells cultured in high glucose medium had a 0.51 fold increase in damage over 24 hours which was independent of treatment ($p=0.03$), and the chronic dose resulted in 0.45 times greater damage than the control at 0 hours ($p=0.030$), but this was not significant after 24 hours ($p=0.10$). In cells cultured in low serum medium, damage following chronic dosing was 0.42-fold greater than after an acute dose, this was independent of time ($p=0.045$). The chronic dose resulted in 0.54 times more damage than the control at 0h ($p=0.037$) and 0.76 times more damage at 24 hours ($p=0.013$). The acute dose had no significant damage at 0 hours and 0.51 times more damage than the control at 24 hours ($p=0.011$). No significant differences were found between the three media conditions with each treatment.

In summary, cells cultured in all three media conditions had no overall significant differences in mtDNA when compared directly. Cells cultured in galactose medium had significant changes in damage over 24h, which accounted for decreasing damage in the coding region of the mtDNA and increasing damage in the non-coding region. The level of initial damage was dependant on the dose and the region of mtDNA, an acute dose produced the highest levels of damage in the coding region, whereas chronic doses produced more initial damage in the non-coding region and remained more constant over 24h after the final dose.

4.4.4 Chronic dosing causes a daily increase in mtDNA damage

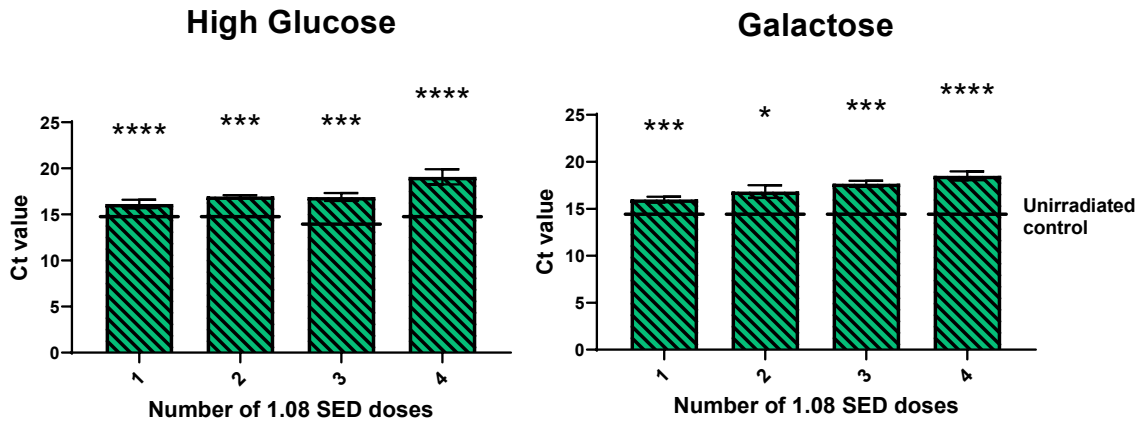

Figure 4-14. Daily increase in mtDNA damage in 11 kb region at 0 hours post 1.08 SED solar irradation each day.
Doses 1 and 4 from previous experiments, data from 2 and 3 taken from separate experiment and each condition compared to individual controls (indicated on each bar as black line); n=3. Statistical differences between doses determined by two-tailed unpaired t-test to control; *p<0.05, ***p<0.001, ****p<0.0001; data represents mean±SD.

Figure 4-14 shows the mtDNA damage from daily doses of 1.08 SED, which were added to the previous results of 1x and 4x conditions in Figure 4-13. Each dose produced significantly higher damage in both media conditions. In cells cultured in high glucose media, this damage increased from; 1.6 Ct difference after the first dose ($p<0.0001$), both dose 2 and 3 had an increase of 2.4 Ct from control ($p=0.0003$ and $p=0.0009$, respectively) and dose 4 had 4.5 Ct increase in mtDNA damage ($p<0.0001$). When cultured in galactose media, dose 1 increased by 1.7 Ct ($p=0.0002$) followed by 2.4 Ct increase at dose 2 ($p=0.0119$), 3.2 Ct at dose 3 ($p=0.0002$) and 4.1 Ct at dose 4 ($p<0.0001$). This shows that after chronic dosing, cells cultured in high glucose and galactose media have a similar increase in mtDNA damage per dose, and an increase in damage every day.

4.4.5 mtDNA increases over 24h in high serum media following solar irradiation

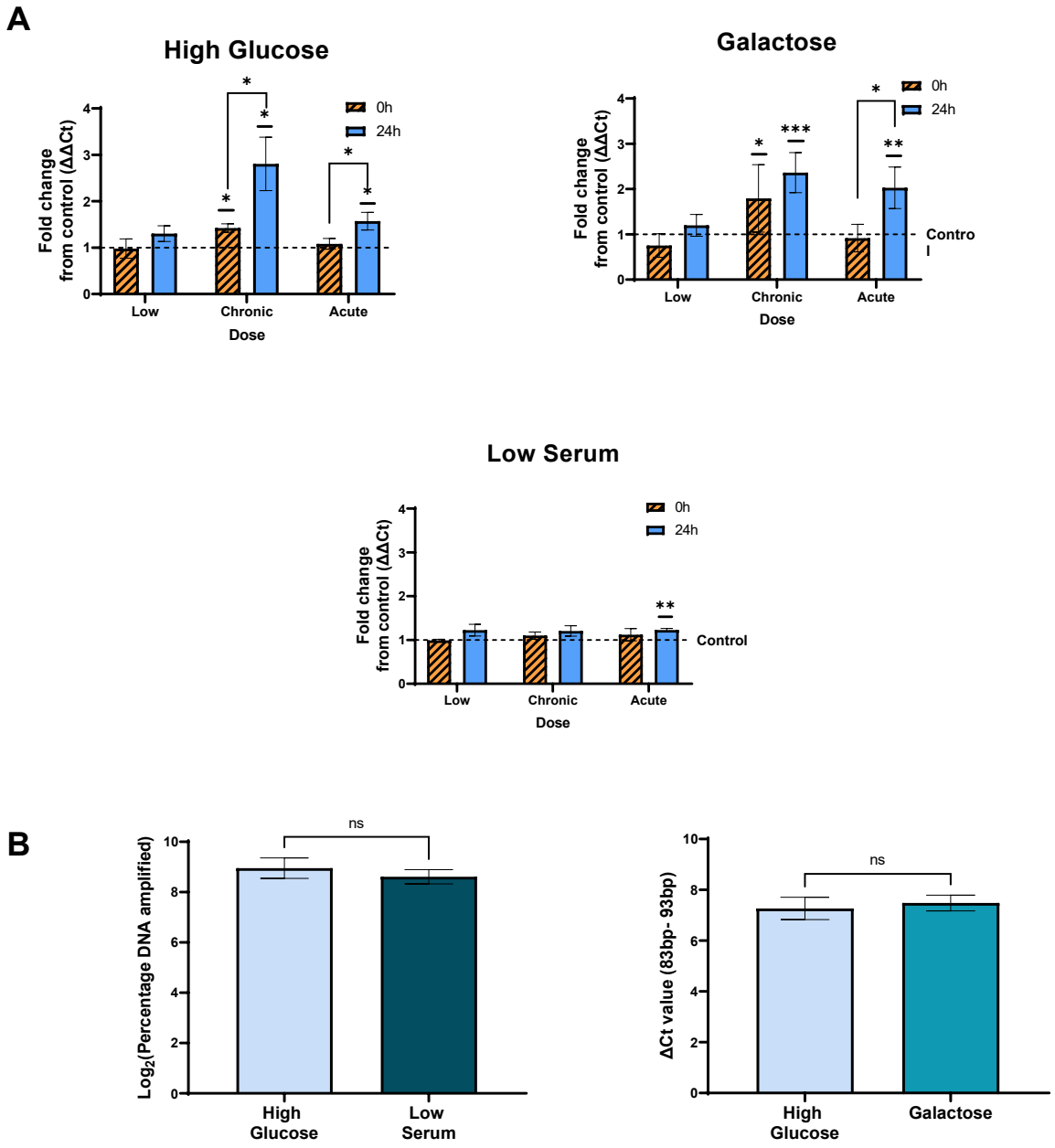

Figure 4-15. Mitochondrial copy number analysis.
Samples from Figure 4-13 rediluted and 83 bp mtDNA and 93bp nDNA housekeeping qPCR assays performed on the same dilutions. A) Effect of dosing on mtDNA copy number change from control; High glucose media n=3, Galactose media n=5, Low serum media n=3; *p<0.05, **p<0.01, ***p<0.001, ****p<0.0001; Statistical differences between treatments by one-way ANOVA on log2 transformed data, one sample t-test to control, and between time points by unpaired t-test. B) Comparison between controls in each growth medium. High glucose medium and low serum were run with standard curve, analysis represents the difference in percentage amplification between 83 bp and 93bp assays, n=6; galactose (n=4) and high glucose (n=2) were run on the same plate, analysis represents change in Ct value between the 83 bp and 93bp assays; Statistical differences between media conditions by Welch's unpaired t-test; data represents mean±SD.

Mitochondrial copy number was affected by both dose and media condition (Figure 4-15A). mtDNA content did not change significantly from control at 0h when cultured in low serum media, though at 24 hours after the acute dose this increase from control by 1.22 ($p=0.006$). Chronic dosing in high glucose medium condition resulted in a 1.44 times increase in mtDNA compared to the control at 0h ($p=0.012$) which increased to 2.8 times at 24h ($p=0.012$), this was a significant increase over the 24h period ($p=0.019$). The acute dose also had a 1.45 increase in mtDNA over 24h ($p=0.019$), which was significantly greater than control at 24 hours ($p=0.026$). The low dose had no change at either time point.

Cells grown in galactose media had a 1.79 times increase in mtDNA at 0h after a chronic dose compared to the control ($p=0.038$), this remained elevated at 24 hours with a 2.38 times increase from control ($p=0.008$), although there was no significant change between the two time points. At 24h post exposure, the acute dose had a 2.02 times increase ($p=0.004$), this was significantly increased from mtDNA at 0h ($p=0.007$).

Comparison between the control groups in each media condition found no difference in mtDNA copy number between the galactose and the high glucose culture conditions ($p=0.517$) or between the high glucose and low serum condition ($p=0.128$) (Figure 4-15B).

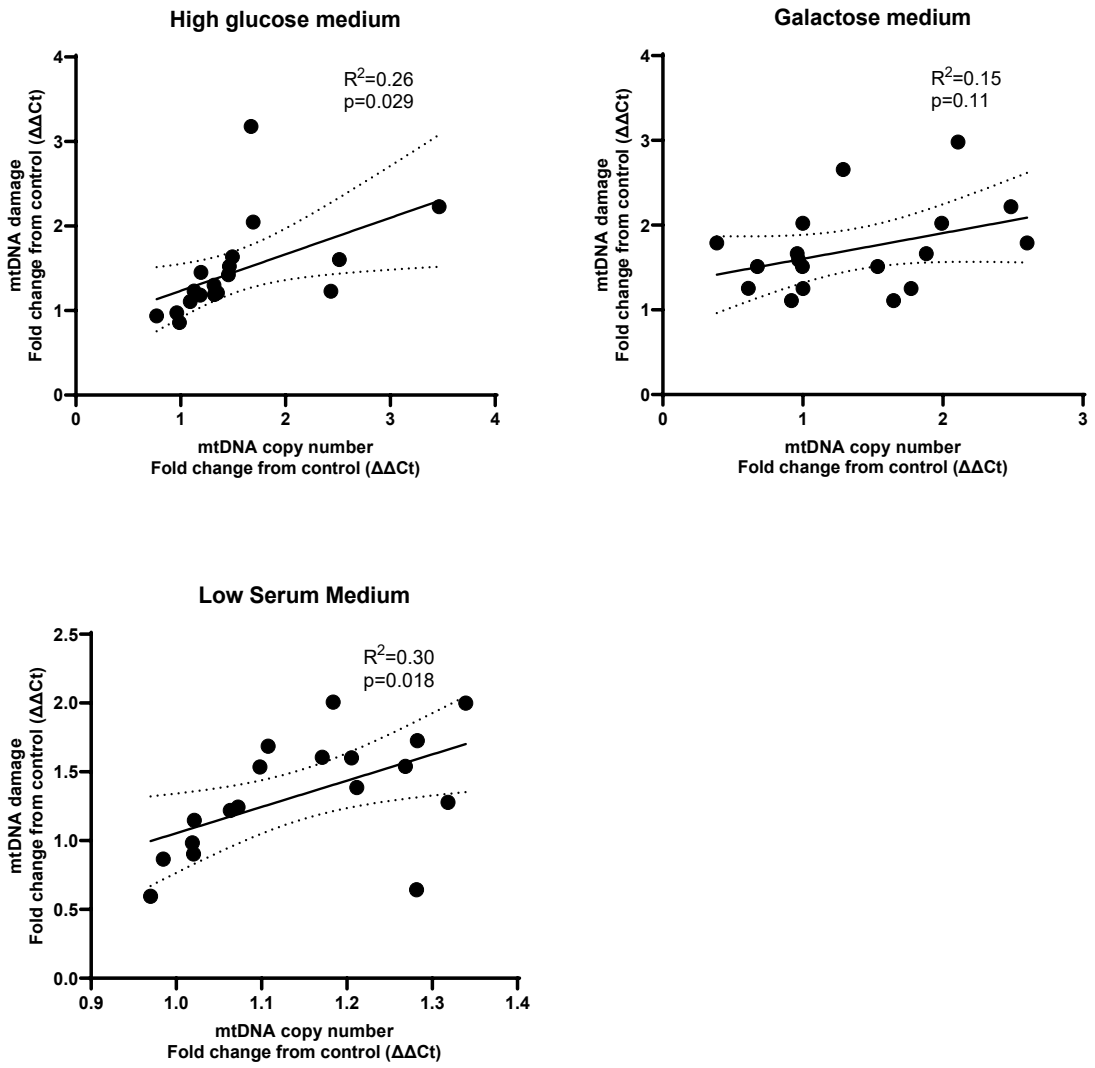

Figure 4-16. Linear regression between fold change mtDNA damage and mtDNA copy number analysis.
Graphs include data from all dosing conditions (chronic solar dose equivelant to 1.08 SED of solar simulated light each day for 4 days, low dose equivalent to a single 1.08 SED dose on the final day, acute dose equivalent to 4.32 SED solar simulated light on final day). High glucose media condtion equals 25mM glucose DMEM with 10% FBS, glactose equals 25mM galactose in glucose free DMEM with 10% FBS and low serum equals 25mM glucose DMEM with 2% FBS. Statistical differences by Pearson's correlation of $\log_2$ transformed data; data shown as mean±95% CI; n=18.

There appeared to be a similar pattern between the fold change in damage and mtDNA copy number so this was investigated further by linear regression (Figure 4-16). A signifcant correlation was found in the high glucose media ($p=0.033$, $R^2= 0.26$) and the low serum media ($p=0.018$, $R^2=0.3$), but not in the galactose media ($p=0.114$, $R^2= 0.14$).

4.4.6 New primer designed with reference in the coding region

The 83 bp reference region has been used to determine mtDNA copy number in many publications (O'Hara et al., 2019, Hsieh et al., 2018). The correlation between mtDNA copy number using the 83 bp assay and the damage profile of the 1 kb assay was concerning; the apparent damage could be due to a true effect of mtDNA replication occurring simultaneously with damage, an effect of normalisation using a housekeeping amplicon in the non-coding region or an effect of the target amplicon. Previous publications have used the D-Loop region to quantify replication status of mtDNA using a D-loop:ND1 ratio (Grünewald et al., 2016), this method could come with its own pitfalls as the ND1 gene lies within the 3895 bp deletion region. However, other research has supported the D-Loop region as a replication status marker with up to 1.5 fold increase in mtDNA copy number found when using the D-loop over other genes in the mitochondrial genome of rats (Li et al., 2018).

To investigate this relationship further, new primers were designed to span the boundary between the Cytochrome B gene and the tRNA threonine (mt-TT) gene. This region is not affected by either the 4977 bp common deletion or the 3895 bp deletion and is outside the D-loop. Primers were designed using the Primer3 tool in Benchling. The region of interest was entered, and the parameter set to find product size of 80-90 bp and Tm of 55-65˚C with an optimum of 60˚C. An 88bp region was selection spanning 15874-15961 nucleotides with annealing temperature calculated using ThermoFisher's online tool to be 63.3˚C and 60.4˚C for the forward and reverse primer, respectively. This chapter only concerns human fibroblasts in cell culture, but further chapters use the 83 bp reference gene for skin cells obtained through skin swabs. The skin was swabbed with 70% ethanol wipes but cannot guarantee that the skin microflora would not be taken up with the sample, it was therefore necessary to determine the specificity of the primers for human mtDNA against known taxonomy orders of microorganisms found in the skin's microbiome (Timm et al., 2020, Tutka et al., 2020).

Order	Common Genus found in skin
Bacteria	
Firmicutes	*Staphylococcus; Streptococcus*
Proteobacteria	*Escherichia; Roseomonas*
Actinobacteria	*Corynebacterium; Cutibacterium*
Bacteriodetes	*Prevotella; Chryseobacterium*
Fungus	
Eurotiales	*Penicillium; Aspergillus*
Capnodiales	*Cladnosporum*
Mucoromycota	*Mucor*

Table 4-3. Order of Bacteria and Fungus and common Genus found in skin samples

Figure 4-17. Nuclear targets of HKBT 1 and 2 primers and corresponding mismatches

Results of NCBI primer blast search had no complete matches to any bacteria within the search (Table 4-3), nor any partial matches below 1000 base pairs. A broad search was used to determine any other off target products without a specified organism, with no products found. Nuclear mtDNA segments occur when cytoplasmic mtDNA transposes into the nuclear genome, partial targets on chromosomes 3, 5 and 17 with 3-5 mismatches per primer (Figure 4-17); there was a possibility this could amplify as an unintended target meaning an upper limit of 3 additional mtDNA copy number could be amplified per nuclear genome.

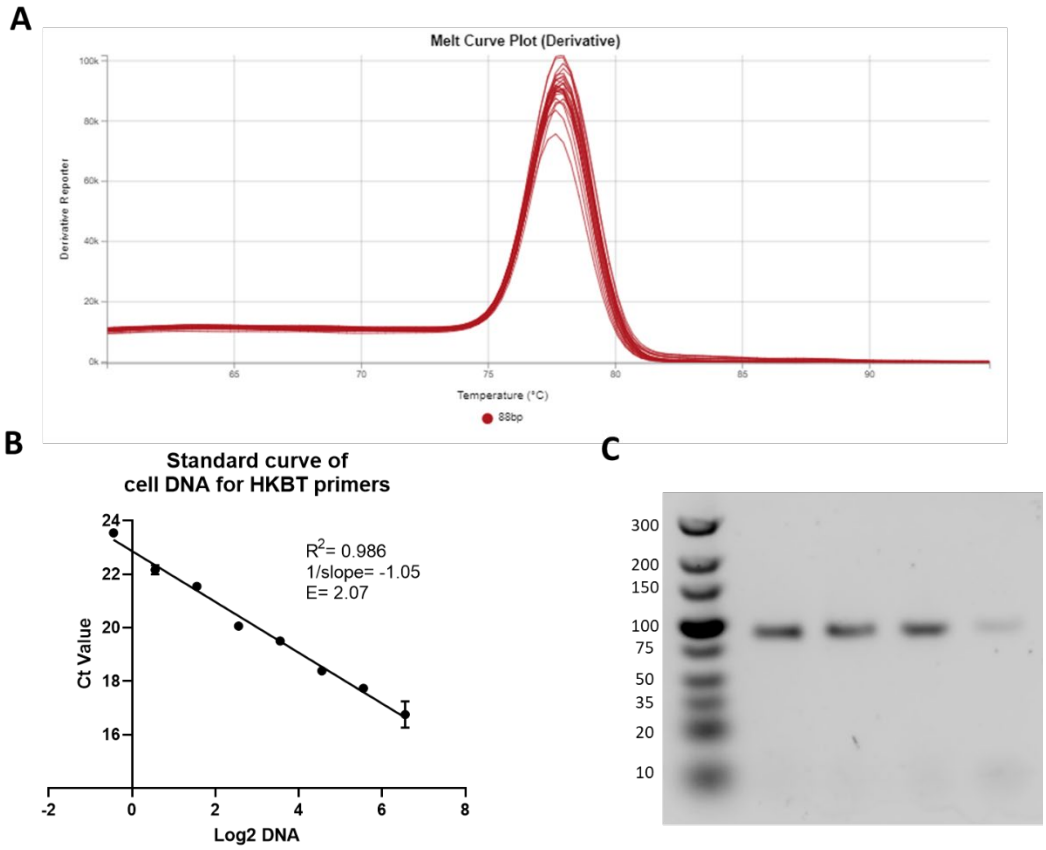

Figure 4-18. Analysis of HKBT primers.
A) Melt curve of qPCR analysis. B) Standard curve of 1:2 serial dilution with simple linear regression analysis. C) Gel electrophersis of PCR product of four dilutions of same sample 100 ng, 50 ng, 25 ng and 12.5 ng from right to left (size 87 bp).

Primers were checked for efficiency and specificity using a 1:2 serial dilution of whole cell DNA in a range of 100 ng to 0.78 ng. QPCR results showed a single melt curve peak at 79˚C confirming a single PCR product (Figure 4-18A) and the Ct values were plotted against Log_2DNA concentration (Figure 4-18B), primer efficiency was calculated to be 107%. The PCR product was confirmed to be a single product with a band size of 88bp using gel electrophoresis (Figure 4-18C).

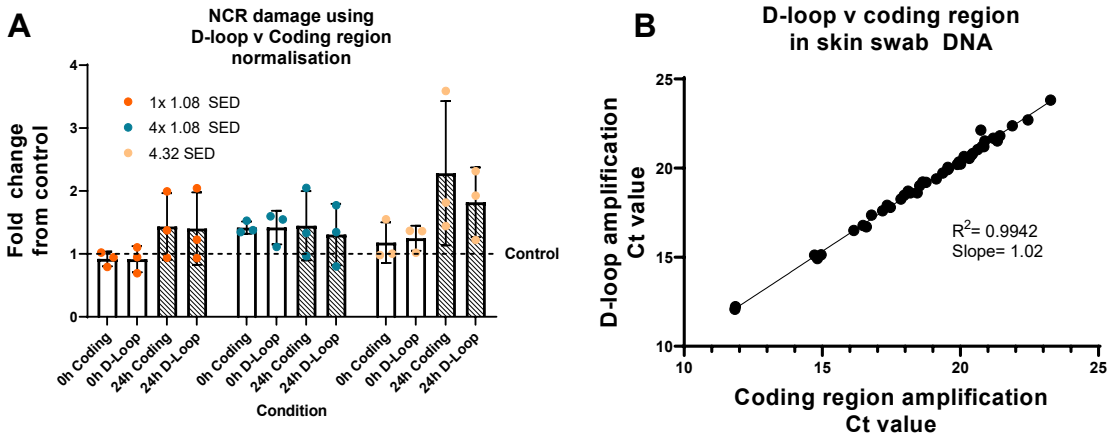

Figure 4-19. Comparison between D-loop and coding region as housekeeping for mtDNA copy number. A) Comparison of 1 kb NCR strand break assay when normalised to D-loop and coding region housekeeping; no significant differences found after normalisation between the D-loop and coding region. Samples were stored at -20˚C for 1 year between experiments; housekeeping and subsequent strand break assay were performed on the same sample dilutions. Statistical differences determined by one-way ANOVA on log2 transformed data; data represents mean±SD. B) Ct value comparison between the D-loop and coding region of skin swab DNA; n=40 including 4 independent samples (from 4 body sites: 2 upper inner arm, left cheek and right cheek) in 10 participatants; statistical analysis performed by simple linear regression and both assays were run on separate plates.

To check the 1 kb strand break assay results were not influenced by replicative status of the mtDNA during the normalisation process, samples were rerun using the new HKBT primers then the same dilutions were amplified by the 1 kb assay. Both results were transformed into fold change of damage using the ΔΔCt method (Figure 4-19A). There was no significant difference between results normalised by housekeeping regions in the D-loop or the cytochrome B/mt-TT gene coding region, therefore it was concluded that the results for the mtDNA copy number were accurate. To confirm the housekeeping DNA results were not influenced by the amplicon region in skin swab samples, the D-loop region Ct value was compared to the coding region in 40 independent samples (Figure 4-19B). The slope of the line after linear regression was equal to 1 (R^2= 0.99), which confirmed both amplicon regions were comparable.

4.4.7 Short chronic dosing does not lead to increase in common deletions

Optimisation of both deletion markers was carried out on positive controls. The 4977 bp marker used a plasmid of the break point and the 3895 bp used a positive control from a patient sample, both controls had been previously validated (Latimer, 2013). Both primer sets were run on the same plate, using the same reaction mixture and run method; 4977 used a range of 1 ng to 0.001 ng in 1:10 dilution and 3895 a range of 100 ng to 6.25 ng in 1:2 dilutions (due a lower starting

concentration and finite sample). Serial dilutions confirmed high efficiencies of both primers, but low level of deletion in the 3895 bp control sample (Figure 4-20A).

The fragment size was confirmed on a 3% TBE agarose gel, 108 bp single band was detected for the 4977 bp (Figure 4-20E) and 131bp for the 3895 bp deletion (Figure 4-20C). Both qPCR runs have 40 cycles and it is clear that any amplification it picks up is low level; for each sample the 3895 deletion had a Ct value in the late 20s and there was no signal for the 4977 before 30 Ct with high standard deviation between replicates.

The 4977 positive wells are sporadic between and within the samples which suggests there is some presence of the 4977 deletion in cells, but the level is so low it cannot be evenly distributed in the sample during dilution. The PCR products of 4977 bp deletion assay were run on a gel with corresponding Ct values shown to determine a cut-off Ct value for true amplification (Figure 4-20D and E). It is not unusual to pick up some of this deletion in a normal population, so it was determined that positive amplification was not induced by the treatment conditions.

The 3895 deletion results had low standard deviation between wells ($SD<0.2$); only a treatment independent decrease in deletion was detected over 24 hours within the high glucose medium condition, but with borderline significance ($p=0.05$) (Figure 4-20B). No other significant differences were found between media conditions, treatments, or time.

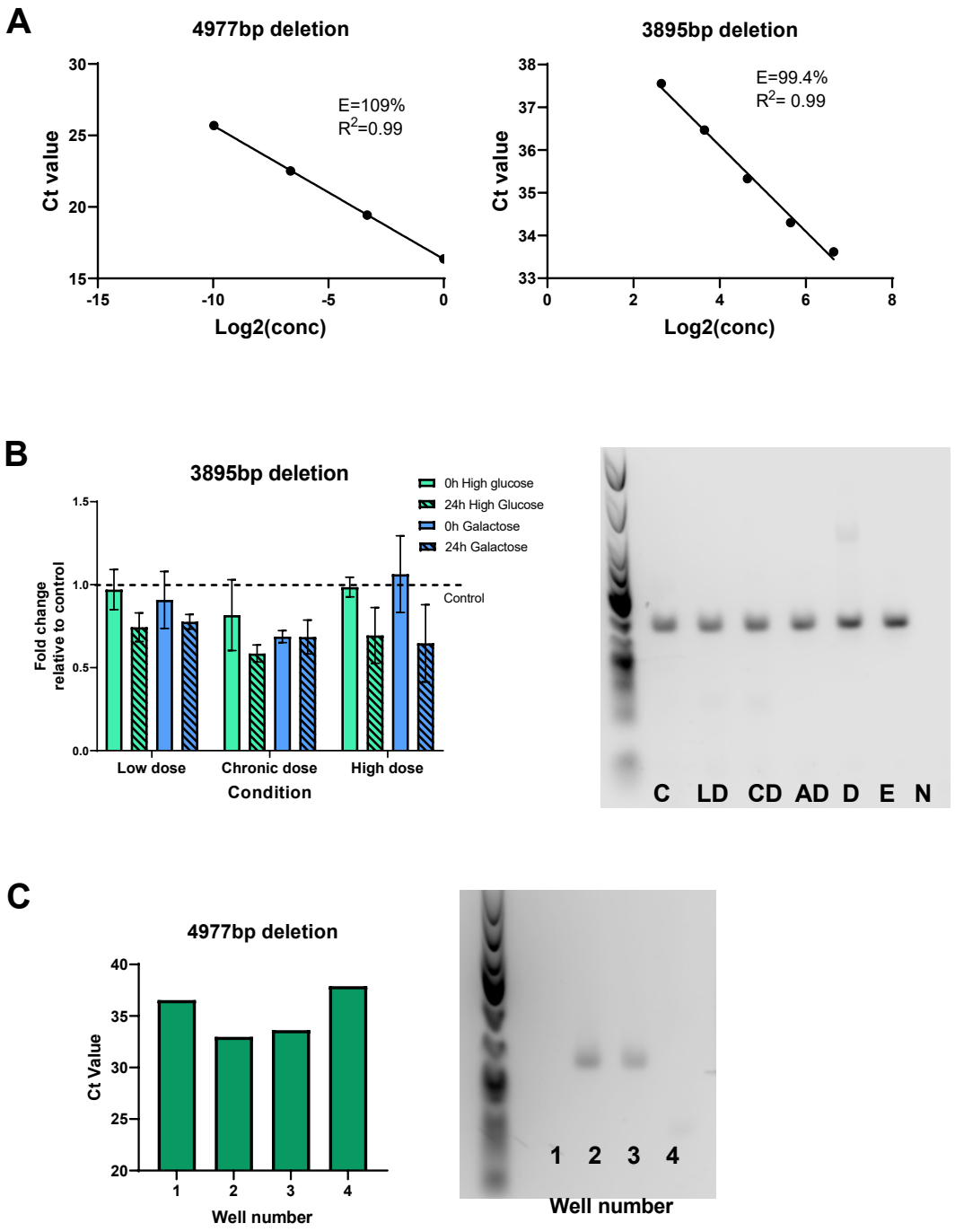

Figure 4-20 Analysis of common deletions using qPCR.
Serial dilutions of 4977 and 3895 primers with respective efficiencies (E) and R^2 values. B) Results for 3895 bp deletion qPCR assay using samples from 11 kb test (Figure 4-13) and gel confirmation of 131 bp qPCR product; data plotted as mean ±SD; statistical differences were determined within media conditions by factorial measures ANOVA, and between media conditions by one-way ANOVA, of log2 transformed data; n=3-4; C=control. LD= low dose, CD= chronic dose, AD= acute dose, D= dermis control sample, E= epidermis control sample, N= negative control. C) Ct value of samples from specific wells in 4977 qPCR assay and corresponding gel of matched qPCR product.

4.4.8 Preliminary correlations between ROS production and mtDNA damage

The flow cytometry and qPCR data were plotted against the change in mtDNA damage over a 24h period. Neither the acute dose nor chronic dose had any correlation between change in mtDNA and ROS production in the 1 kb, non-coding region ($p>0.5$ for all combinations) Figure 4-21A and B). An increase in whole cell ROS (DCF-DA) following the acute dose had a significant effect on change in mtDNA damage in the 11 kb, coding region; lower levels of whole cell ROS appear to have a reduction of mtDNA, but higher levels see an increase in mtDNA damage over 24h ($p=0.0166$). A borderline significance was seen with the chronic dose; increasing damage over 24h appears to coincide with increasing superoxide (MitoSOX) production ($p=0.069$). However, there is only one point that is out-with a cluster of all other data point causing the slope to increase, so more data would be needed to understand if this is a true correlation (Figure 4-21D).

Overall, only the change in damage in the coding region has any correlation with ROS production. Increasing whole cell ROS could have an effect on the cells ability to repair/remove damaged DNA, superoxide may also have a correlation with change in damage in this region. More data would be required to confirm these effects, but it is an interesting observation.

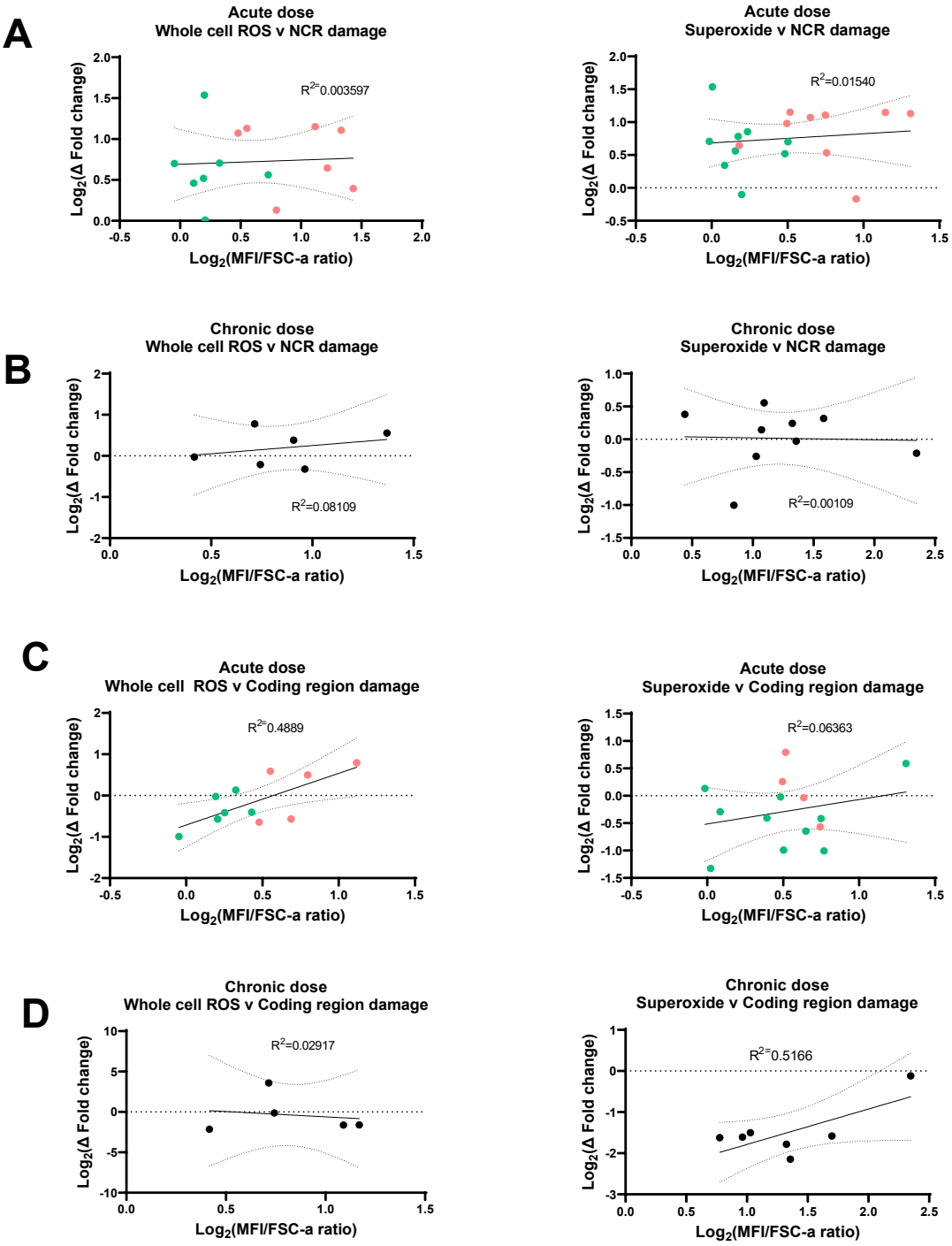

Figure 4-21. Correlations between ROS production and mtDNA damage in all media conditions. A + B) mtDNA damage in the D-loop region (1 kb). C+D) mtDNA damage in the coding region (11 kb). Acute dose where both the 1.08 SED low dose (●) and 4.32 SED large acute dose (●) are plotted together; Δ fold change= 24h fold change- 0h fold change; statistical differences determined by simple linear regression; data presented as mean±95% CI.

4.5 **Discussion**

4.5.1 Cells in 2% FBS have characteristics consistent with a quiescent state

MTS manufacturer information suggest the colorimetric assay occurs through the reduction of tetrazolium compound by NAD(P)H-dependant dehydrogenase enzymes in metabolically active cells, producing a formazan product which is soluble in cell culture medium. NAD(P)H dependant dehydrogenases are important for lipid metabolism and nucleic acid generation and NADH dependant enzymes are involved in mitochondrial respiration, both integral to cell proliferation. Serum deprivation with 0.1% FBS is regularly used to synchronise cells by inducing a G_0 state and forcing the cells into a reversible quiescence, which dermal fibroblasts have been found to tolerate without apoptosis for up to 30 days (Pollina et al., 2008). In this state, primary HDFn cells have been shown to divert glucose to the pentose phosphate pathway resulting in upregulated activity (Lemons et al., 2010). This pathway is involved in the generation of NADPH and can contribute to an increase in NAD(P)H-dependant dehydrogenase activity in the reduced serum cells. Lemons et al. (2010) further found an increase in fatty-acid and protein degradation which would reduce the accumulation of unutilised cellular components, and an increase in both the concentration of reduced glutathione and ratio of reduced to oxidised forms which suggests a lower level of and an increased capacity to withstand oxidative stress.

High serum concentration (10%) has been found to reduce the absorbance of MTS (Huang et al., 2004), whereby BSA in the FBS binds to formazan and reduces the absorbance. The observation that low percent FBS increased survival during the MTS assay could be due to the cell cycle state the cells are in prior to the assay, and low serum cells in a G_0 state may be sensitised to toxicity.

Taken together, the increase in MTS metabolism despite a decrease in cell number at 2% FBS show cells behaviour is consistent with a quiescent state, which could provide protection against oxidative stress. This also suggests that using MTS as a measure of cell viability and proliferation in response to cytotoxicity, of which it is marketed, may not provide accurate results if the cells have entered a quiescent state in response to treatment. BirdU staining could be a more appropriate marker of cell proliferation, as it incorporates into the DNA during S-phase of replication it would account for quiescence.

4.5.2 Effect of growth condition on ROS production and mtDNA damage

4.5.2.1 Stress response to solar light is significantly altered by media condition

This experiment compared cell culture conditions on stress and mtDNA damage in response to solar light. Metabolic state was altered by culturing cells in regularly used high glucose media compared with galactose media containing no glucose, and the effect of continuous replication was explored by reducing the percentage of FBS. Different methods of solar light stress were also compared by treating cells with low, chronic, and acute doses of solar irradiation. This is the first study of its kind to directly research the effect of media condition on dermal fibroblast ROS productions and mtDNA damage in response to solar light.

Increased ROS production in galactose media compared to high glucose is indicative of increased mitochondrial function, and a switch to mitochondrial metabolism. By keeping a high glucose concentration in culture media, metabolism is maintained through glycolysis and does not use mitochondrial oxidative phosphorylation for energy. Replacing the glucose in cell media with galactose has been found to increase basal and maximal mitochondrial respiration, ATP production, and proton leak (Pereira et al., 2018). Similarly, dermal fibroblasts with and without mitochondrial dysfunction cultured in galactose medium show an increase in HE_t (superoxide specific probe) oxidation compared to high glucose medium, and mitochondrial dysfunction caused increased HE_t oxidation in both media conditions compared to control cells (Voets et al., 2012). The increase in basal hydrogen peroxide production shown in the galactose medium of this study agrees with this. There was no obvious increase in superoxide which could reflect the low MitoSOX fluorescence/ background ratio; Voets et al. (2012) used microscopy to determine fluorescence which would have a different sensitivity of detection. Alternatively, this could be due to an increase in superoxide conversion to hydrogen peroxide, specifically superoxide dismutase 2 activity could be upregulated as an adaptive response to increased mitochondrial oxidative stress in galactose medium which would contribute to the increase in basal hydrogen peroxide.

Interestingly, both acute and chronic stress resulted in a greater increase of superoxide production in the high glucose condition, which does not agree with the hypothesis that induced mitochondrial metabolism would lead to greater ROS. This could be a result of increased cell signalling, a decreased capacity for mitochondrial stress in high glucose medium, or that cells in the galactose medium and low serum media conditions had upregulated antioxidant enzymes due to increased oxidative stress in their growth environment. The latter could also be evidenced by the similar increase in mitochondrial superoxide and whole cell ROS in response

to chronic stress in these conditions, while cells in high glucose media have a significantly greater production of mitochondrial superoxide compared to whole cell ROS. High glucose in dermal fibroblasts has been researched quite extensively in the study of diabetic hyperglycaemia, and specifically the wound healing response which is impaired in high glucose conditions. Compared to 5 mM glucose, treatment of fibroblasts in 25/30 mM glucose had a significant increase in DCF-DA ROS production (Xuan et al., 2014) and an increase in catalase but not superoxide dismutase (SOD) production (Buranasin et al., 2018), all of which suggest overall cellular stress but not necessarily mitochondrial. Furthermore, quiescent cells were found to have elevated SOD2 activity over proliferating cells in two cells types (umbilical vein cell (EA.hy926) and breast epithelial (MCF10a)) with an increase in OXPHOS activity, while glutathione peroxidase was only elevated in EA.hy926 (Blecha et al., 2017). Furthermore, SOD2 has been shown to increase proportionally as the percentage of cells in S-phase decreases, but SOD1 levels remained consistent (Sarsour et al., 2005). From previous studies, it is clear that there is increased mitochondrial activity and stress in the galactose and low serum media condition which could have primed the cells for further mitochondrial stress; but there is also OXPHOS independent stress in high glucose media.

Cells cultured in 2% FBS had elevated whole cell ROS in response to acute dosing, but overall did not have the same loss of cell viability or mitochondrial membrane potential that the two high serum conditions had. Interestingly, the 2% FBS media condition had a similar damage response in the 1 kb region of the mtDNA that the 10% FBS (high glucose media) condition but did not have any resulting change in mtDNA copy number after dosing. Previous studies have shown mtDNA copy number in primary dermal fibroblasts does not change when cells have been in a quiescent state for 10 days (Franzolin et al., 2015), which is consistent with the copy number analysis in this study. This suggests that the increase in copy number over 24 hours post exposure in high serum compared to low serum is independent of initial copy number or initial damage to the mtDNA. Alternatively, the change in seeding density could alter the response between the two conditions. Previous work in keratinocytes has found that cells with higher seeding density respond to low doses of solar light differently than low densities (Zanchetta et al., 2010), though keratinocytes and fibroblasts have different stress responses to solar light (Hudson et al., 2020). This could affect the response observed in the chronic dosing condition as the initial dose in 10% FBS media had a low density compared to the initial dose in the 2% FBS. However, the low and acute doses were seeded to ensure a

similar density between the two media conditions when irradiated on the final day so was unlikely to be the cause of the differences observed these dosing conditions.

4.5.2.2 Differences between 1 kb and 11 kb assay

The mitochondrial D-loop has been found to have increased lesion/10kb DNA in response to H_2O_2 compared to coding regions in neuroblastoma cell lines (Rothfuss et al., 2009), and mouse brain and liver cells (Gureev et al., 2017); showing that the non-coding region in multiple cell types has an increased sensitivity to oxidative damage. However, there is also research that shows that amplification in the non-coding region can be disrupted during mtDNA replication (as discussed in 4.4.6). Our in-house data, amplifying regions of mtDNA 1 kb in size, shows that the increase in damage over 24 hours in response to an acute dose is not specific to the non-coding region, and only 3 regions had a significantly reduced level of damage compared to the non-coding region (unpublished data). Therefore, the difference in results between the 11 kb and 1 kb assays is either due to the size of the amplicon or polymerase stability.

The 1 kb assay master mix uses only a *taq* polymerase, whereas the 11 kb assay master mix incorporates two polymerases; *taq* polymerase with no proofreading ability and *tgo* polymerase with potent 3' to 5' exonuclease activity, determined to produce DNA copies three times more accurately than *taq* alone. DNA templates with 8-oxodA bases, thymidine dimers or abasic lesions have been shown to significantly reduce the amplification efficiency of *taq* polymerase in the early cycles of PCR, resulting in an increased cycle threshold (Sikorsky et al., 2004); while abasic lesions have been shown to reduce the efficiency of *tgo* polymerase, thymidine dimers completely inhibit it with no extension past the lesion (Jozwiakowski et al., 2014). Therefore, the large initial increase in damage after an acute exposure in the 11 kb region could be due to thymidine dimers, as they form immediately after exposure to UVR and have been found to decline in mtDNA over 24 hours in immortalised epidermal (HaCaT) cells after 1 SED dose, this did not coincide with a reduction in mtDNA content (Alhegaili et al., 2019). mtDNA has not been found to have a nucleotide excision repair mechanism capable of repairing thymidine dimers, theorised that unless the mtDNA is synthesised at the same rate of mitophagy, another unknown repair mechanism could be responsible for the reduction in damage over time. Overall, this is an interesting observation as it suggests that the damage quantified from the 1 kb assay could be more specific to oxidative stress and double strand breaks, with the increase in damage over 24 hours indicative of the former. The 11 kb assay is additionally more sensitive to pyrimidine dimers, and the decrease in damage over 24 hours is

either due to selective mitophagy or an unknown mechanism for removal of the dimers. Furthermore, the H-strand replicates before the L-strand and gets displaced by the daughter strand until L-strand synthesis, the whole process takes around 75 mins to 2 hours which would suggest that some portions of the mtDNA could be more abundant for a portion of replication (Holt and Davies, 2020, Korr et al., 1998).

4.5.2.3 Cells undergoing oxidative phosphorylation have more oxidative damage to mtDNA in response to solar light

The greater increase in damage in galactose media compared to high glucose media in response to chronic dose shows that the switch to OXPHOS results in an increase in mtDNA damage, which could be linked to oxidative stress post exposure. The increase in damage over 24 hours post exposure is also consistent with oxidative damage rather than direct damage from UVR exposure as the damage continues to increase after exposure. This data also suggests under induced mitochondrial metabolism conditions the cells could significantly reduce mtDNA damage, which would be necessary as their only mechanism of energy production relies on functional mitochondria. Human dermal fibroblast cell line cultured in galactose media compared to high glucose media have previously been found to have a significant increase in basal mtDNA copy number, and a decrease cell vitality in response to mitotoxicity (Pereira et al., 2018), this was not replicated in this study, which could be due to differences between the BJ cell line and the HDFn cells used in this study. Though both derived from neonatal foreskin origin, BJ cells (CRL-2522, ATCC) have been immortalised and found to have a greater capacity for oxidative stress, a longer lifespan than other fibroblast cell lines; BJ cells are also telomerase negative which could explain differences in results between the two studies. Research in adult primary fibroblasts have shown no difference in mtDNA copy number when cultured in galactose compared to high glucose medium (González-Casacuberta et al., 2019). The correlation between mtDNA copy number and damage in the two high glucose mediums (high and low serum), and the lack of correlation in the glucose media, could point to different mechanisms of mtDNA damage accumulation/ repair. This would have to be investigated further; proposedly though microscopy analysis of mitophagy and double strand breaks.

4.6 **Limitations of study and future work**

MitoSOX and DCF-DA have their limitations as specific ROS markers, this has been reviewed previously (Kalyanaraman et al., 2012, Dikalov and Harrison, 2014). Importantly, DCF-DA is prone to artificial amplification by formation of superoxide under one electron oxidation

conditions (two electron oxidation is required for the fluorescent compound); it does not directly react with hydrogen peroxide and can be oxidised by other ROS and NOS; and it reacts with cytochrome c and increases fluorescence during apoptosis. MitoSOX is superoxide specific, however it can also undergo a separate reaction with other oxidants to produce a different red fluorescence with overlapping emission spectra. Furthermore, superoxide is readily dismutated to hydrogen peroxide, where it can then cross the mitochondrial membrane into the cytoplasm making it difficult to measure (Reviewed by Di Marzo et al. (2018)). ROS markers are never completely specific due to the similarities in reactivity and dynamic formation of different species, but with the limitations taken into consideration they can prove a good indicator of mitochondrially specific superoxide (MitoSOX) and a whole cell ROS indicator when used with an apoptosis marker (DCF-DA).

While the overall number of biological repeats is high enough for good statistical analysis, the repeated measures between the flow and qPCR data is lacking due to experimental failure at some stages during the repeats. Therefore, the correlation data can only show trends and not statistically valid results. Future work would involve extending this part of the study to collect more repeats and increase the power. Furthermore, this project quantified ROS production immediately after solar irradiation but a continuation of this experiment would include more time points for both ROS and mtDNA damage to evaluate this relationship in more depth. This would determine the length of time ROS is elevated post irradiation influences mtDNA damage. Additionally, the low serum experiment was carried out after the high glucose and galactose media, therefore there was no control comparison for basal ROS which would have been beneficial.

This study aimed at comparing mtDNA damage and stress in the normal fibroblast growth medium against that which induced OXPHOS and a medium to reduce cell growth. It would benefit from including a low glucose medium condition that is physiologically comparable with blood serum levels to find the true effect of high glucose medium on cells during experiments of this type.

It would also be of interest in the future to probe the mechanism behind the decrease in mtDNA damage seen in the galactose media. This could be achieved by quantifying specific markers of DNA damage, such as double strand breaks (γH2AX) and thymine dimers by immunolabelling; and western blot and microscopy analysis of mitophagy, fission and fusion using the techniques in chapter 6. The reduced serum condition had a similar damage profile in response to solar light as the high serum cells in high glucose, further work to determine the

response of low serum in galactose media would have been a beneficial addition to this study as it could determine if the similar damage profile was due to glycolysis, and if OXPHOS cells would have a different response with reduced growth.

4.7 **Summary of main findings**

- Comparison between media conditions found that high glucose DMEM with 10% FBS as a standard growth condition could show increased levels of ROS, reduced mtDNA damage to solar light and impaired reduction of specific mtDNA lesions.
- Cells cultured in galactose media were sensitive to oxidative stress, but also showed significant reduction of some mtDNA damage over 24 hours
- Reducing the proliferation of cells in high glucose media altered the ROS response to solar light, improved mitochondrial membrane potential and cell vitality in response to solar light, but resulted in the same level of mtDNA damage.
- Chronic dosing of cells increases mtDNA damage incrementally each day but results in reduced damage increase in the 1 kb region 24 hours post solar irradiation.
- Assessment of mtDNA damage is dependent on polymerase in the PCR reaction, and oxidative damage over 24 hours post exposure to single doses significantly increase mtDNA damage.

Chapter 5. Facial Ageing, Skin damage and Oxidative Stress in Patients with Primary Mitochondrial Disease

5.1 Chapter Overview

This chapter builds on the results of chapter three, four and six, by further investigating the association between facial appearance in patients with mitochondrial disease and perceived age, and the effect of sun exposure stress on skin *in vivo*.

Canfield's Visia CR skin analysis system was used to capture standardised high-quality images during the study. The technology uses pre-set lighting modes, including UV photography which can capture photo-damage in the form of melanin accumulation in the epidermis and dermis as the UVR is attenuated by melanin spots and stimulates fluorescence by collagen (Kollias et al., 1997). This method of assessing sun damage has been reported to correlate significantly with melanoma risk and has a low correlation with visible damage (Gamble et al., 2012), therefore a good marker of invisible damage and melanin production.

mtDNA damage is linked to ageing and is damaged both directly and indirectly by solar light. Assessing damage in the skin *in vivo* would previously require a punch or needle biopsy, which are both invasive and not always practical to assess facial damage. This study optimises and assesses a non-invasive method to detect mtDNA damage on the surface of the skin, as a marker of photo-damage. This method of mtDNA collection has shown a correlation between increased damage and body sites with more sun exposure (Harbottle and Birch-Machin, 2006). A further study using a less sensitive analysis method of the skin swabs found average damage to the nose decreased after holiday (3/4 groups of different sun protection groups), and increased damage had a positive correlation with sunscreen use events (Rodrigues, 2014). Experimental protocol and analysis method were optimised to improve repeatability, and the method was investigated to further understand the quality of mtDNA acquired from the swabs.

This pilot study aimed to assess the role of mitochondrial dysfunction as a predisposition to damage from sun exposure as an exogenous stressor. It was hypothesised that genetic mitochondrial dysfunction could lead to increased photoageing and mtDNA damage in sun exposed areas of the skin, and an increased perceived age due to both skin and facial muscle appearance. Alternatively, prematurely reduced muscle function could result in a reduction of mechanical wrinkle formation and therefore reduced perceived age.

Change in mtDNA heteroplasmy in MD patients is dependent on the type of variant and tissue. For example, the m.3243A>G point variant has been found to remain stable in muscle and

decrease in blood with age (Grady et al., 2018). Deletions show an advantage during replication within a cell; cells with lower heteroplasmy have increased growth due to better mitochondrial health, but heteroplasmy has been found to increase in response to ethidium bromide reduction of copy number due to positive selection of smaller molecules during clonal expansion (Diaz et al., 2002). Nuclear defects of mitochondrial replication machinery can either cause mtDNA depletion syndromes in children or present later in life with a progressive phenotype due to an enhanced burden of mtDNA deletions with age (Wanrooij et al., 2004). Clonal expansion of mtDNA arrangements is not fully understood and varies between cells. Both single large-scale deletions and nuclear defects of mtDNA maintenance are both more likely to present with ptosis (chapter three); extraocular muscles have been shown to have reduced mitochondrial function and increase deletion heteroplasmy with increasing age (Müller-Höcker et al., 1992), and dysfunction at an earlier age than skeletal muscle (Yu-Wai-Man et al., 2010). Consequently, we hypothesised that patients with single large-scale deletions and nuclear defects/ multiple mtDNA deletions could have an increased perceived age due to the presence of ptosis.

Post-mitotic cells, such as skeletal muscle, accumulate deletions with age and mitotic cells, such as skin fibroblasts, often present with fewer deletions. However, it has been hypothesised that mtDNA deletions are formed as a result of mtDNA repair as opposed to replication (Krishnan et al., 2008), and mtDNA deletions are increased in the skin in response to sun-damage and ageing (Powers et al., 2016). Furthermore, cells containing the common deletion have increased oxidative stress than wild type cells, and are predisposed to mitochondrial dysfunction in response to hydrogen peroxide (Peng et al., 2006). Therefore, direct and indirect mtDNA damage and from sun exposure could increase the level of mtDNA deletions in the skin, and dysfunction mitochondria could be more susceptible to damage from solar light.

5.2 Chapter aims

Using facial imaging along with optimised mtDNA damage and oxidative stress measurements, to evaluate the overall skin health of patients with primary mitochondrial disease compared to matched healthy controls.

- Assess the perceived age and skin age features of study participants
- Optimise and test non-invasive assessment of mtDNA damage in skin
- Investigate the connection between non-invasive markers of oxidative stress and facial skin ageing.

5.3 Chapter specific methods

5.3.1 Patient recruitment

This research has been reviewed by the North East- Newcastle and North Tyneside 1 Research Ethics Committee. The Newcastle upon Tyne Hospitals NHS Foundation Trust are the sponsor (REC Ref: 18/NE/0331). Patients were recruited sequentially from the CRESTA clinic in Newcastle upon Tyne and provided with the patient information sheet prior to arrival and informed consent was taken prior to study commencement. All participants were included if they were the age of 18 or older, had capacity to provide informed consent, and able to read and converse in English. Patients included in the study required genetic or biochemical confirmation of mitochondrial disease. Participants were excluded from the study if they had photosensitive epilepsy due to the camera flashes, or a history of full reconstructive surgery unless it was corrective for ptosis/ progressive external ophthalmoplegia.

A questionnaire was taken to provide information on confounding variables in the study, including demographic, relevant medical history, and lifestyle data (Appendix A).

		Number of patients
Point variants	m.3243A>G	9
	m.3365T>C	1
	m.8344A>G	1
	m.12271T>C	1
	m.7497G>A	1
Single large-scale deletion		7
Multiple deletions/ nuclear defects	OPA1 defect	1

Table 5-1. Overview of variants in mitochondrial disease patient cohort.

5.3.2 Facial imaging

5.3.2.1 Visia facial imaging

Images were captured using the Visia CR (clinical research) system, which used RBX® technology to visualise brown and red areas, and UV fluorescence (peak 365 nm) to visualise hyperpigmented spots. Marketing for the CR system focuses on repeatability for clinical imaging but does not include the full software for analysing the image; images were captured using the Lite version and analysis was optimised in ImageJ software for the purposes of this study.

5.3.2.2 Analysis of patient images using Visia CR system

All images (standard, UV, brown and red) were masked to remove the background, eyes, eyebrows, nostrils, and the whole lower jaw area which would contain facial hair. Analysis was performed in ImageJ software.

To obtain a value for hue, images were converted to LAB stack in ImageJ and obtained values for luminance (L*), red-green colour (a*) and blue-yellow (b*). Skin tone by Individual Typology Angle (ITA°) was calculated using the equation (Osto et al., 2022):

$$\text{ITA}° = \arctan\left(\frac{L*-50}{b*}\right) * \frac{180}{\pi}$$ *Equation 4. Individual Typology Angle*

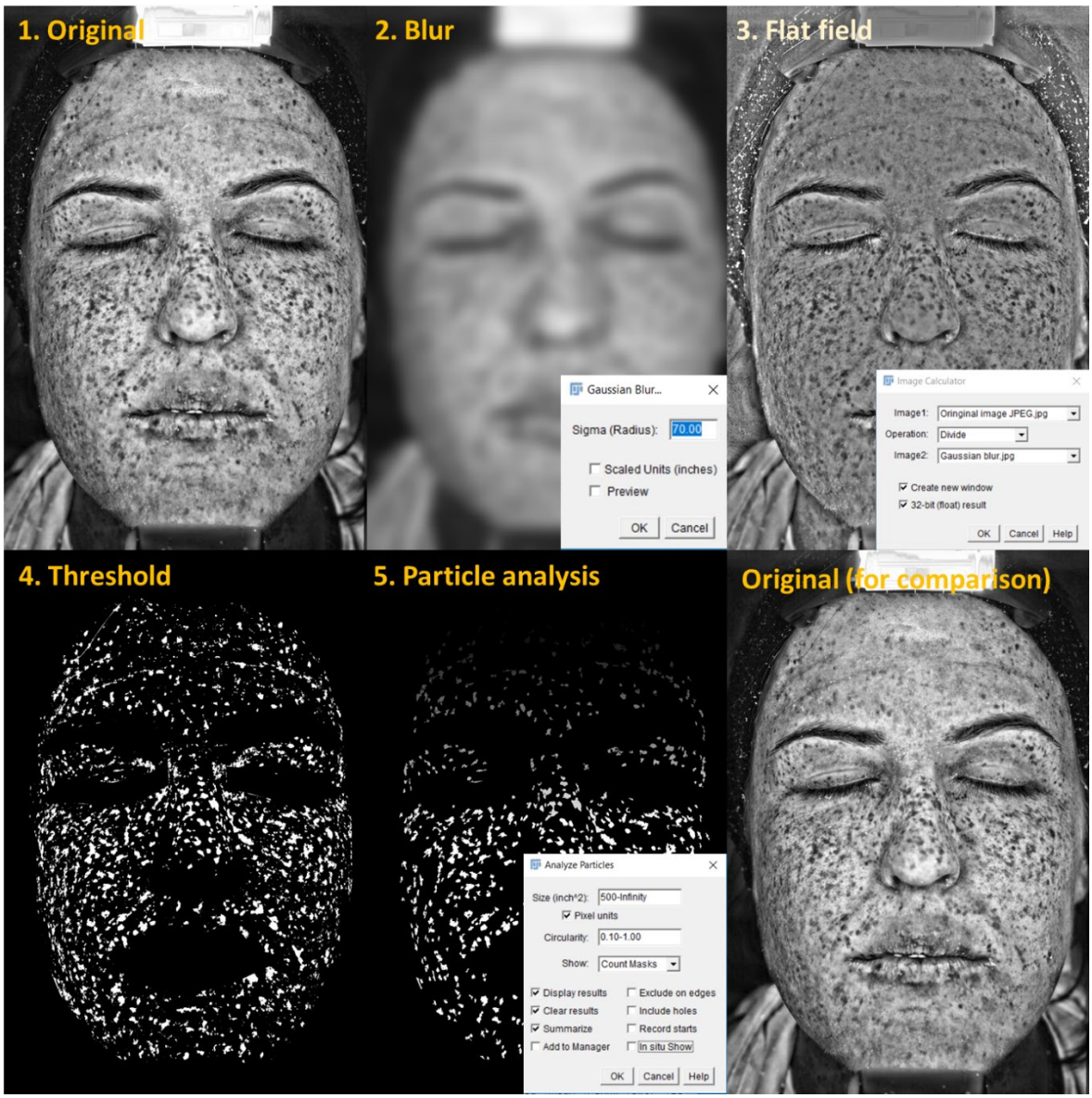

Figure 5-1. Example of particle analysis process on UV spot images.
Images are unmasked, step 4 and 5 have eyelashes, eyebrows, mouth and area around the nose masked for demonstration purposes, permission to include images by R Stout throughout this chapter. Images in JPEG format (1) have a large gaussian blur of sigma 70 added (2). The original image is divided by the blurred image to create a flatfield with no shadows (3), this image is thresholded to mark UV spots (4) and particicles are analysed with filters to remove small pores and lines (5).

Number of UV and pigmented spots were quantified using ImageJ software, using a method devised by Dr Glyn Nelson, Bioimaging department, Newcastle University, UK. Images were converted from 32-bit colour to 8-bit and flat field images were created to produce an even intensity across the face, removing shadows and highlighted areas. A large Gaussian blur was added to the original image (sigma=70) to create a mask (Figure 5-1 step 2), the original image was then divided by the blurred image to create the flat field image, and brightness and contrast was adjusted to view the dark image produced by this process (Figure 5-1 step 3).

Image threshold was adjusted to visualise dark spots (Figure 5-1 step 4), and particle analysis was run with a size range of 0.06-infinity (inch^2) and circularity of 0.02-1. These parameters were optimised to ensure all large spots were included and small spots corresponding with pores and other small artefacts were not, and all fully linear objects corresponding with wrinkles and lines were removed from analysis (Figure 5-1 step 5).

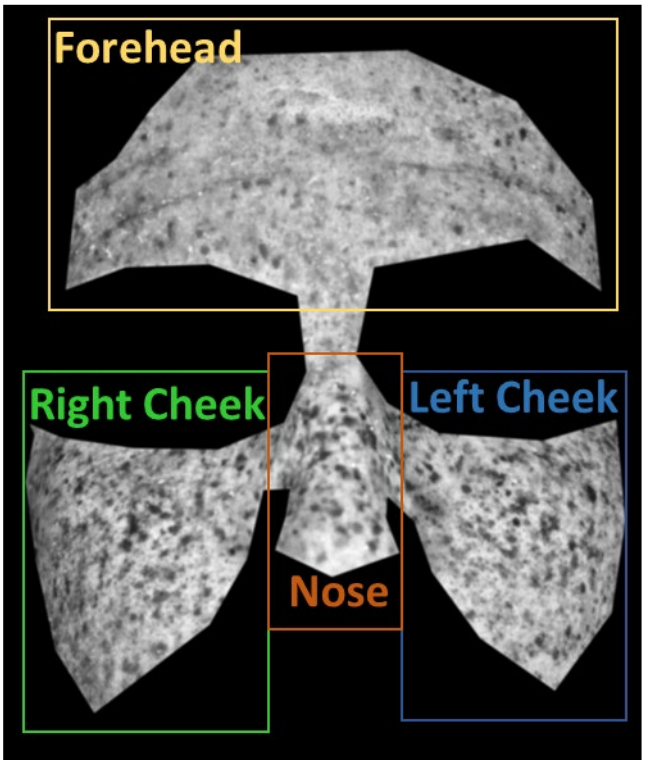

Figure 5-2. Facial regions for UV spot quantification.

After the threshold was set on each image at step 4, they were masked and different regions could be selected for particle analysis, as well as full masked images (Figure 5-2). The total number of particles was divided by the total area to normalise results, and average particle size was also included in analysis.

5.3.2.3 Perceived age assessment

Perceived age was assessed using a convolution neural network (CNN) algorithm (Cao et al., 2020), and previously validated method using naïve assessors (Gunn et al., 2008).
Participants were required to fill out a form while observing the front facing image taken in the Visia booth with eyes open. First, they were required to select an age range they perceived each patient to be before estimating an exact age within the range. Sessions with participants were conducted in person or over Zoom.

A convolution neural network (CNN) algorithm was also used to determine objective perceived age, images were saved in JPEG format and processed with the CNN. Ages were determined to 1 decimal place.

5.3.3 Skin swab and DNA extraction

Skin swabs were taken from the left cheek, right cheek, behind the ear and the inner arm. A large area of skin was wiped thoroughly with a 2% chlorhexidine in 70% isopropyl alcohol skin wipe to clean and left to air dry. A sterile swab (Fisher Scientific, UK) was dipped into a mild detergent skin swab buffer (20mM Tris pH8, 2mM EDTA, 1.2% Triton X-100) and the cleaned area was swabbed 30 times (up and down= 1 swab). Swabs were cut using 70% ethanol cleaned scissors into a 1.5 mL microfuge tube containing 50 µl BLS stabilisation buffer (IsoHelix, UK), vortexed briefly, and stored until subsequent DNA extraction using BuccalPrep Plus kit (IsoHelix, UK) according to the manufactures' instruction.

5.3.4 Previous DNA extraction from skin swab method using Qiagen kit

DNA was extracted from skin swabs using commercially available QiaAMP mini kit (Qiagen) with a modified protocol. Skin swabs were taken without the use of mild detergent buffer or storage in stabilisation buffer. Swabs were stored up to a week before cut into tubes with scissors cleaned with 70% ethanol solution. 400 µl of PBS, 40 µl proteinase K and 400 µl Buffer AL (lysis buffer) was added to each tube and solutions were pulse vortexed for 50s. Each tube containing the swabs was incubated for 30 mins at 56˚C on a heat block, pulse spun to remove condensation in the lid, 400 µl of ethanol (100%) was added before pulse vortexing for 50s and a final pulse spin. 700 µl of the solution was transferred to a spin column and centrifuged at 6000xg for 1 min. The collection tube was replaced, ensuring the outside of the spin column was dry to avoid contamination each time. This was then repeated for the remainder of the solution. 500 µl AW1 buffer was added to the spin column, centrifuged for 1 min at 6000xg and the collection tube was replaced. 500 µl of AW2 was then added and the column was spun at maximum speed (16,000xg) for 3 mins. Finally, the spin column was placed in a clean and sterile 1.5 ml microfuge tube and 60 µl Buffer AE was added to the column, incubated at room temperature for 5 mins and centrifuged at 6000xg for 1 min.

5.3.5 QPCR of skin swab DNA

DNA from skin swabs was assayed the same day as extraction by 83 bp qPCR assay and 1 kb qPCR assay (general methods section). Samples were assayed without Nanodrop quantification as the quantity of DNA obtained from a swab is generally too low for accurate reading. Each PCR was performed with a standard curve of plasmid DNA containing the area of interest.

5.3.6 Oxidative stress test

Finger prick blood samples were taken from either the middle or ring finger using a 2.3 mm lancet (Roche, UK) after cleaning with a 2% chlorhexidine in 70% alcohol skin wipe and air drying. Three 2 µl blood samples were taken using filter tip pipette and each added to 98 µl of Buffer A [0.05% BSA, 1 mM $MgCl_2$, 0.5 mM $CaCl_2$ and 5 mM Glucose in PBS (pH 7.40)], mixed and stored on ice to be analysed within 1 hour. The assay was set up in flat bottom white 96 well plate with each well containing 40 µl blood sample in buffer, 20 µl of 0.05 mg/ml phorbol myristate acetate (PMA) in Buffer A and 200 µl 1mM luminol in Buffer A. A standard curve of H_2O_2 was run with each plate with 20 µl of H_2O_2 in 200 µl 1mM luminol in Buffer A of concentrations 1 mM, 0.8 mM, 0.6 mM, 0.4 mM, 0.2 mM, and 0.1 mM. Luminescence was measured every minute for 25 minutes using Infinite 200 PRO plate reader and i-control software (Tecan, Switzerland). Area under the curve was taken from 8 mins to 23 mins as these are the most consistent readings, and unknown blood samples were plotted against H_2O_2 standard curve to give standardised readings between runs. This assay was adapted previously for capillary blood samples (Clifford et al., 2018), from the methods by Yamazaki *at al.,* (2011) (Yamazaki et al., 2011).

5.3.7 Statistical methods

Statistical differences were determined using GraphPad prism 9 software and specific methods for each analysis are denoted in the results.

Linear regression models were used to model the relationships between outcomes of the study in MiniTab 19. Multiple models were investigated for each relationship to determine confounding variables to the response, based on their effect on the predictor. If a confounder was found to have a 10% effect on the regression coefficient of the predictor it remained in the model based on the change-in-estimate criterion of regression modelling (Mickey and Greenland, 1989), confounder variables were collapsed over based on either no effect or clinically determined insignificance.

5.4 **Results**

5.4.1 Optimisation of oxidative stress test

The oxidative stress assay stimulates the leukocytes in whole blood samples to release intracellular ROS by the addition of PMA, which is crucial for the detection of the chemiluminescent detection by luminol. This reaction in isolated neutrophils is somewhat attenuated by the addition of superoxide dismutase, which suggests a large proportion of the signal to be of superoxide, and therefore mitochondrial origin (Yamazaki et al., 2011). The principle behind this assay therefore relates the level of chemiluminescence detected to the level of ROS in the blood sample at the time it was taken. The assay is measured over time as PMA stimulation effects are not immediate and progress over time before gradually reducing. Due to the dynamic nature of physiological oxidative stress, it was appropriate to determine the variation in testing procedure and reduce this as much as possible. The effect of sample finger on oxidative stress measurement was not significant as shown in Figure 5-3A.

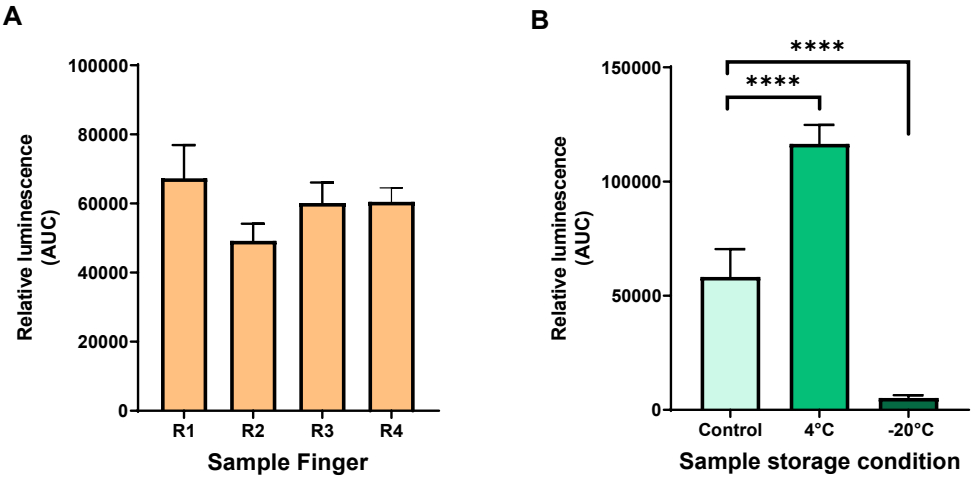

Figure 5-3. Optimisation of blood sampling and storage.
A) The effect of sample finger on oxidative stress measurement from right hand; n=2. B) Effect of sample storage on oxidative stress measurement; assay was performed immediately (control) or stored overnight at 4˚C or -20˚C; n=4; ****P=<0.0001; Statistical differences determined by ordinary one-way ANOVA.

To determine the effects of storage, samples were then taken and measured immediately as a control, then stored at either 4˚C or -20˚C overnight. There was a significant increase of 100% after overnight storage at 4˚C from a mean relative fluorescence of 58,230 to 116,468 (Figure 5-3B). After storage at -20˚C, the chemiluminescence dropped to negligible levels (compared to negative controls). This demonstrated that storage at -20˚C disrupted the blood cells, likely

by lysing the cells in the freeze/thaw process. Storage at 4˚C had an increase of ROS production and therefore could have stressed the cells.

The increase in ROS over time was further investigated to determine whether there was an appropriate amount of time the samples could withstand storage; participant samples needed to be transported between buildings, therefore it was important to determine this parameter. Each sample was stored on ice after collection as this would reflect the transportation method. The time measured equalled the time between sample collection and the start of the assay. Multiple blood samples were taken and collated into a single tube from nine individuals.

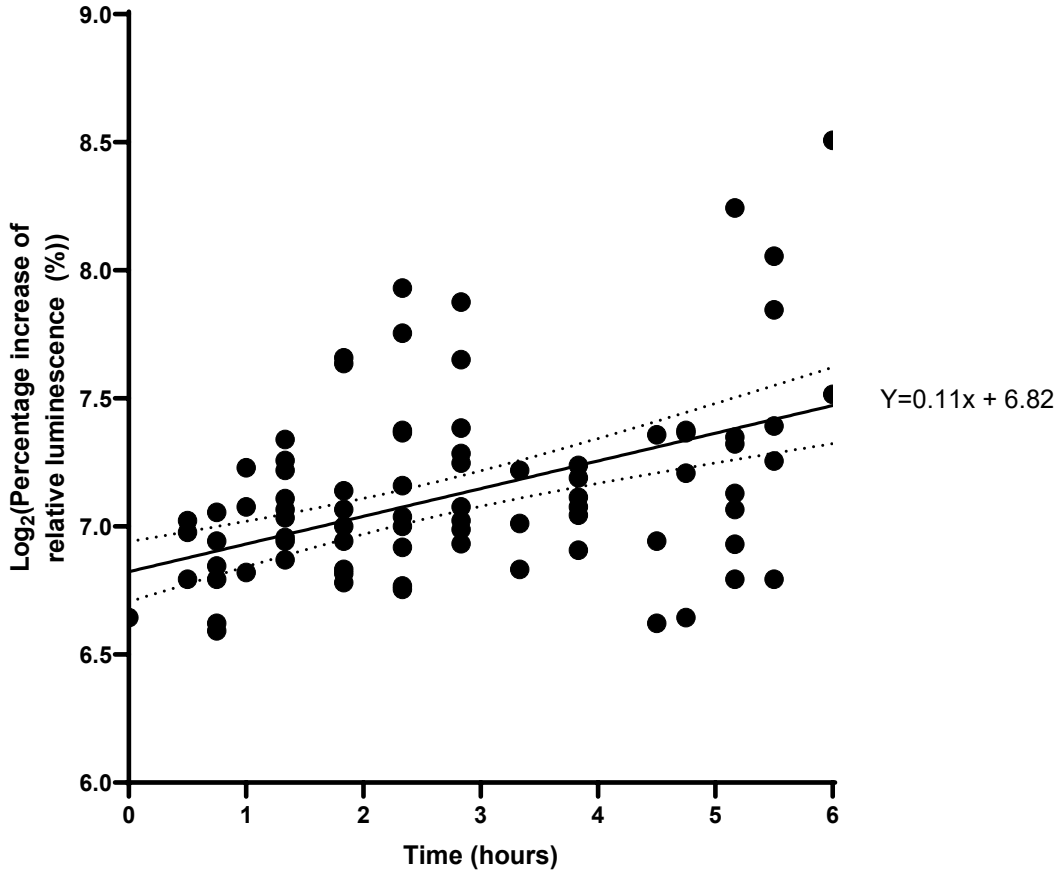

Figure 5-4. Percentage increase of luminescence over time from a single blood sample.
Multiple samples were taken from a single fingerprick and stored on ice until the assay was performed. Significantly deviated from zero (P<0.0001); statistical differences determined by simple linear regression; plotted as individual values with 95% CI lines; N=9, n=2.

From the results in Figure 5-4, there is a significant increase in luminescence over time ($p<0.0001$), with a mean increase of 22.0% every hour up to (calculated from 0 to 6 hours). The assay can reasonably be performed within 1.33 hours of sample collection, paired t-test analysis between 0 and 1.33h showed a mean difference of 34% (CI 16-64%, $p<0.0001$).

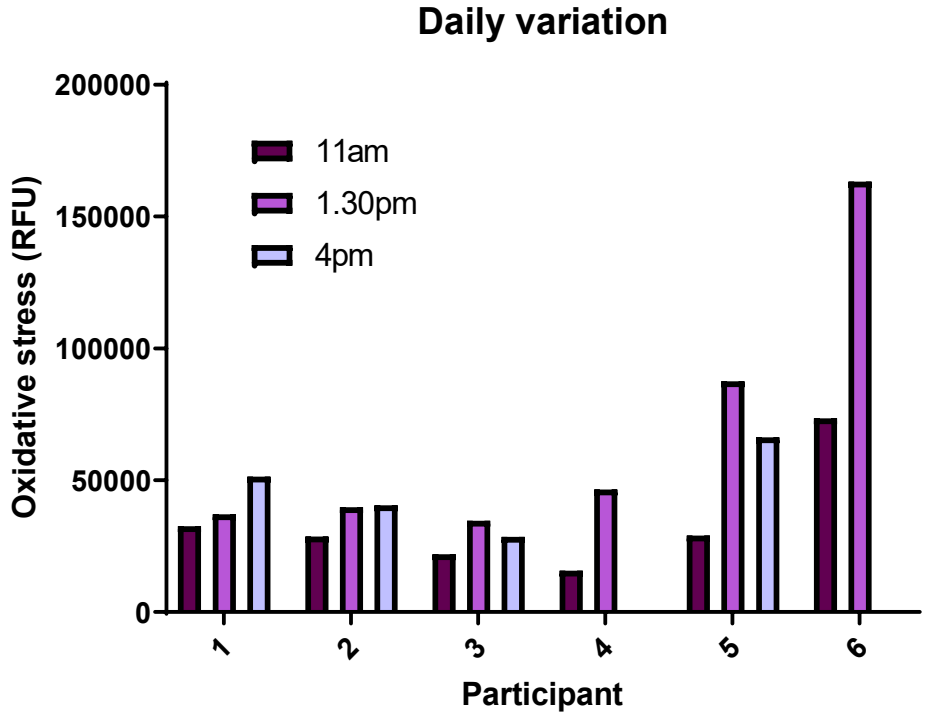

Figure 5-5. Daily variation in oxidative stress levels.
Samples were taken from 6 participants over the course of a day at 11am, 1.30pm and 4pm; 4pm sample not collected for paticipants 4 and 6; n=1.

Daily variation in oxidative stress was found (Figure 5-5), particularly from 11am to 1.30pm which could be a result of just having lunch.

The sample collection was determined to be most appropriate when collected from the middle of ring finger, transported on ice and the assay was started between 1 and 1.33 hours of sample collection. Rested and fasted samples would produce the most accurate results, however due to the variation in patient appointment times, fasted samples were not possible.

5.4.2 Optimisation of skin swab procedure, DNA extraction and storage

The skin swab test is a method of sampling cells from the top layer of skin and using the 83 bp and 1 kb qPCR assays to detect mtDNA damage. The current method used a standard sterile cotton swab, cleaning the area with 70% ethanol wipes and dry swabbing before previously optimised extraction with a modified version of general method for DNA extraction from cell pellets, full details of this in chapter methods.

First, two different swabs were compared to assess the quantity and quality of DNA extracted with two different kits. The current swabs were round cotton with a wooden stick and supplied in a polypropylene tube used in combination with the Qiagen kit. Isohelix^{TM} DNA buccal swabs

has a flat ridged shape on a plastic snappable stick, the Isohelix™ Buccal prep kit was recommended in combination with the swabs. It was hypothesised that the shape of the Isohelix swab would be more abrasive to increase the yield of DNA, the snappable tube would remove the need for scissors to ease the extraction process and the plastic stick would avoid the absorption of the extraction solution to increase the yield. The Isohelix™ Buccal prep kit uses a precipitation-based method whereas the Qiagen kit uses a spin column; it was hypothesised that the Isohelix kit would increase yield by reducing the number of steps and tube transfer of the sample. Customer services at Isohelix also recommended a buffer used by another group to help lift the skin cells during the swab process, this was also tested. The comparison was run with one only repeat due to small test sample size; swabs with buffer and no buffer from the inner arm was assessed as this region consistently obtained a low DNA yield, and a swab from the nose with no buffer was ran as this consistently provided a high yield in previous studies.

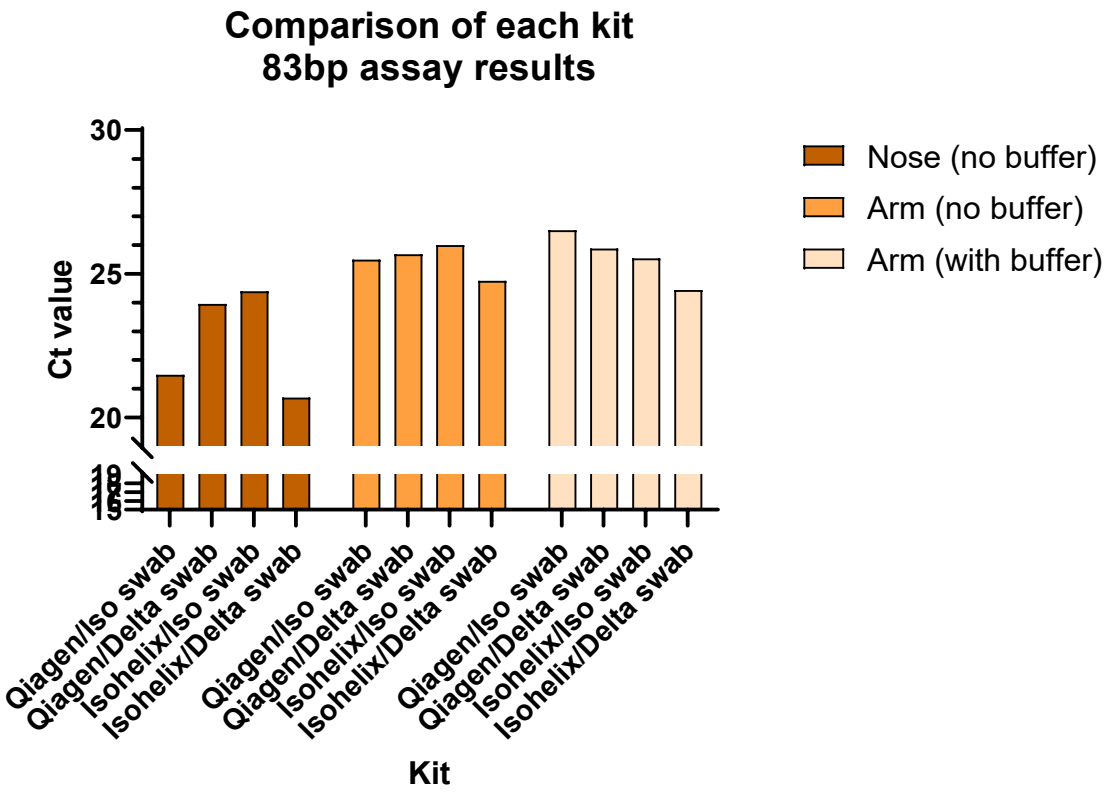

Figure 5-6. Comparison of DNA extraction kits, skin swabs and buffer use on the yield of mtDNA. Two swabs were compared (Deltaswab and Isohelix) and two DNA extraction kits (Qiagen and Isohelix), the use of a buffer with the skin swab was also compared in the arm sample. Results reflect the calculated value for Isohelix based on the difference in initial extraction volumes; n=1.

The tests were performed with different elution volumes, the Qiagen had 60 µl and the Isohelix had 100 µl, the 40 µl difference would be the equivalent of a 1.66x higher concentration in the

Qiagen extracted DNA. Assuming a 100% efficiency in the PCR reaction, this difference can be calculated as E= $2^{0.66}$ -1, meaning the results of the Isohelix kit could have up to 0.58 decrease in Ct value.

From Figure 5-6, each Delta DNA swab had a decreased Ct value (and therefore increase mtDNA yield) using the Isohelix kit compared to the Qiagen kit. This was most apparent in the nose swab with a 3.25 Ct difference; the arm swabs had a 0.92 and 0.98 Ct difference for the dry and buffer, respectively. The Isohelix swab had an increase in Ct value in the Isohelix kit compared to the Qiagen for the nose and arm without buffer swab condition. This was again most apparent in the nose with a 2.90 Ct difference, and 0.50 Ct difference for the arm. The arm swab using buffer seen a 1.44 Ct decrease. The results demonstrated that the Isohelix kit could be more efficient at extracting DNA from the Deltalab swabs, but as this was only performed once and the results were quite variable it was not clear.

The 1 kb assay was performed by PhD student Lizzie Ruddy using the same samples. Results from the 1 kb minus those from the 83 bp results were used as a standardised way to compare these results. Where the difference was smallest, there was a greater amplification of 1 kb fragments compared to the quantity of mtDNA in each sample.

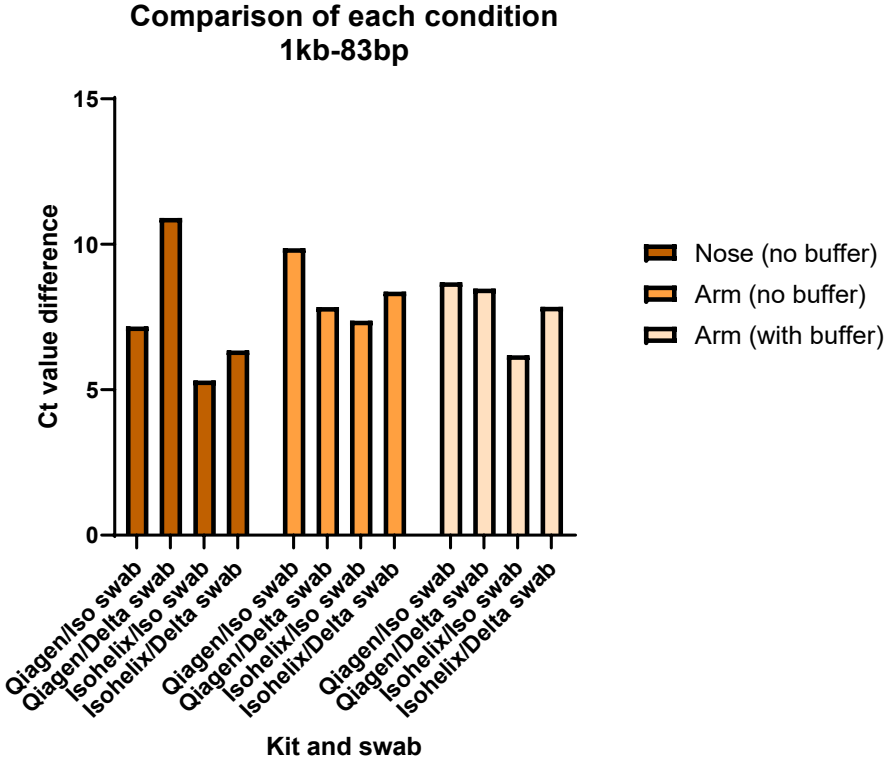

Figure 5-7. Comparison of 1 kb region results from kit, swab and buffer condition.
mtDNA damage was compared for each kit and swab combination from different body sites, the use of a skin swab buffer was tested in the arm sample. Results as 1 kb result minus 83 bp result; n=1.

Three out of four kit/swab combinations had a better amplification of the 1 kb region using the buffer instead of a dry swab (Figure 5-7), therefore the buffer was used in all subsequent skin swabs. The melt curve for the Qiagen kit averaged at 83.15, whereas the Isohelix kit had a melt curve of 84.2 which is reflective of the melt curves seen with good quality DNA in cell DNA extraction. Although the Ct difference were slightly higher using the Deltalab swab than the Isohelix swabs with the Isohelix extraction kit, the overall 83 bp yield was greater with the Deltalab swabs and they had a reduced cost. Therefore, the Deltalab were chosen in combination with the Isohelix kit.

To assess the impact of storing the swab in the Isohelix storage buffer prior to analysis, three participants had swabs taken from the locations on the same cheek. The swabs were kept in buffer BLS from the Isohelix extraction kit and then extracted immediately, after 1 week and after 3 weeks.

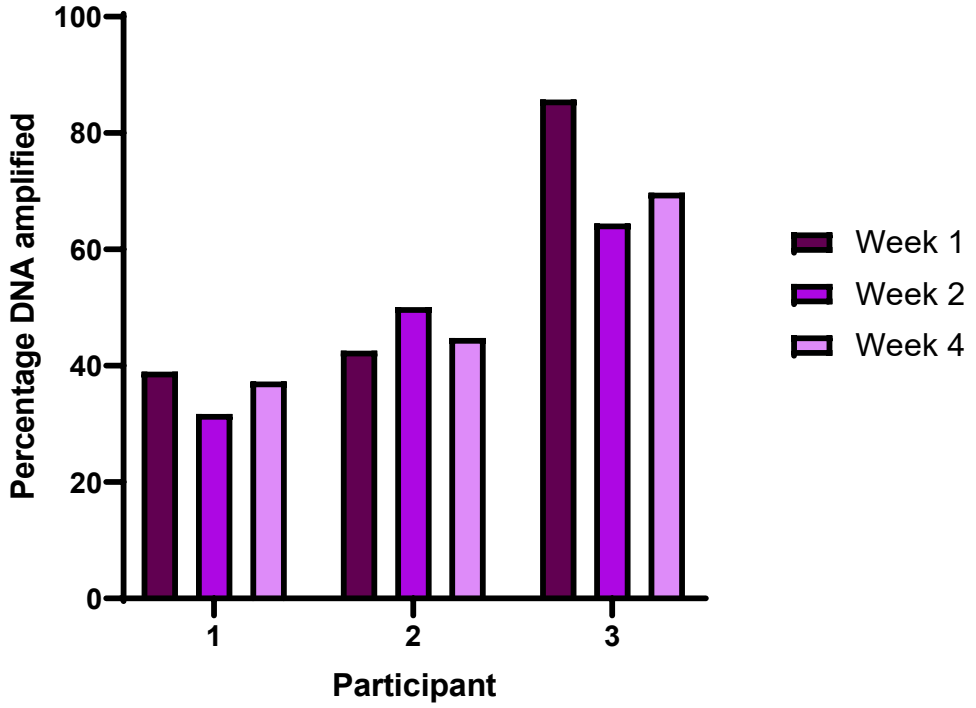

Figure 5-8. Effect of storage in BLS buffer prior to extraction of skin swab.
Swabs were taken from the same cheek, located next to each other from three participants and stored in BLS buffer (Isohelix); N=3, n=1

The results from Figure 5-8 show the percentage of DNA amplified in the target region compared to the control, therefore higher DNA amplified reflects less damage in the DNA. There was no indication that longer storage resulted in a degradation of mtDNA up to 3 weeks when stored in buffer, variability in results in this instance is likely to be intraperson variability

from the different swab locations within the same cheek (see Figure 5-10 for more information).

5.4.3 Skin swab optimisation of analysis technique and biological variability

Previous publications using the skin swab method compared damage in the face, arm, and heel body sites (Harbottle and Birch-Machin, 2006). This method used Picogreen stain to quantify and normalise the DNA loading concentration prior to PCR analysis. Picogreen stain does not distinguish between mitochondrial and nuclear DNA, and biological variation of the skin in different body regions could confound the mtDNA quantification. To determine site variation and compare current qPCR quantification methods with previous whole DNA, a small study was carried out to collect skin swabs from the face, arm, and heel. These were first quantified using the Nanodrop method (chapter 2) and equal DNA concentration was loaded for each sample, before qPCR quantification using the 83 bp housekeeping assay. QPCR was then performed on the nuclear housekeeping region (chapter 2) to compare to the mtDNA results.

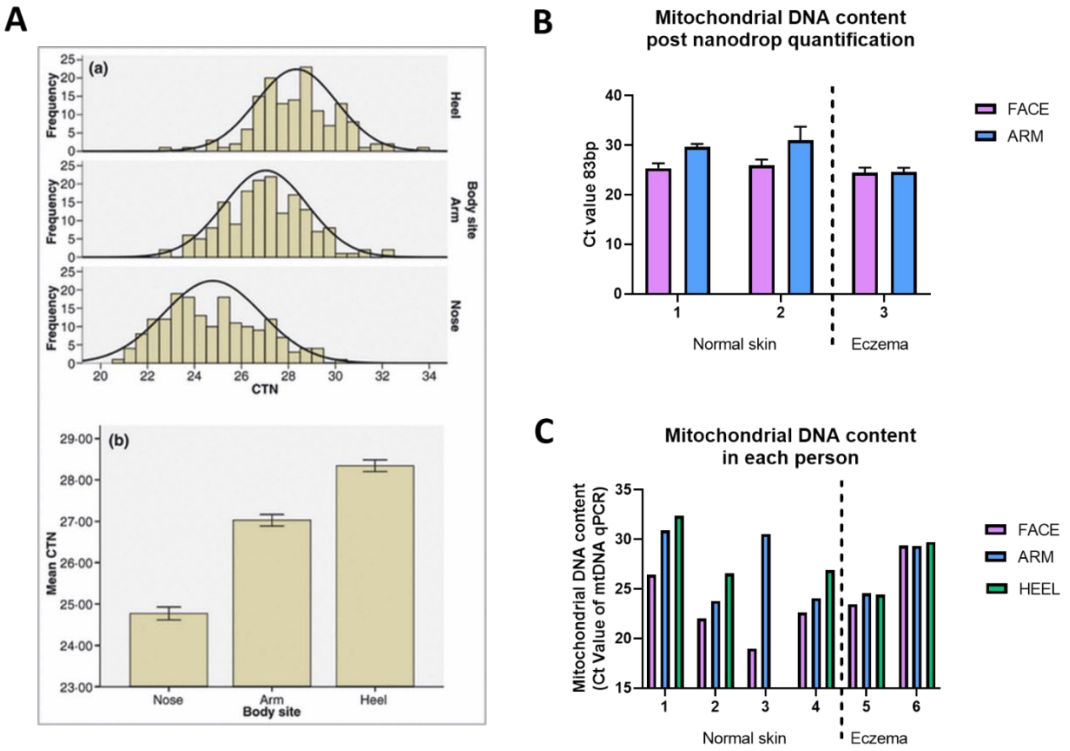

Figure 5-9**.** Skin site region variation in mtDNA quantification.
A) Results from Harbottle and Birch-Machin (2006) paper quantifying 3895bp deletion in different body sites after normalisation of DNA using Picogreen method. B) Face and arm mtDNA quantification post normalisation of DNA using Nanodrop (n=2). C) Quantification of mtDNA in face, arm and heel skin swabs post normalisation based on qPCR of housekeeping region in nuclear DNA (93 bp assay).

The results from the Harbottle paper (Figure 5-9A) determined greater amplification of the 3895 bp deletion from skin swabs in the face (sun exposed region), compared to the arm and heel (non-sun exposed). mtDNA quantification after DNA quantification by Nanodrop (Figure 5-9B) and qPCR of nuclear DNA (Figure 5-9C) show that there is more mtDNA in the face compared to the arm. The results from this study show that the results in the Harbottle paper comparing different body sites could in fact be a result of differing mtDNA content rather than the 3895bp deletion.

An interesting find in this small study, was the lack of body site variation between participants with eczema. The skin swabs only collect the surface of the stratum corneum, and eczema is caused by a disruption in the formation of the stratum corneum. Therefore, the difference in mtDNA quantification between sites could be explained by differing thicknesses of the stratum corneum in each region.

A second small study was carried out to determine intrapersonal variability. Three skin swabs directly after each other in the same location in 5 participants and weekly swabs were taken from 2 participants. This data also provided a scope of the level of interpersonal variability we could expect from future studies.

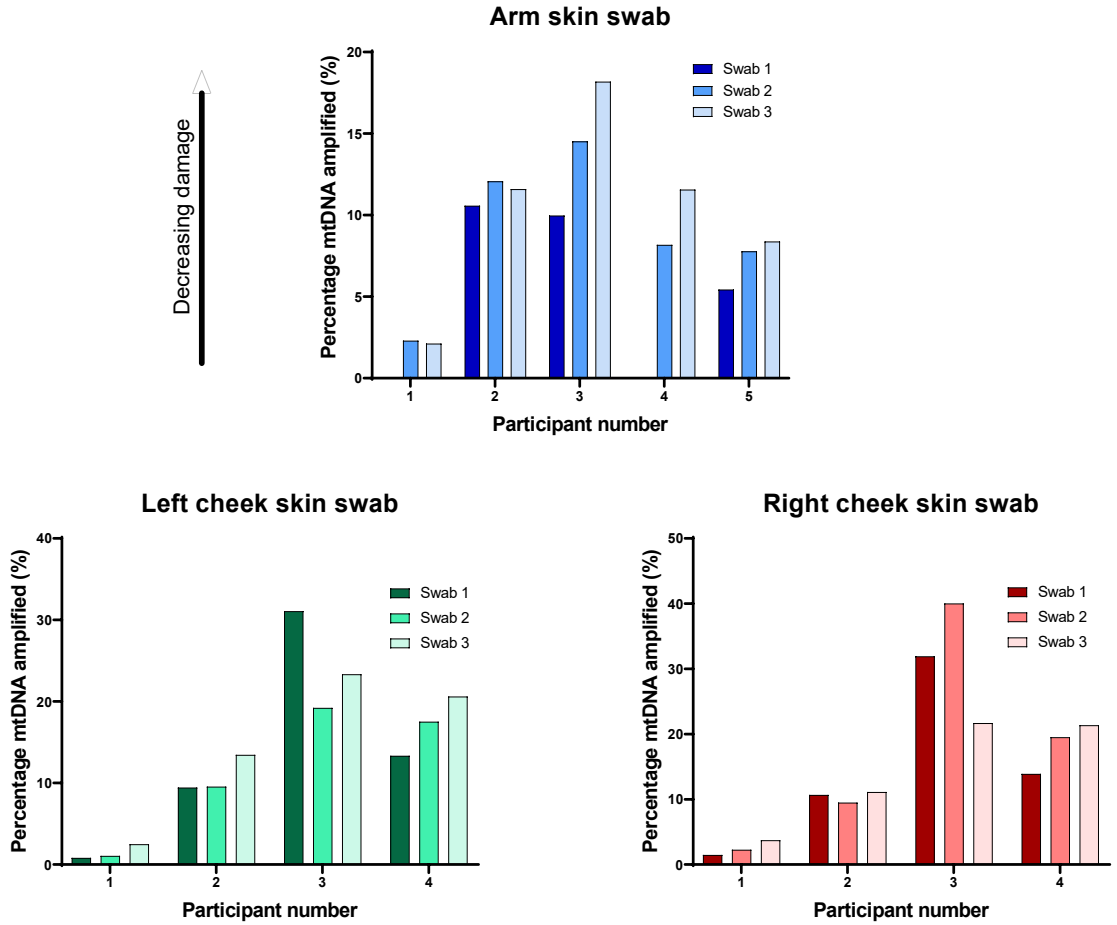

Figure 5-10. Intrapersonal variability of skin swabs**.**
Three swabs of the skin were performed sequentially in the same position, and results show the percentage of 1 kb region amplified. Higher percentage is equal to reduced damage of mtDNA. Five participants provided arm samples and four provided cheek samples. Participant 2 had eczema.

The arm swabs from Figure 5-10 show an increasing trend of 1 kb amplification in each subsequent skin swab, and therefore decreasing damage. Swab 1 from participants' 1 and 4 did not amplify as the sample was too damaged, and participant 2 with eczema did not have the same trend which could be expected due to the damaged stratum corneum. This same pattern in arm skin swabs has been recognised throughout the optimisation process. The skin swabs from the cheeks do not always show the same trend of decreasing damage. This is hypothesised to be due to the thinner stratum corneum on the face compared to the arm. The degree of interpersonal variability ranged from the greatest change of 18.4% between swab 2 and 3 of participant 3 (right cheek), and the lowest 0.17% between swab 2 and 3 of participant 1 arm.

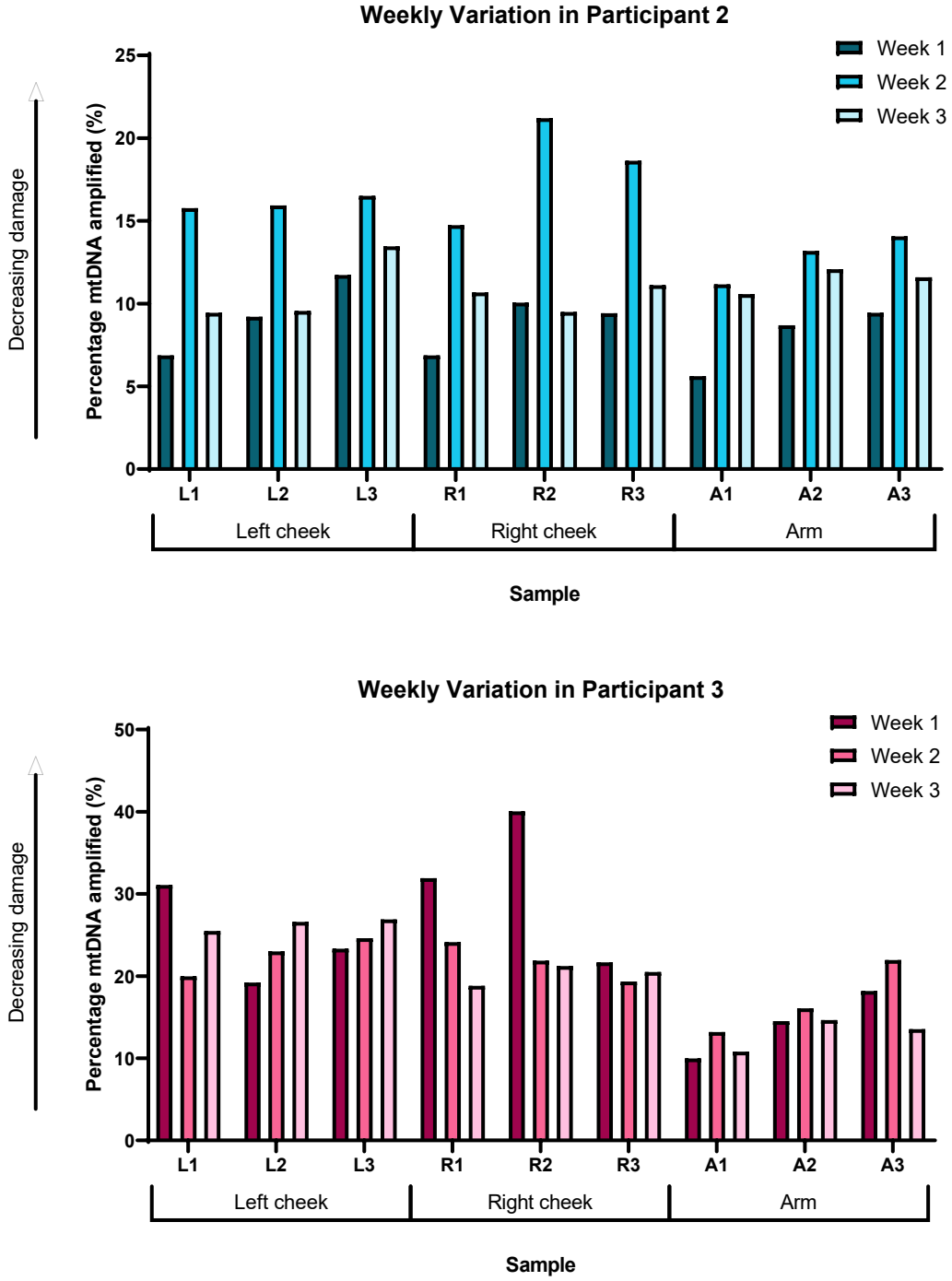

Figure 5-11. Weekly intrapersonal variation in two participants.
Skin swab samples were collected from the left cheek, right cheek, and upper inner arm on the same day each week. Each sample was taken three times, sequentially, in the same region (L1= first swab, L2= second swab etc). Graph plotted as percentage amplification of mtDNA in skin swab.

Weekly variation was to be expected with skin swab results, Figure 5-11 shows variation over three weeks in 2 participants. Three swabs were taken again to determine if taking a sample from a deeper layer resulted in more consistency over time. Participant 2 (with eczema) had the same pattern of damage where week two decrease in damage from week one, and week

three had more damage than week two. On average, the cheek swabs had 8.1% less damage and the arm 4.9% less damage from week one to week two, and the face had 6.5% more damage and the arm 1.4% more damage from week 2 to 3. Participant 3 had an increase in damage in the cheeks by 5.7% and a decrease in damage of 2.8% in the arm form week one to two, and a decrease in damage in the cheeks by 1.1% and an increase in damage in the arm by 4.1% from week two to three. This result demonstrates the importance of consistent swabbing technique and leaving an appropriate length of time between samples to enable to top layer to stabilise, also there is weekly variation in the upper arm swab so it would not be a reliable 'internal control' marker.

The results of this study had two conclusions which impacted the analysis of the skin swab data. Firstly, we could not use a sun exposed and non-exposed region for comparison in any individual. Secondly, comparing the results between individuals would need to take skin conditions into account. Overall, the best method of analysis using the skin swabs would be a time course, comparing a single body site of an individual before and after an intervention. Optimisation of the skin swabs was carried out ethical approval had been given for the patient study; therefore, samples could only be taken from participants on a single day.

5.4.4 Comparison of perceived age assessment in Visia images

Methods of perceived age assessment were compared using forward facing Visia images with a neutral face. Images were processed by the CNN algorithm which provided a perceived age and were independently assessed by thirteen naïve evaluators to determine a mean perceived age. Forward facing images taken by a Nikon camera, set up on a rig were also processed by the CNN algorithm for comparison to the images in the Visia booth format, to determine if the chin and head rests would affect the age assessment.

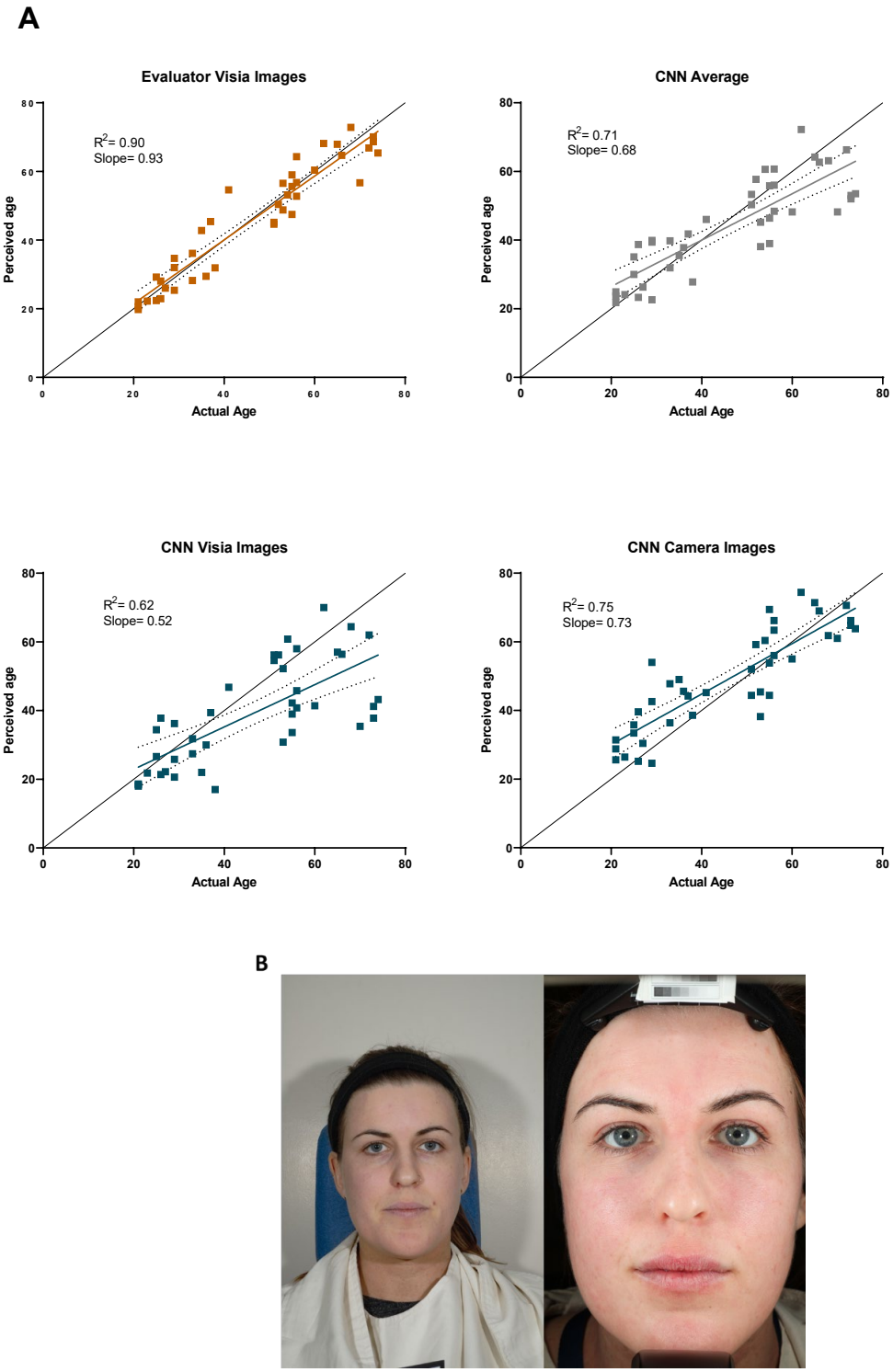

Figure 5-12. Assessment of perceived age of all study participants by independent evaluators and CNN algorithm.
A) Thirteen independent evaluators assessed the images taken in the Visia booth and the average perceived age was plotted against actual age. The CNN algorithm predicted evaluated age for the same Visia booth images, and also images taken via a camera set up on a rig at equal distance from each patient. The average of the CNN algorithm analysis of the Visia and camera images was also plotted (CNN average); correlation was determined by simple linear regression; data presented as mean±95% CI; n=41. B) Camera image and Visia image.

Perceived age as evaluated by human participants had the greatest correlation with actual age (R^2=0.90) (Figure 5-12A). The CNN algorithm had the greatest accuracy with camera images (R^2=0.75) compared to Visia images (R^2=0.62). Averaging of the two imaging methods reduced the accuracy compared to the camera images by 4% but increased the accuracy from the Visia images by 9%. The region in which the 95% confident interval does not contain the reference line determined the CNN algorithm had a greater accuracy in Visia images below the age of 38, and above the age of 48 in the camera image. The actual age was contained within the 95% CI of the evaluator perceived age, showing no bias towards any age groups. The camera captured images of patients from the shoulders and the Visia was exclusively the face, which could have provided the algorithm with additional information of the neck area even with the clothing covered (Figure 5-12B). Additionally, long hair was not always tied up, and was visible behind the headband in some patients in the camera images. The head rest was fixed on the Visia and positioned in the middle of the forehead on some patients which could have affected the assessment. Furthermore, the headband was positioned further down the forehead in some patients, which may have given the impression of a different hairline, though there was no significant effect of hairband or headrest in regression analysis (p=0.816).

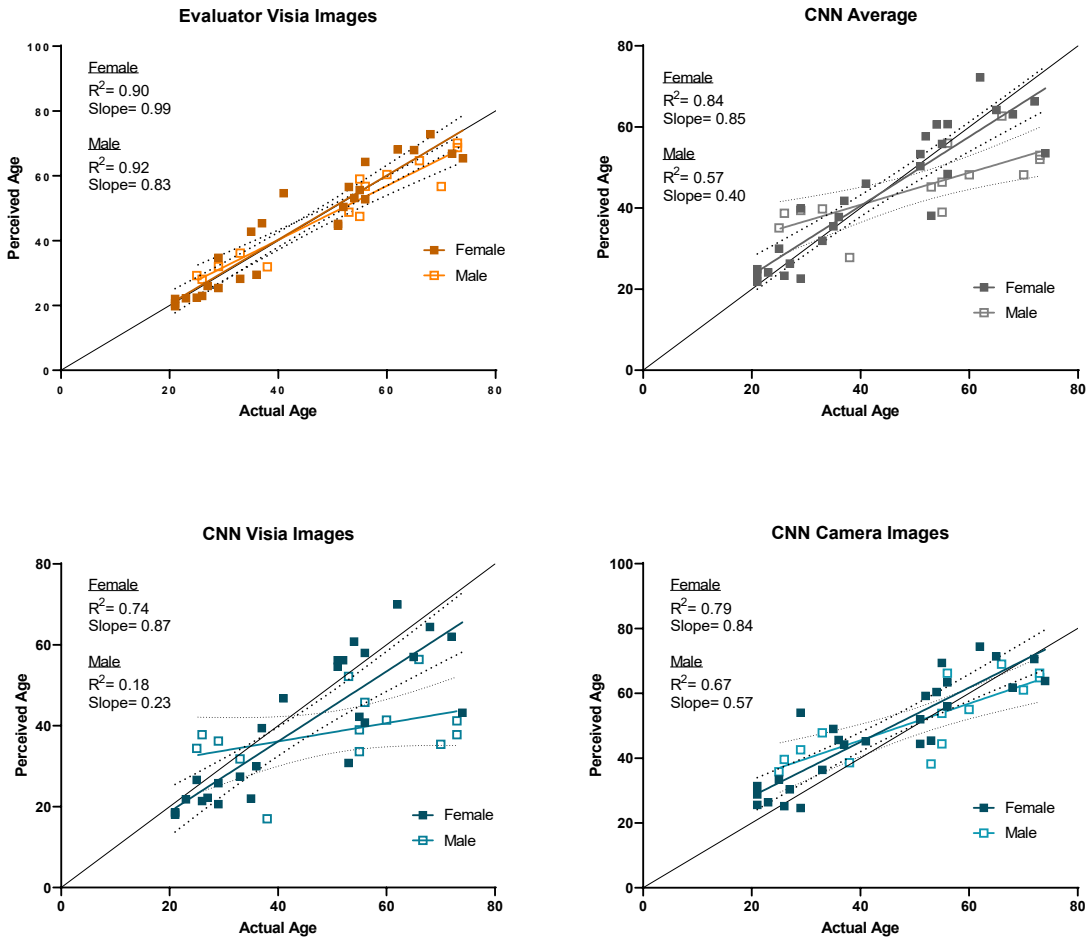

Figure 5-13. Effects of sex on perceived age analysis on all study participants.
Data from Figure 5-12 split into sex groups for evaluators assessment and CNN assessment of perceived age; female n=27, male n =14.

Perceived age assessment by evaluators was not affected by sex (p=0.447), though the slope for female patients was 0.99 compared to 0.87 for males (Figure 5-13). CNN assessment of camera image had a lower accuracy in males, specifically above the age 47, with a slope of 0.57, and had a better accuracy on images of female patients (slope 0.84), though the difference between sex was not significant (p=0.494). The CNN assessment of Visia images had the lowest accuracy in males, with a slope of 0.23, and an improved correlation to actual age in images of female patients compared to the camera (slope=0.87), though not statistically significant there was a trend (p=0.147). Overall, evaluator analysis was determined to assess the perceived age of patients with the greatest accuracy, though the CNN age assessment of camera images was a good estimate and could be improved with further training on the clinical images involved in the study.

5.4.5 Oxidative stress is elevated in patients compared to controls

Patients had elevated oxidative stress equivalent to 81.9 mMol H_2O_2 compared to the control group when controlling for diastolic blood pressure, temperature, exercise, caffeine intake, diabetes, heart condition and high cholesterol ($p=0.039$). Participants with diabetes also had significantly elevated oxidative stress by 163.6 mmol H_2O_2 ($p=0.005$). When the patient group was further characterised by variant type, point variants were found to have the greatest correlation with oxidative stress, with 111.7 mmol H_2O_2 greater than control levels ($p=0.018$). Number of cups of caffeinated drinks per day had a positive correlation with oxidative stress, elevating levels 25.9 mm H_2O_2 per cup.

The introduction of heartrate reduced the significance of the result (69.6 mmol H_2O_2, $p=0.435$). Patients had a significantly higher heartrate than controls by an average of 13.6 beats per minute ($p<0.0001$), which could also be linked to the difference between the two groups.

				Oxidative stress mean
Model 11:	**Patient status (reference control)**		Coefficient	**81.6**
			p-value	***0.039***
	Diastolic BP		Coefficient	-0.75
			p-value	*0.676*
	Temp (°C)		Coefficient	11.2
			p-value	*0.376*
	Exercise (reference at least once per week)	**Mild daily activity**	Coefficient	-75.2
			p-value	*0.1102*
		No	Coefficient	-77.8
			p-value	*0.164*
	Caffeine intake (no. of cups/day)		Coefficient	21.9
			p-value	*0.057*
	Diabetes (reference negative)		Coefficient	**163.6**
			p-value	***0.005***
	Heart condition (reference negative)		Coefficient	-97.6
			p-value	*0.068*
	High cholesterol (reference negative)		Coefficient	-12.4
			p-value	*0.844*

				Oxidative stress mean
Model 13:	**Patient group (reference control)**	**Point variants**	Coefficient	111.7
			p-value	*0.018*
		Single deletion	Coefficient	86.6
			p-value	*0.129*
		Multiple deletions	Coefficient	-58.3
			p-value	*0.518*
	Diastolic BP		Coefficient	-0.89
			p-value	*0.623*
	Temp (°C)		Coefficient	7.9
			p-value	*0.632*
	Exercise (reference at least once per week)	**Mild daily activity**	Coefficient	-98.3
			p-value	*0.049*
		No	Coefficient	-90.1
			p-value	*0.116*
	Caffeine intake (no. of cups/day)		Coefficient	**25.9**
			p-value	***0.03***
	Diabetes (reference negative)		Coefficient	**154.5**
			p-value	***0.007***
	Heart condition (reference negative)		Coefficient	-103.9
			p-value	*0.051*
	High cholesterol (reference negative)		Coefficient	-34.0
			p-value	*0.641*

Table 5-2. Linear regression model of oxidative stress and patient status.
Model 11 determines the mean oxidative stress differences between the patient and control groups, and model 13 categorises the patient groups into point variants, single seletions and multiple deletions. Full iterations can be found in appendix B; significant results are in bold.

5.4.6 Perceived age is a greater predictor of UV spots than actual age

UV spot area had a greater correlation with age over count and size, and evaluator perceived age was able to predict UV spot area better than actual age and the CNN algorithm. In the right cheek, perceived age from all methods and actual age could significantly predict UV spot area, and CNN algorithm assessment of Visia images was not a significant predictor in the left cheek. Evaluator age had contributed to 37.5% of the variation in UV spot area ($p<0.0001$), compared to 35.9% for the CNN algorithm of camera images ($p<0.0001$), 28.2% for actual age ($p=0.003$), and 15.0% for the CNN Visia images ($p=0.012$). There was a reduced predictive outcome of perceived age on the left cheek overall. Evaluator assessment was again the greatest predictor and contributed to 28.8% of the UV spot area variation ($p<0.0001$), compared to 21.5% for CNN camera images ($p=0.002$), 16.5% for actual age ($p=0.008$), and an 8.9% for the CNN of Visia images ($p=0.058$).

After controlling for actual age as a confounder, evaluator assessment of perceived age still had a significant correlation with UV spot area on the right cheek (coefficient= 0.42; $p=0.009$) and left cheek (coefficient= 0.539; $p<0.001$). CNN perceived age of camera images correlated less significantly with UV spot area on the right cheek (coefficient= 0.24; $p=0.038$) and had no correlation on the left check ($p=0.127$). CNN perceived age of Visia images had no correlation with UV spot area on either cheek (right $p=0.956$; left $p=0.955$).

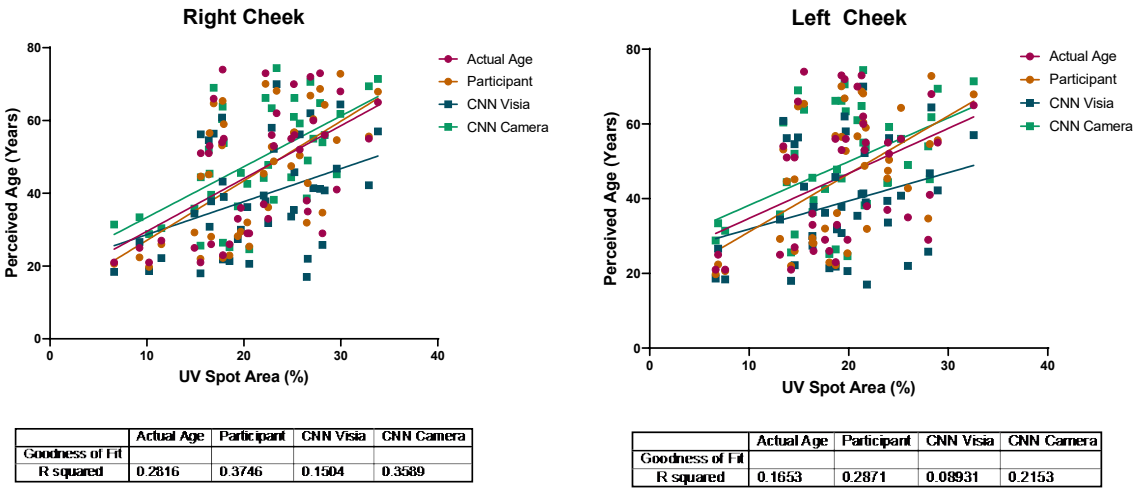

	Actual Age	Participant	CNN Visia	CNN Camera
Goodness of Fit				
R squared	0.2816	0.3746	0.1504	0.3589

	Actual Age	Participant	CNN Visia	CNN Camera
Goodness of Fit				
R squared	0.1653	0.2871	0.08931	0.2153

Figure 5-14. Correlation between percieved age and UV spot area on left and right cheek.
Simple linear regression of UV spot area (% coverage of cheek) compared to actual age and percieved age using the evaluator method and CNN of camera and Visia images; n=41

5.4.7 Patients with single large-scale deletions have a trend for increased perceived age

Perceived age in patients was investigated to first determine if there was an overall effect of patient status on perceived age. A linear regression model was used to control for confounders: hours outdoors, sun protection, alcohol use, age, sex, and smoking status. The null hypothesis would determine no significant difference of perceived between the two groups. The model agreed with the null hypothesis and found that there was no significant change in evaluator determined perceived age (p=0.479), nor CNN assessment of camera (p=0.947) or Visia (p=0.828) images (appendix C).

Patient groups were then categorised into point variants of mtDNA, single large-scale deletions and multiple deletions/ nuclear defects known to cause multiple deletions. While not significant, the CNN evaluation of camera images had a trend of increased perceived age in patients with single large-scale deletions of 7.25 years compared to controls (p=0.095). The CNN assessment of Visia images and the evaluator assessment had no significant outcomes. However, the sample size for each group was small (point variants n=13; single deletions n=7; multiple deletions n=1) (appendix C).

Effect of ptosis on perceived age was assessed in a new model, controlling for the same confounders. Ptosis was available for all patients; although controls were not assessed for ptosis there was no evidence of ptosis in the control participants. Ptosis was not found to have a significant influence on perceived age, though each assessment method had a trend for increasing perceived age with the presence of ptosis [evaluator = +3.39 years (p=0.147); CNN camera = + 4.15 years (p=0.268)]. Ptosis was present in 7 out of 7 patients with single large-scale deletions, 1 out of 1 case with nuclear defects, and 2 out of 9 cases with single point variants.

Overall, there was limited data for grouped variant analysis. However, single large-scale deletions had a trend for increased perceived age when assessed by the CNN algorithm but not by evaluators and ptosis also had a trend for increased perceived age.

5.4.8 Sun protection habits contribution to perceived age, UV spots and skin swab damage

Linear regression models were used to determine the variables which affected skin swab mtDNA damage, below are the models showing the coefficient and *p*-value for each variable of the final models, full iterative models can be found in appendix D.

				mtDNA damage	
				Right cheek	**Left cheek**
Model 9	**Age**		Coefficient	0.00023	0.0014
			p-value	*0.867*	*0.323*
	Sun protection (reference always wears)	**Occasional use**	Coefficient	-0.0631	-0.0946
			p-value	*0.21*	*0.076*
		Never use	Coefficient	**0.1369**	0.0623
			p-value	***0.007***	*0.452*
	Hours outdoors (reference less than 5 hours/week)	**5-10 hours/week**	Coefficient	0.0377	0.031
			p-value	*0.326*	*0.452*
		More than 10 hours/week	Coefficient	0.0253	0.0213
			p-value	*0.614*	*0.702*
	Season of sample collection (reference winter)	**Spring**	Coefficient	0.0965	0.065
			p-value	*0.103*	*0.302*
		Summer	Coefficient	0.1199	**0.165**
			p-value	*0.079*	***0.025***
		Autumn	Coefficient	**0.146**	0.1064
			p-value	**0.03**	0.122
	Alcohol use (reference often use)	**Occasional use**	Coefficient	**0.125**	0.1033
			p-value	***0.037***	*0.08*
		Never use	Coefficient	**0.1803**	**0.24**
			p-value	***0.015***	***0.002***
	Skin type self-assessment	**Type II**	Coefficient	**0.1201**	0.0878
			p-value	***0.05***	*0.199*
		Type III	Coefficient	0.1504	0.0959
			p-value	0.008	0.126
				mtDNA damage	
				Right cheek	**Left cheek**
Model 10: Perceived age with confounders from model 9	**Perceived age (assessors)**		Coefficient	-0.00038	0.00095
			p-value	*0.787*	*0.517*
	Perceived age (CNN camera)		Coefficient	-0.00047	0.00129
			p-value	*0.759*	*0.411*
	Perceived age (CNN Visia)		Coefficient	-0.00046	0.00162
			p-value	*0.729*	*0.221*

Table 5-3. Linear regression model of correlation between age/percieved age and skin swab damage. Full iterations of confounders in models found in appendix D; arcsin(√x) transformation of percentage mtDNA amplified used for analysis; significant results are in bold.

Skin swab damage from the face samples did not correlate with actual age (p=0.867 right; p=0.323 left) or perceived age (p=0.916 right; p=0.431 left), this remained true after controlling for sun protection use, hours spent outdoors, season of sample, alcohol use and skin type (Table 5-3). Self-assessed skin type was used instead of ITA° as it gave a further insight into the skins reactivity to sunlight as opposed to the skin tone alone (Osto et al., 2022).

				mtDNA damage	
				Right cheek	**Left cheek**
Model 8: Add confounder age	**UV spots area**		Coefficient	**-0.00878**	**-0.00787**
			p-value	***0.013***	***0.021***
	Sun protection (reference always use)	**Occasional use**	Coefficient	0.0028	-0.0388
			p-value	*0.95*	*0.414*
		Never use	Coefficient	**0.1686**	**0.1102**
			p-value	***0.001***	***0.02***
	Age		Coefficient	**0.00301**	**0.00285**
			p-value	***0.024***	***0.025***
	Alcohol use (reference often use)	**Occasional use**	Coefficient	0.048	0.0462
			p-value	*0.38*	*0.380*
		Never use	Coefficient	*0.1443*	**0.2244**
				0.055	***0.002***

Table 5-4. Regression modelling of correlation between UV spots and mtDNA damage.
Full iterations of confounders in models found in appendix F; arcsin(√x) transformation of percentage mtDNA amplified used for analysis; siginfiant results are in bold.

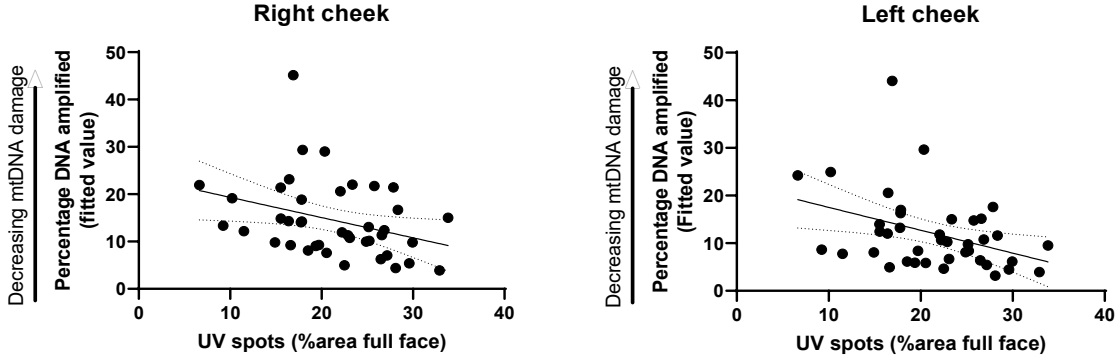

Figure 5-15. Relationship between mtDNA skin swab damage and UV spot area
Fitted values from regression value were transformed back to percent DNA amplified for plotting ($\sin(x^2)*100$) against percentage of UV spot covarage on the right cheek and left cheek; n=41

UV spots area had a significant correlation with skin swab damage after controlling for age, sun protection use, and alcohol (Table 5-4). On the right cheek, there is a 0.59% increase in skin swab damage per percent area increase in UV spots (p=0.013), and the similar on the left cheek (0.50% increase damage/1% increase UV spot area p=0.021) (Figure 5-15). Therefore, UV spot area increases as mtDNA swab damage increases, and sun protection and alcohol use were significant confounding variables. There was still a significant correlation between UV

spots and skin swab damage when controlling for age only (right=0.66% increase, p=0.03; left=0.72% increase, p=0.024).

				Change in perceived age
Model 7:	**Sun protection (reference always wears)**	**Occasional use**	Coefficient	2.11
			p-value	*0.363*
		Never use	Coefficient	***4.82***
			p-value	***0.041***
	Age		Coefficient	-1.063
			p-value	*0.099*
	Patient status (reference control)		Coefficient	1.64
			p-value	*0.354*
	Hours outdoors (reference less than 5 hours/week)	**5-10 hours/week**	Coefficient	0.91
			p-value	*0.635*
		More than 10 hours/week	Coefficient	-1.2
			p-value	*0.641*
	Alcohol use (reference often use)	**Occasional use**	Coefficient	-3.95
			p-value	*0.123*
		Never use	Coefficient	-1.89
			p-value	*0.56*
	Season of sample collection (reference winter)	**Spring**	Coefficient	-3.16
			p-value	*0.264*
		Summer	Coefficient	-3.44
			p-value	*0.292*
		Autumn	Coefficient	-0.318
			p-value	0.318

Table 5-5. Linear regression model of correlation between perceived age and sun protection use. Full iterations of linear regression model can be found in appendix E; significant results are in bold.

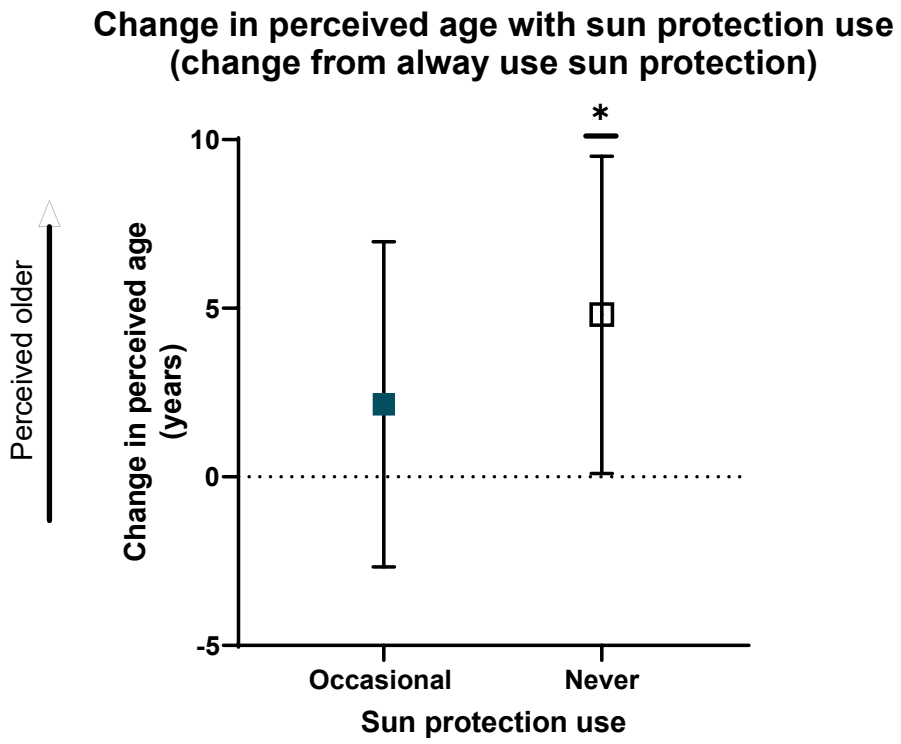

Figure 5-16. Change in perceived age with sun protection use.
Statistical differences determined by linear regression analysis, controlling for confounders shown in table (Table 5-5); reference category was "always use" sun protection; data presented as mean with 95% CI; always use n= 22; occasional use n= 10; never use n=10.

A regression model was performed to assess the correlation between sun protection use and perceived age, controlling for; actual age, patient status, hours outdoors, alcohol use and season of collection (Table 5-5). Patient status, sex, smoking status, BMI, and exercise were found to have no significant contribution to the model (appendix E). Sun protection provided the only unique, statistically significant contribution to the predicted outcome. Participants who self-reported using no sun protection were found to be perceived on average 4.82 years older than those who reported always wearing sun protection (p=0.041), and those who reported occasional use had no significant difference in perceived age than those who always wore sun protection (p=0.363) (Figure 5-16). When perceived age was assessed by the CNN, sun protection was no longer a predictor of perceived age (camera p=0.703; Visia p=0.312). This suggests that skin appearance may be less of a factor in age determination of the algorithm than it is to the evaluators.

5.4.9 UV spots accumulate with age and are reduced in MD patients

A regression model was used to evaluate predictors of UV spot area (Table 5-6; full model in appendix D). While not significant, participants who reported never using sun protection had a trend for a greater percentage area of UV spot coverage on both the left (+3.81%, p=0.127) and right side (+3.38%, p=0.159), controlling for patient status, age, skin type, hours outdoors and month (Figure 5-17). In the same model, patients were found to have significantly reduced percent area of UV spots on the right side (-4.14%, p=0.029) and a similar trend on the left (-3.29%, p=0.089). Additionally, a significant correlation between age and UV spots was found on each side of the face, increasing 0.25% per year on the right (p<0.0001) and 0.18% on the left (p=0.005). Age was also found to significantly predict UV spots count (-0.039/inch^2/year, p=0.002) and size (+0.003 inch^2/year, p=0.003) on the right cheek, and similarly on the left cheek with less significance (size: +0.002 inch^2/year, p=0.003; count: -0.03/inch^2/year, p=0.05). UV spot count has an inverse relationship with UV spot size and %area covered (p<0.0001). The model found no seasonal differences were found in UV spot area (right p=0.415; left p=0.578) or count (right p=0.520; left p=0.625).

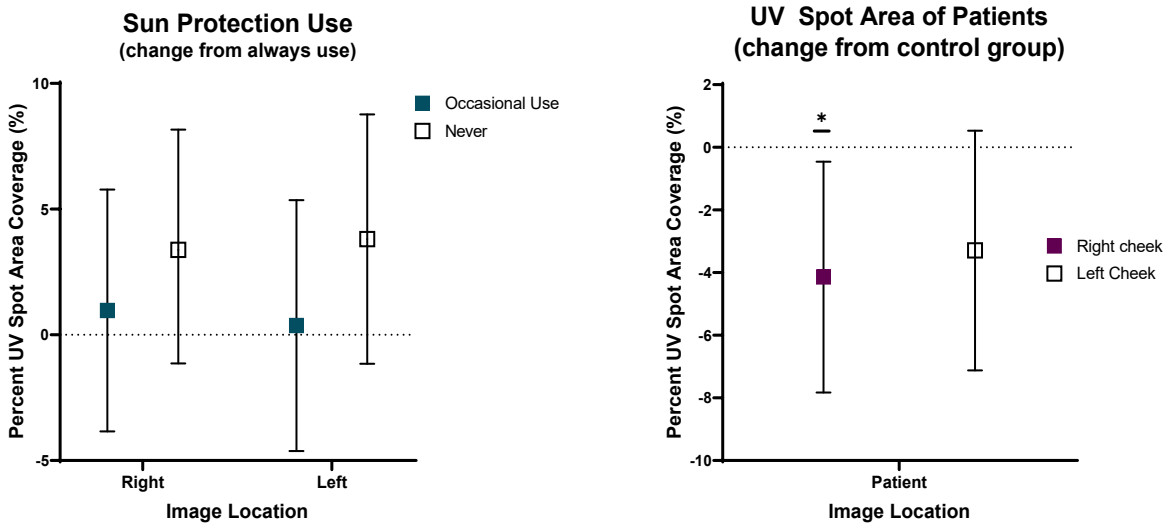

Figure 5-17. UV spot analysis with sun protection use and patient status
Statistical differences determined by linear regression analysis of age, sun protection use, month, skin type, patient status, and hours spent outdoors; reference category for sun protection was was always use and patient UV spot area was control group; data presented as mean with 95% CI; always use n= 22, occasional use n= 10, never use n=10; control n=21, patient n=20.

				UV spot area (% coverage)	
				Right cheek	**Left cheek**
Model 9:	**Sun protection (reference always wears)**	**Occasional use**	Coefficient	0.97	0.37
			p-value	*0.684*	*0.881*
		Never use	Coefficient	3.38	3.81
			p-value	*0.159*	*0.127*
	Age		Coefficient	**0.2498**	**0.1833**
			p-value	***0.000***	***0.005***
	Patient status (reference control)		Coefficient	**-4.14**	-3.29
			p-value	***0.029***	*0.089*
	Hours outdoors (reference less than 5 hours/week)	**5-10 hours/week**	Coefficient	-2.35	-2.44
			p-value	*0.241*	*0.241*
		More than 10 hours/week	Coefficient	-3.26	-3.14
			p-value	*0.203*	*0.237*
	Season of sample collection (reference winter)	**Spring**	Coefficient	-3.41	-3.24
			p-value	0.238	*0.276*
		Summer	Coefficient	-3.18	-2.67
			p-value	*0.326*	*0.424*
		Autumn	Coefficient	-5.32	-4.4
			p-value	0.1	*0.186*
	Skin type self-assessment	**Type II**	Coefficient	-0.017	-0.63
			p-value	*0.957*	*0.847*
		Type III	Coefficient	-3.82	-3.39
			p-value	0.178	0.247

Table 5-6. Linear regression model of predictors of UV spot coverage (%area).
Full iterations can be found in appendix G. Full model contributed to 31.55% (right cheek) and 13.64% (left cheek) of the variability in UV spot area coverage, significant results are in bold.

5.4.10 Skin swab damage is affected by sun protection, seasonal change, skin type and alcohol use

The linear regression model from Table 5-3 was further assessed to evaluate other predictors of skin swab damage. Age was removed from the model to assess sun protection and seasonal change as it was found to have no effect on the coefficient (appendix H). mtDNA damage in the skin swabs had an inverse relationship with sun protection (Figure 5-18).

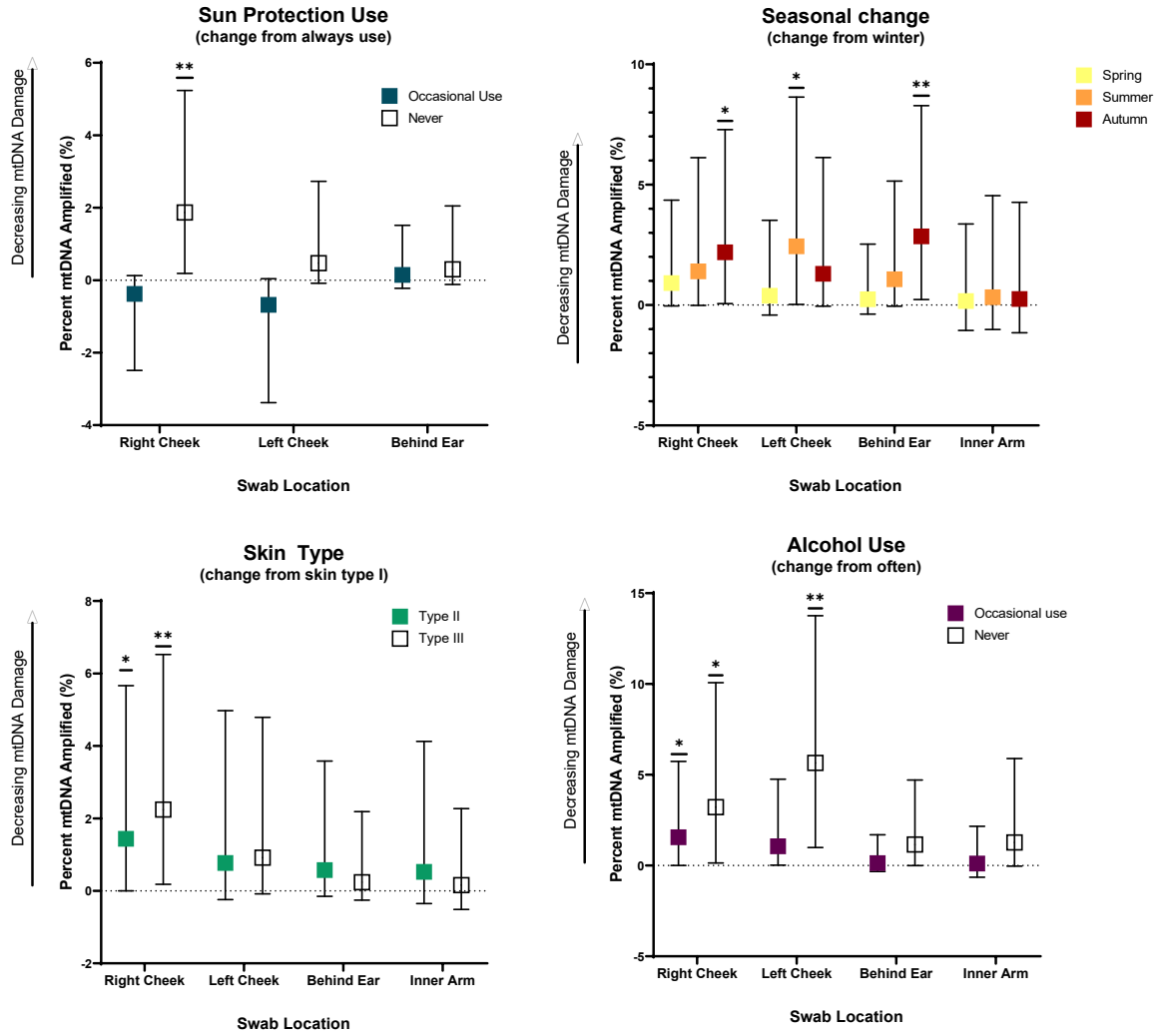

Figure 5-18. Change in skin swab mtDNA damage with sun exposure, skin type and alcohol use
Statistical differences determined by linear regression analysis model using arsin(√x) transformation of mtDNA damage data, with predictors: sun protection, month, skin type, hours outdoors and alcohol use; data presented as mean with 95% CI. Self-reported sun protection use: reference category was always use sun protection; always use n= 22; occasional use n= 10; never use n=10. Seasonal change determined by month skin swab was collected: reference category winter; winter (Dec-Feb) n= 6; spring (Mar-May) n= 18; summer (Jun-Aug) n= 9; autumn (Sep-Nov) n=9. Skin type determined by questionnaire analysis of hair colour and ability to tan: reference skin type I; skin type I n= 6; skin type II n= 12; skin type III n= 24. Self-reported alcohol use: reference often use; often use n= 8; occasional use n= 26; never use n= 8. Full iterations of regression model can be found in appendix H.

A 1.87% decrease in damage was found in the right cheek swab when participant always used sun protection (p=0.006), and no significant change was found in any swab location with occasional use (right cheek p=0.204, left cheek p=0.109, behind ear p=0.37). Similar to the right cheek, there was a trend for decreased damage in the left cheek in those who reported never using sun protection though this was not a significant change (0.47% p=0.161). The inner arm had no change and was removed from the graph due to high CI bars (occasional use p=0.647, never use p=0.897). Seasonal variation was found in the skin swab results, which again was the inverse of expected damage due to sun exposure. Right cheek swabs had a decreasing trend of damage from samples taken in the winter, decreasing by a mean of 0.91% in spring (p=0.098), 1.40% in summer (p=0.075) and 2.19% in autumn (p=0.021). The left cheek had a similar trend, the decreasing damage peaked in summer rather than autumn with no change from winter in spring (p=0.323), a decrease of 2.44% in summer (p=0.031) and a trend for a lesser decrease in damage in autumn of 1.3% (p=0.096). Behind the ear samples had the same trend as the right cheek, with greater effect. No change in damage was found in the spring compared to winter (p=0.369), summer had a trend of 1.07% decrease in damage (p=0.101) and swabs taken in autumn had a 2.86% decrease in damage (p=0.008). Inner arm samples had no seasonal change (spring p=0.562, summer p=0.463, autumn p=0.518). These results are consistent with results from Ruddy (2022, thesis yet unpublished), whereby repeated swabs were taken from individuals in spring, summer, and autumn. mtDNA damage was found to be significantly reduced in the summer and autumn samples compared to the spring, this effect was found in both cheeks and the inner arm sample.

Skin type and alcohol use were also found to effect mtDNA damage in the skin swabs (Figure 5-18), with age included as a confounding variable. The right cheek swabs had 2.25% less damage from participants with skin type III compared to skin type I (p=0.008), and skin type II had 1.44% less damage compared to skin type I (p=0.05). The left cheek had no significant change in damage from skin type I (type II p=0.199; type III p=0.126), nor was any change found in the behind ear sample (type II p=0.185, type III p=0.324) or the inner arm (type II p=0.267, type III p=0.467). A relationship between increasing alcohol use and increased DNA damage in the swab was found in the cheek and behind ear sample, a similar trend was also observed in the inner arm. Participants who reported no alcohol use had on average 3.21% less damage in the right cheek (p=0.015), 5.65% less damage in the left cheek (p=0.002), and 1.15% less damage behind the ear (p=0.057). The occasional use group also had significantly reduced

damage than the often use in the right cheek (1.55%, p=0.037) and a similar trend in the left cheek (1.06% p=0.08), but not behind ear (p=0.428) or the inner arm (0.55).

5.5 Discussion

5.5.1 Skin swab method of mtDNA damage linked to oxidative stress and stratum corneum health

Mitochondrial network fragmentation by autophagy has been found to be a key signal for the initiation of the cornification process, later followed by depolarisation of the mitochondrial network in mitochondria with elongated networks, and DNA degradation the final step in the process (Ipponjima et al., 2020). Mitochondrial ROS production from lysosome signalling, together with calcium signalling, was found to be integral to epidermal differentiation, disruption to the production of mitochondrial ROS was found to result in undifferentiated cells that retained nuclei (parakeratosis) (Monteleon et al., 2018). Furthermore, mtDNA can be sequenced from hair shafts and are regularly used in forensics of cold cases (Hühne et al., 1999), but the amount of mtDNA recoverable increased the closer the sample was to the hair root, and DNA from older hairs had degraded considerably (Almeida et al., 2011). This suggests the longer the mtDNA is retained in the cell after keratinisation, the more degraded it becomes. Although this has not been assessed in the stratum corneum the process is similar. Taken together, increased mitochondrial ROS and mitochondrial dysfunction initiate autophagic degradation of damaged mitochondria, and as healthy mitochondria undergo depolarisation without autophagic degradation later in the process, it could be hypothesised that increased level of healthy mitochondria at the initiation of cornification could result in greater percentage of mtDNA amplification in the skin swab samples. However, mtDNA continues to degrade after cornification, therefore thicker stratum corneum or slower turnover could be perceived to have more damage to the mtDNA.

Results from skin swab optimisation consistently determined swabs from the arm had greater mtDNA damage than the face, this was in contradiction to previous results with skin swab studies that determined the arm to have less damage than the face (5.4.3). This pattern is consistent was differing stratum corneum thickness between the sites found in the literature, whereby the face was found to have 10±3 layers of stratum corneum in the cheek and nose, 14 layers were measured in the upper inner arm, and 86±46 layers in the heel (Ya-Xian et al., 1999a). In addition, the face (forehead) has been found to have a faster epidermal turnover rate of 1 week compared to 2 weeks on the volar forearm, which could be a result of the differing

thicknesses (Baker and Kligman, 1967). The thicker stratum corneum on the arm/ heel compared to the face could be the reason for the apparent increased damage in those sites compared to the face. Results from the participants with eczema (dysfunctional stratum corneum development) showed no variation in body site of mtDNA quantity, while participants with normal stratum corneum consistently showed a greater percentage amplification in the face, compared to the arm, with the heel having the lowest percentage of mtDNA amplified. Parakeratosis is found in inflamed skin (including eczema) with increased epidermal turnover, whereby cellular structure including the nucleus and mitochondria are retained even in normal appearing skin (Sakurai et al., 2002). This could explain the mtDNA quantity and site variation of the skin swab samples from the eczema participants, further demonstrating the body site variation to be an artefact of differing stratum corneum properties. Interestingly, the weekly change in damage of the eczema participant had a global pattern of increase/ decrease in the face and arm, whereas the normal skin participant varied in damage change between the two body sites. While this was a small sample size for proof of concept, further investigation into this observation could provide a useful understanding of the results of the skin swabs, particularly how internal ROS from different factors affects the mtDNA damage in the skin could be assessed multiple body sites. Overall, the results from the optimisation of the skin swabs show that while there is a link of mtDNA damage to the stratum corneum, there are other confounding factors that affect the change in damage over time.

Stratum corneum thickness and turnover in a single site is influenced by a number of factors. Previous research has determined males have a significantly thicker stratum corneum compared to females (Czekalla et al., 2019), number of years smoking has a negative correlation with stratum corneum thickness but not epidermal thickness, darker skin pigmentation correlate positively with the thickness of the stratum corneum, however age did not have any significant effect (Sandby-Møller et al., 2003). Ya-Xian et al. (1999b) found a slight positive correlation between age and stratum corneum thickness in males but not females (R=0.67). Repeated exposure to low dose solar light (below 1 MED) was found to significantly increase stratum corneum thickness in human participants (Lavker et al., 1995) and mice (Kambayashi et al., 2001), and in response to repeated UVA exposure (Pearse et al., 1987). However, short term response to a 1 MED dose of UVB can result in parakeratosis 4-10 days post irradiation (van der Vleuten et al., 1996). This suggests that while the stratum corneum thickens in response to solar light, it may contain higher levels of intact mtDNA due to poor keratinocyte

differentiation and could give the appearance of lower levels of mtDNA damage in response to solar light.

The level of mtDNA in the skin swab sample is likely affected by the thickness, turnover rate, and health of the stratum corneum. This can be affected significantly by body site and disease state of the skin, without further research it would be difficult to make an accurate comparison between participants. The results of the patient study found no association with level of mtDNA damage from the skin swabs and sex, age, or current smoking status (though only two participants were currently smokers). Increased sun exposure, darker skin tones and reduced alcohol use all appear to have a protective effect on skin swab mtDNA damage. The decreased damage in skin swab samples taken in sunnier months, and in participants who reported never using sun protection could be a result of stratum corneum disruption and incomplete differentiation of keratinocytes, or it could be a result of skin barrier dysfunction due to other atmospheric changes, such as low humidity and drier skin in the winter. Conversely, darker skin tones and reduced alcohol use could result in a true protective effect due to increased antioxidant capacity of eumelanin in darker skin tones (Song et al., 2009a), and reduced oxidative damage/ reduced skin dryness that can result from drinking alcohol (Jiang et al., 2013, Liu et al., 2010).

Interestingly, the correlation between increased skin swab damage and increased UV spots, respective of self-reported sun exposure and alcohol use, could suggests is a direct relationship between melanin production and mtDNA damage. However, this data shows that UV spots are independent of skin type, and perhaps a specific marker of damage. The link between UV spots and skin swab damage could be independent of sun exposure and the association with sun protection use could imply use of an overall skin care regime; use of moisturised could improve barrier function and affect the skin swab results independent of sun exposure. Similarly, the use of skin products could have a damaging effect on the skin and increase damage in the swabs; compounds in sun protection themselves induce stress in skin cells (Wright et al., 2017). Alternatively, the correlation between UV spots and skin swab damage could be related to sun exposure as the month of collection, hours outdoor and skin type were not confounding factors, though the method self-reporting in the questionnaire requires amendments for clarity (discussed in paragraph 5.5.4). Skin swab damage is not associated with age, whereas UV spot area is, which suggests the skin swab damage is transient compared to the age associated accumulation of UV spots.

Overall, the swabs could be used as a method of tracking the skin condition of an individual over time, though there are a number of confounding factors that need to be considered during study set up and analysis.

5.5.2 Perceived age has a higher correlation with UV spots than actual age

UV spots area was a greater predictor of perceived age by evaluators, than actual age or CNN perceived age. CNN is a deep learning algorithm that has been trained using the APPA-REAL database (Clapes et al., 2018), a database of 7591 images with real and apparent ages. However, the algorithm has not been used in a clinical setting so the results were experimental and would require further refinement using the standardised images from the study, without hair or clothing indicators of age. The CNN algorithm had a better performance on camera images than the Visia images, which could be a result of the size of the photographs (including the shoulders in the camera images), or that the Visia images did not contain the full face due to the chin and headrest, or the area in which the Visia camera covered. The dataset used to train the CNN were lower quality images than those taken in this study, therefore the difference in perceived age between the two methods could be a result of the algorithm not assessing fine details of skin ageing. After controlling for actual age, evaluator assessment of perceived age maintained the most significant correlation with UV spot area, which suggests that skin condition from sun damage was a significant driver of perceived age. This was not necessarily expected, the algorithm was not trained specifically to assess skin markers, however, analysis of skin texture in a previous model found blurring skin texture returned a younger age that was more prominent in images of older people (Barney et al., 2018). However, this could suggest the CNN algorithm assesses skin texture of classic signs of chronological ageing but not from extrinsic ageing.

Overall, this data shows that photo-damage from sun exposure is linked to a higher perceived age.

5.5.3 Oxidative stress and UV spots in patients

Oxidative stress is one of the leading causes of complications in diabetes, and is a result of multiple pathways including the modification of proteins by glucose, resulting in induced levels of ROS (Giacco et al., 2010). The results in this study were consistent with the literature, and participants with diabetes were found to have increased levels of oxidative stress.

Increased oxidative stress is also a marker of mitochondrial dysfunction, and patients were found to have elevated oxidative stress to the control participants. This was specifically attributed to patients with point variants, of which 9 out of 13 had the point variant m.3243A>G. This variant has been found to cause elevated oxidative stress *in vivo* and *in vitro*, for example, in patient stem cell derived endothelial cells (Pek et al., 2019), in stroke-like brain lesions of patients (Katayama et al., 2009), patient fibroblasts (Seo et al., 2018) and cybrids of the variant (Pang et al., 2001). Defects in nuclear genes associated with deletions are not associated with increased oxidative stress in this dataset. There was only one patient with this genotype in the study, however, similar results are found in the literature. Defects of the OPA1 gene were not found to affect basal ROS production in skin fibroblasts (Spinazzi et al., 2008), and mtDNA deletions as a consequence of POLγ defects in mice have no evidence of increased oxidative stress in mice mutator models (Trifunovic et al., 2005). Finally, cybrid experiments inducing the 4977 bp single large-scale deletion found that basal ROS levels were increased compared to wild type mitochondria, and this increased proportionally with heteroplasmy (Indo et al., 2007, Peng et al., 2006). Increased sensitivity to exogenous oxidative stress has been found in all of the mentioned genotypes (Pang et al., 2001, Trifunovic et al., 2005, Peng et al., 2006, Indo et al., 2007). This study only took resting oxidative stress levels at a single time point, and optimisation data demonstrated a significant change in oxidative stress throughout the day. The most appropriate method would be to have the patient rested and fasted prior to the sample, however the study set up and recruitment was based on the time of the patients' appointment at the clinic and therefore impractical to get a fasted sample. Further studies could take a sample at the start and end of the visit to test for variability over time.

UV spot area was significantly lower in patients with mitochondrial disease. This could be an artefact due to reduced mobility leading to less time spend outside (Apabhai et al., 2011), the questionnaire amendments could correct for this gap in data in future studies (see 5.5.4). Mitochondria are linked to melanin production, and ROS is a key signalling molecule in melanin synthesis. Upregulation of ATP5B (OXPHOS complex V subunit) and ATP levels coincide with increase production of melanin in response to H_2O_2 treatment of melanoma cells (Kim and Lee, 2013). However, exogenous H_2O_2 can induce cell death in cells with mtDNA aberrations and could result in dysfunctional melanocytes. Furthermore, endogenous H_2O_2 build up in the epidermis of vitiligo patients and contributed to the degeneration of melanocytes (Schallreuter et al., 1999). Alternatively, reduced ATP production from patients' cells could reduce the level of melanin produced in response to stress. Defective ATP production was

found in melanocytes from non-lesional skin of vitiligo subjects, compared to control subjects with no vitiligo, which suggests an integral role of mitochondrial metabolism in the production of melanin (Dell'Anna et al., 2017). Overall, the reduced level of UV spots in patients could be a result of reduced mitochondrial metabolism in the melanocytes or linked to less time spent outdoors in the patient cohort.

5.5.4 Questionnaire issues and amendments

The questionnaire used in this study (appendix A) could benefit from amendments to the lifestyle and health, and sun exposure sections to improve clarification of responses.

Question 16 (Do you participate in physical activity, exercise, or sport?) had only three response categories of yes (at least once a week), mild daily activity (i.e., climbing stairs, walk), and no. Patients may be less likely to take part in physical activity due to myopathy, so the expectation of physical activity intensity in the patient cohort could be lower than the control cohort. To understand exercise as a confounding variable in oxidative stress and perceived age, this question would benefit from more information on what counts at physical activity (i.e., enough to elevate heart rate) and an extra category that reflects the NHS guidelines of 150 mins of moderate or 75 mins of vigorous exercise per week. Question 17 (do you drink alcohol?) has the response categories of no, occasional social use and yes (at least 3 times a week). There is an indicator of what alcoholic drinks count as 1 unit but does not detail in the response categories how many units count as 3 times per week. Instead, this question could benefit from responses that include an indication of how many units per week. Question 20 (how many times do you spend in activities outside, on average throughout the year?) had categories of hours per week as a response, though outdoor activities can be largely weather dependant. This question would benefit from separating the responses into weather scenarios and asking many hours would you likely spend outdoors per week in good/bad weather. Question 21 (do you normally use sun protection for your face when you go outside?) could also benefit from weather scenarios, as sun exposure during the winter can also cause sun damage and the response of 'yes' could imply when it is sunny or everyday regardless of weather. Appropriate responses could be 'always or most days, regardless of the weather', 'always when it is sunny', 'most days when it is sunny', 'occasionally', 'only when sunbathing', and 'never'. Question 22 (have you ever had sunburn on your face?) was a difficult question for most participants as it asks specifically how many instances during their life and requires extensive recall. For clarity, this question could ask if the participant had sun burn on their face in the last year, or

the responses ‘yes’, ‘no’, and ‘unsure’ for the question of ever having sunburn, with a further question asking how many times in the last year. Finally, question 24 (do you normally use sunbeds or tanning lamps?) has the responses never, occasionally (less than 10 times), and very regularly (more than 10 times) but does not specific the timescale for the number of times. This could be improved by having responses never, occasionally but not currently, regularly but not currently, occasionally (less than 1 per month), and regularly (more than 1 per month).

5.5.5 Limitations and future work

The outcomes in this pilot study have provided interesting observations of age analysis techniques, differences in oxidative stress and UV spots in PMD patients, and optimisation of skin swabs as an objective and non-invasive method to detect mtDNA damage in skin.

The sequential recruitment method in this study was used to obtain a wide scope of PMD diagnoses, as it was yet undetermined which variants might influence perceived age and skin damage. Due to the heterogeneity of symptoms associated with the diagnosis, further studies into the association between PMD and ageing would benefit from selecting specific variants. Importantly, controls were not assessed for the ptosis which should be added to the analysis of this data in future. Furthermore, clinical assessment of ptosis severity/ impact of surgical correction would be a useful addition for analysis, as would information of facial muscle weakness and age of onset as this could affect wrinkle development. As a pilot study, the number of participants was small, further expansion of the study to include more participants would be beneficial for a more in-depth determination of facial appearance and ageing with PMD. From the data in this study, patients with ptosis trend for higher perceived age, therefore further interrogation of patients with single and multiple deletions may be most appropriate to further investigate perceived age.

5.6 **Summary of main findings**

- Higher perceived age was associated with single large-scale deletions, presence of ptosis and sun damage.
- Patients on average had increase oxidative stress and lower UV spots levels.
- Decreased skin swab damage correlated with higher self-assessed skin type, lower alcohol use and lower self-assessed sun protection use. Decreased damage was found in participants during sunnier months.
- Skin swab damage was positively correlated with UV spots, damage from the skin swabs appears to be more transient and affected by a number of confounders.

Chapter 6. Mitochondrial Network Response to Stress in Primary Skin Cells

6.1 Chapter Overview

Mitochondrial dynamics requires biogenesis, fusion, fission and mitophagy to maintain integrity. Fusion and fission alter the mitochondrial network in response to its environment, biogenesis is the formation of mitochondria, and mitophagy is controlled degradation through lysosomes. Fusion increases the mitochondrial network connections, inducing a filamentous network morphology; fission causes the network to fragment.

OPA1 is a dynamin GTPase which exists in a long form (L-OPA1) and a short form (S-OPA1), L-OPA1 is unprocessed and S-OPA is proteolytically processed by the ATP-dependant proteases when mitochondrial respiration is dysfunctional, and Oma1 when the mitochondrial membrane is depolarised (Ehses et al., 2009). In response to stress, L-OPA1 is cleaved to S-OPA1 and the balance of long to short isoforms determines the fusion state of the mitochondria. L-OPA1 alone is sufficient for pore opening during mitochondrial fusion, and the addition of low expression of S-OPA increases efficiency of pore opening (Ge et al., 2020). However, increased cleavage and accumulation of S-OPA1 in response to stress mediates mitochondrial fragmentation due to release of OPA1 (Griparic et al., 2007).

Mitochondrial network fragmentation is triggered in response to solar irradiation (Jugé et al., 2016), isolating mitochondria enables the mitophagic removal of the dysfunctional mitochondria without impacting the healthy mitochondria. In multiple cell lines, mitochondrial network elongation occurs upon induction of autophagy and protects against mitophagy (Gomes et al., 2011). Fusion precedes fission, with fission predominantly resulting in a depolarised and a hyperpolarised daughter mitochondria (Twig et al., 2008). Hyperpolarised mitochondria could re-fuse quickly, but the depolarised mitochondrion would then either re-polarise or remain depolarised and undergo mitophagy within hours. Furthermore, mitochondrial quality control mitophagy appears to be dependent on a fragmented network, and high energy cells (e.g., muscle) with long filamentous networks have reduced mitophagy resulting in an accumulation of dysfunctional mitochondria (Malena et al., 2016). This reinforces that fission isolates dysfunctional mitochondria, and also highlights that fusion is a selective process for functional mitochondria.

Guillery et al. (2008) described the mechanisms contributing to fission in skin fibroblasts of controls and PMD patients with variants affecting mitochondria OXPHOS of nDNA and

mtDNA origin. Control cells showed severe network fragmentation (punctate structures) upon treatment with CCCP, a drug which induces depolarisation of the inner mitochondrial membrane; treatment with inhibitors of glycolysis or complexes I, III, IV and V had decreased filament sizes (intermediate structures) but did not show the same punctate structures as with CCCP. Patient fibroblasts with severe OXPHOS deficit showed the same punctate structures upon glycolysis inhibition, whereas those with mild OXPHOS deficiencies maintained longer filamentous structures. This research combined with that of Twig et al. (2008), shows that mitochondrial fission and fusion is selective and dependant on mitochondrial membrane potential, decreased membrane potential can either precede mitophagy or a regain of membrane potential, and severe OXPHOS deficiency is capable of severely fragmenting the mitochondrial network when other sources of energy production (glycolysis) are removed.

Ribonucleotide reductase M2B (RRM2B) gene encodes a p53-inducible ribonucleic acid subunit (p53R2). P53R2 is signalled during cell cycle arrest to form part of the ribonucleotide reductase enzyme in response to DNA damage, which catalyses the *de novo* synthesis of nucleotides by the reduction of ribonucleotide diphosphates to their resultant deoxyribonucleotide diphosphates (Wang, 2016). This maintains the pool of dNTPs during mtDNA repair, and mtDNA synthesis in G_0-G_1 state. P53R2 expression is upregulated from 6 hours (which was the first time point after 0 hours) in HDFn cells in response to DNA damage, and remained elevated up to 48 hours (maximum time point) (Tanaka et al., 2000). Defects of the RRM2B gene can result in severe mtDNA depletion syndrome with infant mortality, or present later more commonly with mtDNA deletions (Pitceathly et al., 2012). Fibroblasts are highly proliferative, and therefore show less mtDNA damage in response to high dose irradiation (UVC) than serum starved cells (Pontarin et al., 2012) . However, this study is interested in the network response and mtDNA response to a sub-lethal dose in cycling cells, without inducing mtDNA depletion through serum starvation.

Overall, visualisation of mitochondrial dynamics in response to stressors can obtain a breadth of knowledge about mitochondrial health and ability to recover. So far, mitochondrial dynamics in fibroblasts have not been researched in response to solar irradiation; visualising the mitochondrial network over time following a sub-lethal dose of solar radiation will give insight to mitochondrial recovery post exposure.

6.2 **Chapter aims**

To assess the mitochondrial dynamics response after a moderate dose of solar light in healthy and mitochondrially dysfunctional human dermal fibroblast cells.

- Visualising mitochondrial network post irradiation.
- Determining protein expression of OPA1 and mitochondrial ATP5a as a marker of fusion and mitochondrial content post exposure, respectively.
- Using qPCR to assess mtDNA damage and content, as a marker of repair and mitophagy

6.3 **Chapter specific methods**

6.3.1 Cell seeding and dosing conditions

For imaging, cells were seeded at a density of $4x10^3$ cells per well in a black, 10- well slide with Advanced™ TC treatment (Greiner bio-one, UK). Cells were left to adhere for at least 24 hours prior to dosing. The Advanced™ TC treatment was delicate, so the removal of media was carried out using a P200 tip and media was carefully added using a 1 ml stripette; the addition and removal of media was optimised to prevent the treatment lifting from the well edges. For Western blot and qPCR, cells were seeded at $2x10^5$ cells per 60mm cell culture dish and left to adhere for 24 hours before dosing. Cells were grown in their respective media and washed with PBS prior to dosing. Cells received a dose of 2.16 SED of total solar simulated light for the subsequent analysis.

6.3.2 Imaging of mitochondrial network

6.3.2.1 Plasmid transformation, transfection, and storage

Mito-mCherry and mito-GFP plasmids were kindly gifted from Mag Aushev and Mary Herbert, MitoQC was kindly gifted by Viktor Korolchuk, and photoactivatable-GFP (PA-GFP) was a gift from Karel Svoboda (Addgene plasmid # 18697 http://n2t.net/addgene:18697 ; RRID:Addgene_18697). Transformation was performed in a flame sterile environment in NEB 5-alpha *E.coli* (New England Biosciences, USA) according to manufacturer's protocol. *E.coli* cells were thawed on ice for 10mins and 1ng of plasmid DNA was pipetted directly into the tube and mixed. The mixture was placed on ice for 30 mins, heat shocked at 42˚C for 30 seconds, and placed on ice again for 5 mins before adding 950 µl of SOC was added and the tube was incubated at 37˚C for 60 mins at 250 rpm. Cells were then serially diluted in SOC, 100 µl was spread onto nutrient agar selection plates [2% (w/v) Lysogeny broth (ThermoFisher, UK), 1.5% (w/v) nutrient agar (ThermoFisher, UK); 100 µg/ml ampicillin; mQ water], and plates were incubated overnight at 37˚C before individual colonies were expanded in LB broth [2% (w/v) Lysogeny broth (Thermofisher, UK); 100 µg/ml ampicillin; mQ water]. The resulting culture was either stored short term at -20 ˚C before plasmid purification using plasmid mini prep kit (Qiagen, UK) as per manufacturer's protocol, or stored long-term at -80˚C with 7% DMSO.

Lipofectamine LTX (Thermofisher, UK), XFect (Takara Bio, France), and Viromer Red and Viromer Plasmid (Lipocalyx, Germany) were all tested as transfection reagents in HDFn cells, optimisation was carried out for each as per manufacturers' protocol.

6.3.2.2 CellLight® transduction

CellLight®, BacMam 2.0 reagents mitochondria GFP and mitochondria RFP (ThermoFisher, UK) which target the leader sequence of the E1 alpha pyruvate dehydrogenase were added to visualise the mitochondria. Each reagent was added with the equivalent of 40 particles per cell per reagent. Experimental cells were transduced with both GFP and RFP, a single fluorophore control was set up for each RFP and GFP, and an unstained control for each irradiated and un-irradiated. Cells were dosed after a minimum of 16 hours incubation.

6.3.2.3 Final staining protocol for cell imaging

Cells were dosed at intervals prior to imaging, and imaging for all time points was performed together within 45 mins of staining. After dosing, cells were incubated for 30 mins with phenol red and FBS free media containing 200 mM MitoTracker Green FM (ThermoFisher) and 75 mM LysoTracker Red DND-99 (Thermofisher). Cells were washed twice in PBS and phenol red free media with 5% FBS was added, and imaging was carried out immediately.

6.3.3 Imaging

Images were taken using Zeiss LSM800 confocal microscope at x40 magnification with 1.3 NA at 37°C supplemented with 5% CO_2. 15-20 images were taken at random per condition with the 581nm laser with bandpass filter 565-795nm for RFP and 488nm laser with bandpass filter 496-542nm for GFP, using definite focus to automate the imaging and reduce the time taken to capture.

6.3.3.1 Quantification of mitochondrial network parameters

Deconvolution of images for performed using deconvolution wizard in Huygens Essential software (Scientific Volume Imaging, Holland). This process uses mathematical basis for removing out of focus light that can cause blurring on the images, producing a clearer image. Background was set independently for the green and red images to account for electronic offset and indirect light in the image, and signal to noise was set to adjust the sharpness of the outcome. Data was then collected using ImageJ software and single cells were isolated from

each image. MiNA plug in was used to assess the mitochondrial network, this gave results for mitochondrial footprint, number of branches within the network, and length of network branches. The plugin has optional pre-processing steps to clean the image, of which the optimised parameters were used: mean filter of radius 2; unsharp mask of radius 2 and mask weight 0.5; and Enhanced local contrast (CLAHE) of block 99, histogram 256 and max slope of 1.5. The software then uses an automatic threshold (optimal method used in this analysis was oshu), ridge detection to find the mitochondrial network, it then skeletonises the thresholded image for the final data collection.

Mitophagy assessment was achieved in ImageJ software by isolating regions with red and green fluorescence, this is where mitochondrial stain co-referenced with a lysosome. Red and green channel images were selected, and calculations were performed on the maximum intensity of the images (Z-project function). Threshold of the images is adjusted for maximum entropy which is an algorithm which maximises the certainty an event has taken place, and dark background and stacked histogram options were selected. Image calculator function was used to identify areas with green and red co-referenced fluorescence, positive results were selected based on particle size of 0.01 microns^2 -infinity and circularity of 0.6-1 using the Analyse Particle algorithm, these parameters account for the large and circular appearance of mitophagy artefacts. Mitophagy results were shown as number of event/ mitochondrial volume to normalise results.

6.3.4 Protein analysis of mitochondrial fission and fusion

$2x10^5$ cells were seeded in 60mm cell culture dishes and incubated overnight at 37˚C supplemented with 5% CO_2 prior to dosing. Media was replaced with 5ml PBS prior to 2.16 SED total solar light irradiation, the PBS was then replaced with media and cells were incubated until cell lysis. Cells were washed with ice cold PBS and lysed in 100 µl/well ice cold 1x RIPA buffer (Merck, Germany) supplemented with 1x protease inhibitor cocktail and 1x phosphatase inhibitor cocktail I (Abcam, UK) for 30 mins on ice. Samples were pulse sonicated twice for 5 seconds each at an amplitude of 7 microns at 23 kHz frequency and centrifuged for 10 mins at 12,000xg at 4˚C to remove insoluble particles. Protein was quantified in the samples using Pierce BCA protein assay kit (ThermoFisher, UK) and 10 µg of protein was used for the Western Blotting. Samples were heated at 95˚C for 5 mins with 1x Laemmli sample buffer (BioRad, UK) and 10% β-mercaptoethanol (ThermoFisher, UK). Proteins were separated by SDS-Page with 4-20% Novex^{TM} Tris-Glycine pre-cast polyacrylamide gels

(ThermoFisher, UK) in running buffer [0.25 M Tris base; 1.92 M Glycine; 1% (w/v) SDS; in 1L mQ water at pH 8.3] at 100V for 10 mins before increasing to 125V until the dye front ran off the gel. Protein was transferred to pre-cut and soaked 0.2 μM nitrocellulose membranes (BioRad, UK) in the TransBlot turbo transfer system using the mixed MW setting. Membranes were blocked for 1 hour at room temperature in 5 % (w/v) bovine serum albumin (BSA; Thermofisher, UK) in Tris-buffered saline (TBS; 200 mM Tris base, 1.5 M NaCl, pH 7.6), incubated overnight with primary antibodies [OPA1 (MAB96506) from R&D systems; ATP5a (51) and Fis1 (B-5) from Santa Cruz; GAPDH (AM4300) and VDAC (PA581300) from Thermofisher] in 5% BSA in TBS-T (0.1% Tween-20 in TBS) and incubated for 1 hour at room temperature with IRDye fluorophore tagged secondary antibodies (LiCOR, USA). Membranes were imaged using LiCOR Odyssey FC imaging system at the appropriate light wavelength.

6.3.5 QPCR analysis of mtDNA damage

The 83 bp, 93 bp, 1 kb and 11 kb mtDNA content and damage assays were performed as described in general methods.

6.4 **Results**

6.4.1 Optimisation of imaging techniques

6.4.1.1 Visualisation of plasmid efficiencies

Initially, plasmids were used to establish mitochondrial imaging but the HDFn cells had a low transfection efficiency, and those cells which did uptake the plasmid did not appear viable. Transfection tests were carried out using mito-mCherry as fluorescence was strong in cells successfully transfected, it was therefore a good positive control. Neither Viromer Red nor Viromer Plasmid showed any fluorescence in healthy cells using 25 ng to 200ng of plasmid, Viromer Plasmid showed minor signs of toxicity in some wells and no toxicity was seen with Viromer Red (data not shown).

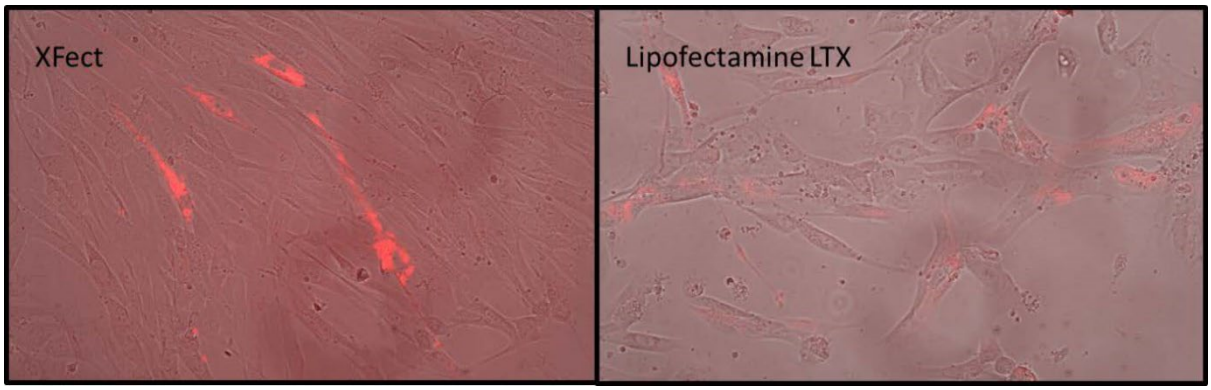

Figure 6-1. Transfection efficiencies with XFect and Lipofectamine LTX transfection reagents in HDFn cells**.**
Both images showing the best results using 2 µg of mito-mCherry plasmid.

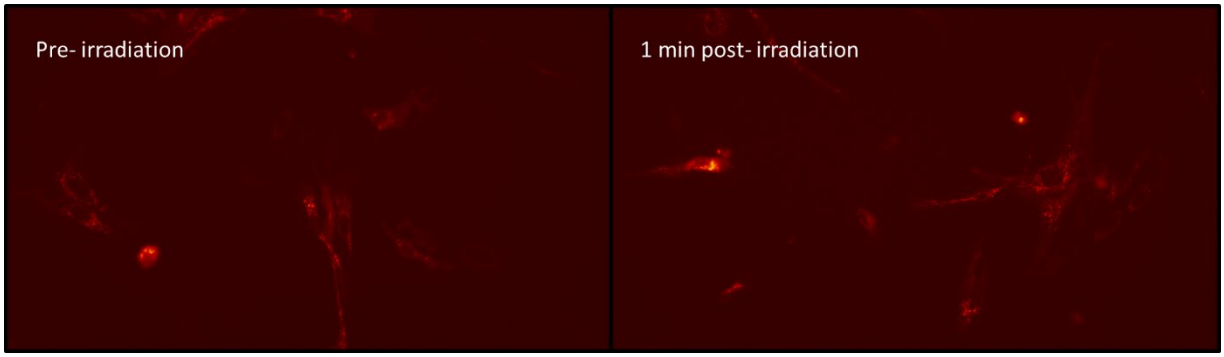

Figure 6-2. Transduction of cells with CellLight® mitochondria-RFP pre and post irradiation of 1 minute total solar light.

LTX had a better transfection efficiency than XFect with mito-mCherry (Figure 6-1), but neither had success with mito-EGFP transfection. The results were inconsistent between attempts, and the cell health was a concern with the plasmid transfection as fibroblasts are a

notoriously difficult cell type to transfect (Kucharski et al., 2021). No further attempts were tried with other plasmid transfection techniques, as they tend to be more damaging to the cells. CellLight® uses insect baculovirus to deliver fluorescent proteins tagged for the mitochondria into the cell. The system was found to have no visible toxicity and no immediate loss of signal after irradiation. Fluorescence was still visible in cells at 5 days post transduction and the process did not involve the removal and addition of new media as with transfection reagents, which had previously resulted in loss of cell adherence with the Advanced^{TM} TC treatment in the wells.

6.4.1.2 Analysis of network dynamics using CellLight in HDFn cell line

Imaging was trialled using CellLight®, BacMam 2.0 in HDFn fibroblast cells. Live cell imaging was captured every 20 mins from 2 hours to 14 hours post exposure to solar light to gauge an appropriate time course for future experiments. To balance the number of images required to obtain an appropriate number of cells with over exposure from overnight imaging, images were captured at 20x magnification on CD7 microscope. Individual particles were counted using ImageJ analyse particle function after a threshold was applied to the image, which gave the total count and the average area of each fragment. Red and green fluorescent proteins (RFP and GFP) were used to determine if it was an appropriate method to calculate the number of mitophagy events. RFP is more stable at lower pH than GFP, therefore during mitophagy the GFP will degrade while the RFP will remain stable. This method relies on consistent uptake of RFP and GFP within the mitochondrial network of a single cell. Mitophagy was determined by subtracting the green channel from the red channel and analysing particles above 2 μm in size and 0.6 in circularity. Additionally, this requires cells to be pre-treated with the CellLight before irradiation, so irradiation could affect the fluorescent properties and therefore the result.

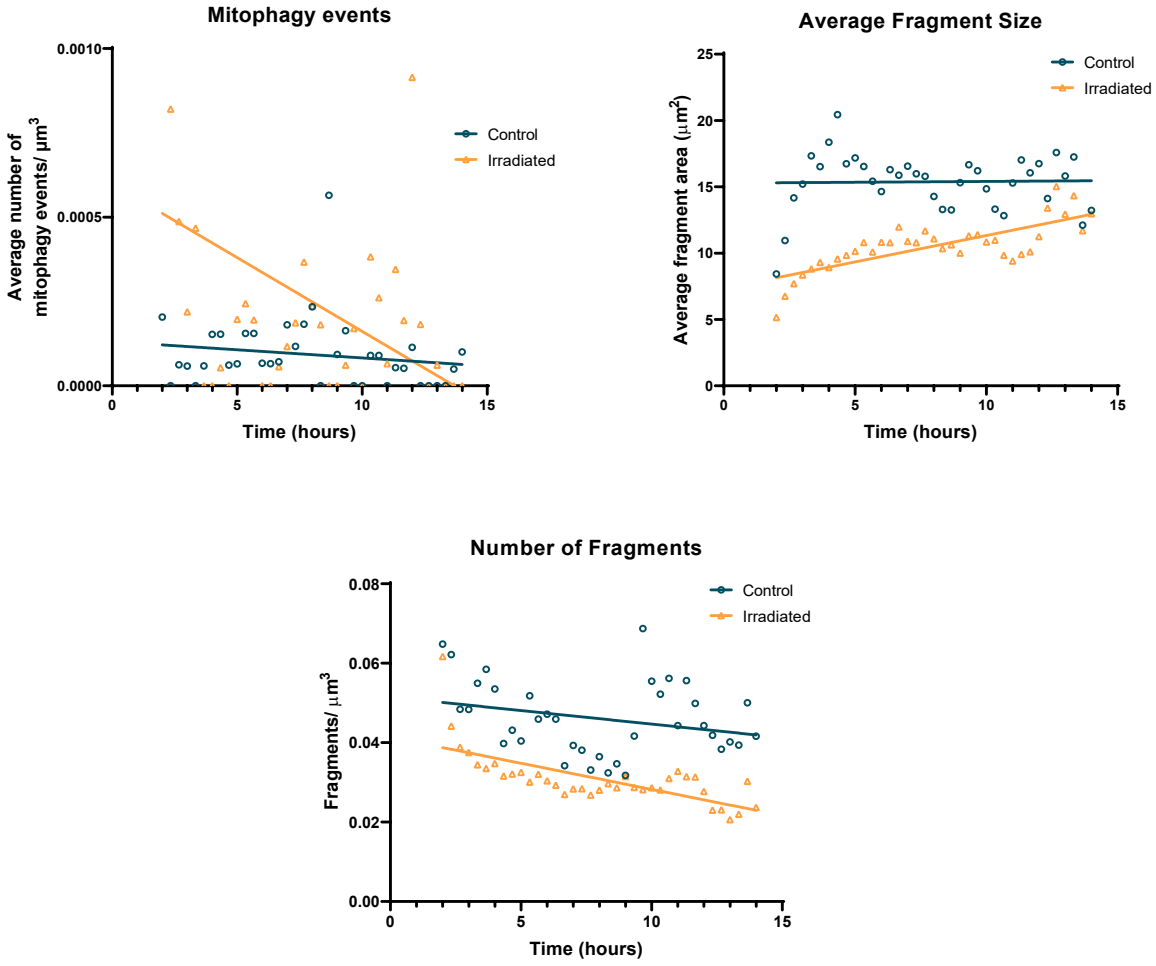

Figure 6-3. Mitophagy events, fragment size and number of HDFn cells post irradiation.
HDFn cells were transduced with CellLights MitoRFP and MitoGFP one day before irradation. Cells were irradiated by 2.16 SED solar simulated light and imaging was performed on live cells at 20x magnification following irradiation. Mitophagy events and number of fragments counted as total number per µm^3 of total mitochondrial network density per frame; cells were images every 20 mins from 2-14 hours post exposure; N=6, n=1.

The number of mitophagy events appeared to remain constant for the control cells and were initially elevated in the irradiated cells, which decreased over time. The technical repeats determined the line to be borderline significantly non-zero ($p=0.055$). The irradiated cells had a smaller fragment size initially and increased over time from 2-14 hours ($p<0.0001$), while the control cells had a consistent fragment size ($p=0.95$). The number of fragments remained consistent for the control cells over time ($p=0.48$) and decreased in the irradiated cells ($p<0.0001$). While the mitophagy events and fragment size in the irradiated cells returned to control levels after around 14 hours, the number of fragments in the irradiated cells was less than the control cells initially and further decreased over time. This could be due to the method of calculating the number of fragments; as it was determined per total cell density in each scene

rather than per cell, it would depend on the cell region that was present in the scene. Cells have larger single fragments around the nucleus, and increasing fragmentation tends to occur further as the distance from the nucleus increases. However, if this was an artefact of the cell region in each scene, a similar effect would be expected in the fragment size. The decreased number of fragments in the irradiated group could therefore be a result of fluorophore bleaching during the irradiation. This could impact the results of the experiment, and a method of staining post irradiation was used for subsequent experiments.

6.4.1.3 Fixed mitochondrial network and lysosomes via staining

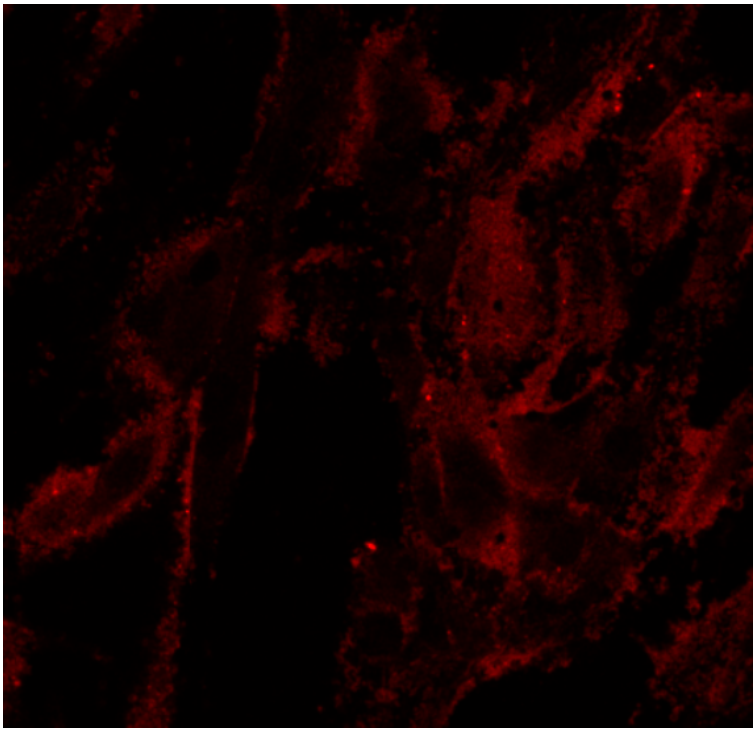

Figure 6-4. Representative image of MitoView fix 640 staining after fixing in 4% PFA
Staining was not retained in the mitochondrial network after staining for 1 hour at 75nm or 150nm concentration (image shown at 75 nm concentration).

Optimisation of imaging was tested on fixed cells. Cells were stained with MitoView fix 640 stain (Biotium, USA), fixed for 15 mins in 4% paraformaldehyde (PFA) in PBS and washed in PBS before imaging. MitoView staining was not retained after fixing (Figure 6-4). Staining required upwards of 1 hour, and therefore was not appropriate for the subsequent imaging experiment to analyse the mitochondrial network at a shorter interval post irradiation.

6.4.2 Optimisation of western blot techniques

Cells for western blotting were initially lysed using a buffer made in the lab (100 mM Tris-HCL (pH7.4), 100mM sodium chloride, 25 mM sodium fluoride, 1 mM benzamidine, 2mM EDTA, 0.1 mM sodium orthovanadate, 1% Triton X100, 1% protease inhibitor cocktail), with the primary antibodies diluted in 5% non-fat milk (NFM) in TBS-T and a Precision Plus protein ladder (BioRad, UK). This had low protein yield and produced smeared blots upon imaging. First 5% NFM was exchanged for 5% bovine serum albumin (BSA) to dilute the primary antibodies, as this is a single purified protein as opposed to multiple mixed proteins found in NFM and can reduce background caused by cross reactivity. Additionally, a new protein standard was used to obtain a clearer ladder. This step reduced the background; however, the protein yield was still low. To counter this, RIPA buffer was used in place of the lab made lysis buffer and an additional sonication step was added to increase protein yield. The initial blocking stage was performed in TBS instead of TBS-T. Antibody tests found no additional bands for the selected targets ATP5a and OPA1 (Figure 6-5).

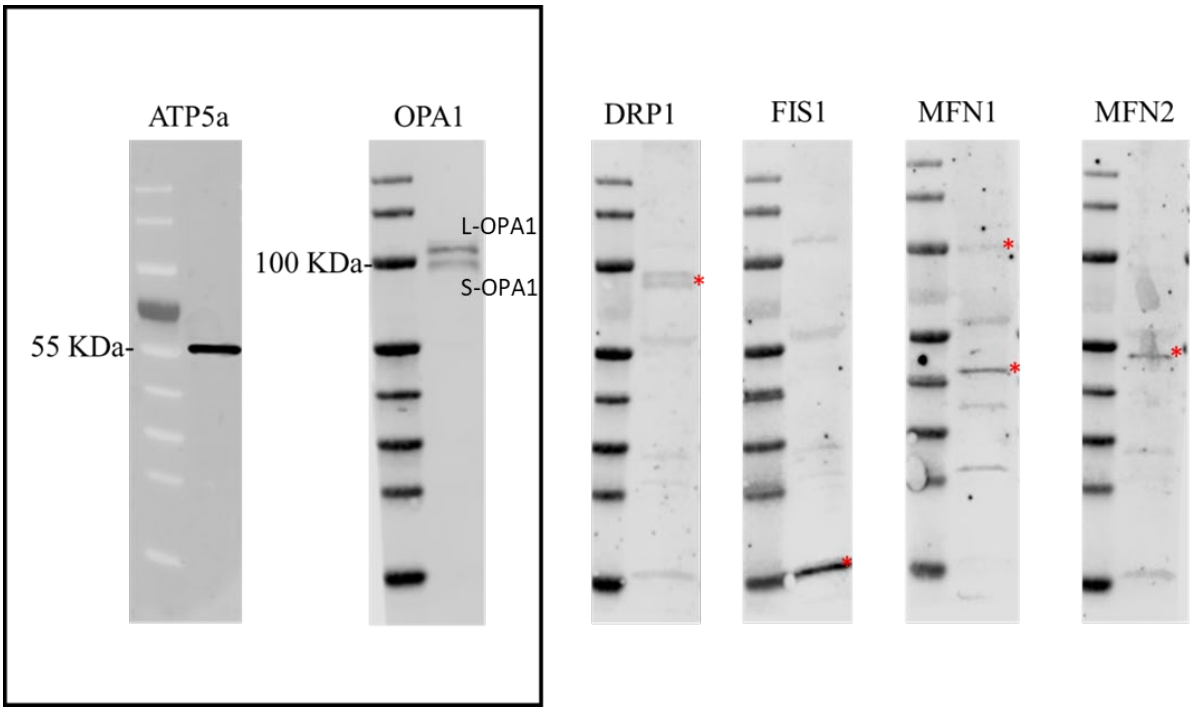

Figure 6-5. Single blot analysis of target proteins.
OPA1 (mitochondrial inner membrane fusion) and ATP5a (mitochondrial complex V protein as content marker) were . DRP1 and FIS1 (mitochondrial fission proteins), MFN1 and MFN2 (mitochondrial outer membrane fusion proteins); samples from whole cell lysates of patient cell line M1096; *denotes expected bands.

6.4.3 *No differences in mtDNA damage or content were found between patient and control cells*

Analysis of average mtDNA damage (1 kb) and content between control and patient cells found no significant change in response to low dose solar light (data not shown). Analysis of individual cell lines found mtDNA content decreased by 0.26 fold change for patient 1 at 4 hours ($p=0.043$) and control 1 at 8 hours ($p=0.042$) post exposure. Patient 1 also had a 0.88 fold increase in 1 kb damage from control at 24 hours post irradiation ($p=0.015$), but no other significant change was found in any other donors.

More significant levels of damage were found after the 11 kb assay. Control 1 had elevated damage for the first 8 hours after exposure (damage at 4 hours was highly variable ranging from 1.04 Ct difference to 4.78 Ct difference and was not found to be significantly elevated from control at this time point ($p=0.106$)). Damage was elevated by a mean of 3.81 Ct from control at 0 hours ($p=0.001$) and reducing to 3.45 Ct at 8 hours ($p=0.011$), damage returned to non-significant levels at 24 hours ($p=0.154$). Patient 1 had elevated damage for the entire time course ($p<0.0001$), starting at 2.65 Ct difference at 0h ($p=0.003$) and increasing to 3.45 Ct at 8h ($p=0.003$), there was still a 1.9 Ct increase in damage after 24 hours ($p=0.003$). Patient 2 had the lowest damage of all 3 cells, with an increase of 2.1 Ct damage at 1 hour post exposure ($p=0.021$) and no significant change from control at any other time point. At 1 hour post exposure, patient 2 had significantly less damage than control 1 (1.8 Ct; $p=0.036$) and at 8 hours post exposure, this cell line had significantly less damage than control 1 (1.49 Ct; $p=0.033$) and patient 2 (1.7 Ct; $p=0.047$). Control 2 was unable to amplify for the 11 kb due to issues with the assay at the time.

The levels of mtDNA damage and content did not have a direct trend from 0h, therefore change from the 24 hour sample was tested to determine at which time point the mtDNA content/damage started to change towards the final 24 hour level. mtDNA content had no significant change from 24 hours in any cell line (m1171 $p=0.33$; m0528 $p=0.36$; m1096 $p=0.075$; m1582 $p=0.21$). Damage from the 1 kb assay found only patient 1 cells had any significant change from 24 hour, there was a 2-fold increase in damage from 1 hour ($p=0.0087$) and a 1.7 fold increase in damage from 4 hours ($p=0.024$). No significant change was found from 0 hours ($p=0.088$) or 8 hours ($p=0.31$). No change was found in Control 1 (m1171) ($p=0.2$), m0528 ($p=0.87$) or m1582 ($p=0.64$).

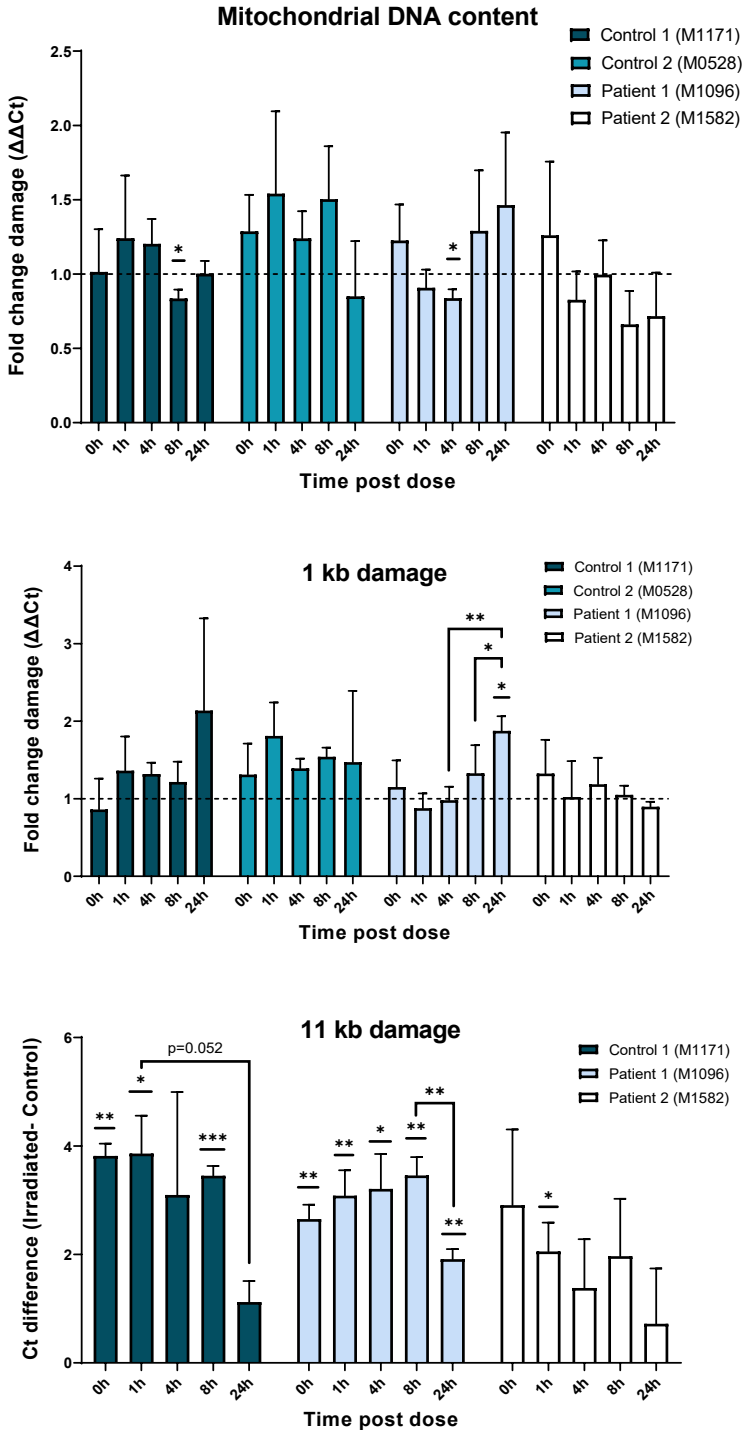

Figure 6-6. Time course changes in mtDNA content and damage after exposure to solar light.
Cells were dosed with 2.16 SED at intervals prior to DNA extraction, mtDNA content was detemined using the 83 bp (mtDNA) and 93 bp (nDNA) assays, and mtDNA damage was determined in the 1 kb and 11 kb region and control for my mtDNA content. Statistical differences between unirradiated control and irradiated samples were determined by one-sample t-Test; Fold change data was $\log_2$ transformed for analysis; one-way ANOVA multiple comparion test with Bonferroni's correction was used to assess changes between time points, change from 24 hours was tested for each marker; ***p<0.001, **p<0.01, *p<0.05; M1171 (n=3), M1096 (n=3), M1582 (n=3, 24 hours n=2), M0528 (n=2).

Change in damage from the 11 kb assay showed no significant change from 24 hours at any time point in patient 2 (m1582) cells (p=0.43). Patient 1 cells had a significant decrease in damage of 1.5 Ct from 8 hours to 24 hours (p=0.004), damage at 1 hour and 4 hours were both significantly higher than at 24 hours (1.17 Ct p=0.024 and 1.3 Ct p=0.013, respectively), and no change was found from 0 hours (p=0.21). Control 1 cells (m1171) had no significant changes from 24 hours, but a borderline 2.69 Ct decrease was observed from 0 hours (p=0.056) and 2.73 Ct from 1 hour (p=0.052). With no significant change from 4 hours (p=0.21) or 8 hours (p=0.11). 24 hour sample for control 1 only had n=2 which could account for the low statistical power.

Change in mtDNA content was assessed between the cell lines, Patient 1 cells (M1096) were found to have significant lower levels of mtDNA compared to Control 1 (M1171) (p=0.0068) and Patient 2 cells (p=0.0302).

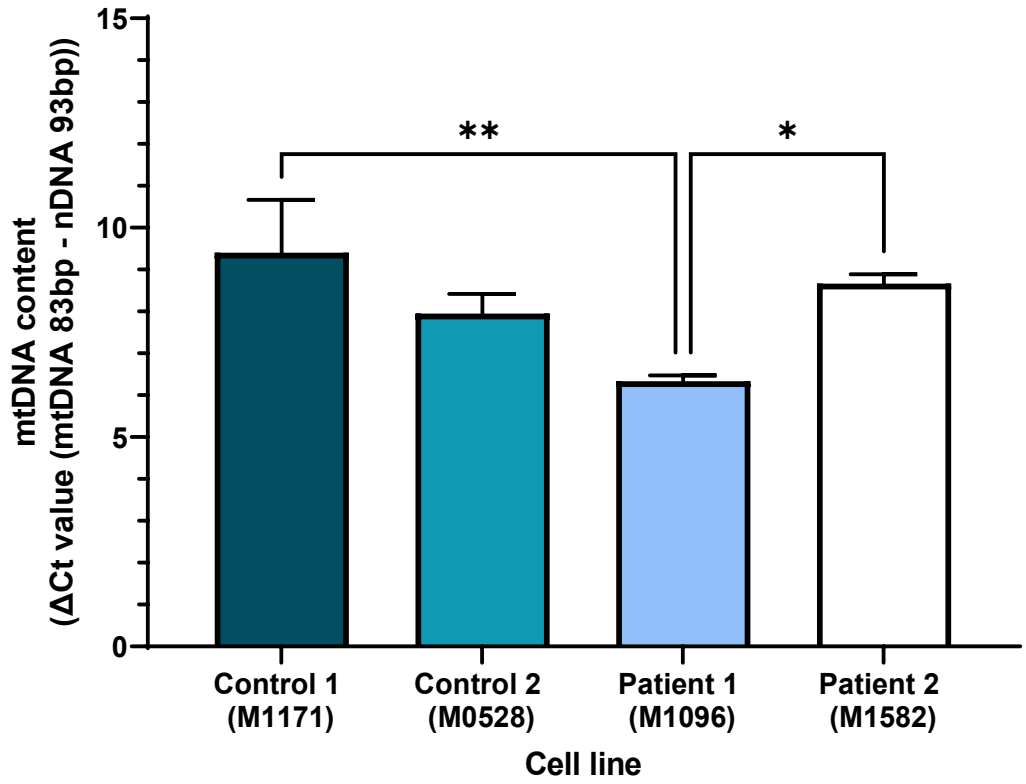

Figure 6-7. mtDNA content of each cell line
MtDNA content was assessed in each cell line by determining the change in Ct value between the 83 bp mtDNA housekeeping amplicon and the 93 bp nuclear housekeeping in the control cells at 0h post exposure; statistical differences were determined by one way ANOVA with Bonferonni's correction; **p<0.01, *p<0.05; n=3 (M0528 n=2)

6.4.4 Decline in mitochondrial content and early changes to OPA1 post irradiation

Protein expression of western blot images was calculated by normalising to either GAPDH or ATP5a (whole cell protein and mitochondrial protein, respectively). Change in mitochondrial fusion proteins was variable over time, fibroblasts from patient 1 had a 43% decrease in L-OPA1 at 1 hour post exposure that returned to control levels by 4 hours ($p=0.02$), and a 59.6% decrease in ATP5a expression was observed from 0 to 8 hours post exposure ($p=0.038$). Patient 2 cells had no significant change in ATP5a ($p=0.822$), L-OPA ($p=0.389$), or S-OPA1 ($p=0.942$) levels from control at each time point, nor was there any change from the 0 hour time point. Control 1 cells had no significant change in ATP5a expression from control at each time point, and a decrease of 67.8% expression from 0 to 8 hours post exposure ($p=0.0106$). L-OPA1 expression was decreased by 24.6% from control at 0 hours ($p=0.049$) and increased by 9.2% from control at 8 hours post exposure ($p=0.046$). No significant change was found in S-OPA levels, though at 8 hours there was a borderline significant increase of 42.7% ($p=0.057$).
Analysis of control 2 (M0528) cells could not be performed as the reduced growth due to the health of the cells resulted in low protein yield, likely due to the apoptotic nature observed during imaging.

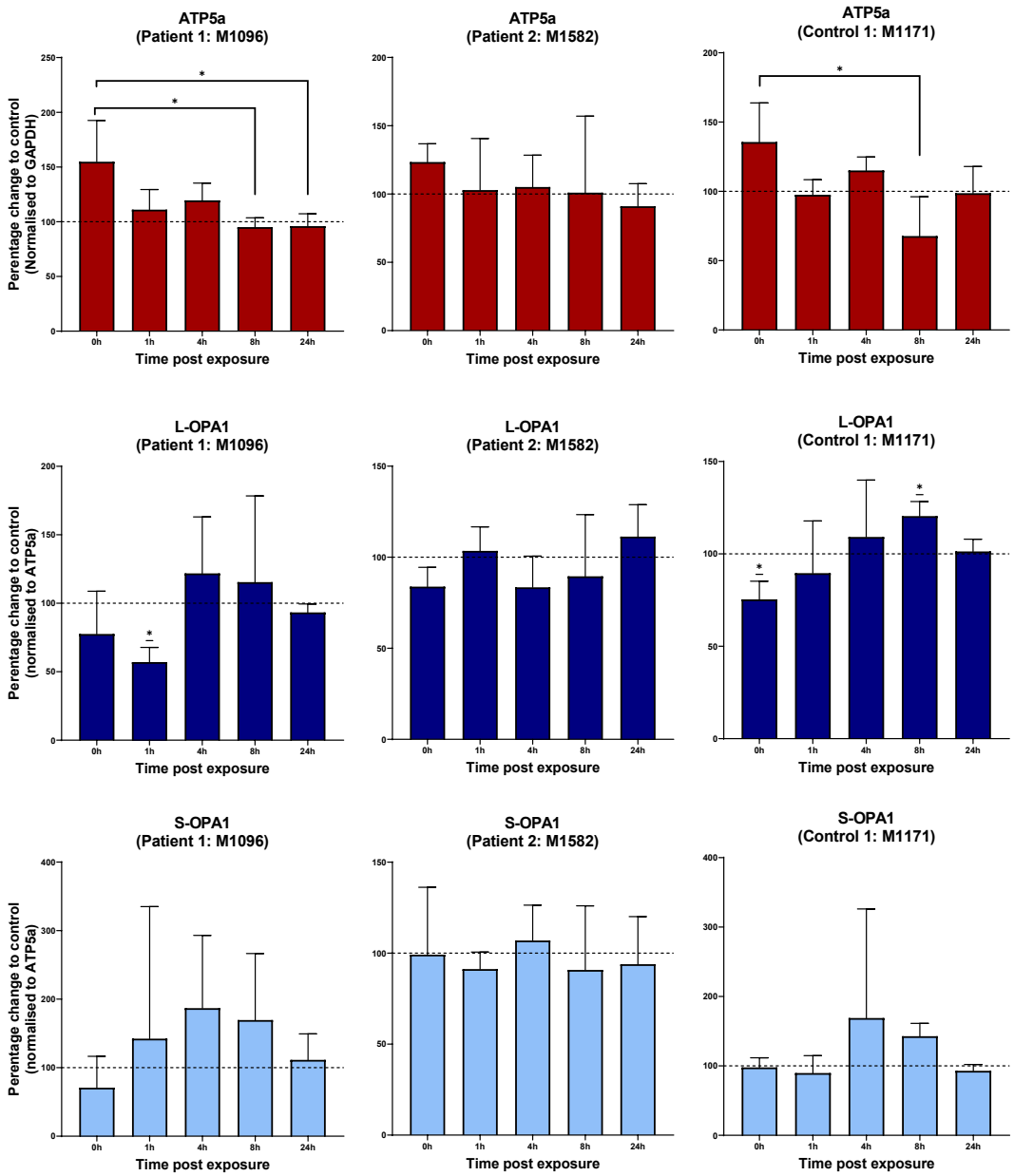

Figure 6-8. Protein levels of ATP5a, L-OPA1 and S-OPA1 post 2.16 SED irradiation in patient cells ATP5a normalised to GAPDH and OPA1 normalised to ATP5a expression levels; L-OPA1 top band and S-OPA1 lower band of the OPA1 blot; statistical differences from control determined by one sample two-tailed t-test from hypothetical value of 100, and differences from 0h determined by one way ANOVA multiple comparison test with Bonferonni"s correction; *p<0.05; n=3.

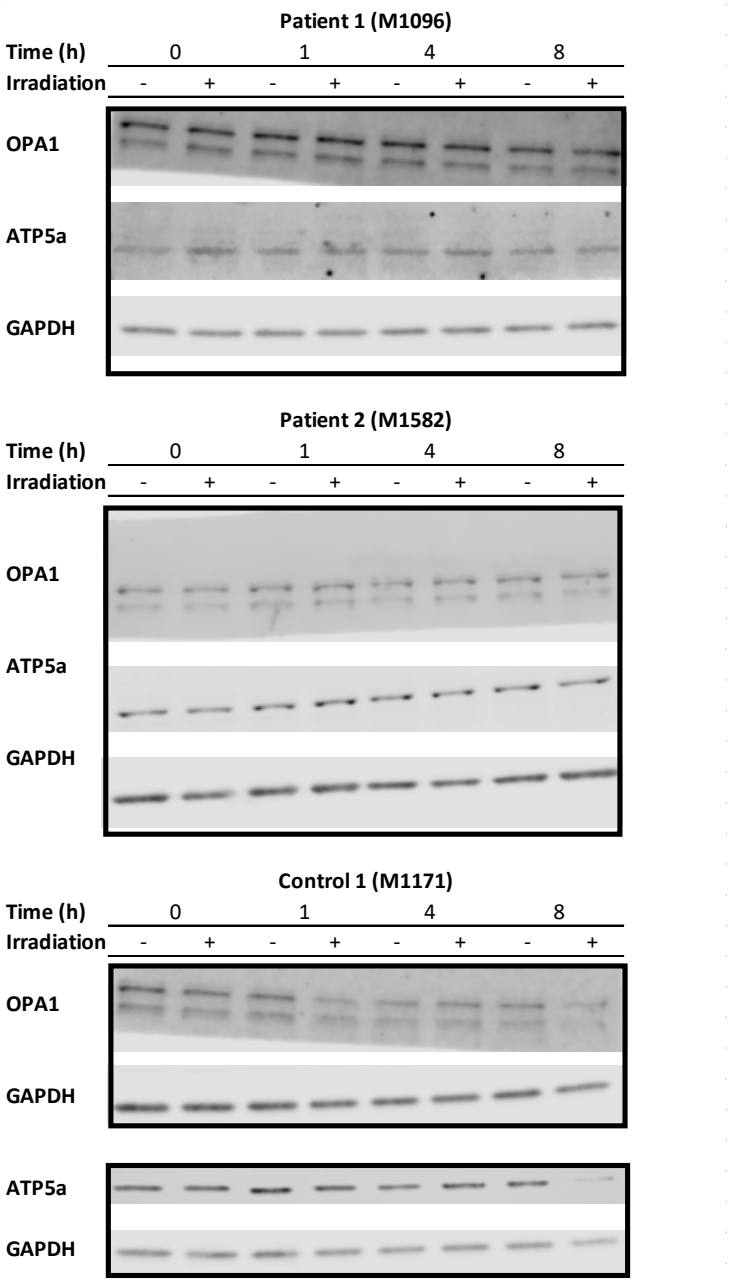

Figure 6-9. Representative Western blot images 0h to 8h post 2.16 SED solar irradiation exposure.

6.4.5 Mitochondrial network analysis of images

Mitochondrial network imaging was performed on both patient cell lines, however both control cell lines experienced issues and were highly apoptotic during imaging so were not analysed (representative images in appendix I).

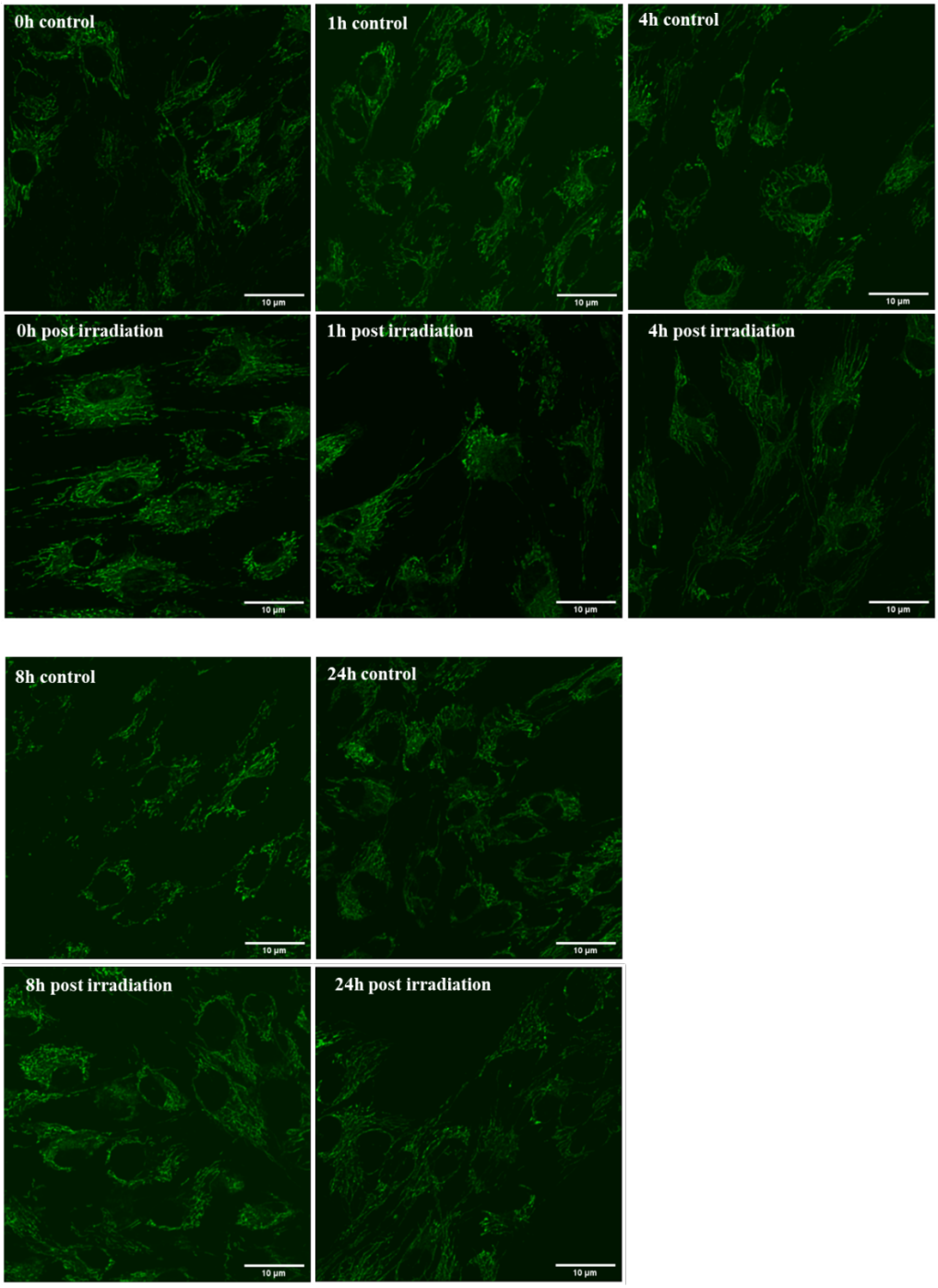

Figure 6-10. Representative images of mitochodnrial network in patient M1096 cells.
Cells were dosed with 2.16 SED solar simulated light at intervals prior to imaging, and images were taken at 40x magnification on LSM800 confocal microscope; Control= no irradiation; n=3.

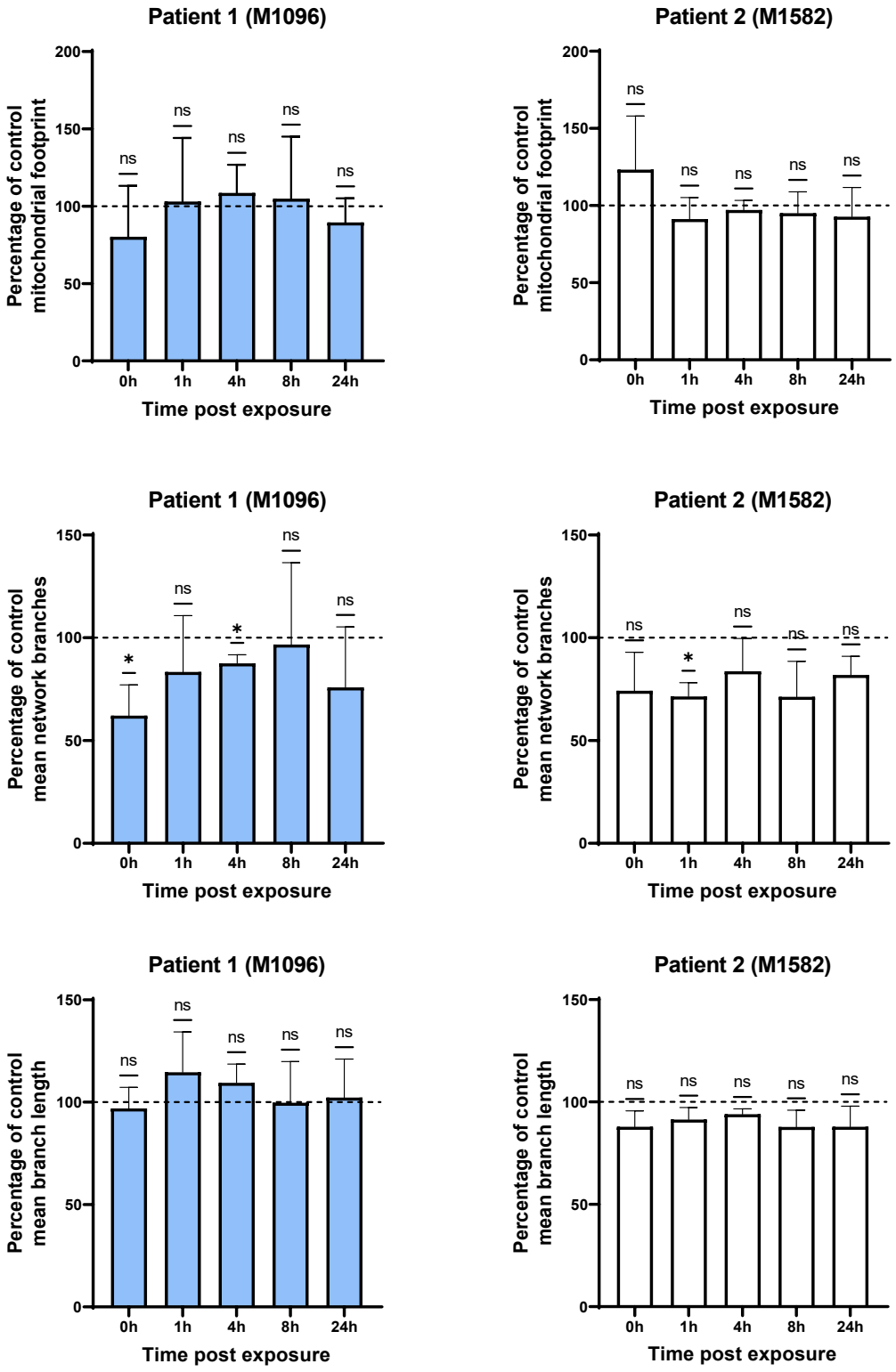

Figure 6-11. Mitochondrial network analysis from imaging of cells after 2.16 SED solar simulated light irradiation.
Graph shows the change from control in mitochondrial footprint, mean number of network branches and mean length of network branches as calculated using MiNA software in immortalised primary

dermal fibroblasts; statistical differences were determined by one sample t-test from hypothetical mean of 100; *$p<0.05$; n=3.

Results from mitochondrial network analysis show variation in the first 4 hours after dosing. At 0h (with staining and set up, this time is equivalent to 1 hour post exposure), patient one had 38% less network branches than the control ($p=0.048$) and also had 23% less network branches at 4h post dose ($p=0.036$). There was no significant difference from control at 1h ($p=0.40$), though a trend of increasing network branches was observed from 0h to 8h. Patient 2 had significantly less network branches than the control at 1h ($p=0.02$) but not at 0h post exposure. There was no change in mitochondrial footprint or the length of the network branches at any time point.

LysoTracker Red analysis determined it would be necessary to obtain images at x63 magnification for co-reference analysis, though it was a useful marker to determine apoptosis in cells during mitochondrial network analysis (representative images from each cell line in appendix I). For the experimental set up to determine an appropriate time course for future experiments it was necessary to use a lower magnification to obtain more cells per image.

6.4.6 Combined summary analysis of mtDNA, protein and imaging data

The results of this study show that changes in mitochondrial dynamics occur within the first 8h after irradiation, and changes to mtDNA damage occur between 8 and 24 hours. Comparison of ATP5a expression and mtDNA content showed all cell lines had similar trends up to 4 hours post exposure, patient 1 cells had a trend for increasing in mtDNA copy while ATP5a levels remained stable; patient 2 had a downward trend while ATP5a remained stable; and control one had a reduced trend of both at 8 hours while returned to control levels at 24 hours (Figure 6-12).

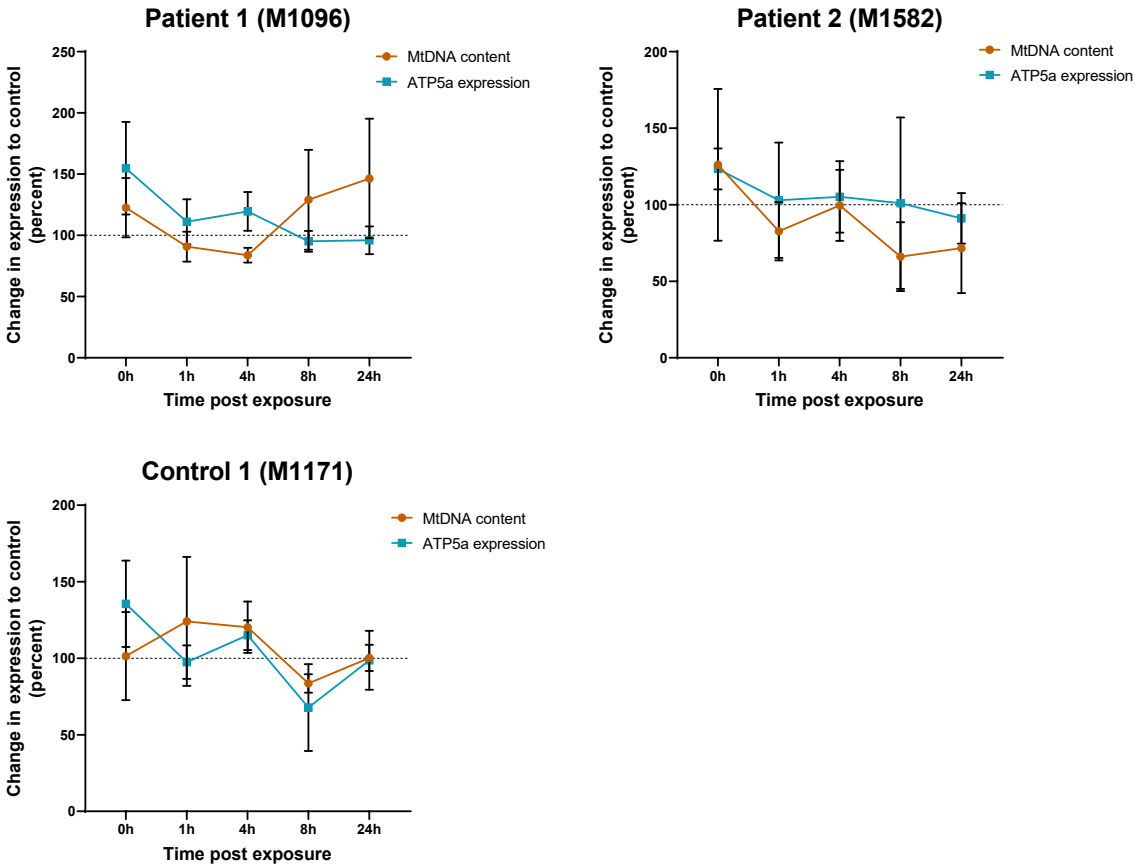

Figure 6-12. Comparison of mtDNA content and ATP5a expression in each cell line.
Immortalised primary dermal fibroblast cells were dosed with 2.16 SED solar simulated light at intervals prior to harvesting for DNA and protein, mtDNA content was determined by the 83 bp mtDNA housekeeping qPCR compared to 93 bp nDNA housekeeping region; ATP5a expression was determined by western blot analysis. Data replotted from Figure 6-6 and Figure 6-8, n=3 (M1171 24 hour sample n=2).

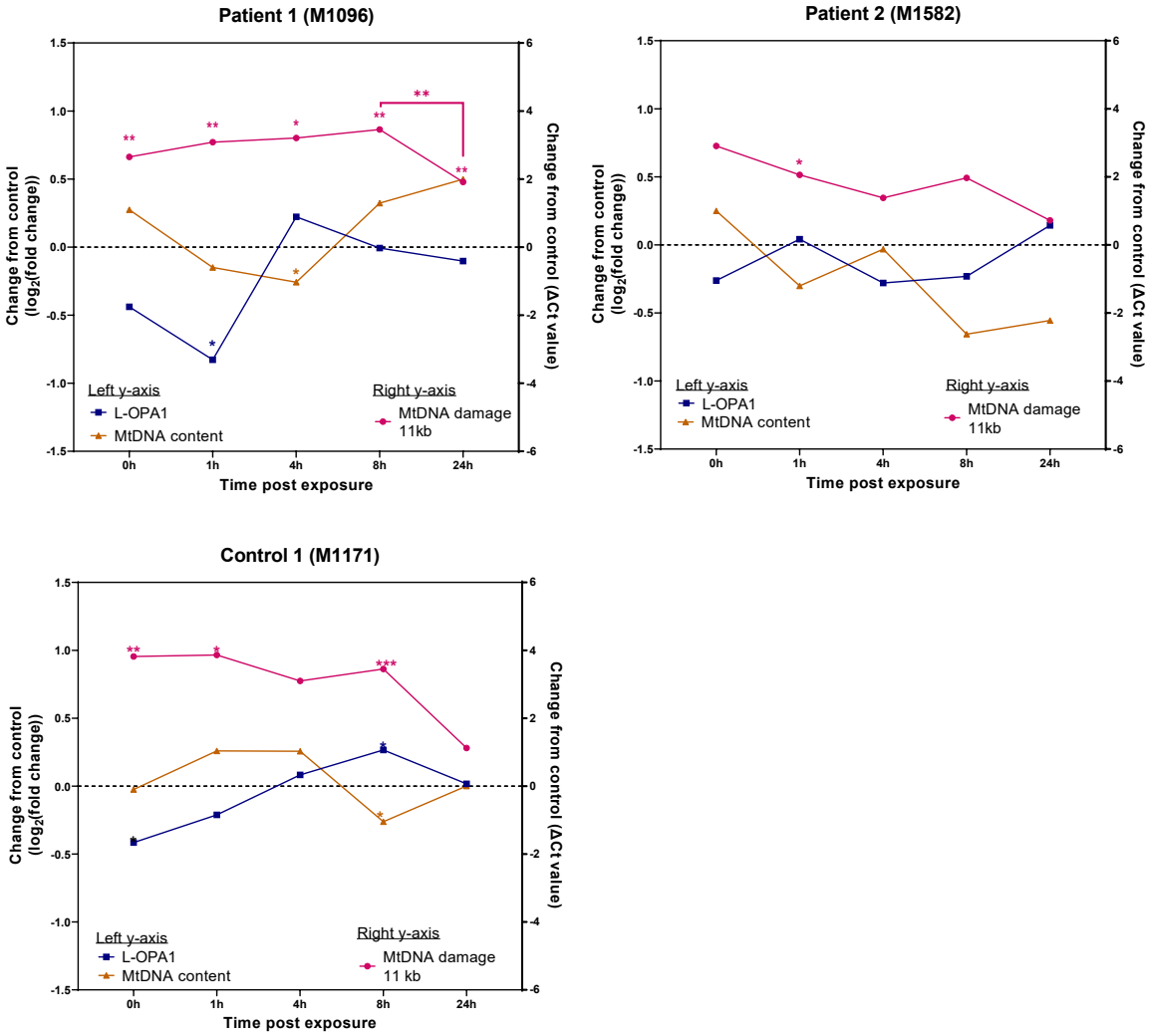

Figure 6-13. Comparison of mtDNA content, 11 kb damage and L-OPA1 expression in each cell line. Immortalised primary dermal fibroblast cells were dosed with 2.16 SED solar simulated light at intervals prior to harvesting for DNA and protein, mtDNA content was determined by the 83 bp mtDNA housekeeping qPCR compared to 93 bp nDNA housekeeping region; 11 kb mtDNA damage was determined by the 11 kb assay controlled for mtDNA content by the 83 bp mtDNA housekeeping region; L-OPA1 expression was determined by western blot analysis. Data replotted from Figure 6-6 and Figure 6-8; ***p<0.001, **p<0.01, *p<0.05; n=3 (M1171 24 hour sample n=2).

Figure 6-13 compares the levels of L-OPA1 to mtDNA damage and content over time. Patient 1 had a decrease in mtDNA content at 4 hours post exposure, and also a decrease in the number of network branches up to 4 hours and a significant reduction in L-OPA1 expression at 1 hour post exposure. Network branches are significantly reduced at 2 hours post exposure and increase in number up to 5 hours, before returning to non-significant levels at 9 hours. L-OPA1 levels are returned to control levels at 4 hours post exposure, and mtDNA damage in the 11 kb region reduces from 8 to 24 hours, but still retains significant damage compared to non-irradiated control. Taken together, this shows the decrease in L-OPA1 correlated with network fragmentation and return of the network to control levels occurred before mtDNA reduced in

damage. The reduction of mtDNA content occurred during mitochondrial network fragmentation, and the mtDNA damage recovery coincided with the increase in mtDNA content.

Patient 2 had no significant change to mtDNA content or 1 kb damage in the 24 hours following exposure, and only significant 11 kb damage at 1 hour post exposure which returned to non-significant levels by 4 hours. This coincided with a significant reduction in number of mitochondrial network branches at 2 hours post exposure, which suggests mitochondrial fission preceded repair in the 11 kb region. However, this change observed in microscopy was not observed in protein expression of OPA1, which could be a result of the time point differences and the repair/ fusion could occur between 1 and 4 hours.

Control 1 cells had a significant loss of L-OPA1 expression at 0h post exposure, which increased to significantly elevated levels at 8 hours post exposure. Mitochondrial content was lower than un-irradiated levels at this time point and return to control levels by 24 hours. This cell line also decreased in mtDNA damage to the 11 kb region between 8 hours and 24 hours.

Both control 1 and patient 1 had elevated oxidative stress damage to the non-coding region at 24 hours, and a greater mitochondrial network response to solar damage than patient 2 which had no oxidative mtDNA damage at 24 hours. Furthermore, patient 2 had lower levels of mtDNA damage in the 11 kb region than the other two cell lines from 1 hour post exposure. Without both controls, no comparison can be made to the patient cell response to solar light.

6.5 **Discussion**

6.5.1 Irradiation causes immediate changes in ATP5a protein expression

While not significant, each cell line had elevated ATP5a expression in each repeat immediately after irradiation (after irradiation of ~2 mins, cells were washed in PBS and then RIPA buffer was added; process took <10 mins). This effect could either be due to an increase in ATP5a expression or a decrease in GAPDH expression, however there was no obvious pattern of reduced GAPDH from the densitometry analysis when comparing the irradiated sample to the control at 0h. GAPDH has been shown to have an immediate reduction enzyme activity but not protein level in response to H_2O_2 stress in yeast (Shenton et al., 2002), and no change in mRNA levels were found in response to UVB irradiation at 12 hours (Li et al., 2011). Taken together, this suggests the immediate increase in ATP5a expression is not due to a reduction in GAPDH expression, though there is limited data on the immediate effects of solar light stress.

ATP5a is encoded by the nuclear gene ATP5F1A, and is a sub-unit of complex V in the ETC. Although there is little information in the literature regarding the short-term expression of ATP5a, a decreasing trend in expression was found after 4 hours treatment with CCCP, which has been shown to increase mitochondrial membrane permeability and uncouples mitochondrial OXPHOS (Choong et al., 2021). Mitochondrial membrane potential loss is a rapid process and can occur within 5-10 seconds of stress (Walsh et al., 2017) and, although there is a high degree of variability in time from signal to translation, protein expression of ATP5a could be upregulated within 10 mins in stress conditions (Wang et al., 2016a, Ben-Ari et al., 2010). Furthermore, mitochondrial mass is significantly increased in keratinocytes at 15 mins post exposure (first time point) of 0.5 SED of solar simulated light as measured by MitoTracker green, which increased up to 1 hour before decreasing between 1 and 3 hours (Zanchetta et al., 2010). The subsequent decrease in ATP5a appears to be due to mitophagic loss, as it coincides with a reduction in mtDNA content and is consistent with a decreased number of mitochondrial network branches (m1096) and decreased expression of L-OPA1 (m1096 and m1171) preceding the loss of mtDNA. The control 1 cells appear to regain L-OPA1 and simultaneously regain mtDNA content and reduce mtDNA damage, suggesting that post fragmentation, the network regains a normal structure and mtDNA replication occurs.

6.5.2 mtDNA damage response is not equal in all cells

The patient 1 cell line appears to have a delayed response between the increase in mtDNA and reduction in damage, and after 24 hours the damage is still significantly higher than the control, this could be due to the lower level of initial mtDNA to the other cell lines. The comparative reduction in mtDNA to that observed in control cells m1171 could have been less and may not have been sufficient to remove all damaged mitochondria in 24 hours. This failure to return damage to control levels could also be linked to the increase in oxidative damage observed in the non-coding region, as ROS in response to mitochondrial damage can increase damage to the mtDNA (Pontarin et al., 2012). The downward trend in mtDNA damage and content in patient m1582 and the lower number of network branches when compared to the control at each time point (though not significant) could suggest the response in this cell line is modest compared to the others, and there is also a slow progressive loss of mtDNA content in response to the low level of damage but not as a result of significant mitophagy. MtDNA degradation is a mechanism of removing high levels of mtDNA damage that are unable to undergo repair (Shokolenko et al., 2009, Zhao, 2019), independent of mitophagy.

The differing responses could be linked the level of initial damage, and subsequent oxidative stress. Mitophagy is initiated when stress levels reach a threshold and is followed by isolation of defective mitochondria as discussed in the chapter introduction. Membrane depolarisation could also initiate mitophagy in response to stress and is an almost immediate response (Walsh et al., 2017), which could be the mechanism behind the immediate loss of mtDNA and subsequent regain of mtDNA content that appears independent of mtDNA repair. Mitophagic clearance of cells with mtDNA damage might have a delayed response to initiation, as DNA damage might not become apparent until subsequent mitochondrial dysfunction. A few studies have tried to elucidate the role of mtDNA damage on mitophagy, with the conclusion that deleterious mtDNA is selectively removed by mitophagy (Suen et al., 2010, Dan et al., 2020). Suen et al. (2010) found that PARKIN promotes the mitophagic removal of mtDNA variants in cybrid cells, though these variants cause considerable mitochondrial dysfunction and subsequent increases in ROS production which could cause the initiation of mitophagy in these cells (Rana et al., 2000). Without a time course following mtDNA damage, it is difficult to conclude whether this response would occur as quickly as the initiation through irradiation. Dan et al. (2020) concluded that mtDNA damage repair was an initiator of mitophagy from 8h following irradiation dose, though the methods of dosing was gamma radiation and therefore not specific to mtDNA damage, and as a result of ROS initiation. Though the results could not

be attributed to mtDNA damage repair, it does show that future work should include a time point between 8 and 24 hours.

6.5.3 Limitations and future work

This research suffered from two major issues which resulted in incomplete data. Firstly, the two control cell lines were not as healthy as the patient cell lines, which could be due to the donor or the immortalisation procedure, and they did not have any demographic information. This meant that only 2 repeats for the mtDNA analysis was carried out on one control cell line (m0528) as it had a slow proliferation and therefore expanding the number of cells to the amount needed for the study was an issue. The control cell lines were also less adherent than the patient, which resulted in fewer cells available for image analysis and of low quality which could be cell senescence cause by inefficient immortalisation. This was a pilot study to determine both a suitable dose and time post dose in which an observable change was seen in each cell line. The 2.16 SED dose was adequate for analysis of mtDNA damage with the 11 kb assay, changes in L-OPA1, mtDNA content and the 1 kb damage region for some of the cell lines. To improve this study in the future, age and sex matched controls control cells of similar quality, and at least three cell lines of control and patients' cells would be required for adequate comparison.

From the data in this study, a 2.16 SED dose of solar light has been shown to increase levels of mtDNA damage for at least 8 hours when assessed using large-scale (11kb) mtDNA damage. Mitochondrial network analysis has determined both patient cell lines had observable network fragmentation that returned to control levels at 4 hours (m1582), and 8h hours (m1096) post irradiation. L-OPA1 levels were reduced at 1 hour post exposure and returned to control levels by 4 hours. This has determined that 2.16 SED is a large enough dose to cause observable fragmentation of the mitochondrial network through microscopy and protein analysis that return to control levels by 8 hours. Observing relevant time points is crucial during cell culture experiments, and many of the discrepancies and low significance of the results could be due to changes at the specific time-point, even if the trend is similar between repeats. Future studies could introduce further hourly time points between 0h and 8h after a 2.16 SED dose, and an increased the number of repeats.

Further work could assess the mechanisms involved in the mtDNA repair between the cell lines, including assessing DNase activity to determine the level of mtDNA degradation, expression of mtDNA repair proteins (Wisnovsky et al., 2016), and mitophagy proteins

PINK1and PARKIN (Ashrafi and Schwarz, 2013). Analysis of ROS using methods in chapter 4 would improve the understanding of the level of damage sustained by each cell line.

6.6 Summary of main findings

- Damage to the mtDNA is mostly repaired between 8 and 24 hours post an exposure of 2.16 SED.
- Oxidative damage affects cells in the 8-24 hour time window
- Cellular network dynamic changes return to control levels at 8 hours post irradiation
- Patient cell lines had differing response to solar irradiation

Chapter 7. Discussion

7.1 Overview

Mitochondrial dysfunction is an established inducer of oxidative stress and further mitochondrial dysfunction. UVR can damage mtDNA and increase levels of ROS production which can facilitate the breakdown of collagen leading to the appearance of wrinkles and uneven pigmentation (Pandel et al., 2013). Primary mitochondrial disease can disrupt the OXPHOS machinery and induce mtDNA deletions, which can lead to an increase in oxidative stress (Hayashi and Cortopassi, 2015). We hypothesised this could induce premature signs of facial and skin ageing. Few studies so far have assessed premature ageing in primary mitochondrial disease. Premature ageing with limited information was mentioned in three case reports from the systemic review in chapter 3, and POLG mutator mice with acquired mtDNA deletions exhibit a premature ageing phenotype (Geurts et al., 2020). The role of mitochondria in ageing, specifically skin photo-ageing, is well research. However, there is no research to date which investigates to relationship between PMD in patients, skin ageing and sub-clinical susceptibility to extrinsic ageing.

7.2 Facial appearance and sun damage effects perceived age

Assessing facial appearance in the literature was problematic as there is no consensus for reporting symptoms in PMD patients, ptosis was either not assessed or mentioned, or categorised with ophthalmoplegia. Furthermore, ptosis is progressive which might present after the report and point variants are not as commonly associated with ptosis as deletions, so was often not acknowledged in reports from those patients. Facial weakness was also often not assessed unless there was clinic significance, which could have an effect on overall facial appearance as a diagnostic marker or perceived age. It was not possible to comment on skin or facial ageing from the literature alone. The review determined ptosis and ophthalmoplegia to be more prevalent in patients with mtDNA deletions/ nuclear defects known to cause deletions which was consistent with the larger studies. However, severity and symmetry was very rarely commented on, and few reports had details on heteroplasmy which makes it difficult to determine diagnostic value in the review alone. It was clear that there are facial characteristics that could potentially be further investigated for diagnostic purposes in future research.

Sun damage is a leading cause of extrinsic skin ageing, and it can result in the appearance of prematurely aged skin. Increased perceived age by human evaluators correlated with level of

UV spots as a marker of photo induced skin damage, which links sun damage to perceived age in this cohort. There was no difference in perceived age between patients and controls, though ptosis had a trend for increased perceived age from human assessors, but not from the CNN algorithm. Ptosis presents with increasing age and also significantly in some PMD patients (Kaur et al., 2015), therefore presence of ptosis would be expected to increase perceived age. Patients had a reduced level of UV spots, which could be due to abnormal melanin production or less time spend outdoors due to mobility. Therefore, perceived age in patients could be confounded by reduced photoageing. Furthermore, facial muscle weakness was not assessed in patients. Wrinkles can develop due to repeated movement of facial muscles over time (Fujimura and Hotta, 2012), and patients with facial muscle weakness may exhibit less wrinkles due to chronological age. Analysis of the literature in chapter three found on three mentions of premature ageing, however there was no specific details and there was no mention of skin ageing. Overall, this analysis determined perceived age was associated with photo-ageing and could be associated with ptosis with further investigation, however there was no difference between the patient and control group which could be the result of confounding factors not collected during this pilot study.

7.3 Fibroblast response to solar stress

Investigation into the effect of solar light on mitochondria in dermal fibroblasts was performed to contribute to the understanding of how cell metabolism and dosing affected the damage profile. mtDNA damage and ROS were selected as markers of damage, and mtDNA content was assessed to understand whether repair coincided with a loss of mtDNA. The results determined mitochondrial damage from solar light was dependant on cell proliferation and glucose in the media, chronic low doses did not have the same collective damage as larger doses, and chapter 6 highlighted the variability in damage over time and the importance of multiple time points in mtDNA damage assays.

Cells with reduced proliferation had elevated whole cell ROS production and increased oxidative damage following solar light, also increased mitochondrial membrane potential and cell viability in response to chronic solar light doses. The cells exhibited a similar oxidative damage profile to those with high proliferation, even with elevated whole cell ROS. Cells cultured in galactose media had elevated oxidative damage to the mtDNA but lower mitochondrial superoxide production to high glucose cells in 10% media condition, a similar level of cell viability after solar light stress, and enhanced repair in the 11 kb region. The

response in mtDNA damage was taken after 24 hours although, as shown in chapter 6, the time course for repair is variable and further time points past the 24 hours could prove key to discerning the differences between the OXPHOS states. If the oxidative stress is more transient it could peak earlier before repair/removal, whereas lower level sustained damage could continue an increasing trend of damage. Chronic doses do not produce the same level of damage as an acute dose does in OXHOS or glycolysis media, and they result in less damage over the 24 hours post dosing than an acute dose does. Interestingly, chronic dosing caused a spike in mitochondrial superoxide in the high proliferating high glucose cells, which could suggest there is less SOD2 enzymatic activity. The implications of this in ageing and sun exposure studies are an increased response to oxidative damage and a perceived increased damage response to solar light. Dermal fibroblasts receive a very low level of UVR as they are protected by the stratum corneum and melanin, therefore this method of culture could be further exacerbating an already increased damage than would be expected from sun. Cell culture models are already far removed from normal physiology of the skin, and neonatal dermal fibroblasts provide an easy to use, fast growing and relatively cost effective cell for research. However, there are differences in stress response when grown in different metabolic states, and perhaps more research could determine an appropriate level of glucose/ serum that represent the levels of replication in skin.

7.4 Predisposition of PMD patients to solar light damage

This project theorised that based on the mitochondrial theory of ageing, genetic mitochondrial dysfunction would accelerate the process and predispose patient's skin to damage from solar light. This study found that patients had less UV spots as a marker of photo-damage. There is evidence that melanocytes are sensitive to stress from hydrogen peroxide, but also patients may be less likely to spend time outside due to reduced mobility. The questionnaire attempted to account for time spent outside, but the question had some ambiguity and did not account for time spent outdoors in different seasons. Reduced melanin has been found in patients with m.3242A>G variant, and patients with point variants (predominantly m.3242A>G) were found to have elevated oxidative stress compared to the other genotype groups. This suggests that oxidative stress could be the mechanism behind the reduced melanin in patients, and this may not be the best method to assess photo-damage in PMD patients. The role of melanin and oxidative stress could also be a confounding factor in the mechanisms behind photo-ageing in PMD patients. Furthermore, as previously mentioned, wrinkles due to facial muscle action

could be reduced as a result of facial muscle weakness, so analysis of wrinkles may not provide conclusive results. Overall, this could suggest the markers previously used to assess skin ageing may not be relevant in PMD patients, and the level of mtDNA damage between sun-exposed and non-exposed areas could provide a more useful comparison. The data from the mtDNA skin swabs show a correlation with UV spots as a marker of photo-damage, however during optimisation it was concluded that there was body site variation that would confound the results. MtDNA damage through needle biopsy have been shown to have a good correlation with age and could provide an alternative, though more invasive method (Krishnan et al., 2004). Unfortunately, the cell culture data in chapter 6 did not have an adequate control, therefore there could be no comparison made between patient fibroblasts and controls in response to solar light stress.

7.5 Future work

The patient study in this thesis was a pilot study, and the data showed interesting point of analysis to include in future expansion. Determining a link between perceived age in patients would provide substantial evidence in the field for mitochondria and ageing, however this pilot study was small and had a wide range of genetic diagnoses. Limiting the range of genomic defects to specifically mtDNA deletions would be the most appropriate for an initial investigation into the link between perceived age and PMD, as deletions are more commonly associated with ptosis but also found commonly in ageing tissues. However, there are confounding results between skin appearance and facial structure and skin wrinkles could be a strong indicator of perceived age. Further studies of perceived age in PMD could benefit from more in-depth markers of facial structure including assessing facial muscle weakness, this could control for weakness as a confounder for wrinkle development. More in depth questions on attitudes to sun exposure and time spent outside would limit the effect of extrinsic ageing from sun exposure as a confounder. Cell culture investigation of PMD patient fibroblasts would provide a good model of predisposition to extrinsic stress, and this study has provided details of suitable dosing and time scales for damage and mitochondrial network analysis. However, a more suitable model would work in parallel with the patient study and include primary fibroblasts from patients involved in the research. This could match the cellular response to the perceived age and provide a more robust model of skin ageing in PMD.

In addition to the perceived age aspect of the patient study, further collaborative work seeks to determine the diagnostic prospects of facial appearance in PMD to reduce the time taken for

diagnosis and referral to a specialist. The systematic review determined limited analysis of facial features in case reports of PMD, as well as unstandardized reporting. The Newcastle Mitochondrial Disease Scale for Adults (NMDAS) was developed in 2006 to help standardise reporting of mitochondrial disease, it has been used widely in mitochondrial research and a step forward for combining mitochondrial research internationally. However, reporting of facial features (mostly ptosis and ophthalmoplegia) is often mentioned without severity or combined into a single feature in reports. More transparent and detailed reporting in research would be beneficial to mitochondrial research overall and not only for the future of facial imaging studies.

7.6 **Key findings**

Overall, this study has investigated the role genetic mitochondrial dysfunction plays in ageing using PMD as a model. Firstly, there is little information facial features or premature ageing in PMD in the literature. Secondly, high glucose media and highly proliferative dermal fibroblasts used to investigate the role sun damage plays on mitochondria in the skin could be masking mtDNA repair and inducing mROS. Finally, in terms of overall facial ageing, clinical features of PMD create a complexity in assessing perceived age; while ptosis and sun damage cannot be ruled out as factors in increased perceived age, facial muscle weakness and mobility issues preventing time outdoors could be confounders.

Appendix A: Lifestyle and environmental-related factor questionnaire

DEMOGRAPHICS

1. What is your date of birth? ……. / ……. / …….
DAY MONTH YEAR

2. What is your gender? □ M □ F □ Other (please specify) ……
3. Marital status: □ Single □ Partnered □ Married
□ Widowed □ Separated
4. Highest education: □ Less than high school □ High school
□ Higher education □ Degree
5. What country do you live in? …… # years you have lived there ……
Have you lived anywhere else? □ N □ Y # years you have lived there ……
Location you previously lived …….
6. Please tick the closest description to describe your skin type:
□ Fair skinned Caucasian, burn very easily and never tan
□ Fair skinned Caucasian, burn easily and tan slowly and with difficulty
□ Medium skinned Caucasians, burn rarely and tan relatively easily
□ Darker skinned Caucasian, virtually never burn or tans readily, e.g. Mediterranean ancestry
□ Asian or Indian skin
□ Afro-Caribbean or Black skin
Facial Imaging Page 20 of 34 Version 6.0 – 09/11/2020
Protocol

DERMATOLOGICAL HISTORY

7. Please indicate if you have had previous or have current skin conditions:
Location Age Treatment & Frequency of treatment
□ Basal cell carcinoma ……. …… ……
□ Squamous cell carcinoma ……. …… ……
□ Melanoma ……. …… ……
□ Unknown skin cancer ……. …… ……
□ Atypical/dysplastic moles ……. …… ……
□ Actinic Keratosis ……. …… ……
□ Chronic skin disease (please specify) ……
□ Tendency to scar (please specify) ……
□ Other (please specify) ……

8. Please indicate if a close family member has previous or has any current skin conditions:
Location Age Treatment & Frequency of treatment
□ Basal cell carcinoma ……. …… ……
□ Squamous cell carcinoma ……. …… ……
□ Melanoma ……. …… ……
□ Unknown skin cancer ……. …… ……
□ Atypical/dysplastic moles ……. …… ……
□ Actinic Keratosis ……. …… ……
□ Chronic skin disease (please specify) ……
□ Other (please specify) ……

9. Please indicate if you currently undergo, or if you have ever had the following treatments:

Location Age Frequency

□ Botox injections ……. …… ……

□ Collagen injections ……. …… ……

□ Fillers ……. …… ……

□ Light treatments ……. …… ……

□ Laser resurfacing ……. …… ……

□ Microdermabrasion ……. …… ……

□ Chemotherapy ……. …… ……

□ Radiotherapy ……. …… ……

□ Other (please specify) ……. …… ……

MEDICAL HISTORY

10. Please indicate if you currently experience, or if you have ever had:

□ Heart problems □ Migraines □ Anaemia □ Thyroid disease

□ High blood pressure □ Seizures/Epilepsy □ HIV/AIDS □ Kidney disease

□ High cholesterol □ Stroke □ Hepatitis □ Liver disease

□ Diabetes □ Hay fever □ Blood disorder □ Eating disorder

□ Jaundice □ Arthritis □ Vitamin D deficiency

□ Lung disease (please specify) ……

□ Cancer (please specify) ……..…

□ Other (please specify) ……

11. Please indicate if you currently experience, or if you have ever had the following eye conditions:

□ Cataracts □ Glaucoma

□ Contact lenses □ Age-related macular degeneration

□ Diabetic retinopathy

□ Other (please specify) ……

12. Please indicate if you have had previous eye surgery:

Surgery # surgeries Age Other details (timing etc.)

□ Left eye ……. …… …… ……

□ Right eye ……. …… …… ……

13. Please list any allergies:

……

14. Please list any medications that you are currently taking:

Name Dose/how often you take it Reason # years

…… …… …… ……

15. Please indicate if you are currently taking any of the following vitamin and mineral tablets, powders, drops or supplements

□ CoQ10 □ Zinc □Vit-A/Retinol □ Vit-B7/Biotin

□ Resveratrol □ Calcium □ Vit-B1/Thiamin □ Vit-B12

□ Lycopene □ Iron □ Vit-B2/Riboflavin □ Vit-C/Ascorbic acid

□ β-carotene □ Chromium □ Vit-B3/Niacin □ Vit-D

□ Flavenoids □ Magnesium □ Vit-B6/Pyridoxine □ Vit-E

□ Selenium □ Manganese □ Folic acid □ Vit-K
□ Genistein □ Molybdenum □ Lutein □ Probiotics
□ Collagen
□ other (please specify)
……
Details (dose, how many a day)
……

LIFESTYLE & HEALTH

16. Do you participate in physical activity, exercise or sport?
□ Yes (at least once a week)
□ Mild daily activity (i.e., climb stairs, walk)
□ No

17. Do you drink alcohol?
□ No
□ Occasional social use
□ Yes (at least 3 times a week) 1 unit= ½ pint beer/ 1 pub measure spirits/1 glass wine

18. Do you smoke?
□ Never smoked
□ Previously quit # of years smoked …… Cigarettes- packets/day ……
□ Yes # of years smoked …… Cigarettes- packets/day ……

19. Do you drink caffeine?
□ No
□ Yes # of cups or cans/day ……

SUN EXPOSURE

20. How many hours do you spend in activities outside, on average throughout the year?
□ Up to 5 hours/week
□ 5-10 hours/week
□ Greater than 10 hours/week

21. Do you normally use sun protection for your face when you go outside?
□ Yes SPF …… Product name ……
□ Occasionally
□ No

22. Have you had been sunburn on your face?
□ No
□ Yes # of times

23. Do you normally use sunglasses when outdoors when you go outside?
□ Yes
□ Occasionally
□ No

24. Do you normally use sunbeds or indoor tanning sunlamp?
□ Never
□ Occasionally (less than 10 times)
□ Very regularly (more than 10 times)

Do you have any additional comments/further information in relation to Lifestyle & Health (questions 16 - 19) or Sun Exposure (questions 20 - 24)

_____

Appendix B: Linear regression model: Oxidative stress and patient status

				Oxidative stress mean
Model 1	**Patient status (reference control)**		Coefficient	37.4
			p-value	*0.232*

				Oxidative stress mean
Model 2: Add age	**Patient status (reference control)**		Coefficient	37.4
			p-value	*0.232*
	Age		Coefficient	0.503
			p-value	*0.574*

				Oxidative stress mean
Model 3: Remove age, add systolic BP	**Patient status (reference control)**		Coefficient	42
			p-value	*0.202*
	Systolic BP		Coefficient	0.376
			p-value	*0.67*

				Oxidative stress mean
Model 4: Add alcohol intake	**Patient status (reference control)**		Coefficient	44.4
			p-value	*0.205*
	Systolic BP		Coefficient	0.45
			p-value	*0.666*
	Alcohol use often never use)	**Occasional use**	Coefficient	9
			p-value	*0.851*
		Never use	Coefficient	-1.6
			p-value	*0.978*

				Oxidative stress mean
Model 5: Remove alcohol intake, add diastolic BP	**Patient status (reference control)**		Coefficient	40.8
			p-value	*0.206*
	Systolic BP		Coefficient	-0.97
			p-value	*0.427*
	Diastolic BP		Coefficient	2.93
			p-value	*0.121*

				Oxidative stress mean
Model 6: Remove systolic BP	**Patient status (reference control)**		Coefficient	44.4
			p-value	*0.164*
	Diastolic BP		Coefficient	1.89
			p-value	*0.157*

				Oxidative stress mean
Model 5: Add temperature	**Patient status (reference control)**		Coefficient	68.1
			p-value	*0.054*
	Diastolic BP		Coefficient	2.54
			p-value	*0.085*
	Temp		Coefficient	-2.28
			p-value	*0.347*

				Oxidative stress mean
Model 6: Add exercise	**Patient status (reference control)**		Coefficient	79.5
			p-value	*0.035*
	Diastolic BP		Coefficient	2.24
			p-value	*0.155*
	Temp		Coefficient	-2.5
			p-value	*0.309*
	Exercise (reference at least once per week)	**Mild daily activity**	Coefficient	-5.7
			p-value	*0.895*
		No	Coefficient	-63.5
			p-value	*0.249*

				Oxidative stress mean
Model 7: Add caffeine intake	**Patient status (reference control)**		Coefficient	84.6
			p-value	*0.029*
	Diastolic BP		Coefficient	4.53
			p-value	*0.412*
	Temp (°C)		Coefficient	-1.79
			p-value	*0.501*
	Exercise (reference at least once per week)	**Mild daily activity**	Coefficient	-20.4
			p-value	*0.673*
		No	Coefficient	-67.9
			p-value	*0.226*
	Caffeine intake (no. of cups/day)		Coefficient	8.9
			p-value	*0.474*

				Oxidative stress mean
Model 8: Add diabetes	**Patient status (reference control)**		Coefficient	53.4
			p-value	*0.152*
	Diastolic BP		Coefficient	0.56
			p-value	*0.748*
	Temp (°C)		Coefficient	0.01
			p-value	*0.998*
	Exercise (reference at least once per week)	**Mild daily activity**	Coefficient	-63.2
			p-value	*0.193*
		No	Coefficient	-81.2
			p-value	*0.121*
	Caffeine intake (no. of cups/day)		Coefficient	12.9
			p-value	*0.269*
	Diabetes (reference negative)		Coefficient	118.3
			p-value	*0.022*

				Oxidative stress mean
Model 9: Add heart condition	**Patient status (reference control)**		Coefficient	69
			p-value	*0.069*
	Diastolic BP		Coefficient	-0.66
			p-value	*0.724*
	Temp (°C)		Coefficient	0.33
			p-value	*0.893*
	Exercise (reference at least once per week)	**Mild daily activity**	Coefficient	-74.8
			p-value	*0.119*
		No	Coefficient	-74.8
			p-value	*0.141*
	Caffeine intake (no. of cups/day)		Coefficient	19.7
			p-value	*0.109*
	Diabetes (reference negative)		Coefficient	146.6
			p-value	*0.007*
	Heart condition (reference negative)		Coefficient	-81.2
			p-value	*0.115*

				Oxidative stress mean
Model 10: Add arthritis	**Patient status (reference control)**		Coefficient	66
			p-value	*0.095*
	Diastolic BP		Coefficient	-0.7
			p-value	*0.711*
	Temp (°C)		Coefficient	0.36
			p-value	*0.885*
	Exercise (reference at least once per week)	**Mild daily activity**	Coefficient	-74.3
			p-value	*0.129*
		No	Coefficient	-72.3
			p-value	*0.167*
	Caffeine intake (no. of cups/day)		Coefficient	20.6
			p-value	*0.108*
	Diabetes (reference negative)		Coefficient	144
			p-value	*0.01*
	Heart condition (reference negative)		Coefficient	-79.2
			p-value	*0.133*
	Arthritis (reference negative)		Coefficient	-17.6
			p-value	*0.738*

				Oxidative stress mean
Model 11: Remove arthritis add high cholesterol	**Patient status (reference control)**		Coefficient	81.6
			p-value	*0.039*
	Diastolic BP		Coefficient	-0.75
			p-value	*0.676*
	Temp (°C)		Coefficient	11.2
			p-value	*0.376*
	Exercise (reference at least once per week)	**Mild daily activity**	Coefficient	-68.3
			p-value	*0.161*
		No	Coefficient	-60.7
			p-value	*0.255*
	Caffeine intake (no. of cups/day)		Coefficient	21.9
			p-value	*0.057*
	Diabetes (reference negative)		Coefficient	163.6
			p-value	*0.005*
	Heart condition (reference negative)		Coefficient	-97.6
			p-value	*0.068*
	High cholesterol (reference negative)		Coefficient	-12.4
			p-value	*0.844*

Model 12: Remove diabetes, heart disease and high cholesterol; add heart rate

			Oxidative stress mean
Patient status (reference control)		Coefficient	69.6
		p-value	*0.106*
Diastolic BP		Coefficient	1.31
		p-value	*0.49*
Temp (°C)		Coefficient	-1.74
		p-value	*0.516*
Exercise (reference at least once per week)	**Mild daily activity**	Coefficient	-30.8
		p-value	*0.542*
	No	Coefficient	-77.3
		p-value	*0.182*
Caffeine intake (no. of cups/day)		Coefficient	9.3
		p-value	*0.46*
Heart rate (beats/min)		Coefficient	1.25
		p-value	*0.435*

Model 13: Add sex

			Oxidative stress mean
Patient status (reference control)		Coefficient	74.2
		p-value	*0.09*
Diastolic BP		Coefficient	1.82
		p-value	*0.363*
Temp (°C)		Coefficient	-1.7
		p-value	*0.526*
Exercise (reference at least once per week)	**Mild daily activity**	Coefficient	-30.8
		p-value	*0.545*
	No	Coefficient	-71.2
		p-value	*0.224*
Caffeine intake (no. of cups/day)		Coefficient	14.7
		p-value	*0.3*
Heart rate (beats/min)		Coefficient	0.88
		p-value	*0.598*
Sex (reference female)		Coefficient	-42
		p-value	*0.386*

				Oxidative stress mean
Model 13: From model 11, change patient status to variant type	**Patient group (reference control)**	**Point variants**	Coefficient	111.7
			p-value	*0.018*
		Single deletion	Coefficient	86.6
			p-value	*0.129*
		Multiple deletions	Coefficient	-58.3
			p-value	*0.518*
	Diastolic BP		Coefficient	-1.14
			p-value	*0.547*
	Temp (°C)		Coefficient	2.7
			p-value	*0.879*
	Exercise (reference at least once per week)	**Mild daily activity**	Coefficient	-98.3
			p-value	*0.049*
		No	Coefficient	-90.1
			p-value	*0.116*
	Caffeine intake (no. of cups/day)		Coefficient	25.4
			p-value	*0.045*
	Diabetes (reference negative)		Coefficient	153.7
			p-value	*0.01*
	Heart condition (reference negative)		Coefficient	-97.1
			p-value	*0.085*
	High cholesterol (reference negative)		Coefficient	-46.4
			p-value	*0.547*

Appendix C: Linear regression model: Change in percieved age and patient status

				Change in perceived age (assessor)
Model 1	**Patient status (reference control)**		Coefficient	2.63
			p-value	*0.119*

				Change in perceived age (assessor)
Model 2: Add sun protection	**Patient status (reference control)**		Coefficient	2.2
			p-value	*0.185*
	Sun protection (reference always wears)	**Occasional use**	Coefficient	-0.58
			p-value	*0.771*
		Never use	Coefficient	3.48
			p-value	*0.09*

				Change in perceived age (assessor)
Model 3: Add hours outdoors age	**Patient status (reference control)**		Coefficient	1.58
			p-value	*0.344*
	Sun protection (reference always wears)	**Occasional use**	Coefficient	0.04
			p-value	*0.985*
		Never use	Coefficient	3.95
			p-value	*0.056*
	Hours outdoors (reference less than 5 hours/week)	**5-10 hours/week**	Coefficient	1.16
			p-value	*0.534*
		More than 10 hours/week	Coefficient	-269
			p-value	*0.232*

				Change in perceived age (assessor)
Model 4: Add alcohol intake	**Patient status (reference control)**		Coefficient	1.28
			p-value	*0.456*
	Sun protection (reference always wears)	**Occasional use**	Coefficient	0.31
			p-value	*0.882*
		Never use	Coefficient	3.61
			p-value	*0.098*
	Hours outdoors (reference less than 5 hours/week)	**5-10 hours/week**	Coefficient	0.96
			p-value	*0.613*
		More than 10 hours/week	Coefficient	-2.79
			p-value	*0.227*
	Alcohol use often never use)	**Occasional use**	Coefficient	-1.48
			p-value	*0.51*
		Never use	Coefficient	0.74
			p-value	*1.69*

				Change in perceived age (assessor)
Model 5:Add smoking status	**Patient status (reference control)**		Coefficient	0.59
			p-value	*0.743*
	Sun protection (reference always wears)	**Occasional use**	Coefficient	0.28
			p-value	*0.894*
		Never use	Coefficient	3.79
			p-value	*0.084*
	Hours outdoors (reference less than 5 hours/week)	**5-10 hours/week**	Coefficient	0.6
			p-value	*0.76*
		More than 10 hours/week	Coefficient	-2.09
			p-value	*0.381*
	Alcohol use often never use)	**Occasional use**	Coefficient	-1.15
			p-value	*0.612*
		Never use	Coefficient	0.56
			p-value	*0.845*
	Smoking status (reference never smoked)	**Previously smoked**	Coefficient	-3.28
			p-value	*0.185*
		Currently smoke	Coefficient	1.46
			p-value	*0.36*

				Change in perceived age (assessor)
Model 6:Add age	Patient status (reference control)		Coefficient	1.15
			p-value	*0.525*
	Sun protection (reference always wears)	Occasional use	Coefficient	0.97
			p-value	*0.645*
		Never use	Coefficient	4.08
			p-value	*0.059*
	Hours outdoors (reference less than 5 hours/week)	5-10 hours/week	Coefficient	0.95
			p-value	*0.626*
		More than 10 hours/week	Coefficient	-0.53
			p-value	*0.832*
	Alcohol use often never use)	Occasional use	Coefficient	-2.82
			p-value	*0.251*
		Never use	Coefficient	-1.99
			p-value	*0.535*
	Smoking status (reference never smoked)	Previously smoked	Coefficient	-2.65
			p-value	*0.277*
		Currently smoke	Coefficient	1.8
			p-value	*0.657*
	Age		Coefficient	-0.984
			p-value	*0.113*

				Change in perceived age (assessor)	Change in perceived age (CNN camera)	Change in perceived age (CNN Visia)
Model 7:Add sex	**Patient status (reference control)**		Coefficient	1.3	-0.24	-0.86
			p-value	*0.479*	*0.947*	*0.828*
	Sun protection (reference always wears)	**Occasional use**	Coefficient	1.15	-0.82	2.79
			p-value	*0.592*	*0.845*	*0.55*
		Never use	Coefficient	4.09	3.7	8.15
			p-value	*0.061*	*0.374*	*0.084*
	Hours outdoors (reference less than 5 hours/week)	**5-10 hours/week**	Coefficient	1.27	0.98	-0.16
			p-value	*0.529*	*0.802*	*0.971*
		More than 10 hours/week	Coefficient	0.34	0.78	-6.6
			p-value	*0.905*	*0.888*	*0.287*
	Alcohol use often never use)	**Occasional use**	Coefficient	-3.34	-4.2	8.54
			p-value	*0.2*	*0.407*	*0.135*
		Never use	Coefficient	-2.63	-7.88	0.78
			p-value	*0.437*	*0.233*	*0.915*
	Smoking status (reference never smoked)	**Previously smoked**	Coefficient	-2.42	-1.46	-4.3
			p-value	*0.328*	*0.763*	*0.425*
		Currently smoke	Coefficient	1.18	-0.85	3.63
			p-value	*0.778*	*0.918*	*0.691*
	Age		Coefficient	-1.041	-0.279	-0.292
			p-value	*0.1*	*0.027*	*0.037*
	Sex (reference female)		Coefficient	-1.4	-1.39	-1.7
			p-value	*0.497*	*0.731*	*0.704*

				Change in perceived age (assessor)	Change in perceived age (CNN camera)	Change in perceived age (CNN Visia)
Model 8: Genotype analysis	**Patient group (reference control)**	**Point variants**	Coefficient	0.86	-0.95	-0.138
			p-value	*0.681*	*0.761*	*0.751*
		Single deletion	Coefficient	2.82	7.25	3.51
			p-value	*0.322*	*0.095*	*0.550*
		Multiple deletions	Coefficient	-0.12	-6.81	-2.9
			p-value	*0.985*	*0.467*	*0.825*

			Change in perceived age (assessor)	Change in perceived age (CNN camera)	Change in perceived age (CNN Visia)
Model 9: ptosis analysis	**Ptosis (reference negative)**	Coefficient	3.39	4.15	1.36
		p-value	*0.147*	*0.268*	*0.783*

Appendix D: Linear regression model: predictors of skin swab mtDNA damage

				mtDNA damage	
				Right cheek	**Left cheek**
Model 1	**Age**		Coefficient	0.0006	0.0006
			p-value	*0.615*	*0.643*

				mtDNA damage	
				Right cheek	**Left cheek**
Model 2: Add confounder patient status	**Age**		Coefficient	0.00065	0.00061
			p-value	*0.592*	*0.636*
	Patient status (reference control)		Coefficient	0.0236	0.0355
			p-value	*0.428*	*0.428*

				mtDNA damage	
				Right cheek	**Left cheek**
Model 3: Remove patient status and add sex	**Age**		Coefficient	0.00069	0.00062
			p-value	*0.574*	*0.65*
	Sex (reference female)		Coefficient	-0.0205	-0.0029
			p-value	*0.657*	*0.955*

				mtDNA damage	
				Right cheek	**Left cheek**
Model 4: Add confounder sun protection use	**Age**		Coefficient	-0.00005	0.00022
			p-value	*0.963*	*0.873*
	Sun protection (reference always use)	**Occasional use**	Coefficient	0.0188	-0.0216
			p-value	*0.703*	*0.715*
		Never use	Coefficient	0.1388	0.0802
			p-value	*0.007*	*0.165*

				mtDNA damage	
				Right cheek	**Left cheek**
Model 5: Add confounder hours outdoors	**Age**		Coefficient	-0.00052	-0.00079
			p-value	*0.668*	*0.591*
	Sun protection (reference always use)	**Occasional use**	Coefficient	0.002	-0.0338
			p-value	*0.996*	*0.563*
		Never use	Coefficient	0.1333	0.0742
			p-value	*0.01*	*0.191*
	Hours outdoors (reference less than 5 hours/week)	**5-10 hours/week**	Coefficient	0.0463	0.0312
			p-value	*0.295*	*0.533*
		More than 10 hours/week	Coefficient	0.0748	0.1115
			p-value	*0.181*	*0.082*

				mtDNA damage	
				Right cheek	**Left cheek**
Model 6: Add confounder season of sample collection	**Age**		Coefficient	-0.00078	-0.00055
			p-value	*0.528*	*0.7*
	Sun protection (reference always use)	**Occasional use**	Coefficient	-0.0335	-0.0772
			p-value	*0.523*	*0.189*
		Never use	Coefficient	0.0981	0.0276
			p-value	*0.063*	*0.622*
	Hours outdoors (reference less than 5 hours/week)	**5-10 hours/week**	Coefficient	0.0598	0.0543
			p-value	*0.173*	*0.265*
		More than 10 hours/week	Coefficient	0.0735	0.1012
			p-value	*0.192*	*0.113*
	Season of sample collection (reference winter)	**Spring**	Coefficient	0.0997	0.0983
			p-value	*0.099*	*0.16*
		Summer	Coefficient	0.1272	0.2044
			p-value	*0.072*	*0.014*
		Autumn	Coefficient	0.149	0.1324
			p-value	0.041	0.101

				mtDNA damage	
				Right cheek	**Left cheek**
Model 7: Add confounder ITA°	**Age**		Coefficient	-0.00122	0.00049
			p-value	*0.404*	*0.744*
	Sun protection (reference always use)	**Occasional use**	Coefficient	-0.0291	-0.0694
			p-value	*0.585*	*0.228*
		Never use	Coefficient	0.0993	0.0359
			p-value	*0.065*	*0.514*
	Hours outdoors (reference less than 5 hours/week)	**5-10 hours/week**	Coefficient	0.0613	0.0677
			p-value	*0.174*	*0.164*
		More than 10 hours/week	Coefficient	0.064	0.1224
			p-value	*0.278*	*0.058*
	Season of sample collection (reference winter)	**Spring**	Coefficient	0.0895	0.096
			p-value	*0.148*	*0.163*
		Summer	Coefficient	0.1153	0.2166
			p-value	*0.113*	*0.008*
		Autumn	Coefficient	0.1458	0.1291
			p-value	0.049	0.102
	ITA°		Coefficient	-0.00134	0.00274
			p-value	*0.451*	*0.124*

				mtDNA damage	
				Right cheek	**Left cheek**
Model 8: Add confounder alcohol use	**Age**		Coefficient	0.00032	0.00198
			p-value	*0.836*	*0.186*
	Sun protection (reference always use)	**Occasional use**	Coefficient	-0.0404	-0.0785
			p-value	*0.45*	*0.147*
		Never use	Coefficient	0.1223	0.0606
			p-value	*0.021*	*0.224*
	Hours outdoors (reference less than 5 hours/week)	**5-10 hours/week**	Coefficient	0.0446	0.0504
			p-value	*0.304*	*0.242*
		More than 10 hours/week	Coefficient	0.0334	0.0466
			p-value	*0.559*	*0.441*
	Season of sample collection (reference winter)	**Spring**	Coefficient	0.0613	0.0655
			p-value	*0.191*	*0.31*
		Summer	Coefficient	0.1001	0.1797
			p-value	*0.18*	*0.02*
		Autumn	Coefficient	0.1156	0.0986
			p-value	0.111	0.165
	ITA°		Coefficient	-0.0022	0.00079
			p-value	*0.213*	*0.637*
	Alcohol use (reference often use)	**Occasional use**	Coefficient	0.092	0.0811
			p-value	*0.142*	*0.173*
		Never use	Coefficient	0.1861	0.2329
			p-value	*0.028*	*0.006*

				mtDNA damage	
				Right cheek	**Left cheek**
Model 9 (remove ITA and assess self-assessed skin type)	**Age**		Coefficient	0.00023	0.0014
			p-value	*0.867*	*0.323*
	Sun protection (reference always wears)	**Occasional use**	Coefficient	-0.0631	-0.0946
			p-value	*0.21*	*0.076*
		Never use	Coefficient	0.1369	0.0623
			p-value	*0.007*	*0.452*
	Hours outdoors (reference less than 5 hours/week)	**5-10 hours/week**	Coefficient	0.0377	0.031
			p-value	*0.326*	*0.452*
		More than 10 hours/week	Coefficient	0.0253	0.0213
			p-value	*0.614*	*0.702*
	Season of sample collection (reference winter)	**Spring**	Coefficient	0.0965	0.065
			p-value	*0.103*	*0.302*
		Summer	Coefficient	0.1199	0.165
			p-value	*0.079*	*0.025*
		Autumn	Coefficient	0.146	0.1064
			p-value	0.03	0.122
	Alcohol use (reference never use)	**Occasional use**	Coefficient	0.125	0.1033
			p-value	*0.037*	*0.08*
		Often use	Coefficient	0.1803	0.24
			p-value	*0.015*	*0.002*
	Skin type self-assessed	**Type II**	Coefficient	0.1201	0.0878
			p-value	*0.05*	*0.199*
		Type III	Coefficient	0.1504	0.0959
			p-value	0.008	0.126

			mtDNA damage	
			Right cheek	**Left cheek**
Model 10: Perceived age with confounders from model 7	**Perceived age (assessors)**	Coefficient	-0.00038	0.00095
		p-value	*0.787*	*0.517*
	Perceived age (CNN camera)	Coefficient	-0.00047	0.00129
		p-value	*0.759*	*0.411*
	Perceived age (CNN Visia)	Coefficient	-0.00046	0.00162
		p-value	*0.729*	*0.221*

Appendix E: Linear regression model: perceived age and sun protection

				Change in perceived age
Model 1	**Sun protection (reference always wears)**	**Occasional use**	Coefficient	-0.75
			p-value	*0.71*
		Never use	Coefficient	3.75
			p-value	*0.069*

				Change in perceived age
Model 2: Add confounder age	**Sun protection (reference always wears)**	**Occasional use**	Coefficient	0.28
			p-value	*0.89*
		Never use	Coefficient	4.78
			p-value	*0.23*
	Age		Coefficient	-0.0937
			p-value	*0.061*

				Change in perceived age
Model 3: Add confounder patient status	**Sun protection (reference always wears)**	**Occasional use**	Coefficient	0.45
			p-value	*0.821*
		Never use	Coefficient	0.451
			p-value	*0.03*
	Age		Coefficient	-0.0941
			p-value	*0.057*
	Patient status (reference control)		Coefficient	2.22
			p-value	*0.166*

				Change in perceived age
Model 4: Add confounder hours outdoors	**Sun protection (reference always wears)**	**Occasional use**	Coefficient	0.64
			p-value	*0.753*
		Never use	Coefficient	*4.63*
			p-value	*0.027*
	Age		Coefficient	-0.0802
			p-value	*0.12*
	Patient status (reference control)		Coefficient	1.76
			p-value	*0.283*
	Hours outdoors (reference less than 5 hours/week)	**5-10 hours/week**	Coefficient	1.45
			p-value	*0.432*
		More than 10 hours/week	Coefficient	-1.58
			p-value	*0.489*

				Change in perceived age
Model 5: Add confounder exercise	**Sun protection (reference always wears)**	**Occasional use**	Coefficient	0.64
			p-value	*0.761*
		Never use	Coefficient	*4.94*
			p-value	*0.023*
	Age		Coefficient	-0.0818
			p-value	*0.113*
	Patient status (reference control)		Coefficient	1.67
			p-value	*0.334*
	Hours outdoors (reference less than 5 hours/week)	**5-10 hours/week**	Coefficient	1.39
			p-value	*0.474*
		More than 10 hours/week	Coefficient	-2.06
			p-value	*2.37*
	Exercise (reference at least once per week)	**Mild daily activity**	Coefficient	-1.7
			p-value	*0.413*
		No	Coefficient	1.71
			p-value	*0.581*

				Change in perceived age
Model 6: Remove exercise and add alcohol	**Sun protection (reference always wears)**	**Occasional use**	Coefficient	1.02
			p-value	*0.622*
		Never use	Coefficient	*3.97*
			p-value	*0.062*
	Age		Coefficient	-1.079
			p-value	*0.076*
	Patient status (reference control)		Coefficient	1.81
			p-value	*0.286*
	Hours outdoors (reference less than 5 hours/week)	**5-10 hours/week**	Coefficient	1.35
			p-value	*0.466*
		More than 10 hours/week	Coefficient	-0.9
			p-value	*0.711*
	Alcohol use often never use)	**Occasional use**	Coefficient	-3.27
			p-value	*0.175*
		Never use	Coefficient	2.19
			p-value	*0.487*

				Change in perceived age
Model 7: Add confounder season of sample collection	**Sun protection (reference always wears)**	**Occasional use**	Coefficient	2.11
			p-value	*0.363*
		Never use	Coefficient	*4.82*
			p-value	*0.041*
	Age		Coefficient	-1.063
			p-value	*0.099*
	Patient status (reference control)		Coefficient	1.64
			p-value	*0.354*
	Hours outdoors (reference less than 5 hours/week)	**5-10 hours/week**	Coefficient	0.91
			p-value	*0.635*
		More than 10 hours/week	Coefficient	-1.2
			p-value	*0.641*
	Alcohol use often never use)	**Occasional use**	Coefficient	-3.95
			p-value	*0.123*
		Never use	Coefficient	-1.89
			p-value	*0.56*
	Season of sample collection (reference winter)	**Spring**	Coefficient	-3.16
			p-value	*0.264*
		Summer	Coefficient	-3.44
			p-value	*0.292*
		Autumn	Coefficient	-0.318
			p-value	0.318

				Change in perceived age

Model 8: Add confounder body mass index	**Sun protection (reference always wears)**	**Occasional use**	Coefficient	2.19
			p-value	*0.369*
		Never use	Coefficient	*4.81*
			p-value	*0.049*
	Age		Coefficient	-0.1198
			p-value	*0.136*
	Patient status (reference control)		Coefficient	1.89
			p-value	*0.344*
	Hours outdoors (reference less than 5 hours/week)	**5-10 hours/week**	Coefficient	0.87
			p-value	*0.663*
		More than 10 hours/week	Coefficient	-1.04
			p-value	*0.704*
	Alcohol use often never use)	**Occasional use**	Coefficient	-4.2
			p-value	*0.132*
		Never use	Coefficient	1.88
			p-value	*0.575*
	Season of sample collection (reference winter)	**Spring**	Coefficient	-3.4
			p-value	*0.262*
		Summer	Coefficient	-3.68
			p-value	*0.287*
		Autumn	Coefficient	-3.32
			p-value	0.324
	Body Mass Index		Coefficient	0.051
			p-value	*0.749*

				Change in perceived age
Model 9: Remove body mass index and add smoking status	**Sun protection (reference always wears)**	**Occasional use**	Coefficient	1.91
			p-value	*0.418*
		Never use	Coefficient	*4.83*
			p-value	*0.045*
	Age		Coefficient	-961
			p-value	*0.148*
	Patient status (reference control)		Coefficient	1.07
			p-value	*0.576*
	Hours outdoors (reference less than 5 hours/week)	**5-10 hours/week**	Coefficient	0.67
			p-value	*0.74*
		More than 10 hours/week	Coefficient	-0.84
			p-value	*0.751*
	Alcohol use often never use)	**Occasional use**	Coefficient	-3.48
			p-value	*0.187*
		Never use	Coefficient	-1.87
			p-value	*0.575*
	Season of sample collection (reference winter)	**Spring**	Coefficient	-3.05
			p-value	*0.295*
		Summer	Coefficient	-2.98
			p-value	*0.384*
		Autumn	Coefficient	-2.95
			p-value	0.38
	Smoking status (reference never smoked)	**Previously smoked**	Coefficient	-2.6
			p-value	*0.304*
		Currently smoke	Coefficient	0.79
			p-value	*0.856*

Appendix F: Linear regression model: UV spots v skin swab damage

				mtDNA damage	
				Right cheek	**Left cheek**
Model 1	**UV spots area**		Coefficient	-0.00484	-0.00667
			p-value	*0.142*	*0.069*

				mtDNA damage	
				Right cheek	**Left cheek**
Model 2: Add confounder patient status	**UV spots area**		Coefficient	-0.00474	-0.0064
			p-value	*0.169*	*0.09*
	Patient status (reference control)		Coefficient	0.0055	0.0168
			p-value	*0.899*	*0.709*

				mtDNA damage	
				Right cheek	**Left cheek**
Model 3: Remove patient status and add sex	**UV spots area**		Coefficient	-0.00478	0.00669
			p-value	*0.169*	*0.072*
	Sex (reference female)		Coefficient	0.0055	0.0089
			p-value	*0.899*	*0.853*

				mtDNA damage	
				Right cheek	**Left cheek**
Model 4: Remove sex and add sun protection use	**UV spots area**		Coefficient	-0.0074	-0.00891
			p-value	*0.015*	*0.015*
	Sun protection (reference always use)	**Occasional use**	Coefficient	0.0307	-0.0089
			p-value	*0.492*	*0.864*
		Never use	Coefficient	0.01696	0.1215
			p-value	*0.001*	*0.024*

				mtDNA damage	
				Right cheek	**Left cheek**
Model 5: Add confounder hours outdoors	**UV spots area**		Coefficient	-0.00772	-0.00909
			p-value	*0.012*	*0.012*
	Sun protection (reference always use)	**Occasional use**	Coefficient	0.0073	-0.0318
			p-value	*0.873*	*0.54*
		Never use	Coefficient	0.1617	0.1044
			p-value	*0.001*	*0.046*
	Hours outdoors (reference less than 5 hours/week)	**5-10 hours/week**	Coefficient	0.0375	0.0204
			p-value	*0.36*	*0.658*
		More than 10 hours/week	Coefficient	0.0845	0.1044
			p-value	*0.089*	*0.056*

				mtDNA damage Right cheek	Left cheek
Model 6: Remove hours outdoors and add confounder season of sample collection	**UV spots area**		Coefficient	-0.00677	-0.00819
			p-value	*0.028*	*0.019*
	Sun protection (reference always use)	**Occasional use**	Coefficient	0.0006	-0.0453
			p-value	*0.991*	*0.385*
		Never use	Coefficient	0.141	0.0827
			p-value	*0.007*	*0.117*
	Season of sample collection (reference winter)	**Spring**	Coefficient	0.0494	0.0296
			p-value	*0.387*	*0.64*
		Summer	Coefficient	0.0865	0.1582
			p-value	*0.195*	*0.034*
		Autumn	Coefficient	0.1141	0.0995
			p-value	0.087	0.172

				mtDNA damage Right cheek	Left cheek
Model 7: Remove season of sample collection and add confounder skin type	**UV spots area**		Coefficient	-0.0079	-0.00872
			p-value	*0.007*	*0.013*
	Sun protection (reference always use)	**Occasional use**	Coefficient	0.0091	-0.0381
			p-value	*0.83*	*0.452*
		Never use	Coefficient	0.1701	0.1089
			p-value	*0.001*	*0.041*
	Skin Type	**Type**	Coefficient	0.1129	0.1469
			p-value	*0.057*	*0.041*
		Often use	Coefficient	0.1325	0.1433
			p-value	*0.009*	*0.021*

				mtDNA damage Right cheek	Left cheek
Model 8: Add confounder age	**UV spots area**		Coefficient	-0.01056	-0.01075
			p-value	*0.003*	*0.006*
	Sun protection (reference always use)	**Occasional use**	Coefficient	0.0123	-0.0308
			p-value	*0.782*	*0.569*
		Never use	Coefficient	0.1608	0.1048
			p-value	*0.001*	*0.053*
	Age		Coefficient	0.00219	0.00183
			p-value	*0.088*	*0.187*

				mtDNA damage	
				Right cheek	**Left cheek**
Model 8: Add confounder age	**UV spots area**		Coefficient	-0.00878	-0.00787
			p-value	*0.013*	*0.021*
	Sun protection (reference always use)	**Occasional use**	Coefficient	0.0028	-0.0388
			p-value	*0.95*	*0.414*
		Never use	Coefficient	0.1686	0.1102
			p-value	*0.001*	*0.02*
	Age		Coefficient	0.00301	0.00285
			p-value	*0.024*	*0.025*
	Alcohol use (reference often use)	**Occasional use**	Coefficient	0.048	0.0462
			p-value	*0.38*	*0.380*
		Never use	Coefficient	*0.1443*	0.2244
				0.055	*0.002*

			mtDNA damage	
			Right cheek	**Left cheek**
Model 9: Remove sun protection and alcohol use	**UV spots area**	Coefficient	-0.00853	-0.009
		p-value	*0.03*	*0.024*
	Age	Coefficient	0.00245	0.00205
		p-value	*0.088*	*0.139*

Appendix G: Linear regression model: predictors of UV spots

				UV spot area (% coverage)	
				Right cheek	**Left cheek**
Model 1	**Sun protection (reference always use)**	**Occasional use**	Coefficient	1.75	0.53
			p-value	*0.48*	*0.813*
		Never use	Coefficient	3.02	3.28
			p-value	*0.224*	*0.153*

				UV spot area (% coverage)	
				Right cheek	**Left cheek**
Model 2: Add confounder age	**Sun protection (reference always use)**	**Occasional use**	Coefficient	-0.36	-0.93
			p-value	*0.873*	*0.672*
		Never use	Coefficient	0.92	1.82
			p-value	*0.68*	*0.41*
	Age		Coefficient	0.1915	0.1332
			p-value	*0.001*	*0.016*

				UV spot area (% coverage)	
				Right cheek	**Left cheek**
Model 3: Add patient status	**Sun protection (reference always use)**	**Occasional use**	Coefficient	-0.6	-1.11
			p-value	*0.782*	*0.609*
		Never use	Coefficient	1.3	2.1
			p-value	*0.55*	*0.338*
	Age		Coefficient	0.192	0.1336
			p-value	*0.001*	*0.015*
	Patient status (reference control)		Coefficient	-3.13	-2.34
			p-value	*0.074*	*0.178*

				UV spot area (% coverage)	
				Right cheek	**Left cheek**
Model 4: Add hours outdoors	**Sun protection (reference always use)**	**Occasional use**	Coefficient	0.04	-0.51
			p-value	*0.986*	*0.82*
		Never use	Coefficient	1.68	2.46
			p-value	*0.445*	*0.268*
	Age		Coefficient	0.2135	0.153
			p-value	*0.000*	*0.008*
	Patient status (reference control)		Coefficient	-3.51	-2.65
			p-value	*0.053*	*0.14*
	Hours outdoors (reference less than 5 hours/week)	**5-10 hours/week**	Coefficient	-2.05	-2.2
			p-value	*0.306*	*0.274*
		More than 10 hours/week	Coefficient	3.37	-3.11
			p-value	*0.18*	*0.216*

Model 5: Add hours outdoors.01056 -.00853

			UV spot area (% coverage)	
			Right cheek	**Left cheek**
Sun protection (reference always use)	**Occasional use**	Coefficient	0.04	-0.51
		p-value	*0.986*	*0.82*
	Never use	Coefficient	1.68	2.46
		p-value	*0.445*	*0.268*
-Age		Coefficient	0.2135	0.153
		p-value	*0.000*	*0.008*
Patient status (reference control)		Coefficient	-3.51	-2.65
		p-value	*0.053*	*0.14*
Hours outdoors (reference less than 5 hours/week)	**5-10 hours/week**	Coefficient	-2.05	-2.2
		p-value	*0.306*	*0.274*
	More than 10 hours/week	Coefficient	3.37	-3.11
		p-value	*0.18*	*0.216*

Model 6: Add season of sample collection

			UV spot area (% coverage)	
			Right cheek	**Left cheek**
Sun protection (reference always use)	**Occasional use**	Coefficient	1.48	0.71
		p-value	*0.532*	*0.797*
	Never use	Coefficient	3.05	3.61
		p-value	*0.204*	*0.141*
Age		Coefficient	0.2179	0.1559
		p-value	*0.001*	*0.011*
Patient status (reference control)		Coefficient	-3.59	-2.78
		p-value	*0.052*	*0.133*
Hours outdoors (reference less than 5 hours/week)	**5-10 hours/week**	Coefficient	-2.56	-2.65
		p-value	*0.207*	*0.199*
	More than 10 hours/week	Coefficient	-3.8	-3.6
		p-value	*0.145*	*0.173*
Season of sample collection (reference winter)	**Spring**	Coefficient	-4.73	-4.25
		p-value	*0.095*	*0.138*
	Summer	Coefficient	-4.63	-3.8
		p-value	*0.15*	*0.242*
	Autumn	Coefficient	-4.84	-4
		p-value	0.14	*0.227*

				UV spot area (% coverage)	
				Right cheek	**Left cheek**
Model 7: Add season of sample collection	**Sun protection (reference always use)**	**Occasional use**	Coefficient	1.48	0.71
			p-value	*0.532*	*0.797*
		Never use	Coefficient	3.05	3.61
			p-value	*0.204*	*0.141*
	Age		Coefficient	0.2179	0.1559
			p-value	*0.001*	*0.011*
	Patient status (reference control)		Coefficient	-3.59	-2.78
			p-value	*0.052*	*0.133*
	Hours outdoors (reference less than 5 hours/week)	**5-10 hours/week**	Coefficient	-2.56	-2.65
			p-value	*0.207*	*0.199*
		More than 10 hours/week	Coefficient	-3.8	-3.6
			p-value	*0.145*	*0.173*
	Season of sample collection (reference winter)	**Spring**	Coefficient	-4.73	-4.25
			p-value	*0.095*	*0.138*
		Summer	Coefficient	-4.63	-3.8
			p-value	*0.15*	*0.242*
		Autumn	Coefficient	-4.84	-4
			p-value	0.14	*0.227*

				UV spot area (% coverage)	
				Right cheek	**Left cheek**
Model 8: Add sex	**Sun protection (reference always use)**	**Occasional use**	Coefficient	1.4	0.71
			p-value	*0.559*	*0.772*
		Never use	Coefficient	2.99	3.61
			p-value	*0.219*	*0.148*
	Age		Coefficient	0.2185	0.156
			p-value	*0.001*	*0.013*
	Patient status (reference control)		Coefficient	-3.58	-2.78
			p-value	*0.055*	*0.14*
	Hours outdoors (reference less than 5 hours/week)	**5-10 hours/week**	Coefficient	-2.76	-2.65
			p-value	*0.186*	*0.212*
		More than 10 hours/week	Coefficient	-4.43	-3.61
			p-value	*0.123*	*0.214*
	Season of sample collection (reference winter)	**Spring**	Coefficient	-4.9	-4.26
			p-value	*0.09*	*0.147*
		Summer	Coefficient	-4.71	-3.8
			p-value	*0.148*	*0.25*
		Autumn	Coefficient	-5.12	-4.01
			p-value	0.127	*0.239*
	Sex (reference female)		Coefficient	1.19	0.03
			p-value	*0.568*	*0.99*

				UV spot area (% coverage)	
				Right cheek	**Left cheek**
Model 9: Remove sex add skin type	**Sun protection (reference always use)**	**Occasional use**	Coefficient	0.97	0.37
			p-value	*0.684*	*0.881*
		Never use	Coefficient	3.38	3.81
			p-value	*0.159*	*0.127*
	Age		Coefficient	0.2498	0.1833
			p-value	*0.000*	*0.005*
	Patient status (reference control)		Coefficient	-4.14	-3.29
			p-value	*0.029*	*0.089*
	Hours outdoors (reference less than 5 hours/week)	**5-10 hours/week**	Coefficient	-2.35	-2.44
			p-value	*0.241*	*0.241*
		More than 10 hours/week	Coefficient	-3.26	-3.14
			p-value	*0.203*	*0.237*
	Season of sample collection (reference winter)	**Spring**	Coefficient	-3.41	-3.24
			p-value	0.238	*0.276*
		Summer	Coefficient	-3.18	-2.67
			p-value	*0.326*	*0.424*
		Autumn	Coefficient	-5.32	-4.4
			p-value	0.1	*0.186*
	Skin type self-assessment	**Type II**	Coefficient	-0.017	-0.63
			p-value	*0.957*	*0.847*
		Type III	Coefficient	-3.82	-3.39
			p-value	0.178	0.247

Appendix H: Linear regression model: skin swab damage in all body sites

				mtDNA damage			
				Right cheek	**Left cheek**	**Behind Ear**	**Inner Arm**
Model 1: from appendix D	**Age**		Coefficient	0.00023	0.0014	-0.00139	0.00116
			p-value	*0.867*	*0.323*	0.24	0.385
	Sun protection (reference always use)	**Occasional use**	Coefficient	-0.0631	-0.0946	0.0458	0.0153
			p-value	*0.21*	*0.076*	0.284	*0.754*
		Never use	Coefficient	0.1369	0.0623	0.0635	-0.0127
			p-value	*0.007*	*0.452*	0.158	*0.8*
	Hours outdoors (reference less than 5 hours/week)	**5-10 hours/week**	Coefficient	0.0377	0.031	-0.0158	0.036
			p-value	*0.326*	*0.452*	0.657	0.391
		More than 10 hours/week	Coefficient	0.0253	0.0213	-0.0056	-0.0047
			p-value	*0.614*	*0.702*	0.903	*0.926*
	Season of sample collection (reference winter)	**Spring**	Coefficient	0.0965	0.065	0.0417	0.0433
			p-value	*0.103*	*0.302*	0.446	*0.542*
		Summer	Coefficient	0.1199	0.165	0.0951	0.0617
			p-value	*0.079*	*0.025*	0.131	*0.431*
		Autumn	Coefficient	0.146	0.1064	0.1827	0.0416
			p-value	0.03	0.122	0.005	*0.597*
	Alcohol use (reference often use)	**Occasional use**	Coefficient	0.125	0.1033	0.0368	0.0335
			p-value	*0.037*	*0.08*	0.428	*0.55*
		Never use	Coefficient	0.1803	0.24	0.1077	0.1131
			p-value	*0.015*	*0.002*	0.057	*0.09*
	Skin type self-assessment	**Type II**	Coefficient	0.1201	0.0878	0.0759	0.0726
			p-value	*0.05*	*0.199*	0.185	0.267
		Type III	Coefficient	0.1504	0.0959	0.0488	0.0398
			p-value	0.008	0.126	0.324	0.467

				mtDNA damage			
			Right cheek	Left cheek	Behind Ear	Inner Arm
Model 2: Remove age	**Sun protection (reference always wears)**	**Occasional use**	Coefficient	-0.0615	-0.0826	0.038	0.022
			p-value	*0.204*	*0.109*	0.37	0.647
		Never use	Coefficient	0.1371	0.0685	0.0547	-0.0064
			p-value	*0.006*	*0.161*	0.219	*0.897*
	Hours outdoors (reference less than 5 hours/ week)	**5-10 hours/week**	Coefficient	0.0384	0.0332	-0.0165	0.0357
			p-value	*0.0271*	*0.421*	0.646	*0.392*
		More than 10 hours/week	Coefficient	0.0271	0.0419	-0.018	0.007
			p-value	*0.572*	*0.42*	0.69	0.887
	Season of sample collection (reference winter)	**Spring**	Coefficient	0.0957	0.0621	0.0492	0.0409
			p-value	*0.098*	*0.323*	0.369	*0.562*
		Summer	Coefficient	0.1186	0.1568	0.1036	0.057
			p-value	*0.075*	*0.031*	0.101	*0.463*
		Autumn	Coefficient	0.1486	0.1142	0.1698	0.0502
			p-value	0.021	0.096	0.008	*0.518*
	Skin type self-assessment	**Type II**	Coefficient	0.1211	0.0816	0.074	0.0768
			p-value	*0.025*	*0.131*	0.199	*0.237*
		Type III	Coefficient	0.1211	0.2042	0.0378	0.05
			p-value	0.1739	0.002	0.439	*0.349*
	Alcohol use (reference never use)	**Occasional use**	Coefficient	0.1204	0.0975	0.0552	0.0195
			p-value	*0.045*	*0.151*	0.214	*0.714*
		Often use	Coefficient	0.1523	0.1079	0.1381	0.0899
			p-value	*0.005*	*0.081*	0.008	0.134

Appendix I: Representative images of LysoTracker staining

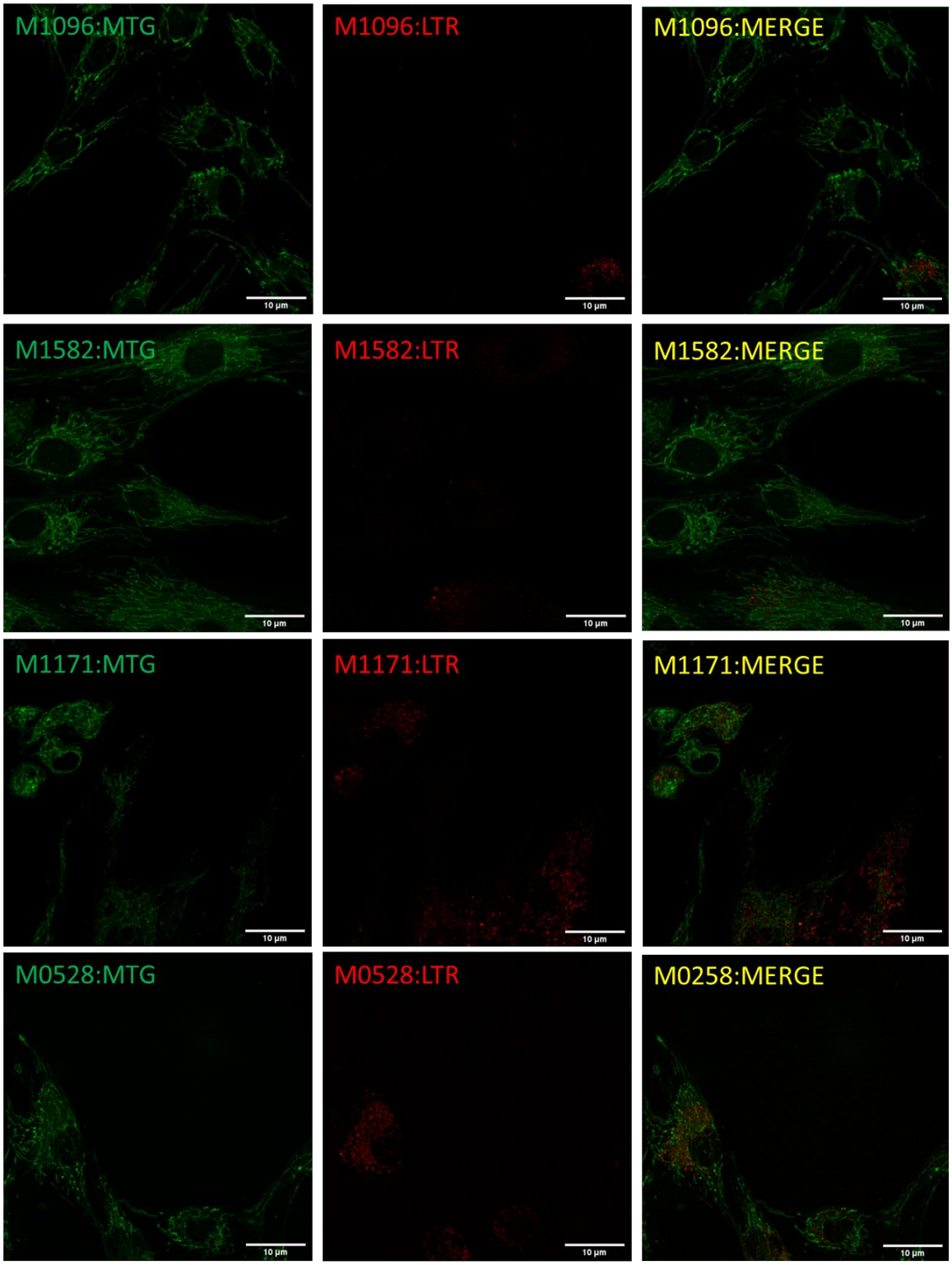

Figure 7-1. Representative images of Mitotracker Green (MTG) and LysoTracker Red (LTR) images for each cell line.

Appendix J: Outcomes of PhD

Manuscripts

Review: Stout, R and Birch-Machin, MA. 2019. Mitochondria's role in skin ageing. *Biology (Basel).* 8

Presentations

Stout, R. 2018. Facial appearance and ageing in mitochondrial dysfunction. *Biochemical Society: The changing landscape of research on ageing: models, mechanisms and therapies.*

Stout, R. 2018. Facial appearance and ageing in mitochondrial dysfunction. *North East Postgraduate conference.*

Posters

Stout, R. 2018. Stressing out mitochondria. *NuGO week: Mitochondria, nutrition and health.*

Stout, R. 2019. Mitochondrial dysfunction in facial appearance and ageing. *FEBS/EMBO Lecture course*: *Mitochondria in life death and disease.*

Stout, R. 2019. Mitochondrial dysfunction in facial appearance and ageing. *10th annual alliance for healthy ageing conference.*

References

AFAQ, F. & MUKHTAR, H. 2001. Effects of solar radiation on cutaneous detoxification pathways. *Journal of Photochemistry and Photobiology B: Biology,* 63**,** 61-69.

ALCÁZAR-FABRA, M., NAVAS, P. & BREA-CALVO, G. 2016. Coenzyme Q biosynthesis and its role in the respiratory chain structure. *Biochimica et Biophysica Acta (BBA) - Bioenergetics,* 1857**,** 1073-1078.

ALHEGAILI, A. S., JI, Y., SYLVIUS, N., BLADES, M. J., KARBASCHI, M., TEMPEST, H. G., JONES, G. D. D. & COOKE, M. S. 2019. Genome-Wide Adductomics Analysis Reveals Heterogeneity in the Induction and Loss of Cyclobutane Thymine Dimers across Both the Nuclear and Mitochondrial Genomes. *International Journal of Molecular Sciences,* 20**,** 5112.

ALLIO, R., DONEGA, S., GALTIER, N. & NABHOLZ, B. 2017. Large Variation in the Ratio of Mitochondrial to Nuclear Mutation Rate across Animals: Implications for Genetic Diversity and the Use of Mitochondrial DNA as a Molecular Marker. *Molecular Biology and Evolution,* 34**,** 2762-2772.

ALMEIDA, M., BETANCOR, E., FREGEL, R., SUÁREZ, N. M. & PESTANO, J. 2011. Efficient DNA extraction from hair shafts. *Forensic Science International: Genetics Supplement Series,* 3**,** e319-e320.

ALVAREZ, L. A., KOVACIC, L., RODRIGUEZ, J., GOSEMANN, J. H., KUBICA, M., PIRCALABIORU, G. G., FRIEDMACHER, F., CEAN, A., GHISE, A., SARANDAN, M. B., PURI, P., DAFF, S., PLETTNER, E., VON KRIEGSHEIM, A., BOURKE, B. & KNAUS, U. G. 2016. NADPH oxidase-derived H2O2 subverts pathogen signaling by oxidative phosphotyrosine conversion to PB-DOPA. *Proc Natl Acad Sci U S A,* 113**,** 10406-11.

ANNA, O. & ADAM, S. 2013. Mitochondria as a pharmacological target: Magnum overview. *IUBMB Life,* 65**,** 273-281.

APABHAI, S., GORMAN, G. S., SUTTON, L., ELSON, J. L., PLÖTZ, T., TURNBULL, D. M. & TRENELL, M. I. 2011. Habitual physical activity in mitochondrial disease. *PloS one,* 6**,** e22294-e22294.

ASHRAFI, G. & SCHWARZ, T. L. 2013. The pathways of mitophagy for quality control and clearance of mitochondria. *Cell Death & Differentiation,* 20**,** 31-42.

AWAD, S. S., MOFTAH, N. H., RASHED, L. A., TOUNI, A. A. & TELEP, R. A. A. 2021. Evaluation of the effect of narrow band-ultraviolet B on the expression of tyrosinase, TYRP-1, and TYRP-2 mRNA in vitiligo skin and their correlations with clinical improvement: A retrospective study. *Dermatologic Therapy,* 34**,** e14649.

BAKER, H. & KLIGMAN, A. M. 1967. Technique for Estimating Turnover Time of Human Stratum Corneum. *Archives of Dermatology,* 95**,** 408-411.

BARNEY, S., STAINTON, S., CATT, M. & DLAY, S. Feature specific analysis of a deep convolutional neural network for ageing classification. 2018 11th International Symposium on Communication Systems, Networks & Digital Signal Processing (CSNDSP), 18-20 July 2018 2018. 1-6.

BASTIAENS, M., HOEFNAGEL, J., WESTENDORP, R., VERMEER, B. J. & BOUWES BAVINCK, J. N. 2004. Solar lentigines are strongly related to sun exposure in contrast to ephelides. *Pigment cell research,* 17**,** 225-229.

BEN-ARI, Y. A., BRODY, Y., KINOR, N., MOR, A., TSUKAMOTO, T., SPECTOR, D. L., SINGER, R. H. & SHAV-TAL, Y. 2010. The life of an mRNA in space and time. *Journal of cell science,* 123**,** 1761-1774.

BERNEBURG, M., GATTERMANN, N., STEGE, H., GREWE, M., VOGELSANG, K., RUZICKA, T. & KRUTMANN, J. 1997. Chronically ultraviolet-exposed human skin shows a higher mutation frequency of mitochondrial DNA as compared to unexposed skin and the hematopoietic system. *Photochemistry and photobiology,* 66**,** 271-275.

BERRY, B. J., TREWIN, A. J., AMITRANO, A. M., KIM, M. & WOJTOVICH, A. P. 2018. Use the Protonmotive Force: Mitochondrial Uncoupling and Reactive Oxygen Species. *Journal of molecular biology,* 430**,** 3873-3891.

BIENERT, G. P. & CHAUMONT, F. 2014. Aquaporin-facilitated transmembrane diffusion of hydrogen peroxide. *Biochim Biophys Acta,* 1840**,** 1596-604.

BIRKET, M. J. & BIRCH-MACHIN, M. A. 2007. Ultraviolet radiation exposure accelerates the accumulation of the aging-dependent T414G mitochondrial DNA mutation in human skin. *Aging Cell,* 6**,** 557-564.

BLECHA, J., NOVAIS, S. M., ROHLENOVA, K., NOVOTNA, E., LETTLOVA, S., SCHMITT, S., ZISCHKA, H., NEUZIL, J. & ROHLENA, J. 2017. Antioxidant defense in quiescent cells determines selectivity of electron transport chain inhibition-induced cell death. *Free Radical Biology and Medicine,* 112**,** 253-266.

BOGENHAGEN, D. F. 2012. Mitochondrial DNA nucleoid structure. *Biochimica et Biophysica Acta (BBA) - Gene Regulatory Mechanisms,* 1819**,** 914-920.

BOGENHAGEN, D. F., OSTERMEYER-FAY, A. G., HALEY, J. D. & GARCIA-DIAZ, M. 2018. Kinetics and Mechanism of Mammalian Mitochondrial Ribosome Assembly. *Cell reports,* 22**,** 1935-1944.

BÖHM, M. & HILL, H. Z. 2016. Ultraviolet B, melanin and mitochondrial DNA: Photo-damage in human epidermal keratinocytes and melanocytes modulated by alpha-melanocyte-stimulating hormone. *F1000Research,* 5.

BOULTON, S. J. & BIRCH-MACHIN, M. A. 2015. Impact of hyperpigmentation on superoxide flux and melanoma cell metabolism at mitochondrial complex II. *The FASEB Journal,* 29**,** 346-353.

BOWMAN, A. & BIRCH-MACHIN, M. A. 2016. Age-dependent decrease of mitochondrial complex II activity in human skin fibroblasts. *Journal of Investigative Dermatology,* 136**,** 912-919.

BRETT, A. K., NELA, D., JEFFREY, M. M., SANTIAGO, C., MARK, A. H., PETER, G., ERIC, A. S. & THOMAS, F. 2007. The Mitochondrial Transcription Factor TFAM Coordinates the Assembly of Multiple DNA Molecules into Nucleoid-like Structures. *Molecular Biology of the Cell,* 18**,** 3225-3236.

BUA, E., JOHNSON, J., HERBST, A., DELONG, B., MCKENZIE, D., SALAMAT, S. & AIKEN, J. M. 2006. Mitochondrial DNA–Deletion Mutations Accumulate Intracellularly to Detrimental Levels in Aged Human Skeletal Muscle Fibers. *The American Journal of Human Genetics,* 79**,** 469-480.

BURANASIN, P., MIZUTANI, K., IWASAKI, K., PAWAPUTANON NA MAHASARAKHAM, C., KIDO, D., TAKEDA, K. & IZUMI, Y. 2018. High glucose-induced oxidative stress impairs proliferation and migration of human gingival fibroblasts. *PloS one,* 13**,** e0201855-e0201855.

CAO, J., WU, H. & LI, Z. 2018. Recent perspectives of pediatric mitochondrial diseases. *Experimental and Therapeutic Medicine,* 15**,** 13-18.

CAO, L., SHITARA, H., SUGIMOTO, M., HAYASHI, J.-I., ABE, K. & YONEKAWA, H. 2009. New Evidence Confirms That the Mitochondrial Bottleneck Is Generated without Reduction of Mitochondrial DNA Content in Early Primordial Germ Cells of Mice. *PLOS Genetics,* 5**,** e1000756.

CAO, W., MIRJALILI, V. & RASCHKA, S. 2020. Rank consistent ordinal regression for neural networks with application to age estimation. *Pattern Recognition Letters,* 140**,** 325-331.

CHAN, C. C. W., LIU, V. W. S., LAU, E. Y. L., YEUNG, W. S. B., NG, E. H. Y. & HO, P. C. 2005. Mitochondrial DNA content and 4977 bp deletion in unfertilized oocytes. *MHR: Basic science of reproductive medicine,* 11**,** 843-846.

CHANG, A. L. S. 2016. Expanding our understanding of human skin aging. *Journal of Investigative Dermatology,* 136**,** 897-899.

CHIANG, H.-M., CHEN, H.-C., LIN, T.-J., SHIH, I.-C. & WEN, K.-C. 2012. Michelia alba extract attenuates UVB-induced expression of matrix metalloproteinases via MAP kinase pathway in human dermal fibroblasts. *Food and Chemical Toxicology,* 50**,** 4260-4269.

CHICHAGOVA, V., HALLAM, D., COLLIN, J., BUSKIN, A., SARETZKI, G., ARMSTRONG, L., YU-WAI-MAN, P., LAKO, M. & STEEL, D. H. 2017. Human iPSC disease modelling reveals functional and structural defects in retinal pigment epithelial cells harbouring the m.3243A > G mitochondrial DNA mutation. *Scientific Reports,* 7**,** 12320.

CHINNERY, P. F. & GOMEZ-DURAN, A. 2018. Oldies but Goldies mtDNA Population Variants and Neurodegenerative Diseases. *Frontiers in Neuroscience,* 12.

CHOONG, C. J., OKUNO, T., IKENAKA, K., BABA, K., HAYAKAWA, H., KOIKE, M., YOKOTA, M., DOI, J., KAKUDA, K., TAKEUCHI, T., KUMA, A., NAKAMURA, S., NAGAI, Y., NAGANO, S., YOSHIMORI, T. & MOCHIZUKI, H. 2021. Alternative mitochondrial quality control mediated by extracellular release. *Autophagy,* 17**,** 2962-2974.

CHOPRA, K., CALVA, D., SOSIN, M., TADISINA, K. K., BANDA, A., DE LA CRUZ, C., CHAUDHRY, M. R., LEGESSE, T., DRACHENBERG, C. B., MANSON, P. N. & CHRISTY, M. R. 2015. A comprehensive examination of topographic thickness of skin in the human face. *Aesthet Surg J,* 35**,** 1007-13.

CLAPES, A., BILICI, O., TEMIROVA, D., AVOTS, E., ANBARJAFARI, G. & ESCALERA, S. From apparent to real age: gender, age, ethnic, makeup, and expression bias analysis in real age estimation. Proceedings of the IEEE Conference on Computer Vision and Pattern Recognition Workshops, 2018. 2373-2382.

CLIFFORD, T., BOWMAN, A., CAPPER, T., ALLERTON, D. M., FOSTER, E., BIRCH-MACHIN, M., LIETZ, G., HOWATSON, G. & STEVENSON, E. J. 2018. A pilot study investigating reactive oxygen species production in capillary blood after a marathon and the influence of an antioxidant-rich beetroot juice. *Appl Physiol Nutr Metab,* 43**,** 303-306.

COLEMAN, S. R. & GROVER, R. 2006. The Anatomy of the Aging Face: Volume Loss and Changes in 3-Dimensional Topography. *Aesthetic Surgery Journal,* 26**,** S4-S9.

CRAVEN, L., ALSTON, C. L., TAYLOR, R. W. & TURNBULL, D. M. 2017. Recent Advances in Mitochondrial Disease. *Annu Rev Genomics Hum Genet,* 18**,** 257-275.

CZEKALLA, C., SCHÖNBORN, K. H., LADEMANN, J. & MEINKE, M. C. 2019. Noninvasive Determination of Epidermal and Stratum Corneum Thickness in vivo Using Two-Photon Microscopy and Optical Coherence Tomography: Impact of Body Area, Age, and Gender. *Skin Pharmacol Physiol,* 32**,** 142-150.

D'MELLO, S. A. N., FINLAY, G. J., BAGULEY, B. C. & ASKARIAN-AMIRI, M. E. 2016. Signaling Pathways in Melanogenesis. *International journal of molecular sciences,* 17**,** 1144.

DĄBROWSKA, A. K., SPANO, F., DERLER, S., ADLHART, C., SPENCER, N. D. & ROSSI, R. M. 2018. The relationship between skin function, barrier properties, and body-dependent factors. *Skin Research and Technology,* 24**,** 165-174.

DAHAL, S., DUBEY, S. & RAGHAVAN, S. C. 2018. Homologous recombination-mediated repair of DNA double-strand breaks operates in mammalian mitochondria. *Cellular and Molecular Life Sciences,* 75**,** 1641-1655.

DAN, X., BABBAR, M., MOORE, A., WECHTER, N., TIAN, J., MOHANTY, JOY G., CROTEAU, D. L. & BOHR, V. A. 2020. DNA damage invokes mitophagy through a pathway involving Spata18. *Nucleic Acids Research,* 48**,** 6611-6623.

DANIELE, T., HURBAIN, I., VAGO, R., CASARI, G., RAPOSO, G., TACCHETTI, C. & SCHIAFFINO, M. V. 2014. Mitochondria and melanosomes establish physical contacts modulated by Mfn2 and involved in organelle biogenesis. *Current Biology,* 24**,** 393-403.

DAO, H., JR. & KAZIN, R. A. 2007. Gender differences in skin: a review of the literature. *Gend Med,* 4**,** 308-28.

DE LAAT, P., KOENE, S., VAN DEN HEUVEL, L. P. W. J., RODENBURG, R. J. T., JANSSEN, M. C. H. & SMEITINK, J. A. M. 2012. Clinical features and heteroplasmy in blood, urine and saliva in 34 Dutch families carrying the m.3243A > G mutation. *Journal of Inherited Metabolic Disease,* 35**,** 1059-1069.

DELL'ANNA, M. L., OTTAVIANI, M., KOVACS, D., MIRABILII, S., BROWN, D. A., COTA, C., MIGLIANO, E., BASTONINI, E., BELLEI, B., CARDINALI, G., RICCIARDI, M. R., TAFURI, A. & PICARDO, M. 2017. Energetic mitochondrial failing in vitiligo and possible rescue by cardiolipin. *Scientific Reports,* 7**,** 13663.

DENAT, L., KADEKARO, A. L., MARROT, L., LEACHMAN, S. A. & ABDEL-MALEK, Z. A. 2014. Melanocytes as instigators and victims of oxidative stress. *Journal of Investigative Dermatology,* 134**,** 1512-1518.

DI MARZO, N., CHISCI, E. & GIOVANNONI, R. 2018. The Role of Hydrogen Peroxide in Redox-Dependent Signaling: Homeostatic and Pathological Responses in Mammalian Cells. *Cells,* 7**,** 156.

DIAZ, F., BAYONA-BAFALUY, M. P., RANA, M., MORA, M., HAO, H. & MORAES, C. T. 2002. Human mitochondrial DNA with large deletions repopulates organelles faster than full-length genomes under relaxed copy number control. *Nucleic acids research,* 30**,** 4626-4633.

DIFFEY, B. 2015. Solar Spectral Irradiance and Summary Outputs Using Excel. *Photochemistry and Photobiology,* 91**,** 553-557.

DIKALOV, S. I. & HARRISON, D. G. 2014. Methods for detection of mitochondrial and cellular reactive oxygen species. *Antioxidants & redox signaling,* 20**,** 372-382.

DING, A., YANG, Y., ZHAO, Z., HÜLS, A., VIERKÖTTER, A., YUAN, Z., CAI, J., ZHANG, J., GAO, W. & LI, J. 2017. Indoor PM2. 5 exposure affects skin aging manifestation in a Chinese population. *Scientific reports,* 7**,** 1-7.

DRISKELL, R. R. & WATT, F. M. 2015. Understanding fibroblast heterogeneity in the skin. *Trends in Cell Biology,* 25**,** 92-99.

DUNNILL, C., PATTON, T., BRENNAN, J., BARRETT, J., DRYDEN, M., COOKE, J., LEAPER, D. & GEORGOPOULOS, N. T. 2017. Reactive oxygen species (ROS) and wound healing: the functional role of ROS and emerging ROS-modulating technologies for augmentation of the healing process. *International Wound Journal,* 14**,** 89-96.

DVORAKOVA, V., KOLAROVA, H., MAGNER, M., TESAROVA, M., HANSIKOVA, H., ZEMAN, J. & HONZIK, T. 2016. The phenotypic spectrum of fifty Czech m.3243A> G carriers. *Molecular Genetics and Metabolism,* 118**,** 288-295.

ECKHART, L., LIPPENS, S., TSCHACHLER, E. & DECLERCQ, W. 2013. Cell death by cornification. *Biochimica et Biophysica Acta (BBA) - Molecular Cell Research,* 1833**,** 3471-3480.

EDWARDS, C., PEARSE, A., MARKS, R., NISHIMORI, Y., MATSUMOTO, K. & KAWAI, M. 2001. Degenerative Alterations of Dermal Collagen Fiber Bundles in Photodamaged Human Skin and UV-Irradiated Hairless Mouse Skin: Possible Effect on Decreasing Skin Mechanical Properties and Appearance of Wrinkles. *Journal of Investigative Dermatology,* 117**,** 1458-1463.

EGEA, J., FABREGAT, I., FRAPART, Y. M., GHEZZI, P., GÖRLACH, A., KIETZMANN, T., KUBAICHUK, K., KNAUS, U. G., LOPEZ, M. G., OLASO-GONZALEZ, G., PETRY, A., SCHULZ, R., VINA, J., WINYARD, P., ABBAS, K., ADEMOWO, O. S., AFONSO, C. B., ANDREADOU, I., ANTELMANN, H., ANTUNES, F., ASLAN, M., BACHSCHMID, M. M., BARBOSA, R. M., BELOUSOV, V., BERNDT, C., BERNLOHR, D., BERTRÁN, E., BINDOLI, A., BOTTARI, S. P., BRITO, P. M., CARRARA, G., CASAS, A. I., CHATZI, A., CHONDROGIANNI, N., CONRAD, M., COOKE, M. S., COSTA, J. G., CUADRADO, A., MY-CHAN DANG, P., DE SMET, B., DEBELEC-BUTUNER, B., DIAS, I. H. K., DUNN, J. D., EDSON, A. J., EL ASSAR, M., EL-BENNA, J., FERDINANDY, P., FERNANDES, A. S., FLADMARK, K. E., FÖRSTERMANN, U., GINIATULLIN, R., GIRICZ, Z., GÖRBE, A., GRIFFITHS, H., HAMPL, V., HANF, A., HERGET, J., HERNANSANZ-AGUSTÍN, P., HILLION, M., HUANG, J., ILIKAY, S., JANSEN-DÜRR, P., JAQUET, V., JOLES, J. A., KALYANARAMAN, B., KAMINSKYY, D., KARBASCHI, M., KLEANTHOUS, M., KLOTZ, L.-O., KORAC, B., KORKMAZ, K. S., KOZIEL, R., KRAČUN, D., KRAUSE, K.-H., KŘEN, V., KRIEG, T., LARANJINHA, J., LAZOU, A., LI, H., MARTÍNEZ-RUIZ, A., MATSUI, R., MCBEAN, G. J., MEREDITH, S. P., MESSENS, J., MIGUEL, V., MIKHED, Y., MILISAV, I., MILKOVIĆ, L., MIRANDA-VIZUETE, A., MOJOVIĆ, M., MONSALVE, M., MOUTHUY, P.-A., MULVEY, J., MÜNZEL, T., MUZYKANTOV, V., NGUYEN, I. T. N., OELZE, M., OLIVEIRA, N. G., PALMEIRA, C. M., PAPAEVGENIOU, N., et al. 2017. European contribution to the study of ROS: A summary of the findings and prospects for the future from the COST action BM1203 (EU-ROS). *Redox biology,* 13**,** 94-162.

EHINGER, J. K., PIEL, S., FORD, R., KARLSSON, M., SJÖVALL, F., FROSTNER, E. Å., MOROTA, S., TAYLOR, R. W., TURNBULL, D. M., CORNELL, C., MOSS, S. J., METZSCH, C., HANSSON, M. J., FLIRI, H. & ELMÉR, E. 2016. Cell-permeable succinate prodrugs bypass mitochondrial complex I deficiency. *Nature communications,* 7**,** 12317-12317.

EHSES, S., RASCHKE, I., MANCUSO, G., BERNACCHIA, A., GEIMER, S., TONDERA, D., MARTINOU, J.-C., WESTERMANN, B., RUGARLI, E. I. & LANGER, T. 2009. Regulation of OPA1 processing and mitochondrial fusion by m-AAA protease isoenzymes and OMA1. *The Journal of cell biology,* 187**,** 1023-1036.

EKBERG, O., HAMDY, S., WOISARD, V., WUTTGE–HANNIG, A. & ORTEGA, P. 2002. Social and Psychological Burden of Dysphagia: Its Impact on Diagnosis and Treatment. *Dysphagia,* 17**,** 139-146.

ELFAKIR, A., EZZEDINE, K., LATREILLE, J., AMBROISINE, L., JDID, R., GALAN, P., HERCBERG, S., GRUBER, F., MALVY, D., TSCHACHLER, E. & GUINOT, C. 2010. Functional MC1R-Gene Variants Are Associated with Increased Risk for Severe Photoaging of Facial Skin. *Journal of Investigative Dermatology,* 130**,** 1107-1115.

EZURE, T. & AMANO, S. 2010. The severity of wrinkling at the forehead is related to the degree of ptosis of the upper eyelid. *Skin Res Technol,* 16**,** 202-9.

FEINGOLD, K. R. 2012. Lamellar Bodies: The Key to Cutaneous Barrier Function. *Journal of Investigative Dermatology,* 132**,** 1951-1953.
FINLAYSON, L., BARNARD, I. R. M., MCMILLAN, L., IBBOTSON, S. H., BROWN, C. T. A., EADIE, E. & WOOD, K. 2021. Depth Penetration of Light into Skin as a Function of Wavelength from 200 to 1000 nm. *Photochemistry and Photobiology,* n/a.
FISHER, G. J., DATTA, S., WANG, Z., LI, X.-Y., QUAN, T., CHUNG, J. H., KANG, S. & VOORHEES, J. J. 2000. c-Jun–dependent inhibition of cutaneous procollagen transcription following ultraviolet irradiation is reversed by all-trans retinoic acid. *The Journal of Clinical Investigation,* 106**,** 663-670.
FONTANA, G. A. & GAHLON, H. L. 2020. Mechanisms of replication and repair in mitochondrial DNA deletion formation. *Nucleic Acids Research,* 48**,** 11244-11258.
FORNI, M. F., PELOGGIA, J., BRAGA, T. T., CHINCHILLA, J. E. O., SHINOHARA, J., NAVAS, C. A., CAMARA, N. O. S. & KOWALTOWSKI, A. J. 2017. Caloric restriction promotes structural and metabolic changes in the skin. *Cell reports,* 20**,** 2678-2692.
FRANZOLIN, E., SALATA, C., BIANCHI, V. & RAMPAZZO, C. 2015. The Deoxynucleoside Triphosphate Triphosphohydrolase Activity of SAMHD1 Protein Contributes to the Mitochondrial DNA Depletion Associated with Genetic Deficiency of Deoxyguanosine Kinase. *J Biol Chem,* 290**,** 25986-96.
FRASER, J. A., BIOUSSE, V. & NEWMAN, N. J. 2010. The neuro-ophthalmology of mitochondrial disease. *Surv Ophthalmol,* 55**,** 299-334.
FUJIMAKI, K., LI, R., CHEN, H., DELLA CROCE, K., ZHANG, H. H., XING, J., BAI, F. & YAO, G. 2019. Graded regulation of cellular quiescence depth between proliferation and senescence by a lysosomal dimmer switch. *Proceedings of the National Academy of Sciences,* 116**,** 22624-22634.
FUJIMURA, T. & HOTTA, M. 2012. The preliminary study of the relationship between facial movements and wrinkle formation. *Skin Res Technol,* 18**,** 219-24.
GALO, R., VITTI, M., MATTOS, M. D. G. C. & REGALO, S. C. H. 2007. Masticatory muscular activation in elderly individuals during chewing. *Gerodontology,* 24**,** 244-248.
GAMBLE, R. G., ASDIGIAN, N. L., AALBORG, J., GONZALEZ, V., BOX, N. F., HUFF, L. S., BARÓN, A. E., MORELLI, J. G., MOKROHISKY, S. T., CRANE, L. A. & DELLAVALLE, R. P. 2012. Sun damage in ultraviolet photographs correlates with phenotypic melanoma risk factors in 12-year-old children. *Journal of the American Academy of Dermatology,* 67**,** 587-597.
GARONE, C., TADESSE, S. & HIRANO, M. 2011. Clinical and genetic spectrum of mitochondrial neurogastrointestinal encephalomyopathy. *Brain,* 134**,** 3326-3332.
GE, Y., SHI, X., BOOPATHY, S., MCDONALD, J., SMITH, A. W. & CHAO, L. H. 2020. Two forms of Opa1 cooperate to complete fusion of the mitochondrial inner-membrane. *eLife,* 9**,** e50973.
GEURTS, J., NASI, S., DISTEL, P., MÜLLER-GERBL, M., PROLLA, T. A., KUJOTH, G. C., WALKER, U. A. & HÜGLE, T. 2020. Prematurely aging mitochondrial DNA mutator mice display subchondral osteopenia and chondrocyte hypertrophy without further osteoarthritis features. *Scientific Reports,* 10**,** 1296.
GIACCO, F., BROWNLEE, M. & SCHMIDT, A. M. 2010. Oxidative Stress and Diabetic Complications. *Circulation Research,* 107**,** 1058-1070.
GNANAPRADEEPAN, K., BASU, S., BARNOUD, T., BUDINA-KOLOMETS, A., KUNG, C.-P. & MURPHY, M. E. 2018. The p53 Tumor Suppressor in the Control of Metabolism and Ferroptosis. *Frontiers in Endocrinology,* 9.

GOMES, L. C., BENEDETTO, G. D. & SCORRANO, L. 2011. During autophagy mitochondria elongate, are spared from degradation and sustain cell viability. *Nature Cell Biology,* 13**,** 589-598.

GONZÁLEZ-CASACUBERTA, I., JUÁREZ-FLORES, D.-L., EZQUERRA, M., FUCHO, R., CATALÁN-GARCÍA, M., GUITART-MAMPEL, M., TOBÍAS, E., GARCÍA-RUIZ, C., FERNÁNDEZ-CHECA, J. C., TOLOSA, E., MARTÍ, M.-J., GRAU, J. M., FERNÁNDEZ-SANTIAGO, R., CARDELLACH, F., MORÉN, C. & GARRABOU, G. 2019. Mitochondrial and autophagic alterations in skin fibroblasts from Parkinson disease patients with Parkin mutations. *Aging,* 11**,** 3750-3767.

GONZALO, S., KREIENKAMP, R. & ASKJAER, P. 2017. Hutchinson-Gilford Progeria Syndrome: A premature aging disease caused by LMNA gene mutations. *Ageing Res Rev,* 33**,** 18-29.

GORDON, J. R. S. & BRIEVA, J. C. 2012. Unilateral Dermatoheliosis. *New England Journal of Medicine,* 366**,** e25.

GORMAN, G. S., SCHAEFER, A. M., NG, Y., GOMEZ, N., BLAKELY, E. L., ALSTON, C. L., FEENEY, C., HORVATH, R., YU-WAI-MAN, P., CHINNERY, P. F., TAYLOR, R. W., TURNBULL, D. M. & MCFARLAND, R. 2015. Prevalence of nuclear and mitochondrial DNA mutations related to adult mitochondrial disease. *Annals of Neurology,* 77**,** 753-759.

GRADY, J. P., PICKETT, S. J., NG, Y. S., ALSTON, C. L., BLAKELY, E. L., HARDY, S. A., FEENEY, C. L., BRIGHT, A. A., SCHAEFER, A. M., GORMAN, G. S., MCNALLY, R. J., TAYLOR, R. W., TURNBULL, D. M. & MCFARLAND, R. 2018. mtDNA heteroplasmy level and copy number indicate disease burden in m.3243A>G mitochondrial disease. *EMBO molecular medicine,* 10**,** e8262.

GRIPARIC, L., KANAZAWA, T. & VAN DER BLIEK, A. M. 2007. Regulation of the mitochondrial dynamin-like protein Opa1 by proteolytic cleavage. *Journal of Cell Biology,* 178**,** 757-764.

GRUBER, J., SCHAFFER, S. & HALLIWELL, B. 2008. The mitochondrial free radical theory of ageing—where do we stand. *Front Biosci,* 13**,** 6554-6579.

GRÜNEWALD, A., RYGIEL, K. A., HEPPLEWHITE, P. D., MORRIS, C. M., PICARD, M. & TURNBULL, D. M. 2016. Mitochondrial DNA Depletion in Respiratory Chain–Deficient Parkinson Disease Neurons. *Annals of Neurology,* 79**,** 366-378.

GUILLERY, O., MALKA, F., FRACHON, P., MILEA, D., ROJO, M. & LOMBÈS, A. 2008. Modulation of mitochondrial morphology by bioenergetics defects in primary human fibroblasts. *Neuromuscular Disorders,* 18**,** 319-330.

GUNN, D. A., MURRAY, P. G., TOMLIN, C. C., REXBYE, H., CHRISTENSEN, K. & MAYES, A. E. 2008. Perceived age as a biomarker of ageing: a clinical methodology. *Biogerontology,* 9**,** 357.

GUREEV, A. P., SHAFOROSTOVA, E. A., STARKOV, A. A. & POPOV, V. N. 2017. Simplified qPCR method for detecting excessive mtDNA damage induced by exogenous factors. *Toxicology,* 382**,** 67-74.

HALLIWELL, B. & GUTTERIDGE, J. M. 1984. Oxygen toxicity, oxygen radicals, transition metals and disease. *The Biochemical journal,* 219**,** 1-14.

HAMANAKA, R. B. & CHANDEL, N. S. 2009. Mitochondrial reactive oxygen species regulate hypoxic signaling. *Current opinion in cell biology,* 21**,** 894-899.

HAMILTON MICHELLE, L., VAN REMMEN, H., DRAKE JESSICA, A., YANG, H., GUO ZHONG, M., KEWITT, K., WALTER CHRISTI, A. & RICHARDSON, A. 2001. Does oxidative damage to DNA increase with age? *Proceedings of the National Academy of Sciences,* 98**,** 10469-10474.

HAMILTON, R. T., WALSH, M. E. & VAN REMMEN, H. 2012. Mouse Models of Oxidative Stress Indicate a Role for Modulating Healthy Aging. *Journal of clinical & experimental pathology,* Suppl 4**,** 005.

HANNA, R., CROWTHER, J. M., BULSARA, P. A., WANG, X., MOORE, D. J. & BIRCH-MACHIN, M. A. 2019. Optimised detection of mitochondrial DNA strand breaks. *Mitochondrion,* 46**,** 172-178.

HARBOTTLE, A. & BIRCH-MACHIN, M. A. 2006. Real-time PCR analysis of a 3895 bp mitochondrial DNA deletion in nonmelanoma skin cancer and its use as a quantitative marker for sunlight exposure in human skin. *British journal of cancer,* 94**,** 1887-1893.

HARMAN, D. 1956. Aging: A Theory Based on Free Radical and Radiation Chemistry. *Journal of Gerontology,* 11**,** 298-300.

HAYASHI, G. & CORTOPASSI, G. 2015. Oxidative stress in inherited mitochondrial diseases. *Free radical biology & medicine,* 88**,** 10-17.

HOLT, A. G. & DAVIES, A. M. 2020. The significance of mitochondrial DNA half-life to the lifespan of post-mitotic cells. *bioRxiv***,** 2020.02.15.950410.

HSIEH, A. Y. Y., BUDD, M., DENG, D., GADAWSKA, I. & CÔTÉ, H. C. F. 2018. A Monochrome Multiplex Real-Time Quantitative PCR Assay for the Measurement of Mitochondrial DNA Content. *The Journal of Molecular Diagnostics,* 20**,** 612-620.

HUANG, K. T., CHEN, Y. H. & WALKER, A. M. 2004. Inaccuracies in MTS assays: major distorting effects of medium, serum albumin, and fatty acids. *BioTechniques,* 37**,** 406-412.

HUDSON, L., RASHDAN, E., BONN, C. A., CHAVAN, B., RAWLINGS, D. & BIRCH-MACHIN, M. A. 2020. Individual and combined effects of the infrared, visible, and ultraviolet light components of solar radiation on damage biomarkers in human skin cells. *The FASEB Journal,* 34**,** 3874-3883.

HÜHNE, J., PFEIFFER, H., WATERKAMP, K. & BRINKMANN, K. 1999. Mitochondrial DNA in human hair shafts--existence of intra-individual differences? *Int J Legal Med,* 112**,** 172-5.

HÜLS, A., VIERKÖTTER, A., GAO, W., KRÄMER, U., YANG, Y., DING, A., STOLZ, S., MATSUI, M., KAN, H. & WANG, S. 2016. Traffic-related air pollution contributes to development of facial lentigines: further epidemiological evidence from Caucasians and Asians. *The Journal of investigative dermatology,* 136**,** 1053-1056.

HUSSAIN, M., KRISHNAMURTHY, S., PATEL, J., KIM, E., BAPTISTE, B. A., CROTEAU, D. L. & BOHR, V. A. 2021. Skin Abnormalities in Disorders with DNA Repair Defects, Premature Aging, and Mitochondrial Dysfunction. *Journal of Investigative Dermatology,* 141**,** 968-975.

HUTCHIN, T. P., HEATH, P. R., PEARSON, R. C. & SINCLAIR, A. J. 1997. Mitochondrial DNA mutations in Alzheimer's disease. *Biochem Biophys Res Commun,* 241**,** 221-5.

ICNIRP 2007. Protecting Workers from Ultraviolet Radiation. *In:* VECCHIA, P., HIETANEN, M., STUCK, B. E., VAN DEVENTER, E. & NIU, S. (eds.). Oberschleißheim, Germany: International Commission on Non-Ionising Radiation Protection.

INDO, H. P., DAVIDSON, M., YEN, H.-C., SUENAGA, S., TOMITA, K., NISHII, T., HIGUCHI, M., KOGA, Y., OZAWA, T. & MAJIMA, H. J. 2007. Evidence of ROS generation by mitochondria in cells with impaired electron transport chain and mitochondrial DNA damage. *Mitochondrion,* 7**,** 106-118.

IPPONJIMA, S., UMINO, Y., NAGAYAMA, M. & DENDA, M. 2020. Live imaging of alterations in cellular morphology and organelles during cornification using an epidermal equivalent model. *Scientific Reports,* 10**,** 5515.

JACKSON, M. 2018. *Investigation of cellular bioenergetics and oxidative stress in ageing & the modulation of these processes with antioxidants.* PhD, Newcastle University.

JANG, Y. C., PÉREZ, V. I., SONG, W., LUSTGARTEN, M. S., SALMON, A. B., MELE, J., QI, W., LIU, Y., LIANG, H., CHAUDHURI, A., IKENO, Y., EPSTEIN, C. J., VAN REMMEN, H. & RICHARDSON, A. 2009. Overexpression of Mn superoxide dismutase does not increase life span in mice. *The journals of gerontology. Series A, Biological sciences and medical sciences,* 64**,** 1114-1125.

JEPPESEN, T. D., DUNO, M. & VISSING, J. 2020. Mutation Load of Single, Large-Scale Deletions of mtDNA in Mitotic and Postmitotic Tissues. *Frontiers in Genetics,* 11.

JIANG, R., CUDJOE, E., BOJKO, B., ABAFFY, T. & PAWLISZYN, J. 2013. A non-invasive method for in vivo skin volatile compounds sampling. *Analytica Chimica Acta,* 804**,** 111-119.

JONCKHEERE, A. I., SMEITINK, J. A. M. & RODENBURG, R. J. T. 2012. Mitochondrial ATP synthase: architecture, function and pathology. *Journal of inherited metabolic disease,* 35**,** 211-225.

JOZWIAKOWSKI, S. K., KEITH, B. J., GILROY, L., DOHERTY, A. J. & CONNOLLY, B. A. 2014. An archaeal family-B DNA polymerase variant able to replicate past DNA damage: occurrence of replicative and translesion synthesis polymerases within the B family. *Nucleic acids research,* 42**,** 9949-9963.

JUGÉ, R., BREUGNOT, J., DA SILVA, C., BORDES, S., CLOSS, B. & AOUACHERIA, A. 2016. Quantification and Characterization of UVB-Induced Mitochondrial Fragmentation in Normal Primary Human Keratinocytes. *Scientific Reports,* 6**,** 35065.

KALYANARAMAN, B., DARLEY-USMAR, V., DAVIES, K. J. A., DENNERY, P. A., FORMAN, H. J., GRISHAM, M. B., MANN, G. E., MOORE, K., ROBERTS, L. J. & ISCHIROPOULOS, H. 2012. Measuring reactive oxygen and nitrogen species with fluorescent probes: challenges and limitations. *Free Radical Biology and Medicine,* 52**,** 1-6.

KAMBAYASHI, H., YAMASHITA, M., ODAKE, Y., TAKADA, K., FUNASAKA, Y. & ICHIHASHI, M. 2001. Epidermal changes caused by chronic low-dose UV irradiation induce wrinkle formation in hairless mouse. *J Dermatol Sci,* 27 Suppl 1**,** S19-25.

KANG, S., CHUNG, J. H., LEE, J. H., FISHER, G. J., WAN, Y. S., DUELL, E. A. & VOORHEES, J. J. 2003. Topical N-acetyl cysteine and genistein prevent ultraviolet-light-induced signaling that leads to photoaging in human skin in vivo. *Journal of Investigative Dermatology,* 120**,** 835-841.

KARVONEN, S. L., HAAPASAARI, K. M., KALLIOINEN, M., OIKARINEN, A., HASSINEN, I. E. & MAJAMAA, K. 1999. Increased prevalence of vitiligo, but no evidence of premature ageing, in the skin of patients with bp 3243 mutation in mitochondrial DNA in the mitochondrial encephalomyopathy, lactic acidosis and stroke-like episodes syndrome (MELAS). *Br J Dermatol,* 140**,** 634-9.

KATAYAMA, Y., MAEDA, K., IIZUKA, T., HAYASHI, M., HASHIZUME, Y., SANADA, M., KAWAI, H. & KASHIWAGI, A. 2009. Accumulation of oxidative stress around the stroke-like lesions of MELAS patients. *Mitochondrion,* 9**,** 306-313.

KAUR, M., GARG, R. K. & SINGLA, S. 2015. Analysis of facial soft tissue changes with aging and their effects on facial morphology: A forensic perspective. *Egyptian Journal of Forensic Sciences,* 5**,** 46-56.

KEEFE, D. L., NIVEN-FAIRCHILD, T., POWELL, S. & BURADAGUNTA, S. 1995. Mitochondrial deoxyribonucleic acid deletions in oocytes and reproductive aging in women**Supported by National Institutes of Health K08 HD01099–01, Bethesda, Maryland and by The American Fertility Society-Ortho Research Award from The American Fertility Society, Birmingham, Alabama (D.K.).††Presented at the 41st Annual Meeting of the Society for Gynecologic Investigation, Chicago, Illinois, March 22 to 26, 1994. *Fertility and Sterility,* 64**,** 577-583.

KEITHLEY, E. M., CANTO, C., ZHENG, Q. Y., WANG, X., FISCHEL-GHODSIAN, N. & JOHNSON, K. R. 2005. Cu/Zn superoxide dismutase and age-related hearing loss. *Hearing research,* 209**,** 76-85.

KIM, H.-E. & LEE, S.-G. 2013. Induction of ATP synthase β by H2O2 induces melanogenesis by activating PAH and cAMP/CREB/MITF signaling in melanoma cells. *The International Journal of Biochemistry & Cell Biology,* 45**,** 1217-1222.

KIM, T.-K., LIN, Z., TIDWELL, W. J., LI, W. & SLOMINSKI, A. T. 2015. Melatonin and its metabolites accumulate in the human epidermis in vivo and inhibit proliferation and tyrosinase activity in epidermal melanocytes in vitro. *Molecular and cellular endocrinology,* 404**,** 1-8.

KLOTZ, L. O., SANCHEZ-RAMOS, C., PRIETO-ARROYO, I., URBANEK, P., STEINBRENNER, H. & MONSALVE, M. 2015. Redox regulation of FoxO transcription factors. *Redox Biol,* 6**,** 51-72.

KOCH, H., WITTERN, K. P. & BERGEMANN, J. 2001. In human keratinocytes the Common Deletion reflects donor variabilities rather than chronologic aging and can be induced by ultraviolet A irradiation. *J Invest Dermatol,* 117**,** 892-7.

KOKOSZKA JASON, E., COSKUN, P., ESPOSITO LUKE, A. & WALLACE DOUGLAS, C. 2001. Increased mitochondrial oxidative stress in the Sod2 (+/−) mouse results in the age-related decline of mitochondrial function culminating in increased apoptosis. *Proceedings of the National Academy of Sciences,* 98**,** 2278-2283.

KOKOTAS, H., PETERSEN, M. B. & WILLEMS, P. J. 2007. Mitochondrial deafness. *Clin Genet,* 71**,** 379-91.

KOLARSICK, P. A. J., KOLARSICK, M. A. & GOODWIN, C. 2011. Anatomy and Physiology of the Skin. *Journal of the Dermatology Nurses' Association,* 3**,** 203-213.

KOLESAR, J. E., SAFDAR, A., ABADI, A., MACNEIL, L. G., CRANE, J. D., TARNOPOLSKY, M. A. & KAUFMAN, B. A. 2014. Defects in mitochondrial DNA replication and oxidative damage in muscle of mtDNA mutator mice. *Free Radic Biol Med,* 75**,** 241-51.

KOLLIAS, N., GILLIES, R., COHÉN-GOIHMAN, C., PHILLIPS, S. B., MUCCINI, J. A., STILLER, M. J. & DRAKE, L. A. 1997. Fluorescence photography in the evaluation of hyperpigmentation in photodamaged skin. *Journal of the American Academy of Dermatology,* 36**,** 226-230.

KORR, H., KURZ, C., SEIDLER, T. O., SOMMER, D. & SCHMITZ, C. 1998. Mitochondrial DNA synthesis studied autoradiographically in various cell types in vivo. *Braz J Med Biol Res,* 31**,** 289-98.

KOWALD, A. 2001. The mitochondrial theory of aging. *Biol Signals Recept,* 10**,** 162-75.

KRISHNAN, K. J., HARBOTTLE, A. & BIRCH-MACHIN, M. A. 2004. The use of a 3895 bp mitochondrial DNA deletion as a marker for sunlight exposure in human skin. *Journal of investigative dermatology,* 123**,** 1020-1024.

KRISHNAN, K. J., REEVE, A. K., SAMUELS, D. C., CHINNERY, P. F., BLACKWOOD, J. K., TAYLOR, R. W., WANROOIJ, S., SPELBRINK, J. N., LIGHTOWLERS, R. N. & TURNBULL, D. M. 2008. What causes mitochondrial DNA deletions in human cells? *Nature Genetics,* 40**,** 275-279.

KROKAN, H. E. & BJØRÅS, M. 2013. Base excision repair. *Cold Spring Harb Perspect Biol,* 5**,** a012583.

KUCHARSKI, M., MROWIEC, P. & OCŁOŃ, E. 2021. Current standards and pitfalls associated with the transfection of primary fibroblast cells. *Biotechnology Progress,* 37**,** e3152.

KURLAND, C. G. & ANDERSSON, S. G. 2000. Origin and evolution of the mitochondrial proteome. *Microbiology and molecular biology reviews : MMBR,* 64**,** 786-820.

LANE, N. & MARTIN, W. 2010. The energetics of genome complexity. *Nature,* 467**,** 929-934.

LATIMER, J. 2013. *Determining the action spectrum of UVR-induced mitochondrial DNA damage, and related UVR-induced cellular effects in human skin.* PhD, Newcastle University.

LAVKER, R. M., GERBERICK, G. F., VERES, D., IRWIN, C. J. & KAIDBEY, K. H. 1995. Cumulative effects from repeated exposures to suberythemal doses of UVB and UVA in human skin. *Journal of the American Academy of Dermatology,* 32**,** 53-62.

LEMONS, J. M. S., FENG, X.-J., BENNETT, B. D., LEGESSE-MILLER, A., JOHNSON, E. L., RAITMAN, I., POLLINA, E. A., RABITZ, H. A., RABINOWITZ, J. D. & COLLER, H. A. 2010. Quiescent Fibroblasts Exhibit High Metabolic Activity. *PLOS Biology,* 8**,** e1000514.

LI, B., KAUSHIK, S., KALINOWSKI, P., KIM, B., GERSHOME, C., CHING, J. & POBURKO, D. 2018. Droplet digital PCR shows the D-Loop to be an error prone locus for mitochondrial DNA copy number determination. *Scientific Reports,* 8**,** 11392.

LI, L., YAN, Y., XU, H., QU, T. & WANG, B. 2011. Selection of reference genes for gene expression studies in ultraviolet B-irradiated human skin fibroblasts using quantitative real-time PCR. *BMC Molecular Biology,* 12**,** 8.

LI, M., SCHRÖDER, R., NI, S., MADEA, B. & STONEKING, M. 2015. Extensive tissue-related and allele-related mtDNA heteroplasmy suggests positive selection for somatic mutations. *Proceedings of the National Academy of Sciences,* 112**,** 2491-2496.

LIANG, L.-P. & PATEL, M. 2004. Mitochondrial oxidative stress and increased seizure susceptibility in Sod2−/+ mice. *Free Radical Biology and Medicine,* 36**,** 542-554.

LIU, F., HAMER, M. A., DEELEN, J., LALL, J. S., JACOBS, L., VAN HEEMST, D., MURRAY, P. G., WOLLSTEIN, A., DE CRAEN, A. J. & UH, H.-W. 2016. The MC1R gene and youthful looks. *Current Biology,* 26**,** 1213-1220.

LIU, S. W., LIEN, M. H. & FENSKE, N. A. 2010. The effects of alcohol and drug abuse on the skin. *Clinics in Dermatology,* 28**,** 391-399.

LUCAS, R., MCMICHAEL, T., SMITH, W. & ARMSTRONG, B. 2006. Solar Ultraviolet Radiation: Global burden of disease from solar ultraviolet radiation *In:* ORGANISATION, W. H. (ed.). Geneva.

MALENA, A., PANTIC, B., BORGIA, D., SGARBI, G., SOLAINI, G., HOLT, I. J., SPINAZZOLA, A., PERISSINOTTO, E., SANDRI, M., BARACCA, A. & VERGANI, L. 2016. Mitochondrial quality control: Cell-type-dependent responses to pathological mutant mitochondrial DNA. *Autophagy,* 12**,** 2098-2112.

MANCUSO, M., ORSUCCI, D., ANGELINI, C., BERTINI, E., CARELLI, V., COMI, G. P., DONATI, A., MINETTI, C., MOGGIO, M., MONGINI, T., SERVIDEI, S., TONIN, P., TOSCANO, A., UZIEL, G., BRUNO, C., IENCO, E. C., FILOSTO, M., LAMPERTI, C., CATTERUCCIA, M., MORONI, I., MUSUMECI, O., PEGORARO, E., RONCHI, D., SANTORELLI, F. M., SAUCHELLI, D., SCARPELLI, M., SCIACCO, M., VALENTINO, M. L., VERCELLI, L., ZEVIANI, M. & SICILIANO, G. 2014. The m.3243A>G mitochondrial DNA mutation and related phenotypes. A matter of gender? *Journal of Neurology,* 261**,** 504-510.

MANCUSO, M., ORSUCCI, D., ANGELINI, C., BERTINI, E., CARELLI, V., COMI, G. P., DONATI, M. A., FEDERICO, A., MINETTI, C., MOGGIO, M., MONGINI, T., SANTORELLI, F. M., SERVIDEI, S., TONIN, P., TOSCANO, A., BRUNO, C., BELLO, L., CALDARAZZO IENCO, E., CARDAIOLI, E., CATTERUCCIA, M., DA POZZO, P., FILOSTO, M., LAMPERTI, C., MORONI, I., MUSUMECI, O., PEGORARO, E., RONCHI, D., SAUCHELLI, D., SCARPELLI, M., SCIACCO, M., VALENTINO, M. L., VERCELLI, L., ZEVIANI, M. & SICILIANO, G. 2015.

Redefining phenotypes associated with mitochondrial DNA single deletion. *Journal of Neurology,* 262**,** 1301-1309.
MANCUSO, M., ORSUCCI, D., ANGELINI, C., BERTINI, E., CARELLI, V., COMI, G. P., MINETTI, C., MOGGIO, M., MONGINI, T., SERVIDEI, S., TONINC, P., TOSCANO, A., UZIEL, G., BRUNO, C., IENCO, E. C., FILOSTO, M., LAMPERTI, C., MARTINELLI, D., MORONI, I., MUSUMECI, O., PEGORARO, E., RONCHI, D., SANTORELLI, F. M., SAUCHELLI, D., SCARPELLI, M., SCIACCO, M., SPINAZZI, M., VALENTINO, M. L., VERCELLI, L., ZEVIANI, M. & SICILIANO, G. 2013. Phenotypic heterogeneity of the 8344A>G mtDNA "MERRF" mutation. *Neurology,* 80**,** 2049-2054.
MANICONE, A. M. & MCGUIRE, J. K. Matrix metalloproteinases as modulators of inflammation. Seminars in cell & developmental biology, 2008. Elsevier, 34-41.
MARESCA, V., FLORI, E., BRIGANTI, S., CAMERA, E., CARIO-ANDRÉ, M., TAÏEB, A. & PICARDO, M. 2006. UVA-Induced Modification of Catalase Charge Properties in the Epidermis Is Correlated with the Skin Phototype. *Journal of Investigative Dermatology,* 126**,** 182-190.
MARKS, R. 2004. The Stratum Corneum Barrier: The Final Frontier. *The Journal of Nutrition,* 134**,** 2017S-2021S.
MARLOW, F. L. 2017. Mitochondrial matters: Mitochondrial bottlenecks, self-assembling structures, and entrapment in the female germline. *Stem Cell Research,* 21**,** 178-186.
MARTÍNEZ-REDONDO, D., MARCUELLO, A., CASAJÚS, J. A., ARA, I., DAHMANI, Y., MONTOYA, J., RUIZ-PESINI, E., LÓPEZ-PÉREZ, M. J. & DÍEZ-SÁNCHEZ, C. 2010. Human mitochondrial haplogroup H: The highest VO2max consumer – Is it a paradox? *Mitochondrion,* 10**,** 102-107.
MATSUZAKI, Y., UMEMOTO, T., TANAKA, Y., OKANO, T. & YAMATO, M. 2015. β2-Microglobulin is an appropriate reference gene for RT-PCR-based gene expression analysis of hematopoietic stem cells. *Regen Ther,* 1**,** 91-97.
MCELHINNEY, D. B., HOFFMAN, S. J., ROBINSON, W. A. & FERGUSON, J. 1994. Effect of melatonin on human skin color. *Journal of investigative dermatology,* 102**,** 258-259.
MCFARLAND, R., SCHAEFER, A. M., GARDNER, J. L., LYNN, S., HAYES, C. M., BARRON, M. J., WALKER, M., CHINNERY, P. F., TAYLOR, R. W. & TURNBULL, D. M. 2004. Familial myopathy: new insights into the T14709C mitochondrial tRNA mutation. *Ann Neurol,* 55**,** 478-84.
MCGETTRICK, A. F. & O'NEILL, L. A. J. 2020. The Role of HIF in Immunity and Inflammation. *Cell Metab,* 32**,** 524-536.
MCKAY, N. D., ROBINSON, B., BRODIE, R. & ROOKE-ALLEN, N. 1983. Glucose transport and metabolism in cultured human skin fibroblasts. *Biochimica et Biophysica Acta (BBA) - Molecular Cell Research,* 762**,** 198-204.
MCVEY, M. & LEE, S. E. 2008. MMEJ repair of double-strand breaks (director's cut): deleted sequences and alternative endings. *Trends in genetics : TIG,* 24**,** 529-538.
MEAGHER, M. & LIGHTOWLERS, R. N. 2014. The role of TDP1 and APTX in mitochondrial DNA repair. *Biochimie,* 100**,** 121-124.
MEYERSON, C., VAN STAVERN, G. & MCCLELLAND, C. 2015. Leber hereditary optic neuropathy: current perspectives. *Clinical Ophthalmology (Auckland, N.Z.),* 9**,** 1165-1176.
MICKEY, R. M. & GREENLAND, S. 1989. THE IMPACT OF CONFOUNDER SELECTION CRITERIA ON EFFECT ESTIMATION. *American Journal of Epidemiology,* 129**,** 125-137.
MIGNON, C., UZUNBAJAKAVA, N. E., RAAFS, B., BOTCHKAREVA, N. V. & TOBIN, D. J. 2017. Photobiomodulation of human dermal fibroblasts in vitro: decisive role of

cell culture conditions and treatment protocols on experimental outcome. *Scientific reports,* 7**,** 2797-2797.
MITRA, M., HO, L. D. & COLLER, H. A. 2018. An In Vitro Model of Cellular Quiescence in Primary Human Dermal Fibroblasts. *Methods in molecular biology (Clifton, N.J.),* 1686**,** 27-47.
MIYAMOTO, S., NANTES, I. L., FARIA, P. A., CUNHA, D., RONSEIN, G. E., MEDEIROS, M. H. G. & DI MASCIO, P. 2012. Cytochrome c-promoted cardiolipin oxidation generates singlet molecular oxygen. *Photochemical & Photobiological Sciences,* 11**,** 1536-1546.
MIYAMURA, Y., COELHO, S. G., WOLBER, R., MILLER, S. A., WAKAMATSU, K., ZMUDZKA, B. Z., ITO, S., SMUDA, C., PASSERON, T., CHOI, W., BATZER, J., YAMAGUCHI, Y., BEER, J. Z. & HEARING, V. J. 2007. Regulation of human skin pigmentation and responses to ultraviolet radiation. *Pigment Cell Research,* 20**,** 2-13.
MONTELEON, C. L., AGNIHOTRI, T., DAHAL, A., LIU, M., REBECCA, V. W., BEATTY, G. L., AMARAVADI, R. K. & RIDKY, T. W. 2018. Lysosomes Support the Degradation, Signaling, and Mitochondrial Metabolism Necessary for Human Epidermal Differentiation. *Journal of Investigative Dermatology,* 138**,** 1945-1954.
MORETTI, G., ELLIS, R. A. & MESCON, H. 1959. Vascular patterns in the skin of the face. *J Invest Dermatol,* 33**,** 103-12.
MOVAFAGH, S., CROOK, S. & VO, K. 2015. Regulation of hypoxia-inducible factor-1a by reactive oxygen species: new developments in an old debate. *J Cell Biochem,* 116**,** 696-703.
MÜLLER-HÖCKER, J., SCHNEIDERBANGER, K., STEFANI, F. H. & KADENBACH, B. 1992. Progressive loss of cytochrome c oxidase in the human extraocular muscles in ageing — a cytochemical-immunohistochemical study. *Mutation Research/DNAging,* 275**,** 115-124.
MULLER, F. L., SONG, W., LIU, Y., CHAUDHURI, A., PIEKE-DAHL, S., STRONG, R., HUANG, T.-T., EPSTEIN, C. J., ROBERTS II, L. J. & CSETE, M. 2006. Absence of CuZn superoxide dismutase leads to elevated oxidative stress and acceleration of age-dependent skeletal muscle atrophy. *Free Radical Biology and Medicine,* 40**,** 1993-2004.
NAIDOO, K. & BIRCH-MACHIN, M. A. 2017. Oxidative stress and ageing: the influence of environmental pollution, sunlight and diet on skin. *Cosmetics,* 4**,** 4.
NAING, A., KENCHAIAH, M., KRISHNAN, B., MIR, F., CHARNLEY, A., EGAN, C. & BANO, G. 2014. Maternally inherited diabetes and deafness (MIDD): Diagnosis and management. *Journal of Diabetes and its Complications,* 28**,** 542-546.
NAUE, J., HÖRER, S., SÄNGER, T., STROBL, C., HATZER-GRUBWIESER, P., PARSON, W. & LUTZ-BONENGEL, S. 2015. Evidence for frequent and tissue-specific sequence heteroplasmy in human mitochondrial DNA. *Mitochondrion,* 20**,** 82-94.
NGUYEN, H. H., PARK, J., PARK, S. J., LEE, C.-S., HWANG, S., SHIN, Y.-B., HA, T. H. & KIM, M. 2018. Long-Term Stability and Integrity of Plasmid-Based DNA Data Storage. *Polymers,* 10**,** 28.
NISHIMURA, T., KATSUMURA, T., MOTOI, M., OOTA, H. & WATANUKI, S. 2017. Experimental evidence reveals the UCP1 genotype changes the oxygen consumption attributed to non-shivering thermogenesis in humans. *Scientific Reports,* 7**,** 5570.
NIYAZOV, D. M., KAHLER, S. G. & FRYE, R. E. 2016. Primary Mitochondrial Disease and Secondary Mitochondrial Dysfunction: Importance of Distinction for Diagnosis and Treatment. *Molecular syndromology,* 7**,** 122-137.
NOORDAM, R., GUNN, D. A., TOMLIN, C. C., MAIER, A. B., MOOIJAART, S. P., SLAGBOOM, P. E., WESTENDORP, R. G. J., DE CRAEN, A. J. M., VAN HEEMST,

D. & LEIDEN LONGEVITY STUDY, G. 2013. High serum glucose levels are associated with a higher perceived age. *Age (Dordrecht, Netherlands),* 35**,** 189-195.
NORDLUND, J. J. & LERNER, A. B. 1977. The effects of oral melatonin on skin color and on the release of pituitary hormones. *J Clin Endocrinol Metab,* 45**,** 768-74.
O'HARA, R., TEDONE, E., LUDLOW, A., HUANG, E., AROSIO, B., MARI, D. & SHAY, J. W. 2019. Quantitative mitochondrial DNA copy number determination using droplet digital PCR with single-cell resolution. *Genome research,* 29**,** 1878-1888.
ORSUCCI, D., ANGELINI, C., BERTINI, E., CARELLI, V., COMI, G. P., FEDERICO, A., MINETTI, C., MOGGIO, M., MONGINI, T., SANTORELLI, F. M., SERVIDEI, S., TONIN, P., ARDISSONE, A., BELLO, L., BRUNO, C., IENCO, E. C., DIODATO, D., FILOSTO, M., LAMPERTI, C., MORONI, I., MUSUMECI, O., PEGORARO, E., PRIMIANO, G., RONCHI, D., RUBEGNI, A., SALVATORE, S., SCIACCO, M., VALENTINO, M. L., VERCELLI, L., TOSCANO, A., ZEVIANI, M., SICILIANO, G. & MANCUSO, M. 2017. Revisiting mitochondrial ocular myopathies: a study from the Italian Network. *Journal of Neurology,* 264**,** 1777-1784.
OSTO, M., HAMZAVI, I. H., LIM, H. W. & KOHLI, I. 2022. Individual Typology Angle and Fitzpatrick Skin Phototypes are Not Equivalent in Photodermatology. *Photochemistry and Photobiology,* 98**,** 127-129.
PANDEL, R., POLJŠAK, B., GODIC, A. & DAHMANE, R. 2013. Skin photoaging and the role of antioxidants in its prevention. *ISRN dermatology,* 2013**,** 930164-930164.
PANG, C.-Y., LEE, H.-C. & WEI, Y.-H. 2001. Enhanced oxidative damage in human cells harboring A3243G mutation of mitochondrial DNA: implication of oxidative stress in the pathogenesis of mitochondrial diabetes. *Diabetes Research and Clinical Practice,* 54**,** S45-S56.
PEARSE, A. D., GASKELL, S. A. & MARKS, R. 1987. Epidermal Changes in Human Skin Following Irradiation With Either UVB or UVA. *Journal of Investigative Dermatology,* 88**,** 83-87.
PEK, N. M. Q., PHUA, Q. H., HO, B. X., PANG, J. K. S., HOR, J.-H., AN, O., YANG, H. H., YU, Y., FAN, Y., NG, S.-Y. & SOH, B.-S. 2019. Mitochondrial 3243A > G mutation confers pro-atherogenic and pro-inflammatory properties in MELAS iPS derived endothelial cells. *Cell Death & Disease,* 10**,** 802.
PENG, T.-I., YU, P.-R., CHEN, J.-Y., WANG, H.-L., WU, H.-Y., WEI, Y.-H. & JOU, M.-J. 2006. Visualizing common deletion of mitochondrial DNA-augmented mitochondrial reactive oxygen species generation and apoptosis upon oxidative stress. *Biochimica et Biophysica Acta (BBA) - Molecular Basis of Disease,* 1762**,** 241-255.
PEREIRA, S. P., DEUS, C. M., SERAFIM, T. L., CUNHA-OLIVEIRA, T. & OLIVEIRA, P. J. 2018. Metabolic and Phenotypic Characterization of Human Skin Fibroblasts After Forcing Oxidative Capacity. *Toxicological Sciences,* 164**,** 191-204.
PÉREZ, V. I., VAN REMMEN, H., BOKOV, A., EPSTEIN, C. J., VIJG, J. & RICHARDSON, A. 2009. The overexpression of major antioxidant enzymes does not extend the lifespan of mice. *Aging Cell,* 8**,** 73-75.
PFAFFL, M. W. 2001. A new mathematical model for relative quantification in real-time RT-PCR. *Nucleic acids research,* 29**,** e45-e45.
PIAO, M. J., AHN, M. J., KANG, K. A., RYU, Y. S., HYUN, Y. J., SHILNIKOVA, K., ZHEN, A. X., JEONG, J. W., CHOI, Y. H., KANG, H. K., KOH, Y. S. & HYUN, J. W. 2018. Particulate matter 2.5 damages skin cells by inducing oxidative stress, subcellular organelle dysfunction, and apoptosis. *Archives of toxicology,* 92**,** 2077-2091.
PICKETT, S. J., GRADY, J. P., NG, Y. S., GORMAN, G. S., SCHAEFER, A. M., WILSON, I. J., CORDELL, H. J., TURNBULL, D. M., TAYLOR, R. W. & MCFARLAND, R.

2018. Phenotypic heterogeneity in m.3243A>G mitochondrial disease: The role of nuclear factors. *Ann Clin Transl Neurol,* 5**,** 333-345.

PITCEATHLY, R. D. S., MORROW, J. M., SINCLAIR, C. D. J., WOODWARD, C., SWEENEY, M. G., RAHMAN, S., PLANT, G. T., ALI, N., BREMNER, F., DAVAGNANAM, I., YOUSRY, T. A., HANNA, M. G. & THORNTON, J. S. 2016. Extra-ocular muscle MRI in genetically-defined mitochondrial disease. *European Radiology,* 26**,** 130-137.

PITCEATHLY, R. D. S., SMITH, C., FRATTER, C., ALSTON, C. L., HE, L., CRAIG, K., BLAKELY, E. L., EVANS, J. C., TAYLOR, J., SHABBIR, Z., DESCHAUER, M., POHL, U., ROBERTS, M. E., JACKSON, M. C., HALFPENNY, C. A., TURNPENNY, P. D., LUNT, P. W., HANNA, M. G., SCHAEFER, A. M., MCFARLAND, R., HORVATH, R., CHINNERY, P. F., TURNBULL, D. M., POULTON, J., TAYLOR, R. W. & GORMAN, G. S. 2012. Adults with RRM2B-related mitochondrial disease have distinct clinical and molecular characteristics. *Brain,* 135**,** 3392-3403.

POCKETT, J. 2010. *Heat Reflecting Paints and a Review of Their Advertising Material*, In: Chemeca 2010: Engineering at the Edge; 26-29 September 2010, Hilton Adelaide, South Australia. Barton, A.C.T.: Engineers Australia, 2010: [2999]-[3011].

POLLINA, E. A., LEGESSE-MILLER, A., HALEY, E., GOODPASTER, T., RANDOLPH-HABECKER, J. & COLLER, H. A. 2008. Regulating the angiogenic balance in tissues: A potential role for the proliferative state of fibroblasts. *Cell Cycle,* 7**,** 2056-2070.

PONTARIN, G., FERRARO, P., BEE, L., REICHARD, P. & BIANCHI, V. 2012. Mammalian ribonucleotide reductase subunit p53R2 is required for mitochondrial DNA replication and DNA repair in quiescent cells. *Proceedings of the National Academy of Sciences,* 109**,** 13302.

POWERS, J. M., MURPHY, G., RALPH, N., O'GORMAN, S. M. & MURPHY, J. E. J. 2016. Mitochondrial DNA deletion percentage in sun exposed and non sun exposed skin. *Journal of Photochemistry and Photobiology B: Biology,* 165**,** 277-282.

RAHMAN, S. & COPELAND, W. C. 2019. POLG-related disorders and their neurological manifestations. *Nature reviews. Neurology,* 15**,** 40-52.

RANA, M., DE COO, I., DIAZ, F., SMEETS, H. & MORAES, C. T. 2000. An out-of-frame cytochrome b gene deletion from a patient with parkinsonism is associated with impaired complex III assembly and an increase in free radical production. *Ann Neurol,* 48**,** 774-81.

REDZA-DUTORDOIR, M. & AVERILL-BATES, D. A. 2016. Activation of apoptosis signalling pathways by reactive oxygen species. *Biochimica et Biophysica Acta (BBA) - Molecular Cell Research,* 1863**,** 2977-2992.

REYNOLDS, W. J., HANSON, P. S., CRITCHLEY, A., GRIFFITHS, B., CHAVAN, B. & BIRCH-MACHIN, M. A. 2020. Exposing human primary dermal fibroblasts to particulate matter induces changes associated with skin aging. *The FASEB Journal,* 34**,** 14725-14735.

RHIE, G. E., SEO, J. Y. & CHUNG, J. H. 2001. Modulation of catalase in human skin in vivo by acute and chronic UV radiation. *Mol Cells,* 11**,** 399-404.

RINNERTHALER, M., DUSCHL, J., STEINBACHER, P., SALZMANN, M., BISCHOF, J., SCHULLER, M., WIMMER, H., PEER, T., BAUER, J. W. & RICHTER, K. 2013. Age-related changes in the composition of the cornified envelope in human skin. *Exp Dermatol,* 22**,** 329-35.

RISTOW, M. & ZARSE, K. 2010. How increased oxidative stress promotes longevity and metabolic health: The concept of mitochondrial hormesis (mitohormesis). *Experimental Gerontology,* 45**,** 410-418.

RIVERA-TORRES, J., ACÍN-PEREZ, R., CABEZAS-SÁNCHEZ, P., OSORIO, F. G., GONZALEZ-GÓMEZ, C., MEGIAS, D., CÁMARA, C., LÓPEZ-OTÍN, C., ENRÍQUEZ, J. A., LUQUE-GARCÍA, J. L. & ANDRÉS, V. 2013. Identification of mitochondrial dysfunction in Hutchinson–Gilford progeria syndrome through use of stable isotope labeling with amino acids in cell culture. *Journal of Proteomics,* 91**,** 466-477.

ROCHA, M. C., ROSA, H. S., GRADY, J. P., BLAKELY, E. L., HE, L., ROMAIN, N., HALLER, R. G., NEWMAN, J., MCFARLAND, R., NG, Y. S., GORMAN, G. S., SCHAEFER, A. M., TUPPEN, H. A., TAYLOR, R. W. & TURNBULL, D. M. 2018. Pathological mechanisms underlying single large-scale mitochondrial DNA deletions. *Annals of neurology,* 83**,** 115-130.

RODRIGUES, A. 2014. *Systematic development of a behavioural intervention to promote sun-protection behaviours amongst holidaymakers.* PhD, Newcastle University.

ROGERS, J., HARDING, C., MAYO, A., BANKS, J. & RAWLINGS, A. 1996. Stratum corneum lipids: the effect of ageing and the seasons. *Archives of Dermatological Research,* 288**,** 765-770.

ROK, J., RZEPKA, Z., KOWALSKA, J., BANACH, K., BEBEROK, A. & WRZEŚNIOK, D. 2021. Molecular and Biochemical Basis of Minocycline-Induced Hyperpigmentation—The Study on Normal Human Melanocytes Exposed to UVA and UVB Radiation. *International Journal of Molecular Sciences,* 22**,** 3755.

RONG, Z., TU, P., XU, P., SUN, Y., YU, F., TU, N., GUO, L. & YANG, Y. 2021. The Mitochondrial Response to DNA Damage. *Frontiers in Cell and Developmental Biology,* 9.

ROTHFUSS, O., GASSER, T. & PATENGE, N. 2009. Analysis of differential DNA damage in the mitochondrial genome employing a semi-long run real-time PCR approach. *Nucleic Acids Research,* 38**,** e24-e24.

RÜNGER, T., EPE, B. & MÖLLER, K. 1995. Processing of directly and indirectly ultraviolet-induced DNA damage in human cells. *Skin Cancer: Basic Science, Clinical Research and Treatment.* Springer.

SAKURAI, K., SUGIURA, H., MATSUMOTO, M. & UEHARA, M. 2002. Occurrence of patchy parakeratosis in normal-appearing skin in patients with active atopic dermatitis and in patients with healed atopic dermatitis: a cause of impaired barrier function of the atopic skin. *J Dermatol Sci,* 30**,** 37-42.

SANDBY-MOLLER, J., POULSEN, T. & WULF, H. C. 2003. Epidermal thickness at different body sites: relationship to age, gender, pigmentation, blood content, skin type and smoking habits. *Acta Derm Venereol,* 83**,** 410-3.

SANDBY-MØLLER, J., POULSEN, T. & WULF, H. C. 2003. Epidermal thickness at different body sites: relationship to age, gender, pigmentation, blood content, skin type and smoking habits. *Acta Derm Venereol,* 83**,** 410-3.

SANZ, A., PAMPLONA, R. & BARJA, G. 2006. Is the Mitochondrial Free Radical Theory of Aging Intact? *Antioxidants & Redox Signaling,* 8**,** 582-599.

SANZ, A. & STEFANATOS, R. K. A. 2008. The Mitochondrial Free Radical Theory of Aging: A Critical View. *Current Aging Science,* 1**,** 10-21.

SARSOUR, E. H., AGARWAL, M., PANDITA, T. K., OBERLEY, L. W. & GOSWAMI, P. C. 2005. Manganese Superoxide Dismutase Protects the Proliferative Capacity of Confluent Normal Human Fibroblasts *. *Journal of Biological Chemistry,* 280**,** 18033-18041.

SCHAAR, C. E., DUES, D. J., SPIELBAUER, K. K., MACHIELA, E., COOPER, J. F., SENCHUK, M., HEKIMI, S. & VAN RAAMSDONK, J. M. 2015. Mitochondrial and

cytoplasmic ROS have opposing effects on lifespan. *PLoS genetics,* 11**,** e1004972-e1004972.

SCHALLREUTER, K. U., MOORE, J., WOOD, J. M., BEAZLEY, W. D., GAZE, D. C., TOBIN, D. J., MARSHALL, H. S., PANSKE, A., PANZIG, E. & HIBBERTS, N. A. 1999. In Vivo and In Vitro Evidence for Hydrogen Peroxide (H2O2) Accumulation in the Epidermis of Patients with Vitiligo and its Successful Removal by a UVB-Activated Pseudocatalase. *Journal of Investigative Dermatology Symposium Proceedings,* 4**,** 91-96.

SCHRIER, S. A. & FALK, M. J. 2011. Mitochondrial Disorders and The Eye. *Current opinion in ophthalmology,* 22**,** 325-331.

SCHRINER SAMUEL, E., LINFORD NANCY, J., MARTIN GEORGE, M., TREUTING, P., OGBURN CHARLES, E., EMOND, M., COSKUN PINAR, E., LADIGES, W., WOLF, N., VAN REMMEN, H., WALLACE DOUGLAS, C. & RABINOVITCH PETER, S. 2005. Extension of Murine Life Span by Overexpression of Catalase Targeted to Mitochondria. *Science,* 308**,** 1909-1911.

SCHULZ, E., WENZEL, P., MÜNZEL, T. & DAIBER, A. 2014. Mitochondrial redox signaling: Interaction of mitochondrial reactive oxygen species with other sources of oxidative stress. *Antioxidants & redox signaling,* 20**,** 308-324.

SCIACCO, M., PRELLE, A., COMI, G. P., NAPOLI, L., BATTISTEL, A., BRESOLIN, N., TANCREDI, L., LAMPERTI, C., BORDONI, A., FAGIOLARI, G., CISCATO, P., CHIVERI, L., PERINI, M. P., FORTUNATO, F., ADOBBATI, L., MESSINA, S., TOSCANO, A., MARTINELLI-BONESCHI, F., PAPADIMITRIOU, A., SCARLATO, G. & MOGGIO, M. 2001. Retrospective study of a large population of patients affected with mitochondrial disorders: Clinical, morphological and molecular genetic evaluation. *Journal of Neural Transmission,* 108**,** 778-788.

SEIBERG, M. 2001. Keratinocyte-melanocyte interactions during melanosome transfer. *Pigment Cell Res,* 14**,** 236-42.

SEO, K.-S., KIM, J.-H., MIN, K.-N., MOON, J.-A., ROH, T.-C., LEE, M.-J., LEE, K.-W., MIN, J.-E. & LEE, Y.-M. 2018. KL1333, a Novel NAD+ Modulator, Improves Energy Metabolism and Mitochondrial Dysfunction in MELAS Fibroblasts. *Frontiers in Neurology,* 9.

SHENTON, D., PERRONE, G., QUINN, K. A., DAWES, I. W. & GRANT, C. M. 2002. Regulation of Protein S-Thiolation by Glutaredoxin 5 in the Yeast Saccharomyces cerevisiae *. *Journal of Biological Chemistry,* 277**,** 16853-16859.

SHOKOLENKO, I., VENEDIKTOVA, N., BOCHKAREVA, A., WILSON, G. L. & ALEXEYEV, M. F. 2009. Oxidative stress induces degradation of mitochondrial DNA. *Nucleic Acids Research,* 37**,** 2539-2548.

SICILIANO, G., MANCUSO, M., CERAVOLO, R., LOMBARDI, V., IUDICE, A. & BONUCCELLI, U. 2001. Mitochondrial DNA rearrangements in young onset parkinsonism: two case reports. *Journal of Neurology, Neurosurgery & Psychiatry,* 71**,** 685-687.

SIKORSKY, J. A., PRIMERANO, D. A., FENGER, T. W. & DENVIR, J. 2004. Effect of DNA damage on PCR amplification efficiency with the relative threshold cycle method. *Biochemical and Biophysical Research Communications,* 323**,** 823-830.

SKLAR, L. R., ALMUTAWA, F., LIM, H. W. & HAMZAVI, I. 2012. Effects of ultraviolet radiation, visible light, and infrared radiation on erythema and pigmentation: a review. *Photochemical & Photobiological Sciences,* 12**,** 54-64.

SLOMINSKI, A. & PRUSKI, D. 1993. Melatonin inhibits proliferation and melanogenesis in rodent melanoma cells. *Experimental cell research,* 206**,** 189-194.

SLOMINSKI, A. T., SEMAK, I., FISCHER, T. W., KIM, T. K., KLESZCZYŃSKI, K., HARDELAND, R. & REITER, R. J. 2017. Metabolism of melatonin in the skin: Why is it important? *Experimental dermatology,* 26**,** 563-568.

SNYDER, J. R., HALL, A., NI-KOMATSU, L., KHERSONSKY, S. M., CHANG, Y.-T. & ORLOW, S. J. 2005. Dissection of melanogenesis with small molecules identifies prohibitin as a regulator. *Chemistry & biology,* 12**,** 477-484.

SOLOMON, N. P., MAKASHAY, M. J., HELOU, L. B. & CLARK, H. M. 2017. Neurogenic Orofacial Weakness and Speech in Adults With Dysarthria. *American journal of speech-language pathology,* 26**,** 951-960.

SONG, X., MOSBY, N., YANG, J., XU, A., ABDEL-MALEK, Z. & KADEKARO, A. L. 2009a. α-MSH activates immediate defense responses to UV-induced oxidative stress in human melanocytes. *Pigment Cell & Melanoma Research,* 22**,** 809-818.

SONG, X., MOSBY, N., YANG, J., XU, A., ABDEL-MALEK, Z. & KADEKARO, A. L. 2009b. α-MSH activates immediate defense responses to UV-induced oxidative stress in human melanocytes. *Pigment cell & melanoma research,* 22**,** 809-818.

SPINAZZI, M., CAZZOLA, S., BORTOLOZZI, M., BARACCA, A., LORO, E., CASARIN, A., SOLAINI, G., SGARBI, G., CASALENA, G., CENACCHI, G., MALENA, A., FREZZA, C., CARRARA, F., ANGELINI, C., SCORRANO, L., SALVIATI, L. & VERGANI, L. 2008. A novel deletion in the GTPase domain of OPA1 causes defects in mitochondrial morphology and distribution, but not in function. *Human Molecular Genetics,* 17**,** 3291-3302.

SREEDHAR, A., AGUILERA-AGUIRRE, L. & SINGH, K. K. 2020. Mitochondria in skin health, aging, and disease. *Cell death & disease,* 11**,** 444-444.

STAMATAS, G. N., ZMUDZKA, B. Z., KOLLIAS, N. & BEER, J. Z. 2004. Non-Invasive Measurements of Skin Pigmentation In Situ. *Pigment Cell Research,* 17**,** 618-626.

STILES, A. R., SIMON, M. T., STOVER, A., EFTEKHARIAN, S., KHANLOU, N., WANG, H. L., MAGAKI, S., LEE, H., PARTYNSKI, K., DORRANI, N., CHANG, R., MARTINEZ-AGOSTO, J. A. & ABDENUR, J. E. 2016. Mutations in TFAM, encoding mitochondrial transcription factor A, cause neonatal liver failure associated with mtDNA depletion. *Mol Genet Metab,* 119**,** 91-9.

STOUT, R. & BIRCH-MACHIN, M. 2019. Mitochondria's Role in Skin Ageing. *Biology (Basel),* 8.

SUEN, D. F., NARENDRA, D. P., TANAKA, A., MANFREDI, G. & YOULE, R. J. 2010. Parkin overexpression selects against a deleterious mtDNA mutation in heteroplasmic cybrid cells. *Proc Natl Acad Sci U S A,* 107**,** 11835-40.

SWALWELL, H., LATIMER, J., HAYWOOD, R. M. & BIRCH-MACHIN, M. A. 2012. Investigating the role of melanin in UVA/UVB-and hydrogen peroxide-induced cellular and mitochondrial ROS production and mitochondrial DNA damage in human melanoma cells. *Free Radical Biology and Medicine,* 52**,** 626-634.

SWIFT, A., LIEW, S., WEINKLE, S., GARCIA, J. K. & SILBERBERG, M. B. 2021. The Facial Aging Process From the "Inside Out". *Aesthetic surgery journal,* 41**,** 1107-1119.

TADI, S. K., SEBASTIAN, R., DAHAL, S., BABU, R. K., CHOUDHARY, B. & RAGHAVAN, S. C. 2016. Microhomology-mediated end joining is the principal mediator of double-strand break repair during mitochondrial DNA lesions. *Molecular biology of the cell,* 27**,** 223-235.

TADOKORO, T., KOBAYASHI, N., ZMUDZKA, B. Z., ITO, S., WAKAMATSU, K., YAMAGUCHI, Y., KOROSSY, K. S., MILLER, S. A., BEER, J. Z. & HEARING, V. J. 2003. UV-induced DNA damage and melanin content in human skin differing in racial/ethnic origin. *The FASEB Journal,* 17**,** 1177-1179.

TANAKA, H., ARAKAWA, H., YAMAGUCHI, T., SHIRAISHI, K., FUKUDA, S., MATSUI, K., TAKEI, Y. & NAKAMURA, Y. 2000. A ribonucleotide reductase gene involved in a p53-dependent cell-cycle checkpoint for DNA damage. *Nature,* 404**,** 42-49.

TEWARI, A., GRYS, K., KOLLET, J., SARKANY, R. & YOUNG, A. R. 2014. Upregulation of MMP12 and its activity by UVA1 in human skin: potential implications for photoaging. *Journal of Investigative Dermatology,* 134**,** 2598-2609.

THODY, A. J., HIGGINS, E. M., WAKAMATSU, K., ITO, S., BURCHILL, S. A. & MARKS, J. M. 1991. Pheomelanin as well as Eumelanin Is Present in Human Epidermis. *Journal of Investigative Dermatology,* 97**,** 340-344.

TIMM, C. M., LOOMIS, K., STONE, W., MEHOKE, T., BRENSINGER, B., PELLICORE, M., STANICZENKO, P. P. A., CHARLES, C., NAYAK, S. & KARIG, D. K. 2020. Isolation and characterization of diverse microbial representatives from the human skin microbiome. *Microbiome,* 8**,** 58.

TRIFUNOVIC, A., HANSSON, A., WREDENBERG, A., ROVIO, A. T., DUFOUR, E., KHVOROSTOV, I., SPELBRINK, J. N., WIBOM, R., JACOBS, H. T. & LARSSON, N.-G. 2005. Somatic mtDNA mutations cause aging phenotypes without affecting reactive oxygen species production. *Proceedings of the National Academy of Sciences of the United States of America,* 102**,** 17993.

TULINIUS, M., DARIN, N., WIKLUND, L.-M., HOLMBERG, E., ERIKSSON, J. E., LISSENS, W., DE MEIRLEIR, L. & HOLME, E. 2005. A family with pyruvate dehydrogenase complex deficiency due to a novel C>T substitution at nucleotide position 407 in exon 4 of the X-linked E1α gene. *European Journal of Pediatrics,* 164**,** 99-103.

TUTKA, K., ŻYCHOWSKA, M. & REICH, A. 2020. Diversity and Composition of the Skin, Blood and Gut Microbiome in Rosacea-A Systematic Review of the Literature. *Microorganisms,* 8**,** 1756.

TWIG, G., ELORZA, A., MOLINA, A. J. A., MOHAMED, H., WIKSTROM, J. D., WALZER, G., STILES, L., HAIGH, S. E., KATZ, S., LAS, G., ALROY, J., WU, M., PY, B. F., YUAN, J., DEENEY, J. T., CORKEY, B. E. & SHIRIHAI, O. S. 2008. Fission and selective fusion govern mitochondrial segregation and elimination by autophagy. *The EMBO Journal,* 27**,** 433-446.

VALACCHI, G., VAN DER VLIET, A., SCHOCK, B. C., OKAMOTO, T., OBERMULLER-JEVIC, U., CROSS, C. E. & PACKER, L. 2002. Ozone exposure activates oxidative stress responses in murine skin. *Toxicology,* 179**,** 163-170.

VAN DER VLEUTEN, C. J. M., KROOT, E. J. A., DE JONG, E. M. G. J. & VAN DE KERKHOF, P. C. M. 1996. The immunohistochemical effects of a single challenge with an intermediate dose of ultravilet B on normal human skin. *Archives of Dermatological Research,* 288**,** 510-516.

VAN RAAMSDONK, J. M. & HEKIMI, S. 2009. Deletion of the mitochondrial superoxide dismutase sod-2 extends lifespan in Caenorhabditis elegans. *PLoS genetics,* 5**,** e1000361-e1000361.

VARANI, J., DAME, M. K., RITTIE, L., FLIGIEL, S. E. G., KANG, S., FISHER, G. J. & VOORHEES, J. J. 2006. Decreased Collagen Production in Chronologically Aged Skin: Roles of Age-Dependent Alteration in Fibroblast Function and Defective Mechanical Stimulation. *The American Journal of Pathology,* 168**,** 1861-1868.

VARANI, J., WARNER, R. L., GHARAEE-KERMANI, M., PHAN, S. H., KANG, S., CHUNG, J., WANG, Z., DATTA, S. C., FISHER, G. J. & VOORHEES, J. J. 2000. Vitamin A Antagonizes Decreased Cell Growth and Elevated Collagen-Degrading

Matrix Metalloproteinases and Stimulates Collagen Accumulation in Naturally Aged Human Skin1. *Journal of Investigative Dermatology,* 114**,** 480-486.
VICENTINI, F. T., HE, T., SHAO, Y., FONSECA, M. J., VERRI JR, W. A., FISHER, G. J. & XU, Y. 2011. Quercetin inhibits UV irradiation-induced inflammatory cytokine production in primary human keratinocytes by suppressing NF-κB pathway. *Journal of dermatological science,* 61**,** 162-168.
VIERKÖTTER, A., SCHIKOWSKI, T., RANFT, U., SUGIRI, D., MATSUI, M., KRÄMER, U. & KRUTMANN, J. 2010. Airborne particle exposure and extrinsic skin aging. *Journal of investigative dermatology,* 130**,** 2719-2726.
VÍTOR, A. C., HUERTAS, P., LEGUBE, G. & DE ALMEIDA, S. F. 2020. Studying DNA Double-Strand Break Repair: An Ever-Growing Toolbox. *Frontiers in Molecular Biosciences,* 7.
VOETS, A. M., LINDSEY, P. J., VANHERLE, S. J., TIMMER, E. D., ESSELING, J. J., KOOPMAN, W. J. H., WILLEMS, P. H. G. M., SCHOONDERWOERD, G. C., DE GROOTE, D., POLL-THE, B. T., DE COO, I. F. M. & SMEETS, H. J. M. 2012. Patient-derived fibroblasts indicate oxidative stress status and may justify antioxidant therapy in OXPHOS disorders. *Biochimica et Biophysica Acta (BBA) - Bioenergetics,* 1817**,** 1971-1978.
WALSH, D. W. M., SIEBENWIRTH, C., GREUBEL, C., ILICIC, K., REINDL, J., GIRST, S., MUGGIOLU, G., SIMON, M., BARBERET, P., SEZNEC, H., ZISCHKA, H., MULTHOFF, G., SCHMID, T. E. & DOLLINGER, G. 2017. Live cell imaging of mitochondria following targeted irradiation in situ reveals rapid and highly localized loss of membrane potential. *Scientific Reports,* 7**,** 46684.
WALSH, M. E., SHI, Y. & VAN REMMEN, H. 2014. The effects of dietary restriction on oxidative stress in rodents. *Free radical biology & medicine,* 66**,** 88-99.
WANG, C., HAN, B., ZHOU, R. & ZHUANG, X. 2016a. Real-Time Imaging of Translation on Single mRNA Transcripts in Live Cells. *Cell,* 165**,** 990-1001.
WANG, G., CAO, L., LIU, X., SIERACKI, N. A., DI, A., WEN, X., CHEN, Y., TAYLOR, S., HUANG, X., TIRUPPATHI, C., ZHAO, Y. Y., SONG, Y., GAO, X., JIN, T., BAI, C., MALIK, A. B. & XU, J. 2016b. Oxidant Sensing by TRPM2 Inhibits Neutrophil Migration and Mitigates Inflammation. *Dev Cell,* 38**,** 453-62.
WANG, L. 2016. Mitochondrial purine and pyrimidine metabolism and beyond. *Nucleosides, Nucleotides & Nucleic Acids,* 35**,** 578-594.
WANG, T.-Y., SUN, Y., MUTHUKRISHNAN, N., ERAZO-OLIVERAS, A., NAJJAR, K. & PELLOIS, J.-P. 2016c. Membrane Oxidation Enables the Cytosolic Entry of Polyarginine Cell-penetrating Peptides. *The Journal of biological chemistry,* 291**,** 7902-7914.
WANROOIJ, S., LUOMA, P., VAN GOETHEM, G., VAN BROECKHOVEN, C., SUOMALAINEN, A. & SPELBRINK, J. N. 2004. Twinkle and POLG defects enhance age-dependent accumulation of mutations in the control region of mtDNA. *Nucleic acids research,* 32**,** 3053-3064.
WEBB, A. R., KAZANTZIDIS, A., KIFT, R. C., FARRAR, M. D., WILKINSON, J. & RHODES, L. E. 2018a. Colour Counts: Sunlight and Skin Type as Drivers of Vitamin D Deficiency at UK Latitudes. *Nutrients,* 10**,** 457.
WEBB, A. R., KAZANTZIDIS, A., KIFT, R. C., FARRAR, M. D., WILKINSON, J. & RHODES, L. E. 2018b. Meeting Vitamin D Requirements in White Caucasians at UK Latitudes: Providing a Choice. *Nutrients,* 10**,** 497.
WENCZL, E., VAN DER SCHANS, G., ROZA, L., KOLB, R., SMIT, N. & SCHOTHORST, A. 1998. UVA-induced oxidative DNA damage in human melanocytes is related to their (pheo) melanin content. *Journal of Dermatological Science***,** S221.

WICKERSHAM, M., WACHTEL, S., WONG FOK LUNG, T., SOONG, G., JACQUET, R., RICHARDSON, A., PARKER, D. & PRINCE, A. 2017. Metabolic Stress Drives Keratinocyte Defenses against Staphylococcus aureus Infection. *Cell reports,* 18**,** 2742-2751.

WISNOVSKY, S., JEAN, S. R., LIYANAGE, S., SCHIMMER, A. & KELLEY, S. O. 2016. Mitochondrial DNA repair and replication proteins revealed by targeted chemical probes. *Nature Chemical Biology,* 12**,** 567-573.

WOJTOVICH, A. P., SMITH, C. O., HAYNES, C. M., NEHRKE, K. W. & BROOKES, P. S. 2013. Physiological consequences of complex II inhibition for aging, disease, and the mKATP channel. *Biochimica et biophysica acta,* 1827**,** 598-611.

WONG, L.-J. C. 2007. Diagnostic challenges of mitochondrial DNA disorders. *Mitochondrion,* 7**,** 45-52.

WRIGHT, C., IYER, A. K. V., WANG, L., WU, N., YAKISICH, J. S., ROJANASAKUL, Y. & AZAD, N. 2017. Effects of titanium dioxide nanoparticles on human keratinocytes. *Drug and chemical toxicology,* 40**,** 90-100.

XIONG, Z. M., CHOI, J. Y., WANG, K., ZHANG, H., TARIQ, Z., WU, D., KO, E., LADANA, C., SESAKI, H. & CAO, K. 2016. Methylene blue alleviates nuclear and mitochondrial abnormalities in progeria. *Aging Cell,* 15**,** 279-290.

XUAN, Y. H., HUANG, B. B., TIAN, H. S., CHI, L. S., DUAN, Y. M., WANG, X., ZHU, Z. X., CAI, W. H., ZHU, Y. T., WEI, T. M., YE, H. B., CONG, W. T. & JIN, L. T. 2014. High-Glucose Inhibits Human Fibroblast Cell Migration in Wound Healing via Repression of bFGF-Regulating JNK Phosphorylation. *PLOS ONE,* 9**,** e108182.

YA-XIAN, Z., SUETAKE, T. & TAGAMI, H. 1999a. Number of cell layers of the stratum corneum in normal skin - relationship to the anatomical location on the body, age, sex and physical parameters. *Arch Dermatol Res,* 291**,** 555-9.

YA-XIAN, Z., SUETAKE, T. & TAGAMI, H. 1999b. Number of cell layers of the stratum corneum in normal skin – relationship to the anatomical location on the body, age, sex and physical parameters. *Archives of Dermatological Research,* 291**,** 555-559.

YAMASHITA, S., NISHINO, I., NONAKA, I. & GOTO, Y. I. 2008. Genotype and phenotype analyses in 136 patients with single large-scale mitochondrial DNA deletions. *Journal of Human Genetics,* 53**,** 598-606.

YAMAZAKI, T., KAWAI, C., YAMAUCHI, A. & KURIBAYASHI, F. 2011. A highly sensitive chemiluminescence assay for superoxide detection and chronic granulomatous disease diagnosis. *Tropical medicine and health,* 39**,** 41-45.

YANG, L., TANG, H., LIN, X., WU, Y., ZENG, S., PAN, Y., LI, Y., XIANG, G., LIN, Y.-F., ZHUANG, S.-M., SONG, Z., JIANG, Y. & LIU, X. 2020. OPA1-Exon4b Binds to mtDNA D-Loop for Transcriptional and Metabolic Modulation, Independent of Mitochondrial Fusion. *Frontiers in Cell and Developmental Biology,* 8.

YANG, W. & HEKIMI, S. 2010. A Mitochondrial Superoxide Signal Triggers Increased Longevity in Caenorhabditis elegans. *PLOS Biology,* 8**,** e1000556.

YAROSZ, E. L. & CHANG, C.-H. 2018. The Role of Reactive Oxygen Species in Regulating T Cell-mediated Immunity and Disease. *Immune network,* 18**,** e14-e14.

YOSHIMOTO, S., YOSHIDA, M., ANDO, H. & ICHIHASHI, M. 2018. Establishment of Photoaging In Vitro by Repetitive UVA Irradiation: Induction of Characteristic Markers of Senescence and its Prevention by PAPLAL with Potent Catalase Activity. *Photochemistry and Photobiology,* 94**,** 438-444.

YOUSEF, H., ALHAJJ, M. & SHARMA, S. 2019. *Anatomy, Skin (Integument), Epidermis*, StatPearls Publishing, Treasure Island (FL).

YU-WAI-MAN, P., CLEMENTS, A. L., NESBITT, V., GRIFFITHS, P. G., GORMAN, G. S., SCHAEFER, A. M., TURNBULL, D. M., TAYLOR, R. W. & MCFARLAND, R.

2014. A national epidemiological study of chronic progressive external ophthalmoplegia in the United Kingdom - molecular genetic features and neurological burden. *Investigative Ophthalmology & Visual Science,* 55**,** 5109-5109.

YU-WAI-MAN, P., LAI-CHEONG, J., BORTHWICK, G. M., HE, L., TAYLOR, G. A., GREAVES, L. C., TAYLOR, R. W., GRIFFITHS, P. G. & TURNBULL, D. M. 2010. Somatic Mitochondrial DNA Deletions Accumulate to High Levels in Aging Human Extraocular Muscles. *Investigative Ophthalmology & Visual Science,* 51**,** 3347-3353.

ZABIHI DIBA, L., MOHADDES ARDEBILI, S. M., GHARESOURAN, J. & HOUSHMAND, M. 2016. Age-related decrease in mtDNA content as a consequence of mtDNA 4977 bp deletion. *Mitochondrial DNA Part A,* 27**,** 3008-3012.

ŻĄDŁO, A., ITO, S., SARNA, M., WAKAMATSU, K., MOKRZYŃSKI, K. & SARNA, T. 2020. The role of hydrogen peroxide and singlet oxygen in the photodegradation of melanin. *Photochemical & Photobiological Sciences,* 19**,** 654-667.

ZANCHETTA, L. M., KIRK, D., LYNG, F., WALSH, J. & MURPHY, J. E. 2010. Cell-density-dependent changes in mitochondrial membrane potential and reactive oxygen species production in human skin cells post sunlight exposure. *Photodermatology, photoimmunology & photomedicine,* 26**,** 311-317.

ZHANG, J., GUO, J., FANG, W., JUN, Q. & SHI, K. 2015. Clinical features of MELAS and its relation with A3243G gene point mutation. *International Journal of Clinical and Experimental Pathology,* 8**,** 13411-13415.

ZHANG, Y., CAI, Y., SHI, M., JIANG, S., CUI, S., WU, Y., GAO, X.-H. & CHEN, H.-D. 2016. The Prevalence of Vitiligo: A Meta-Analysis. *PloS one,* 11**,** e0163806-e0163806.

ZHANG, Y., UNNIKRISHNAN, A., DEEPA, S. S., LIU, Y., LI, Y., IKENO, Y., SOSNOWSKA, D., VAN REMMEN, H. & RICHARDSON, A. 2017. A new role for oxidative stress in aging: The accelerated aging phenotype in Sod1−/− mice is correlated to increased cellular senescence. *Redox Biology,* 11**,** 30-37.

ZHAO, L. 2019. Mitochondrial DNA degradation: A quality control measure for mitochondrial genome maintenance and stress response. *Enzymes,* 45**,** 311-341.

ZHENG, Y., LUO, X., ZHU, J., ZHANG, X., ZHU, Y., CHENG, H., XIA, Z., SU, N., ZHANG, N. & ZHOU, J. 2012. Mitochondrial DNA 4977 bp deletion is a common phenomenon in hair and increases with age. *Bosnian journal of basic medical sciences,* 12**,** 187-192.

ZIADA, A. S., SMITH, M.-S. R. & CÔTÉ, H. C. F. 2020. Updating the Free Radical Theory of Aging. *Frontiers in Cell and Developmental Biology,* 8.

ZIGMAN, S., REDDAN, J., SCHULTZ, J. B. & MCDANIEL, T. 1996. Structural and functional changes in catalase induced by near-UV radiation. *Photochem Photobiol,* 63**,** 818-24.

ZINOVKINA, L. A. 2018. Mechanisms of Mitochondrial DNA Repair in Mammals. *Biochemistry (Moscow),* 83**,** 233-249.